MECHANISMS OF EXCITATION AND AMPLIFICATION IN THE MAMMALIAN COCHLEA

THOMAS DAVID WEDDELL

2013

The University of Brighton in collaboration with the University of Munich

DECLARATION

I declare that the research contained in this thesis, unless otherwise formally indicated within the text, is the original work of the author. The thesis has not been previously submitted to this or any other university for a degree, and does not incorporate any material already submitted for a degree.

_____

Thomas David Weddell

Date: 18th April 2013

To my dad,

Dr David John Weddell

ACKNOWLEDGEMENTS

I thank my supervisors Professor Ian Russell and Dr. Andrei Lukashkin for their guidance, support and patience during the course of my PHD studies. They have always been generous with their time, have been keen to give me opportunities and have inspired me with their passion for science.

I thank Dr Markus Drexl for the opportunity of working in Germany, his continued support in my studies, for proof reading of this thesis and his hospitality during my time in Munich.

I thank my laboratory colleagues, past and present, for creating a perfect environment in which to engage in science and for their support throughout my studies, particularly I would like to thank James Hartley for his technical expertise and willingness to share his immense knowledge. I would also like to thank Gareth Jones for his help and advice and Victoria Lukashkina for her assistance when learning the mouse preparation.

I thank my former colleagues in the University of Sussex Life Sciences Department and my new colleagues at the University of Brighton for their professionalism and kindness and for giving me numerous teaching opportunities, during my time as a PhD student. I particularly thank Professor George Kemenes for never failing to care for his students and their best interests.

I thank all my family for their patience and encouragement during my prolonged stay in education, particularly my parents David and Jane Weddell and Phil Yates and Jane Weddell without whom I would never have been able to pursue this course. I thank my friends for all their support and so often feeding me and providing a couch to sleep on. I thank my friend John Brinsley for proof reading this thesis.

I thank my wife Anna for her continued love, advice, enthusiasm and limitless patience over the last 3 years.

PREFACE

The research presented in this thesis is the work of Thomas D. Weddell under the supervision of Ian J. Russell and Andrei N. Lukashkin.

This thesis contains 7 chapters and 3 appendices. Chapter 1 contains a general introduction to mammalian hearing and Chapter 2 describes the materials and methods used in the experiments on mice, guinea pigs and humans.

Chapters 3 - 6 are results chapters containing focused introductions to the experiments performed, results and related discussion. Chapter 3 compares low-frequency acoustical biasing of distortion product otoacoustic emissions in humans and guinea pigs. For this chapter data collected from experiments in humans was compared with data collected for guinea pigs from a previously published paper (Lukashkin and Russell, 2005b); the experimental methods used in this work on guinea pigs are presented in appendix 1. Chapter 4 presents data from an investigation into round window stimulation of the cochlea in guinea pigs. Chapter 5 presents data collected from a mouse model (*Otoa*$^{EGFP/EGFP}$) of the human deafness gene, DFNB22. The chapter has been accepted for publication in PNAS and has been modified slightly to fit with the formatting and style of this thesis, certain important topics expanded on and the morphological analysis separated from the electrophysiology and mechanical measurements. The construction of the *Otoa*$^{EGFP/EGFP}$ knockout mouse and all morphological and imaging work presented was performed by Richard Goodyear, Lindsey Welstead, Christine Petit, Kevin Legan and Guy Richardson, the methods for this work can be found in appendix 2 and a copy of the full paper can be found in appendix 3. Data for distortion product otoacoustic emission recordings and compound action potential tuning curves were collected with Dr Victoria Lukashkina. Chapter 6 is concerned with the role of the prestin motor molecule linking extrinsic tuning to neural excitation. This chapter was previously published in the journal Current Biology in September 2011 (Weddell et al., 2011) and has been modified slightly to fit with the formatting and style of this thesis. The methods section, which was previously found in supplementary information in the published article, has been moved to the general methods section in Chapter 2, and the Materials and Methods have been expanded. Figure 6.2 was previously located in the supplementary material in the published paper but has been moved to the main body of the chapter in this thesis. The references have been merged with the main bibliography. The data presented in this paper for prestin KO mice was partially collected by Dr Marcia Maria Mallado Lagarde.

Chapter 7 contains a general discussion of the data presented in this thesis and suggestions for possible future work.

APPENDIX 1 contains experimental methods for distortion product otoacoustic emission recording in the guinea pig preparation.

APPENDIX 2 contains a description of the construction of the *Otoa*$^{EGFP/EGFP}$ knockout mouse and all morphological work performed for Chapter 5.

APPENDIX 3 contains the pre-publication proof of the accepted paper on the *Otoa*$^{EGFP/EGFP}$ mouse that has been accepted for publication in PNAS.

UNIVERSITY OF BRIGHTON

Thomas David Weddell

Mechanisms of excitation and amplification in the mammalian cochlea

ABSTRACT

Mechanisms of cochlea excitation and amplification were investigated experimentally across a range of mammalian species.

Distortion product otoacoustic emissions (DPOAEs) are used to clinically assess hearing. DPOAEs recorded from the ears of human subjects in the presence of a low frequency, high level tone were compared with similar recordings made from guinea pigs. Both guinea pig and human data were found to originate from a common cochlear nonlinearity; the Boltzmann model of DPOAE generation at the output of a spatially localised single-saturating non-linearity. Accordingly, the guinea pig cochlea can be used as a human model system for the study of DPOAE generation.

To further understand mechanical excitation of the cochlea, and as an alternative means of cochlear excitation for subjects without access to the normal middle ear route, the guinea pig cochlea was stimulated by vibrating the round window (RW) membrane using a tiny cylindrical electromagnet. Interferometer measurements of magnet displacement and compound action potential (CAP) recordings revealed RW stimulation to be highly efficient, providing the RW acted normally as a pressure release valve. Measurements of ossicular vibrations during RW stimulation provided an unreliable measure of input into the cochlea and stapes fixation resulted in no change in CAP threshold. It was concluded that the area of the RW not covered by the magnet acts as a pressure shunt and that RW vibrations drive the basilar membrane directly via near-field pressure variations.

In the *Otoa*$^{EGFP/EGFP}$ mouse model of the DFNB22 human deafness mutation, the tectorial membrane (TM), an extracellular matrix that is normally anchored by one edge to the spiral limbus and overlies the organ of Corti, retains its structure and remains in close proximity to Corti's organ, but is detached from the limbal surface. Apart from loss of a second resonance in the BM tuning curve and minor reductions in levels of DPOAEs, tuning and sensitivity of the basilar membrane (BM) responses and cochlea microphonic (CM) were similar in *Otoa*$^{EGFP/EGFP}$ and wild-type (WT) mice. It was concluded that the tectorial membrane provides an inertial mass against which outer hair cells (OHCs) can exert forces and be excited optimally. The thresholds of the CAP in *Otoa*$^{EGFP/EGFP}$ mice were significantly elevated indicating the importance of limbal attachment of the TM in effective inner hair cell (IHC) excitation and that the hearing loss in DFNB22 patients is due to a defect in IHC excitation.

The electromechanical motor protein prestin localised to the OHCs is necessary for cochlea amplification, frequency tuning, and sensitivity. We measured the cochlear responses of the prestin knock-in 499 mouse, where the OHCs have normal axial stiffness but lack somatic motility. The sensitivities of both BM and CAP responses were considerably reduced and BM frequency tuning was shifted to lower frequencies compared with responses from WT mice. BM and electrical recordings from prestin KO mice revealed BM sensitivity to be similar to that of WT mice, but more broadly tuned to lower frequencies. From comparison of BM motion and neural responses from prestin KO, 499 and WT mice it was concluded that prestin is the essential molecular element that mechanically couples OHCs to the BM. Thereby, OHCs are able to amplify tuned vibrations of the BM and relay the exquisitely sensitive, sharply tuned mechanical responses of the cochlea to the IHCs and hence to the auditory nerve.

CONTENTS

LIST OF FIGURES

LIST OF TABLES

ABBREVIATIONS

AC	Alternating current
ABR	Auditory brainstem response
BM	Basilar membrane
CF	Characteristic frequency
CM	Cochlea microphonic
CAP	Compound action potential
CHA	Conventional hearing aid
CNS	Central nervous system
dB	Decibel
DC	Deiter's cell
Dcurr	Direct current
DPOAE	Distortion product otoacoustic emission
ENT	Ear nose and throat
FMT	Floating mass transducer
GAGS	Glycosaminoglycans
HL	Hearing loss
IHC	Inner hair cell
IPC	Inner pillar cell
i.m	Intra-muscular
i.p	Intra-peritoneal
KO	Knock-out
MET	Mechanoelectrical transduction
OAE	Otoacoustic emission
OHC	Outer hair cell
OPC	Outer pillar cell
pm	Post mortem
RL	Reticular laminar
RW	Round window
s.c	Subcutaneous
SPL	Sound pressure level
ST	Scala tympani
SSM	Striated sheet matrix
SV	Scala vestibuli
TM	Tectorial membrane
TTL	Transistor transistor logic
WT	Wild-type

1 GENERAL INTRODUCTION

The mammalian ear's function is the detection and processing of acoustic vibrations, separating sounds into their constituent frequencies whilst maintaining a high degree of sensitivity over an enormous dynamic range. To achieve this role the cochlea relies on the effective mechanical interaction and timings between the structures of which it is composed and an active amplification mechanism localised to one of the two types of mechanosensory cell it contains, the outer hair cells (OHCs). In circumstances where amplification or the mechanics of the cochlea are compromised the results can be that the second mechanosensory cell type, the inner hair cells (IHCs) whose role it is to transduce sound energy into electrical signals to be centrally processed, are not excited effectively. The mechanics of the cochlea and the mechanism that underpins amplification are not fully understood.

1.1 Anatomy of the mammalian ear

The peripheral auditory system can be divided into three broad anatomical divisions: the external ear (or outer ear), the middle ear and the inner ear (Geisler, 1998) (Figure 1.1). These divisions each play important roles in acoustic sensation. The external ears primary function is to funnel acoustic energy to the tympanic membrane and apply basic filtering of specific frequencies. The middle ear's main role is to efficiently transmit behaviourally relevant sound energy from air to the fluids of the cochlea. The inner ear has a dual function; it is responsible for the sensation of acoustic information through the cochlea and it senses rotation and linear acceleration of the head through the vestibular system.

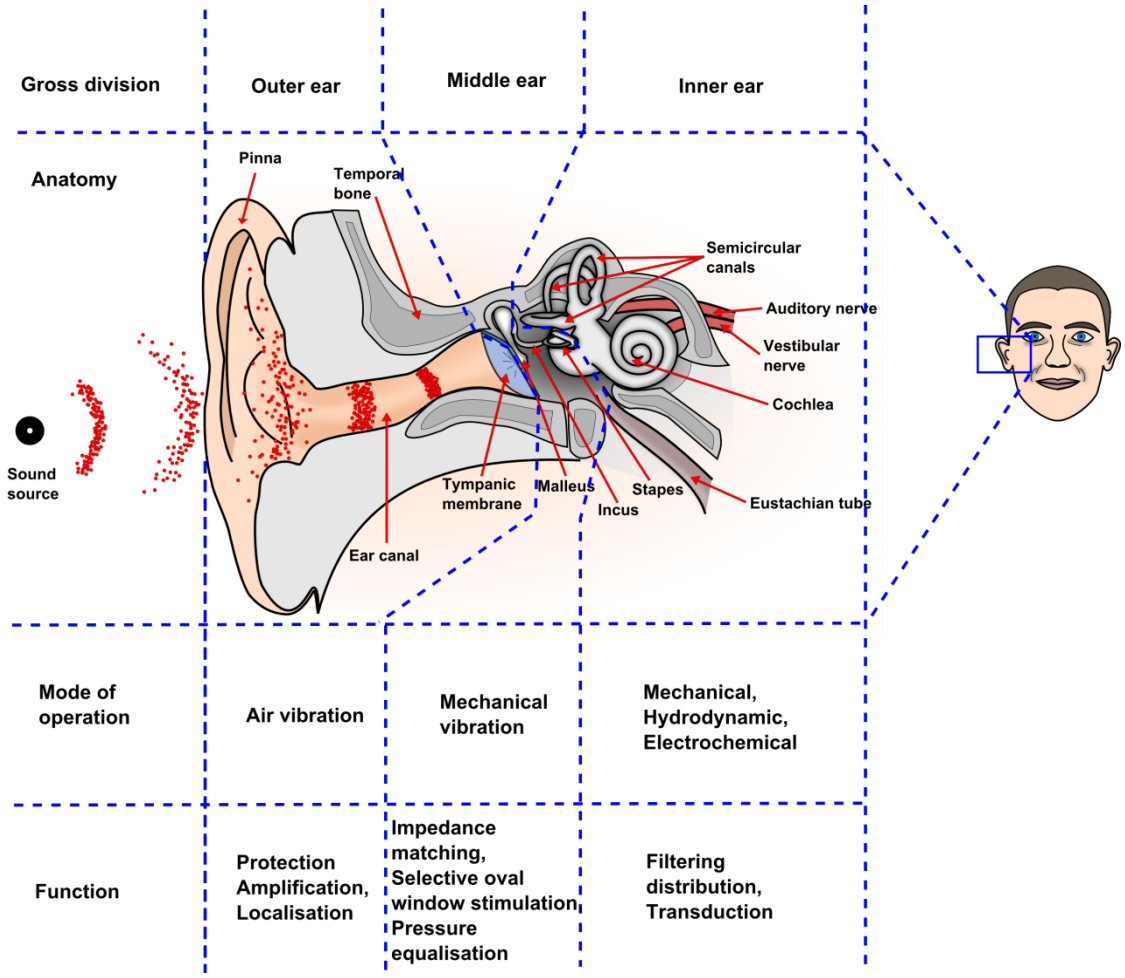

Figure 1.1 Cross section showing broad anatomical divisions of the human ear. The major suggested functions of each division and predominant modes of operation are listed. Adapted from (Yost et al., 2001; Pickles, 2008; Jones, 2012).

1.1.1 The external ear

The external ear consists of an asymmetrical cartilaginous flap of skin called the pinna or auricle which has a multitude of sizes and shapes between mammals that are highly

dependent on the individual species acoustic environment. The shape of the pinna enables animals to amplify behaviourally relevant frequencies of sound, and achieve monoaural sound localisation through a learned process (Van Wanrooij and Van Opstal, 2004) (Figure 1.1). The auricle funnels sound into the ear canal and the sound travels medially towards the middle and inner ear, the combination of which act as a 'collecting horn' that amplify the sound as it enters the auditory system. This acoustic energy is channelled towards the tympanic membrane, which is held in place by fibres and cartilage between the outer and middle ear (Yost et al., 2001).

1.1.2 The middle ear

The tympanic membrane demarcates the lateral border of the middle ear, a hollow, gas filled cavity suspended within which are the three smallest bones in mammals; the malleus, incus and stapes, known collectively as the ossicles. The tympanic membrane provides a large flexible surface area on which compression sound waves are able to impinge and vibrate (Geisler, 1998). The ossicles are mechanically coupled to the movements of the tympanic membrane and the ossicular chain transfers tympanic vibrations via the middle ear and the oval window to the fluids of the cochlea. Through this efficient transfer of acoustic energy from the relatively low impedance air to the relatively high impedance fluids of the cochlear the middle ear primarily acts as an impedance matching devise reducing reflection of acoustic energy. Across species the responses of the ossicular chain are optimal at certain frequencies that are behaviourally relevant to the animal. For humans this is between 1-4Khz, the dominant frequencies of vocal communication (Yost et al., 2001). The middle ear also consists of a Eustachian tube, connected to the nasopharynx. This connection allows equalisation of pressure in the middle ear with atmospheric pressure (Geisler, 1998).

1.1.3 The inner ear

The inner ear broadly comprises the semi-circular canals, the vestibule and the shell like structure of the cochlea, which have two functionally different roles. The semi-circular canals and otolith organs of the vestibular system are responsible for the sensation of linear acceleration (gravity) and rotation of the head; which allow mammals to successfully navigate complex environments. In the cochlea mechanical movements of cochlea fluids are converted to neural electrical impulses interpreted by the CNS as sound. The anatomy, and mechanical and electrical properties of the cochlea are specialised to transduce an enormous dynamic range of environmental sounds that spans over 6 orders of magnitude. Low level sounds are amplified, high level sounds are compressed, and sounds are sharply separated into their constituent frequencies, with frequencies extending over 10 octaves (Dallos, 1992).

1.2 Anatomy and passive properties of the mammalian peripheral auditory system

The passive mechanical properties of the peripheral auditory system can be split into three broad divisions, the middle ear including the tympanic membrane and the ossicles, the broad mechanics of the cochlea including the oval and RW and the organ of Corti including its sensory and supporting cells. In reality in a healthy intact cochlea these structures are mechanically coupled.

1.2.1 Middle ear

Upon entering the peripheral auditory system, the acoustic energy, in the form of compression waves, must first be converted into mechanical movements of the solid structures in order to propagate to the fluids of the cochlea. This is achieved by the highly specialised tympanic membrane. The relatively large surface area and flexible properties of which enable it to be moved by compression sound waves (Geisler, 1998). Frequency-dependent movement of the tympanic membrane is efficiently transmitted to the ossicular chain via its connection with the manubrium of the malleus. The ossicular chain transmits these movements to the fluids of the cochlea via the stapes footplate, which is located in the oval window (Tonndorf and Khanna, 1972). The position of the manubrium can vary dependent on species, such that in smaller mammals with fused malleus-incus joints, (guinea pig and chinchilla, for example) the manubrium divides the membrane largely symmetrically. Conversely, mammals with mobile malleus-incus joints, such as cats and humans, have an asymmetric division of the tympanum by the manubrium. It is thought this difference is related to the differing modes of ossicular movement at high frequencies between larger and smaller mammals (Puria and Steele, 2010). The three bone chain of the ossicles is suspended within the middle ear by a series of ligaments, the axial ligaments, shown schematically in Figure 1.2 (yellow).

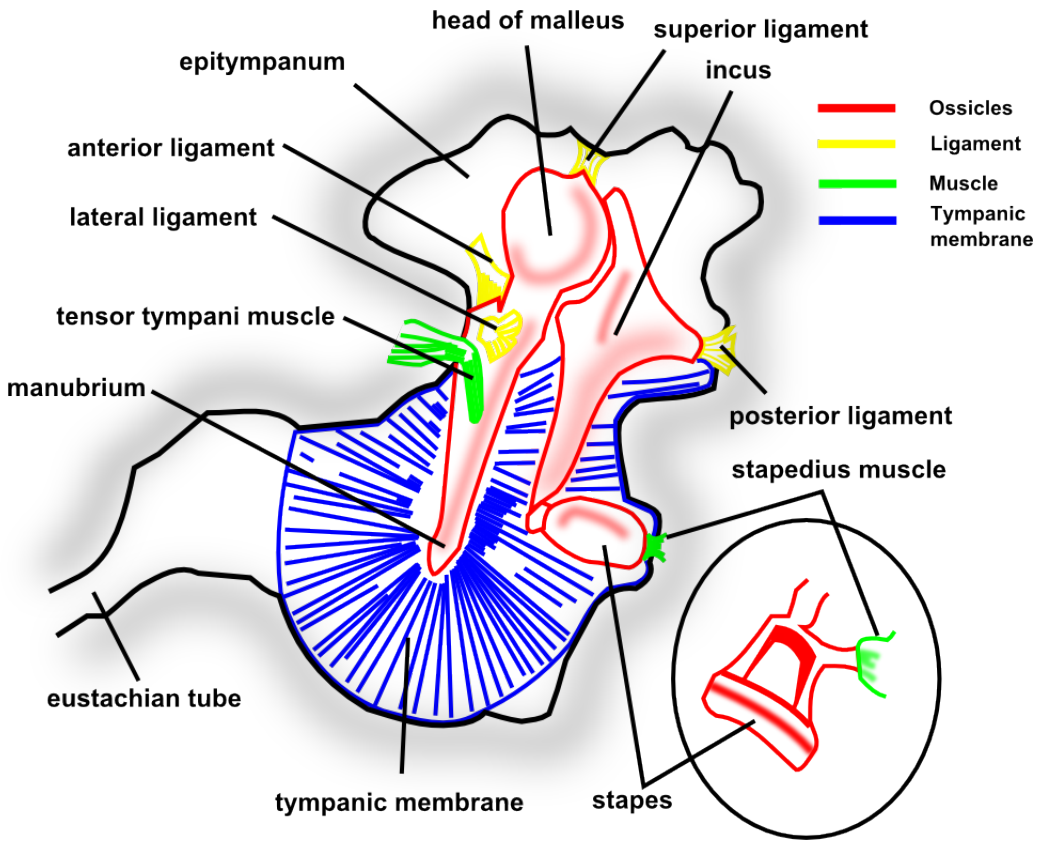

Figure 1.2 Schematic drawing of the human middle ear, indicating the ossicular chain (red), tympanic membrane (blue) and associated muscles (green) and ligaments (yellow), adapted from Moller, 1970.

Figure 1.2 also shows the tensor tympani muscle and the stapedius muscle (green) (Moller, 1970). The tensor tympani and stapedius muscles protect the ear from the potentially damaging effects of high level sound, contracting in response to high intensity sound (above 80 dB), tensing the ossicular chain and resulting in a 10-30 dB attenuation in sound intensity (Yost et al., 2001) delivered to the inner ear. The middle ear muscles may play a significant role in limiting distortion; with larger vibrations of the ossicles causing muscles to increase pressure on the chain, ensuring the ossicular bones do not separate and introduce distortion into the system (Yost et al., 2001). Ossicular movement is frequency and level dependent. At low frequencies this movement acts in a rotary fashion around an axis found in the head of the malleus, which can be likened to the movement of a piston (Békésy, 1960); at higher frequencies, the ossicular motion can become more complex (Decraemer et al., 1989; Decraemer et al., 1991). Recent studies suggest that at these higher frequencies in larger mammals such as humans and cats, the saddle-shaped malleus-incus joint act like a pair of biological gears to compensate for greater ossicular moment of inertia in these species (Puria and Steele, 2010). Ossicular vibrations remain essentially linear under sound intensities of up to 130 dB SPL providing middle ear muscle contractions do not occur (Guinan and Peake,

1967). The ossicles provide some additional amplification approx. 1.3X in humans through leverage (Beskesy, 1960). The vibrations of the ossicles are transmitted to the fluids of the scala vestibuli through contact of the stapes footplate and the oval window (Geisler, 1998; Yost et al., 2001). The morphology of the stapes in mammals varies slightly between species (Hellstrom, 1998), the dimensions of the stapes footplate and oval window are optimised to ensure efficient transfer of vibrational energy into the cochlea. The area of oval window membrane around the stapes has a maximum width of only 0.1mm and a minimum width of 0.015mm in humans: any larger and movement of the stapes would result in fluid movement back around the stapes (Békésy, 1960). The size of the species' cochlea is important in determining the stapes footplate and oval window dimensions; smaller cochleae have fluids with less inertia and so allow for a greater width of membrane surrounding the stapes footplate (Békésy, 1960). The structures of the middle ear have an important functional role in providing an impedance match between the tympanic membrane and the fluids of the cochlea in order to allow efficient transfer of sound energy (Geisler, 1998). The surface area of the tympanic membrane must be of the right size in proportion to the stapes footplate to provide this efficient transfer from air to a fluid medium. Due to the relative impedances of water and air (3880:1), calculations predict that the tympanic membrane should have an area 62x the size of the stapedal footplate. Indeed, this is found to be the approximate ratio in most species (Killion and Dallos, 1979).

1.2.2 Broad mechanics of the cochlea

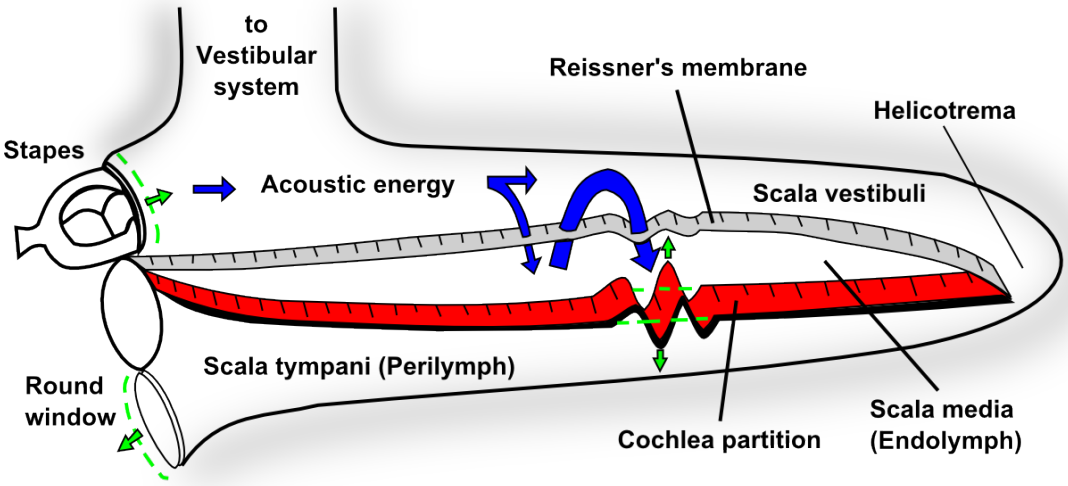

Figure 1.3 Stylised mammalian cochlea, shown rolled out. Indicated are some of the cochlea's broad structures and the progression acoustic energy through the cochlea fluids and structures (adapted from Geisler, 1998).

The cochlea comprises a continuous perilymphatic duct system with two membranous openings into the middle ear, the RW and the oval window (Figure 1.3). The ducts are divided anatomically into, the scala vestibuli and the scala tympani; both are filled with high Na^+ perilymph. Sandwiched between these is a third endolymphatic duct termed the scala media which is separated from the scala vestibule by Reissner's membrane and the scala tymapani by the basilar membrane (BM). The scala media contains the organ of Corti and is filled with high K^+ and low Na^+ endolymph (Sterkers et al., 1988). Figure 1.3 (Geisler, 1998) shows a simplified, uncoiled cochlea represented as having been rolled out length ways from its usual complex coil orientation (Geisler, 1998). In mammals the scalae spiral longitudinally from the base (near the oval window), around a bony central spiral known as the modiolus to the apex of the cochlea. The perilymphatic space forms a hairpin like shape at the tip of which is the helicotrema, which allows the two ducts' fluids to be continuous. Movement of the ossicles displaces the perilymph and increases pressure in the scala vestibuli, this causes a bulging of the BM and increased pressure in the scala tympani. The perilymph contained in the scala tympani is displaced and pushes the round window out; the reverse process occurs when the stapes footplate is pulled out. Reissner's membrane has negligible impedance and for this reason the pressure in the scala media and scala vestibuli are the same during acoustic stimulation (Voss et al., 1996a; Olson, 1998). Early work on human cadavers showed that movement of the ossicules resulted in a travelling wave of displacements on the BM (Békésy, 1960), due to the

relative pressure differences between the scala tympani and scala vestibuli. The movements of the BM are determined by the mass and stiffness of each individual section, which both change gradually along the length of the cochlea. The BM is thinner and stiffer at its base and wider and more flaccid towards the apex (Békésy, 1960). The result of these changing properties is that different sections of the BM will respond maximally to different frequencies of excitation, known as characteristic frequency (CF). This property is described as tonotopic mapping and allows the cochlea to separate sounds into its constituent frequencies. Experiments have also shown that the cochlea can be excited from anywhere along its length, not just by movement of the oval window, and the resultant travelling wave will begin at the base and travel to the apex in the 'normal' forward travelling direction (Békésy, 1960).

1.2.3 Organ of Corti and sensory transduction

The organ of Corti is positioned on the BM within the endolymphatic fluids of the scala media and runs the length of the mammalian cochlea. It consists of numerous cells and materials whose complex structural relationships allow it to decompose sound into its various frequency elements after sound energy entering the cochlea has resulted in BM motion at its CF. This mechanical interaction between the organ of Corti and the BM (the two structures combined are collectively described as the cochlea partition) motion is not present in lower vertebrates such as birds and frogs, who largely rely on electrically tuned hair cells for spatial decomposition of sound (Crawford and Fettiplace, 1981). The evolutionary adaptation of a mechanically based tonotopicity in the mammalian cochlea is believed to have allowed mammals to extend their hearing ranges to far higher frequencies and so given them an evolutionary advantage (Manley, 2000). The cells and structures of the organ of Corti consist of two sets of mechanotransducing hair cells, the tectorial membrane (TM), efferent and afferent nerves, supporting cells and as part of the wider cochlea partition the BM on which the organ itself sits (Figure 1.4).

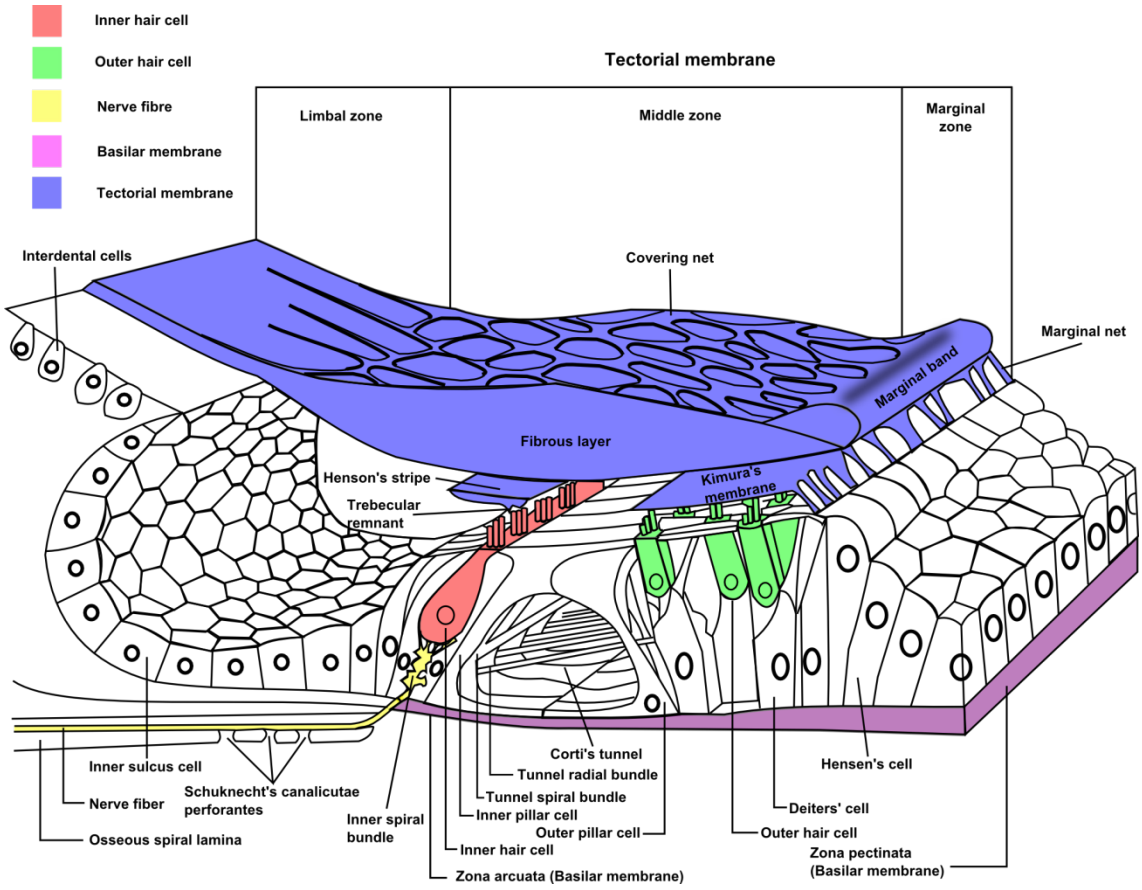

Figure 1.4 Artists conception of the Organ of Corti. Colours highlight structures and cells of particular interest (Lim, 1986).

1.2.3.1 Supporting cells

Despite not directly transducing sound vibrations of the cochlea fluids, the supporting cells of the organ of Corti are vital for the correct functioning of the cochlea partition in auditory sensation, which often results in some unique specialisations and cell morphologies (Figure 1.4). These essential functions include maintaining the unique ionic balance of the endolymph (stria vascularis), ensuring correct motion of the cochlea partition (pillar cells), providing structural rigidity (Henson's cells, Deiter's cells), and a possible role in modulation of electromotility (Deiter's cells) (Bohnke and Arnold, 1998; Yu and Zhao, 2009b).

1.2.3.2 Hair cells

The sensory cells of the peripheral auditory system consist of the IHCs and the OHCs (Geisler, 1998). These highly specialised mechanotransducers are arranged in rows along the length of the cochlea from base to apex, and are located within the complex superstructure of the organ of Corti (Figure 1.4)(Geisler, 1998). A human ear contains approximately 15,000 hair cells, IHCs form a single row on the modiolus side and OHCs form three rows (Figure 1.4), at the base of

the cochlea, located towards the outer edge of the spiral lamina, which can increase to as much as five rows at the apex. IHCs and OHCs have a broadly similar structure, as they are both functionally polarised cells that act as mechanotransducers through cellular specialisations. The most striking specialisation shared by the hair cells ,and indeed the source of their name, is a structure known as the hair bundle which is located at the apical membrane and consists of rigid, actin filament-based stereocilia (Flock and Cheung, 1977; Tilney et al., 1980). The stereocilia are packed full of hundreds of actin filaments that are crosslinked by fimbrin, espin and potentially other proteins. The stereocilia taper at their base towards their insertion into the cellular apex. Although OHCs and IHCs are structurally similar in a broad sense they have numerous aspects of their detailed cellular structure and morphology that are different, these differences reflect their distinct functions within the organ of Corti. Schematic representations of an IHC and an OHC are shown in (Figure 1.5). A gelatinous TM covers the organ of Corti along its entire length and is attached to the limbus and to the tallest row the OHC stereocilia. This arrangement means that displacements of the BM in the transverse plane results in a sliding motion of the TM over the apical part of the organ or Corti (Davis, 1958).

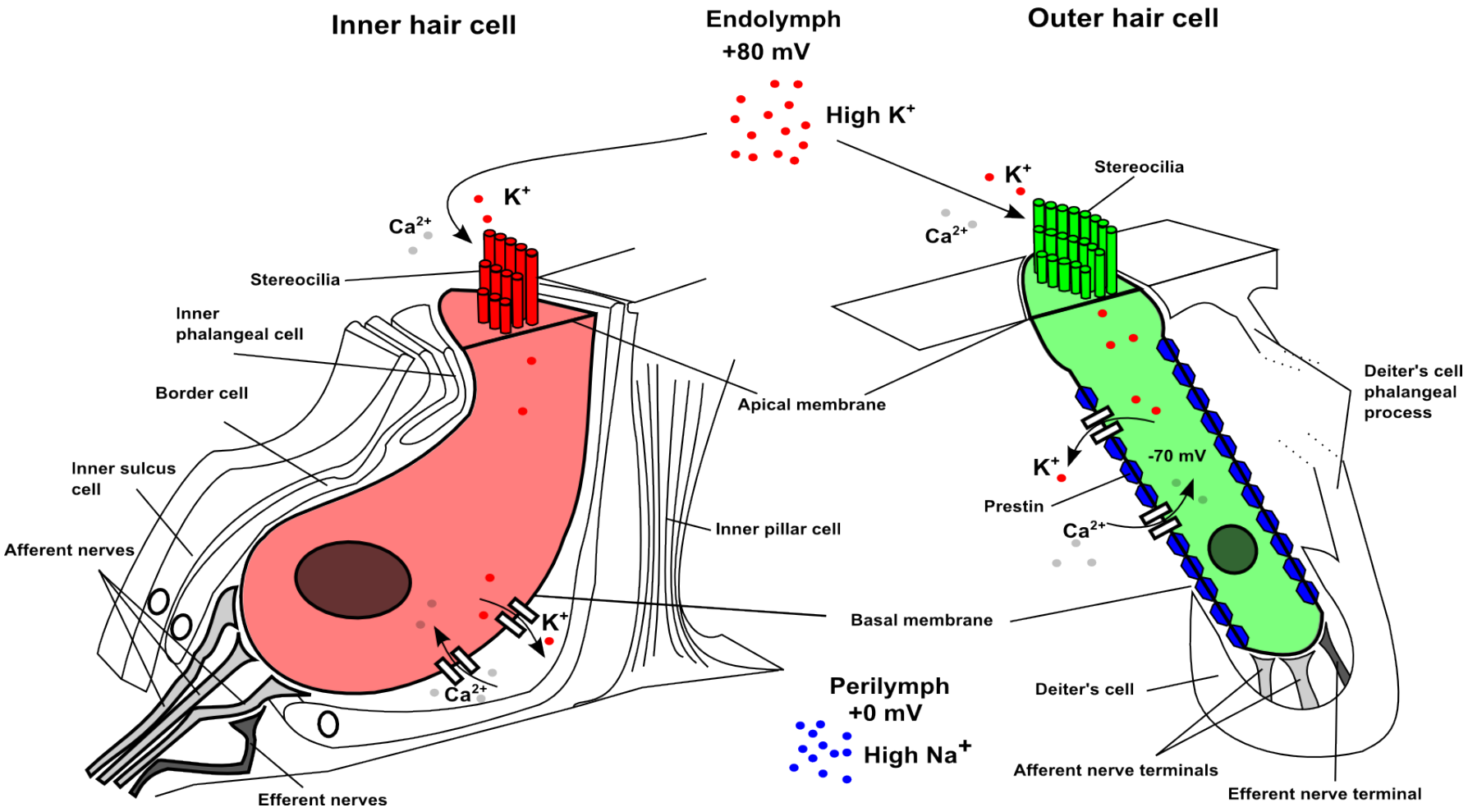

Figure 1.5 Cochlear hair cells. IHCs transduce acoustic vibrations (left). OHCs are mechanically active within of the cochlea partition (right) (adapted from Jones, 2012).

Through electrophysiological recordings and two-photon laser scanning microscopy, (Denk et al., 1995), the hair cells' transduction current has been located to their apical end. Ion channels are believed to be located on stereocilia that protrude into the endolymphatic space (Geisler, 1998). These rigid actin-filled stereocilia form 'W' shaped arrays in OHCs and 'U' shaped arrays in IHCs of increasing height, from the outside of the 'W' or the 'U' to the point, that are linked by extracellular links responsible for maintaining the correct spatial orientation of the hair bundle. One sub-type of the links in the hair bundle are the tip-links (Figure 1.6) (formed of the transmembrane proteins cadherin-23 and protocadherin-15) which are believed to be either closely associated with or directly attached to a mechanotransducing ion channel of unknown identity (Kandel et al., 2000) and are found at the apical end of the hair bundle. When the hair bundle is deflected, as occurs during acoustic stimulation, the hair bundles are displaced as a group in the radial direction and pivot around their base in the cuticular plate (Hudspeth and Jacobs, 1979). Hair bundles are direction sensitive. Displacements in the positive direction (towards the tallest row of stereocilia), increase tension in a gating spring component and raises the open probability of the mechanical electrical transduction (MET) channels. The tip links are likely to be a component of each gating spring but due to their minimal elasticity it is likely that other more compliant elements are involved. These could be located in the MET channel themselves, for example a recent contender for the MET, TRP type sub-units, caused interest because it contained numerous ankyrin repeats that may act compliantly (Corey et al., 2004; Howard and Bechstedt, 2004). Another possibility is that myosin molecules associated with mechanotransduction could act compliantly (Howard and Spudich, 1996). Regardless of the identity of the gating spring the result of increased tension on the tip-links is an increase in the open probability of the ion channels leading extracellular cations to enter the cell and causing depolarisation of the cell body. If pushed in the negative direction (towards the shortest row of stereocilia), the ion channels' open probability is decreased and current flow into the cell reduced, resulting in hyperpolarisation of the cell body (Figure 1.6). The channels therefore mediate the state of excitability of the hair cells and are known as MET channels. The MET channel open probability has a sigmoidal dependence on the hair bundle displacement and resultant receptor current (Kros et al., 1992; Netten and Kros, 2000), demonstrated schematically in the bottom panel of Figure 1.6 as a transducer input-output curve. IHCs and OHCs have differences in the operating characteristics of their input-output curves which reflect their differing functions within the cochlea and, more specifically, the position of the resting operating point (OP), the open probability of the MET channels at rest. The curve demonstrated in (Figure 1.6, lower panels) is more akin to recordings taken from an IHC during hair bundle displacement and reflects its role in transducing auditory signals to the

CNS, its OP is positioned asymmetrically on the input-output curve allowing it to generate DC responses to high frequency tones and signal their response to post synaptic afferent fibres. OHC OP have been found to be positioned on or around the point of inflection of the input-output curve, enabling them to respond with maximum sensitivity and cyclically to displacement of the BM and organ of Corti (Russell et al., 1986). *In vivo* the tallest of the OHC's stereocilia is embedded in the TM meaning that movements of the BM cause deflections of the hair bundle and mechanotransduction to occur (Figure 1.6). The TM is believed to be responsible for setting the OP of OHCs, as it has been found that in mutants lacking a TM (for example Tecta$^{\Delta ENT/\Delta ENT}$) the OHC OP is similar to that found in IHCs (Legan et al., 2000).

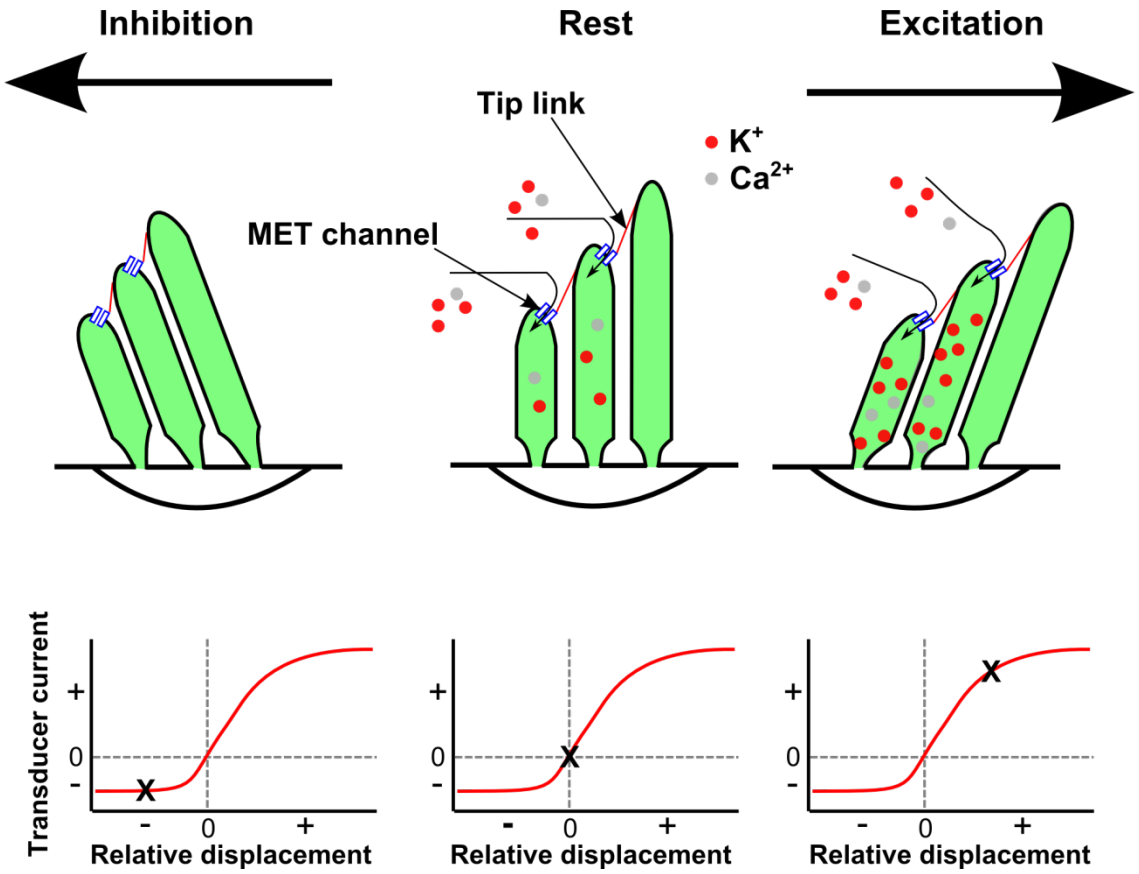

Figure 1.6 Hair bundle stereocilia displacement. Displacement of hair bundle stereocilia in an excitatory direction causes relative movement between stereocilia which opens MET channels. Displacements in the opposite direction closes channels and results in inhibition (adapted from Jones, 2012).

The stereocilia of the IHCs project into the endolymph containing space between the TM and the BM, the sub-tectorial space. The IHC hair bundle does not contact any other structure apically; rather it is believed that fluid movements created by the vibrations of the BM result in the IHC hair bundle displacements (Hudspeth and Jacobs, 1979).

In both IHCs and OHCs, once MET channels are open K^+ and Ca^{2+} flow rapidly down their electrochemical gradients in to the hair cells. This high gradient across the hair cell membrane is created by high concentrations of K^+ in the endolymph, known as the endocochlear potential (+80 mV) and the resting intracellular potentials of IHCs and OHCs, which have been ascertained *in vivo* to be -45mV and -70 mV respectively (Russell and Sellick, 1978; Russell and Sellick, 1983). The transduction of the signal is rapid and the cells so sensitive they can detect 1-2 nanometre displacements of the stereocilia, accounting for a large part of the sensitivity of the mammalian cochlea. The endocochlear potential is maintained through a structure called the stria vascularis and a system of K^+ recycling that regulates the unique ionic composition of the endolymph in the scala media. The importance of this system is highlighted by application of furosemide to the cochlea. This loop-inhibiting diuretic causes a reduction in the endocochlear potential and the hair cell potentials; its effects are to linearize the response of the cochlea and substantially decrease the sensitivity and frequency selectivity of the BM (Robles and Ruggero, 2001).

The OHCs have a more rigid structure than that of the IHCs, their endoplasmic membranes form multiple ordered layers called cisternae lying parallel to the lateral cytoplasmic surface of the plasma membrane (Gulley and Reese, 1977; Saito, 1983). Approximately 25 nm beneath the plasma membrane, and the outer surface of lateral cisternae lies, an unusual protein cytoskeleton known as the cortical lattice (Holley and Ashmore, 1990). Which has multiple links to integral membrane proteins present in the plasma membrane, specifically the membrane protein prestin is found in high densities throughout the plasma membrane of OHCs (Huang and Santos-Sacchi, 1994; Zheng et al., 2000). The properties of prestin, combined with the structural organisation previously described, gives the OHC its motile ability (Zheng et al., 2000). The longest of the OHC stereocilia are embedded in the TM (Kimura, 1966; Lim, 1972). OHCs are heavily innervated by efferent fibres from the superior olivary complex (both ipsilateral and contra-lateral) and are only sparsely innervated by thin non-myelinated afferent fibres (Spoendlin, 1969; Geisler, 1996). The role of OHCs is concerned with the mechanics of the BM, the movements of which are modelled in (Figure 1.7) (Geisler, 1998). Current understanding follows that OHCs are responsible for amplification in the mammalian cochlea, although there is still debate around this subject, feeding energy into BM motion on a cycle-by-cycle basis. The IHCs in contrast are innervated by 90-95 % of afferent fibres which are thickly myelinated (Spoendlin, 1969), through highly specialised ribbon synapses. Current understanding gives their function as transducing the mechanical movement of the BM into electrical signals that represent the frequency of that portion of the BM and are perceived as

sound by the CNS. The afferent fibres that innervate the IHCs have been shown to reflect this same frequency specificity (Tasaki and Spyropoulos, 1959).

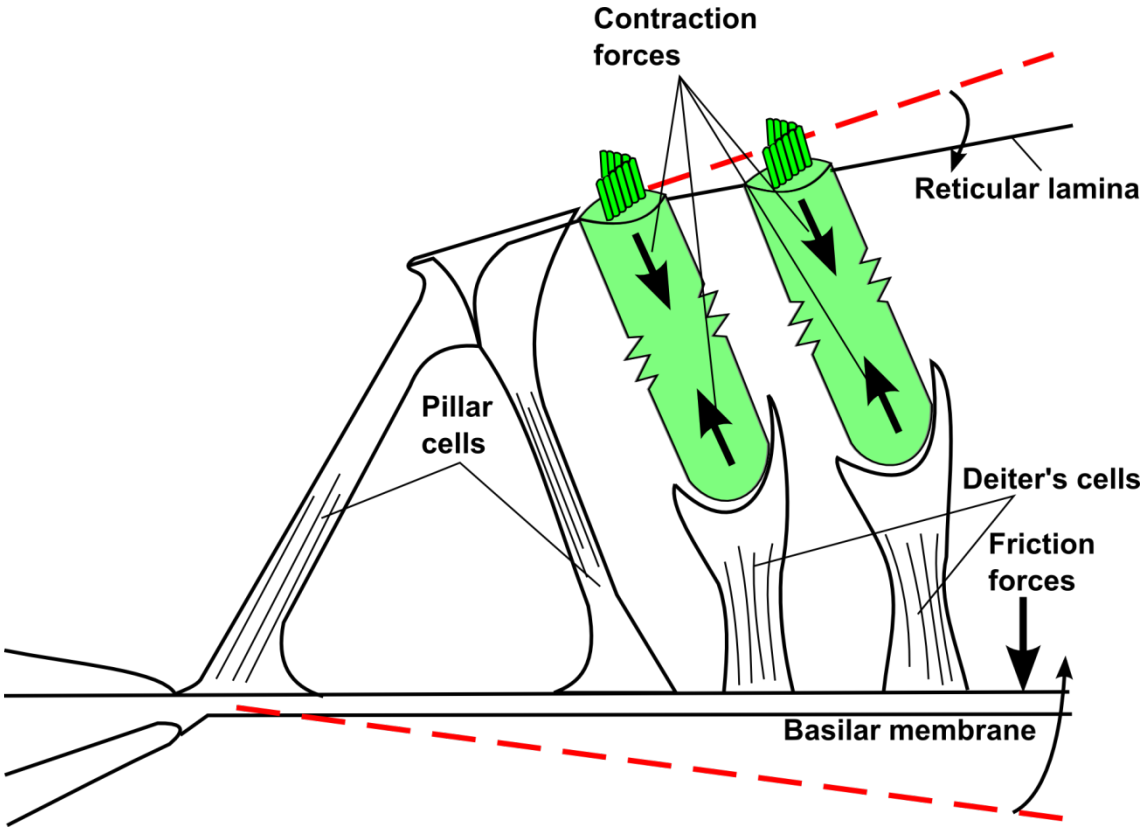

Figure 1.7 Schematic cross section of organ of Corti showing hypothesized effects of outer hair cell contraction and resultant BM and reticular lamina movements. Movement of the basilar membrane is opposed by friction forces in the opposite direction (Geisler, 1998).

1.2.3.3 Basilar membrane

Two extra-cellular matrices are present in the cochlear partition, the BM and the TM. The correct mechanical functioning of both membranes is vital for auditory transduction and the regular propagation of energy along the cochlea. Historically, a number of factors have meant that the BM has received more attention in auditory research than has the TM: the BM is less susceptible to the ionic changes experienced post mortem (pm), it is easier to view *in vitro,* and most importantly, *in vivo* through the RW membrane in the high frequency region of the cochlea.

Despite the BM being the subject of numerous mechanical studies, relatively little is known about its composition when compared to the TM (Amma et al., 2003). The BM is a composite acellular plate containing a thin sheet of fibres and unstructured matrix. It is known to be composed structurally of major filaments 10-12 nm in diameter, imbedded in a matrix of

ground substance (Cabezudo, 1978; Katori et al., 1993). The major BM filaments appear to be largely composed of collagen type II (Thalmann, 1993; Tsuprun and Santi, 2001). These filaments are associated with keratan- and chondroitin-sulfate proteoglycans (Munyer and Schulte, 1991) and the glycoproteins fibronectin and tenascin have been detected in the BM ground substance (Woolf et al., 1992; Swartz and Santi, 1999). The fibres are orientated in the radial direction from the modiolus to the outside wall of the cochlea and account for the BMs radial stiffness. In recent years the exploitation of deaf mouse models has led to new discoveries concerning the BMs composition, identifying the glycoprotein emilin-2 (part of a family of elastic fibres previously identified in heart tissue) to be a major component of the BM (Amma et al., 2003).

Anatomically the BM can be divided radially into two zones, the pars tecta (arcuate zone) and pars pectinata (pectinate zone). The pars tecta extends from the tympanic lip of the spiral limbus to the region under the outer pillar cells and the pars pectinata extends from the region under the outer pillar cells to the basilar crest of the spiral ligament (Figure 1.4). The radially running fibres of the BM are continuous with the fibres of the spiral limbus and spiral ligament and therefore the BM forms a single morphological and functional unit with these structures.

The mechanical properties of the BM have been studied relatively extensively compared to the TM. Its resonant properties vary along its length as a result of changes in stiffness, mass, width, damping and the dimensions of the scalae. The stiffness of the BM varies along its length causing higher frequencies of sound to resonate near the base and lower frequencies to resonate near the apex of the cochlea (Békésy, 1970). Where a particular frequency resonates along the BM is known as the CF or best frequency (BF) (when the cochlea is in a healthy active state). The exact gradation of stiffness along the BM has been difficult to ascertain due to species differences, recording methods, recording positions and difficulties of separating the BM's stiffness contribution from the overall cochlea partition to which it is mechanically linked (Richter et al., 2007). However it is largely recognised that the BM stiffness changes by approximately two orders of magnitude from base to apex (Zwislocki and Cefaratti, 1989) and that these changes are able to account for the changes in CF along its length. The change in mechanical properties along the cochlea and subsequent dependence of frequency on longitudinal position enables linking of specific spatial locations to specific regions of sensory cells. This property is known as tonotopicity and allows the cochlea to act as a frequency analyser, separating incoming sound vibrations into their constituent frequencies (Békésy, 1960).

As described in chapter 1.2.2, movements of the stapes caused by sound result in pressure differences across the BM, which in turn cause a travelling wave to propagate along its length to the CF, of the frequency of stimulation (Békésy, 1960). However longitudinal elastic coupling of individual sections of the BM along the cochlea is very poor. The travelling wave propagates through localised fluid mass coupling caused by the displacement of individual segments of the BM. Once a travelling wave has been stimulated at the base, the resultant pressure difference across the BM that propagates to the point of the CF is very localised to within 5 µm of its surface (Olson, 1998). In regions of the cochlea basal to the point of the CF, the travelling wave initially encounters a section of BM which is stiffness dominated, resulting in small displacements and little difference in phase between ossicular motion and BM motion, which allows the system to conserve energy. As the wave propagates down the length of the cochlea its amplitude and phase difference increase and its velocity decreases, it begins to dissipate more energy. Approaching the CF the mass of the system begins to play an increasing role, until after CF it is dominant and energy is rapidly dissipated as the wave is damped (Gummer et al., 1996). In a passive system, such as pm or in a compromised cochlea, the sharpness of a particular CF point compared to a live healthy cochlea is much reduced, an active process that can overcome the effects of viscous dampening is required to increase the amplitude and sharpness at CF.

1.2.3.4 Tectorial membrane

The TM is an extracellular matrix that runs the entire length of the cochlea partition overlying the organ of Corti. In a healthy cochlea it is attached along its length to the spiral limbus and via Kimura's membrane on its underside to the tallest row of stereocilia of the OHCs (Kimura, 1966; Zwislocki, 1986; Goodyear et al., 2005). Therefore, the TM is able to contribute mechanically to the movements of the cochlea partition and directly to the excitation of the OHCs. However, its position within the central chamber of the scala media, sensitivity to environmental conditions and transparency have often made it difficult to investigate and its movements remain to be observed *in vivo*. For many years the TM was viewed as a rigid surface against which the OHCs could react during stimulation. In recent years investigations have begun to tease apart the functional contribution of the TM to effective sensory transduction, particularly by studying mouse deafness mutations (Lukashkin et al., 2010) and have found that its contribution is far more complex than previously assumed.

The TM is an acellular polyelectrolyte gel that is composed of 97% water; its remaining 3% consisting of diffusible ions and non-diffusible macromolecules, which makes up its dry weight (Tanaka, 1981). This dry weight consists of a mixture of collagen fibres, non-collagenous

glycoproteins and proteoglycans (Freeman et al., 2003a). The collagen fibres make up about 50% of the dry weight of the TM (Thalmann et al., 1986). Collagens type II, V, IX and XI have all been identified in the TM with collagen type II being by far the most numerous (Richardson et al., 1987). Collagen type II is orientated radially along the length of the TM and is responsible for its radial stiffness (Lim 1972, Kronester-Frei 1978) whilst the remaining collagens are believed to regulate the positioning of the type II fibres. Approximately 25% of the TMs dry weight consists of the glycoproteins α-tectorin, β-tectorin and otogelin which are exclusive to the inner ear (Richardson et al., 1987; Cohen-Salmon et al., 1997). These glycoproteins are involved in organising the striated sheet matrix (SSM) of the TM and have undergone intensive research in recent years due to the identification of mutations in the genes that encode α-tectorin and β-tectorin being linked to certain forms of human deafness (Verhoeven et al., 1998). The proteoglycans are glycosylated proteins which contain a core protein and a covalently bonded glycosaminoglycans (GAGS) (Kjellen and Lindahl, 1991). The two GAGS found in the TM are chondroitin sulphate and keratan sulphate which are negatively charged by polysaccharide groups and are able to bind cations (Richardson et al., 1987; Munyer and Schulte, 1991; Thalmann et al., 1993). It is this binding property that allows them to affect TM mechanics.

The TM is divided into a number of zones along its length, consisting of the limbal zone, middle zone and marginal zone (see Figure 1.4). The dimensions of the three zones vary along the length of the organ of Corti; the limbal zone, which attaches on its inside edge to the spiral limbus is widest (radially) at ~45 µm in the base (Gueta et al., 2007) and thinnest transversely at 10 µm (Gueta et al., 2007). The middle zone is ~30 µm wide in the base and has a thickness that increases from ~21.6 µm thick at the base to ~36.4 µm thick in the apex (Russell et al., 2007), it overlies the IHCs and on its underside, opposite the hair bundles of the IHCs is a localised bump known as Henson's stripe which is also present along the length of the TM. The marginal zone overlies the reticular lamina and OHCs, the tallest row of OHCs is imbedded in Kimura's membrane on the underside of this zone (Kimura, 1966). The marginal zone is ~13 µm wide (Gueta et al., 2007) and decreases in thickness from the edge that borders the middle zone at ~20 µm to its marginal edge at ~10 µm. A cover net of tightly packed collagen fibrils sits on top of the TM (Kronester-Frei, 1978).

Past studies assessing the mechanics of the TM has been complicated by factors such as its sensitivity to environmental conditions, dynamic properties and the difficulty of separating its mechanical contribution from the rest of the cochlea partition. Its polyelectrolyte nature means it is extremely sensitive to environmental conditions such as ionic balance and pH

(Freeman et al., 2003b). The TM swells when the pH is increased ≥9 or decreased ≤6 (Weiss and Freeman, 1997), when the concentration of Na^+ in its environment is increased or when osmotic pressure of its surrounding environment is decreased (Shah et al., 1995). Increasing osmotic pressure leads to an increase in Ca^{2+} in the TM's environment which results in shrinking (Shah et al., 1995). Early studies viewed the TM as a rigid structure against which the OHCs could react (Davis, 1965) and it was not until the TM was studied under physiologically relevant conditions that its mechanical properties were viewed as more complex, although Beskesy did note that the TM had both elastic and viscous properties (Békésy, 1953). As with structural changes in the BM along its length, the radial and longitudinal changes in the structure of the TM result in changes in its mechanical properties. The transverse and radial stiffness both reduce from base to apex (-4.0 $dBmm^{-1}$ and 4.9 $dBmm^{-1}$, respectively) (Richter et al., 2007). This change in longitudinal stiffness is mainly confined to the marginal zone as opposed to the limbal and middle zones whose stiffness properties do not change along the cochlea's length (Gueta et al., 2006). Radially the stiffness of the TM varies with the limbal zone being the most stiff and middle zone most floppy.

1.2.3.5 Gradients in the cochlea

The tonotopicity present in the mammalian cochlea is instrumental to its ability to decompose sounds spatially into its constituent frequencies. Whereas in lower vertebrates such as turtles, birds, frogs and lizards this characteristic is largely underpinned by the electrical tuning of hair cells and at higher frequencies a combination of electrical and micromechanical tuning, in mammals tonotopicity relies on mechanical tuning. This mechanical tuning is largely based on structural and mechanical gradients present along the length of the cochlea, that run longitudinally in both directions.

The organ of Corti's stiffness increases from the apex to the base, as does the stiffness of the TM, the BM the OHC hair bundle and the IHC hair bundle. The radial stiffness of the TM decreases from the base to the apex (Gueta et al., 2006; Richter et al., 2007).The changing stiffness of the TM and BM enable the two acellular membranes to act in synergy as two resonating systems and allow effective timings of organ of Corti motion and cellular transduction. As the stiffness of the hair bundles in both hair cell types increase from apex to base the length of these bundles becomes shorter but the number of stereocilia in each hair bundle increases (Lim, 1986; Davis, 2003). The result of these gradients, in height of hair bundles and number of stereocilia, is that hair bundles are more sensitive to organ of Corti displacement in the base than in the apex. This increased sensitivity is due to shorter bundles undergoing larger angular rotation in the base for equivalent BM motion to the apex and

larger numbers of stereocilia resulting in an increased number of channels (He et al., 2004). The magnitude of the mechanotransduction currents become larger whilst their adaptation time becomes shorter from the apex to the base. The larger currents are a consequence of more stereocila resulting in more MET channels and larger single channel conductance in the basal hair cells (Ricci et al., 2003; He et al., 2004). The OHCs become increasingly shorter from the apex to the base, which results in a reduction in membrane capacitance in the same direction (Davis, 2003). There are also inter-species differences between mammalian species in the number of rows of OHCs the cochlea contains, for example the human cochlea shows an increase in the number of rows of OHCs from base to apex, from 3 to 5 rows respectively.

1.3 Active mechanisms in the mammalian cochlea

The passive tuning of the BM found by von Békésy (Békésy, 1960) contrasts with studies on nerve fibre activity that show complex signals to be sharply separated into spectral components at the auditory periphery (Tasaki and Spyropoulos, 1959). How this sharp tuning is achieved was the subject of numerous hypothesises. The discovery of evoked (Kemp, 1978; Kemp and Chum, 1980) and spontaneous (Zurek, 1981) otoacoustic emissions supported the idea that an active process pumping energy into the vibrations of the cochlear partition was present, the term 'cochlea amplifier' would later be coined to describe it (Davis, 1983). This process could account for the frequency selectivity of the auditory nerve fibres (Tasaki and Spyropoulos, 1959), amplification of BM responses at low sound pressure levels (SPL) and compressive non-linearity at high sound pressure levels (Rhode, 1971; Rhode, 1978; Sellick et al., 1982; Robles et al., 1986; Ruggero and Rich, 1991; Cooper and Rhode, 1992; Nuttall and Dolan, 1996). Further evidence for the role of the 'cochlear amplifier' is provided by experiments in which the cochlea is compromised (Figure 1.8) (Cody and Johnstone, 1980), once compromised the mechanics of the BM become progressively more like those of Békésy, 1960 passive cochlea. The existence of a 'cochlear amplifier' is widely accepted in hearing physiology but its exact nature is still an issue of debate.

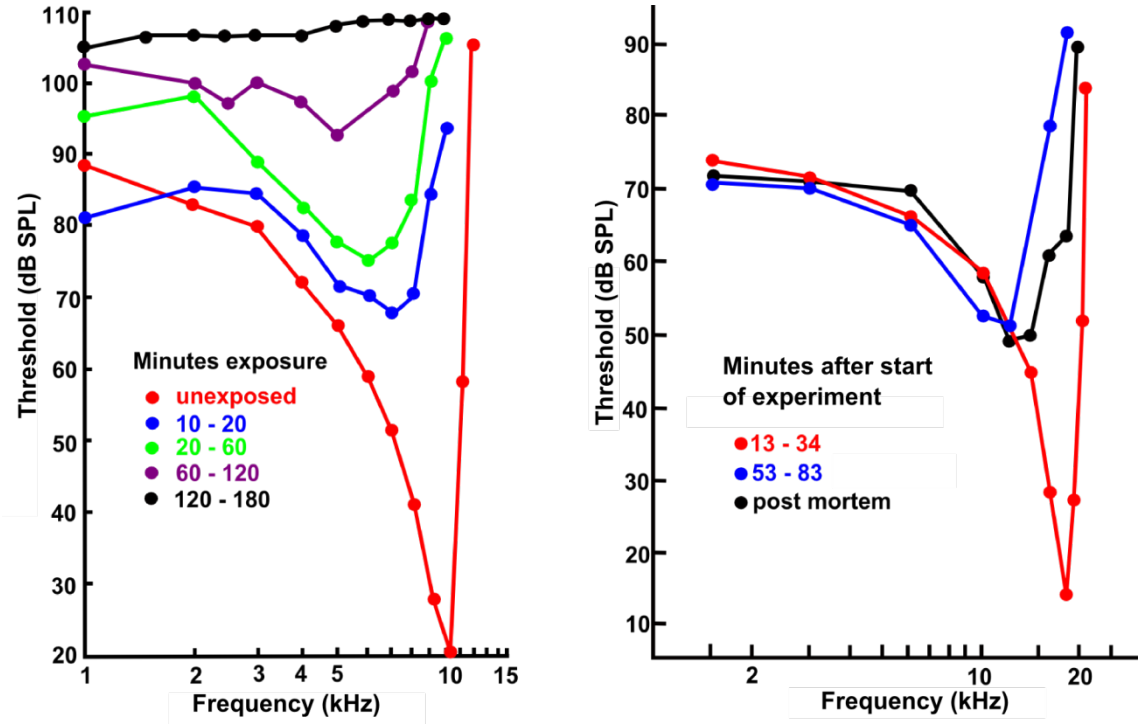

Figure 1.8 Vulnerability of the cochlear amplifier to experimental manipulations. Changes in neural threshold tuning curve before and at numerous stages (inset) during exposure to pure tone over stimulation (black) in a guinea pig (10kHz at 110 dB SPL) (left) (Cody and Johnstone, 1980). Changes in the mechanical frequency tuning curve observed before (red) and after (blue) deterioration of the experimental preparation and PM (black) (right) (Sellick et al., 1982).

1.3.1.1 Cochlea amplifier

Despite early theoretical calculations and predictions made by Gold (Gold, 1948) of the requirement of an amplification mechanism in the cochlea to overcome viscous dampening of fluids and account for its sharp frequency tuning, it was not until the 1970's that serious work began on investigating the basis of this mechanism (Dallos et al., 2008). Investigations using chemical ablation and high intensity noise to induce cochlear lesions that targeted OHCs led to 50 dB increases in hearing thresholds at the affected frequencies. This indicated that the amplification process was localised to the OHCs of the organ of Corti (Kiang et al., 1967; Ryan and Dallos, 1975; Dallos and Harris, 1978; Harrison and Evans, 1979). The mechanism by which the OHCs provide this amplification has been a continual source of debate and investigation for the past 30 years (Dallos et al., 2006).

Two discoveries, both in 1985, have given rise to two proposed mechanisms for amplification in the mammalian cochlea. The first discovery was that OHCs, when electrically stimulated undergo length changes, a process termed electromotility (Brownell et al., 1985) and the second is that ciliated hair bundles (in turtles hair cells) are capable of actively reacting to incoming stimuli and display spontaneous motility (Crawford and Fettiplace, 1985).

Electromotility of OHCs has been shown to be underpinned by the motor molecule prestin (SLC26A5), a member of the SLC26A family of membrane anion transporters (Mount and Romero, 2004). Prestin undergoes voltage dependent shape changes upon stimulation and due to its position and abundance in the membrane of OHCs causes changes in the overall length of the cells. Depolarisation of OHCs shortens the cell and results in an increased diameter. Hyperpolarisation results in lengthening of the cell and narrowing. The length changes can be as great as 4% and can occur at frequencies of 25-80kHz (Gale and Ashmore, 1997; Frank et al., 1999). This ability to respond at high stimulus frequencies has made prestin an extremely attractive candidate for amplification in the mammalian cochlea where, depending on the species, frequencies can range to as high as 120 kHz (Manley, 2010). Transmembrane electrical fields stimulate the changes in hair cell length and these changes are marked by nonlinear membrane capacitance which reflects the prestin molecules structural rearrangement. This process is similar to the movement of gating charge in voltage-sensitive ion channels (Iwasa, 1993; Gale and Ashmore, 1994; Kakehata and Santos-Sacchi, 1995). Investigations have also observed a change in the somatic stiffness of OHCs, indicating that OHCs have an impact on the mechanical properties of the BM (He et al., 2004).

Recent advances in genetics have provided an opportunity to target the genes that encode prestin with the aim of discovering its role in amplification. Work by Liberman et al, 2002 on a mutant prestin knock-out (KO) mouse that left the OHC hair bundles intact in these animals showed a complete lack of amplification in the mutants. However the results of this study needs to be treated with caution as the removal of prestin from OHCs, a major structural protein, caused reductions in the length and stiffness of the hair cells that would make it unlikely that any amplification process, if present, could exert an effect (Hudspeth, 2008). The Prestin-null mice also showed fast rates of age-related deafness and calculations pertaining to the contribution of each prestin motor molecule, on closer inspection, are overly simplified (Patuzzi et al., 1989b; Cheatham et al., 2005). These factors combined mean that no definitive conclusions could be made from this study. A study in which the structural properties of prestin are preserved but its electromotility abolished through substituting 2 residues with the effect of eliminating the molecule's electromotile properties but conserving its structural properties, provided a stronger case for the predominance of the molecule in the amplification process. Results showed that normal sensitivity and frequency selectivity were reduced in these knock-in mice (Dallos et al., 2008). Another study investigating the α-tectorin mouse, in which the TM is detached from the hair bundle, stimulated the cochlea electrically and found normal acoustic emissions were evoked. This study, in trying to separate hair bundle motility

from somatic motility demonstrated that hair bundle motility could not account for the active process (Mellado Lagarde, 2008).

The most significant criticism levelled at prestin based motility is due to the properties of OHC membranes, which act as an electrical low pass filter with a cut-off of <1kHz, which at high frequencies would attenuate the signal (Dallos, 2010). Numerous possible mechanisms have been proposed to overcome this problem; these mechanisms include extracellular voltage changes (Dallos and Evans, 1995), exceptionally speedy voltage-gated ion channels (Ospeck et al., 2003), piezoelectrical properties of hair cells conferring unique properties to OHCs (Weitzel et al., 2003) and local chloride ion interactions occurring within the plasmalemma (Rybalchenko and Santos-Sacchi, 2003). As yet no conclusive proof has been obtained to confirm any one of them. Interestingly, recent experiments concerning the OHC membrane time constant, in which physiologically relevant levels of calcium in the endolymph were used, have predicted it to track the characteristic frequency of the OHCs up to 8 kHz (Johnson et al., 2011). Another criticism of prestin based somatic motility model is that the process is not tuned (Ashmore et al., 2010), postulations have been made of the possible presence of a graded system of filters and the TM resonance has been cited as the possible basis of this (Gummer et al., 1996), but the tuning could also be based on ciliated hair bundle tuning (Ricci et al., 2003). Equally compressive non-linearity has not been sufficiently demonstrated by isolated OHCs and somatic motility (Hudspeth, 2008).

Experiments on turtle hair cells have demonstrated that these cells are capable of producing active movements in response to stimulation enabling their hearing systems to amplify incoming sound (Crawford and Fettiplace, 1985). The process appears to be based upon the fast component of hair bundle adaptation. Adaptation is an important characteristic shared by hair cells, a process whereby hair cells reset their range of sensitivity in response stimulation (Eatock et al., 1987; Gillespie and Corey, 1997). Without adaptation the enormously sensitive hair bundle stimulation would result in rapid saturation with displacements of only a few tens of nanometers. The MET channels of the hair bundle stereocilia have the most complex adaptation system of any mechanosensory receptor which is required to maintain sensitivity across vast frequency ranges.

Evidence suggests there are two mechanisms underlying adaptation in hair cells; a slow adaptation process linked to an ATP driven myosin motor and a fast process linked to calcium interaction with the MET channel. The slow component of hair cell adaptation has been linked to the myosin motors due to the stereocilia being packed with actin filaments (Myosin being

the only known molecular motors to interact with actin) and the presence of many isoforms of myosin in the hair bundles. Myosin-1c is the most likely candidate motor for slow adaptation, as it is localised to where adaptation is thought to occur near the insertional plaque at the upper end of each tip-link (García-Añoveros and Corey, 1997; Gillespie and Corey, 1997). Compelling evidence has also come from transgenic expression of the myosin-1c protein altered by site-directed mutagenesis (Holt et al., 2002; Stauffer et al., 2005). However it is likely that other myosins such as myosin-VIIa (Kros et al., 2001) may be associated with adaptation and indeed other proteins appear to be associated with the slow adaptation process. Fast adaptation involves Ca^{2+} dependent reclosure of transduction channels, which not only involves the reclosure of the MET channels but is associated with a force opposed to the stimulating force (Benser et al., 1996). Although ion replacement studies have established Ca^{2+} as being responsible for initiating MET channel closure the molecular basis of this process is unknown. Proposals for calcium's interaction with the MET complex include; direct interaction of Ca^{2+} with the channel or associated proteins (Corey and Hudspeth, 1983; Crawford et al., 1991), Ca^{2+} binding leading to a relaxation in some elastic element of the channel or channel complex channel reclosure (Martin et al., 2003), or interaction of Ca^{2+} with myosin-1c motor leading to relaxation of the motor and subsequent channel reclosure (Martin et al., 2003; Stauffer et al., 2005).

It is likely that on a cycle-by-cycle basis it is the fast component of hair cell adaptation that underlies amplification in lower vertebrates, as this interaction may act either directly to decrease channel opening probability or act via relaxing some element of the transduction apparatus and thus reduce channel opening probability. Experiments since those originally performed by Crawford and Fettiplace have demonstrated that ciliated bundles are capable of producing active movements at the forces and frequencies required for hearing in various animals including mammals (Assad and Corey, 1992; Benser et al., 1996). Modelling also predicts that OHC hair bundle could have the required force to influence BM motion (Hudspeth, 2008). However these investigations have failed to show comprehensively that hair bundle based amplification occurs *in vivo*.

The ambiguity of the results supporting the two distinct amplification mechanisms in the mammalian cochlea have led to the hypothesis that they may work in synergy, perhaps with amplification being dominated by OHC electromotility and fine tuning being the responsibility of ciliated bundle motility (Kim, 1986; Russell et al., 1986; Chan and Hudspeth, 2005a). The relative roles, if any, of the two mechanisms remains to be resolved (Hudspeth, 2008).

1.3.1.2 Tectorial membrane

The TM plays two vital roles associated with active processes in the cochlea: Through its interaction with the stereocilia of the OHCs, the TM is vital to their effective stimulation during organ of Corti displacements, of particular importance is relative timings of the movements of these two structures in allowing the OHCs to bring about amplification, regardless of the mechanism on which this process is based. The TM is important to the effective excitation of the IHCs, the IHCs stereocilia are not embedded in the TM and are known to be stimulated by fluid in the subtectorial space due to relative motions of the TM and RL (Legan et al., 2000). Therefore the TM affects the output gain of the cochlea.

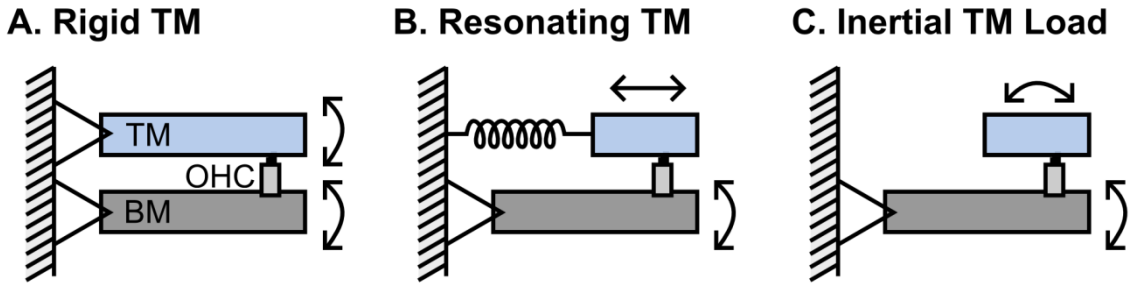

Figure 1.9 Models of radial mechanics of TM and BM. A. Infinite radial and bending stiffness, pivoting around the spiral limbus. B. Mass and stiffness leading to a resonant model. C. Mass dominated model with little or no radial stiffness. (Adapted from Abnet, 1998 and Jones, 2012).

The view of the TMs contribution to cochlear mechanics and effective OHC excitation has changed drastically over the past 20 years (Lukashkin et al., 2010). The TM was originally modelled radially as a rigid plate which pivoted around the spiral limbus allowing radial shear between TM and reticular lamina (RL) (Figure 1.9, A) (Davis, 1958; Davis, 1965; Johnstone and Johnstone, 1966; Rhode and Geisler, 1967; Billone and Raynor, 1973; Neely and Kim, 1983; Steel, 1983). This view of the TM was largely predicated on experiments investigating TM stiffness which used non-physiologically relevant ionic environments. The TM has also been modelled as a simple mass load with negligible radial stiffness (Figure 1.9, C)(Zwislocki et al., 1988; Mammano and Nobili, 1993) and as a model with both mass and stiffness which can include any radial resonant properties of the TM (Figure 1.9, B)(Zwislocki and Kletsky, 1979; Allen, 1980; Gummer et al., 1996).

There are indications of the TM acting as a second resonator in the cochlea (Allen and Fahey, 1993; Gummer et al., 1996; Hemmert et al., 2000). A number of measures both direct and indirect have observed the presence of either a resonance, or what is believed to reflect the presence of a resonance, approximately half an octave below the CF at each cochlea position (Lukashkin et al., 2010). Studies have pointed out that in such a system, timings between TM and BM motion would be very important to bring about effective amplification (Gummer et al.,

1996). Gummer et al., 1996, modelled the effect on feedback in two hypothetical systems, one where the TM acted compliantly or as an inertial mass, as the two different modes effect the timings of hair cell excitation and subsequent timings of forces fed into the cochlear partition by the active amplification mechanism. It was observed that inertial motion, provided the introduction of a 90° phase lag between hair bundle displacement and intracellular receptor potential, would result in effective amplification (Figure 1.10). Although OHC motility due to extracellular potentials would not be accounted for within this model. In a compliant TM system it was predicted that the timings of the structures motion would oppose amplification.

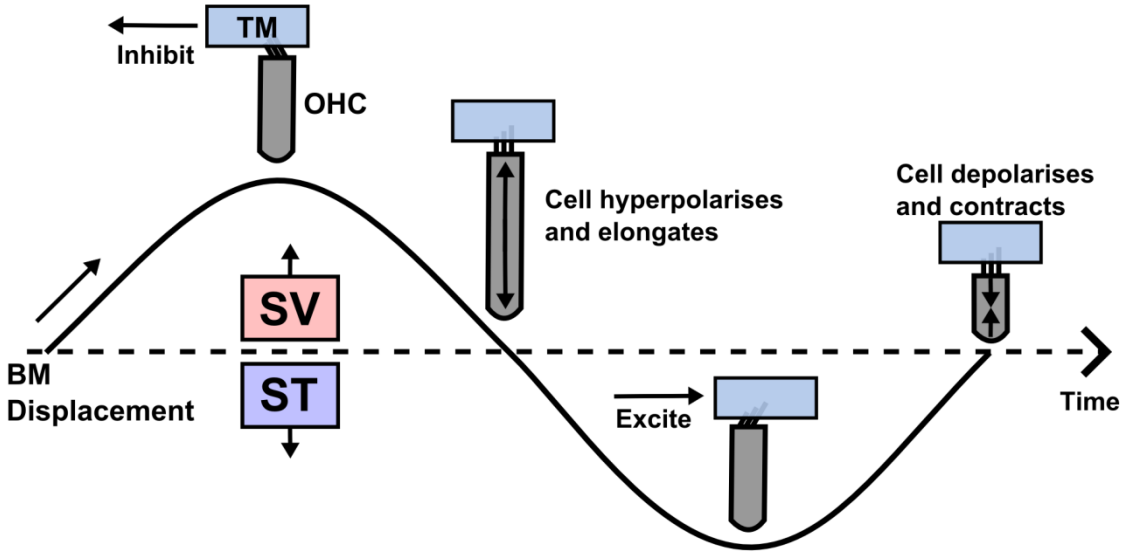

Figure 1.10 Model of electromechanical force interaction of an OHC for inertial motion of the TM. Inertial motion combined with a 90° phase lag of the depolarising receptor potential to stereo ciliary displacement. The consequence of inertial motion of the TM and the phase lag of the driving voltage results in optimum amplification timing (adapted from Gummer et al., 1996 and Jones, 2012).

It is important to note that the majority of models of the tectorial membrane consider it to consist of individual radial elements and that traditionally longitudinal coupling has been considered negligible. Experimental evidence in recent years reveals that this is unlikely to be the case (Ghaffari et al., 2007; Jones, 2012; Jones et al., 2013) and that the TM can support a travelling wave with important implications for shaping cochlea tuning. Indeed TM mouse mutants with changes in sharpness of cochlear tuning have been investigated and these have been hypothesised to result from changes in longitudinal coupling along the TM (Russell et al., 2007).

The hydrodynamical properties of the subtectorial space are vital for effective excitation of the IHCs whose stereocilia are not attached to the TM. The poor accessibility of the subtectorial

space has hampered efforts to understand its hydrodynamical properties with indirect measures such as recordings of IHC potentials being used until recently. Classically the main mode of excitation of the IHCs has been thought of as through flow of fluid as the result of shearing motion between the TM and RL (Billone and Raynor, 1973; Freeman and Weiss, 1990). At low frequencies and low levels of stimulation, the IHCs respond to the velocity of the cochlear partition (Dallos et al., 1972; Sellick and Russell, 1980), and at high frequencies the IHC respond to both velocity and displacement of the cochlear partition (Sellick and Russell, 1980; Russell and Sellick, 1983; Patuzzi and Yates, 1987) *In vitro* recordings have confirmed through direct measurement of the IHC stereocilia these same findings (Fridberger et al., 2006). The existence of excitatory shear is now well established but other modes of excitation of the IHCs have been observed that are based on pulsatile fluid motion. Nowotny and Gummer, 2006, demonstrated that the counter-phasic motion of the TM and RL as a result of OHC contraction could generate fluid flow in the subtectorial space. Other forms of pulsatile fluid motion have also been predicted for IHC excitation with some neural recordings predicting their existence (For review see Guinan Jr, 2012). However it is important to note that all these modes of excitation only occur at frequencies below approximately 3 kHz, at frequencies above this sheer is widely accepted to underpin IHC excitation (Lukashkin et al., 2010).

1.4 Non-linearities and emissions in the cochlea

As with most sound processing systems, the cochlea distorts the input signal it receives to some extent. This distortion can occur at numerous stages and contributes to a general level of non-linearity within the cochlea (Rhode, 1971; Durrant and Dallos, 1972; Russell and Sellick, 1978; Cheatham and Dallos, 1982; Neely and Kim, 1982; Zagaeski et al., 1994). The physiological manifestations of this non-linearity that have been studied intensively are compression, which has been shown in the voltage responses of the hair cells (Dallos and Cheatham, 1989) and BM displacement (Murugasu and Russell, 1995), two-tone suppression, whereby responses to one tone can be suppressed by a second tone of a different frequency, and distortion products, which can be generated by the combination of tones and can be recorded in auditory nerve activity (Sachs and Kiang, 1968; Kim et al., 1980) or in the ear canal as otoacoustic emissions (OAEs) (Kemp, 1978; Kemp and Chum, 1980).

OAEs are sounds detected in the ear canal that are the result of physiological activity in the cochlea driving the peripheral auditory system in reverse (Kemp, 2008). Anecdotal reports had suggested their existence for many years but this was confirmed by Kemp in 1978, and since this time the mechanisms which underlie this phenomenon, as well as its relevance to understanding the cochlea has increased greatly. The OAEs initially observed by Kemp are known as transient evoked otoacoustic emissions (TEOAEs), he also observed spontaneous otoacoustic emissions (SOAE) which occur without any stimulation in a large minority of normal ears, with a higher incidence in women than in men (Bilger et al., 1990; Penner et al., 1993; Penner and Zhang, 1997). SOAEs are currently believed to be the result of standing waves caused by multiple internal coherent reflections at discrete locations in the cochlea of the individual affected, but current evidence predicts that not all OAEs are the result of a single mechanism (Shera, 2004). OAEs can also be evoked via a constant stimulus at a certain frequency played into the ear, causing an OAE of the same frequency to arise in normal subjects. This is known as stimulus frequency otoacoustic emissions (SFOAEs). Another method of evoking OAEs is by a short duration of stimulus that is applied repetitively, as Kemp discovered (either wideband or frequency-limited), in healthy ears, this will result in a frequency-dispersed sound of frequencies mainly present in the stimulus, TEOAEs (Shera, 2004). SFOAEs and TEOAEs are predicted to be the result of coherent reflections due to pre-existing irregularities in cochlear mechanics. What these irregularities consist of is unknown but hypothesises include large morphological discontinuities such as hair cell number and geometry or less visible irregularities such as cell to cell variations in cell biochemistry and structure such as number of prestin molecules present (Shera, 2004). Another form of OAE

which is currently understood to arise mainly through a quite different mechanism to SFOAEs and TEOAEs occurs when two closely related tones (f_1 and f_2), are presented to the cochlea. The resultant OAEs consists of distortion products from the interaction between these two tones, the most prominent of which are the $2f_1$-f_2 and f_2-f_1. These forms of OAE are known as distortion product otoacoutic emissions (DPOAEs) as they arise due to non-linearities acting as sources of cochlear travelling waves. Although the previously described discretely grouped OAEs referred to as a 'mechanism-based taxonomy' is useful as a rough guide to categorising OAEs, the realities found through experiments show a more complex story. For example DPOAEs consist of a mixture of a non-linearity generated sound created in the region of overlap between the f_2 and f_1 characteristic frequency places on the cochlear and a reflection source which results from a forward travelling wave from the aforementioned overlap region that travels to the CF of the sound and is reflected back (Shera, 2004). The two sources of a DPOAE give the resultant sound its fine structure which can be separated.

OAE emissions are an epiphenomenon of the active hearing process in the mammalian cochlea. Despite being of no functional importance to the workings of the peripheral auditory system they do provide both clinicians and researchers with a useful tool for assessing cochlea function. OAEs result from the active processes concerned with amplification and compression in the cochlea which has been localised to the OHCs of the Organ of Corti. OAEs are able to provide non-invasive quantitative data about the physiological health of cochlea. Dead or severely compromised cochleae do not emit OAEs. The two forms of OAEs used most widely in a clinical setting are TEOAEs and DPOAEs as they occur in all healthy ears. Current clinical uses include new-born screening, topological diagnostics, quantitative evaluation of hearing loss and monitoring of cochlea sensitivity over time. Future prospects include assessing cochlea vulnerability and hearing aid fitting parameters (Shera, 2004).

1.5 Thesis Aims

This thesis looks at the acoustic, electrophysiological and mechanical properties of the mammalian cochlea across of a range of species. The broad aims of each of the results chapters are:

Chapter 3 – to compare if DPOAE from guinea pigs and humans can be approximated to a model of generation based on a single-saturating non-linearity.

Chapter 4 – to determine parameters required for effective stimulation of the cochlea during round window stimulation and to determine the mechanisms of this excitation in the cochlear in a guinea pig model.

Chapter 5 – to characterise the acoustic, mechanical and electrophysiological responses of the *Otoa*$^{EGFP/EGFP}$ mutant mouse, a model for DFNB22 deafness in humans, and gain further understanding of the causes of DFNB22 deafness.

Chapter 6 – to compare the mechanical and electrophysiological responses of the prestin knock-out, prestin knock-in and wild-type mice and further understand the function of the motor protein prestin in the mammalian cochlea.

2 MATERIALS AND METHODS

2.1 Introduction

This materials and methods chapter is divided in two. Chapter 2.2 describes acoustic, electrophysiological and mechanical measurements on animals and Chapter 2.3 describes acoustic and psychoacoustic measurements on human subjects.

All experiments were performed in double skinned sound attenuated booths and additionally in animal preparations, experiments were carried out on an inflated gas isolation table (LINOS, technical manufacturing corporation). These measures were a precaution to reduce external noise contamination during experimental procedures.

All procedures involving animals were performed in accordance with UK Home Office regulations with approval from the local ethics committee. For procedures involving human subjects the ethics committee of the University Hospital of the Ludwig-Maximilians University Munich, Germany, in agreement with the Code of Ethics of the World Medical Association (Declaration of Helsinki), approved the procedures, and all subjects gave their informed consent.

2.2 Animal Experimental Methods

2.2.1 Round window stimulation experiments

In order to investigate round window (RW) stimulation of the peripheral auditory system of the guinea pig, surgery was performed on a preparation allowing access to the RW and a small magnet was placed on the RW membrane, in close proximity to an electric coil. On stimulation of the coil and the resultant movement of the magnet, various aspects of the peripheral auditory system's response to RW stimulation were monitored, including electrical responses from the cochlea and mechanical responses of the ossicular chain with and without mechanical interference, using laser interferometry. In addition, measures were taken of magnet displacement required for threshold stimulation of the cochlea.

2.2.1.1 Guinea pig experimental procedure

Pigmented guinea pigs (280-390 g) were anaesthetised with the neurolept anaesthetic technique (0.06 mg/kg body weight atropine sulphate s.c., 30 mg/kg pentobarbitone i.p., 500 µl/kg Hypnorm i.m.). Additional injections of Hypnorm were given every 40 minutes. Additional doses of pentobarbitone were administered as necessary to maintain a non-reflexive state. The heart rate was monitored with a pair of skin electrodes placed on both sides of the thorax. The animals were tracheotomised and artificially respired, and their core temperature was maintained at 38 ˚C, with a heating blanket and head holder. The middle ear cavity of the ear used for the measurements was opened to reveal the RW. Animals were sacrificed at the end of experiments with an overdose of pentobarbital sodium (150 mg/kg body weight, i.p.).

Compound action potentials (CAPs) of the auditory nerve were measured from the cochlear bony ridge in the proximity of the RW membrane, using Teflon-coated silver wire (S in Figure 2.1). Thresholds of the N1 peak of the CAP were estimated visually on an oscilloscope.

For acoustic stimulation sound was delivered to the tympanic membrane by a closed acoustic system comprising two Brüel & Kjær 4134 ½" microphones for delivering tones, and a single Brüel & Kjær 4133 ½" microphone for monitoring sound pressure at the tympanum. The microphones were coupled to the ear canal via 10 mm long, 4 mm diameter tubes to a conical speculum, the 1 mm diameter opening of which was placed approximately 1 mm from the tympanum. The closed sound system was calibrated *in situ* for frequencies of between 1 and 50 kHz (see Chapter 2.2.3.1.2). Known sound pressure levels (SPLs) were expressed in dB SPL re $2x10^{-5}$ Pa.

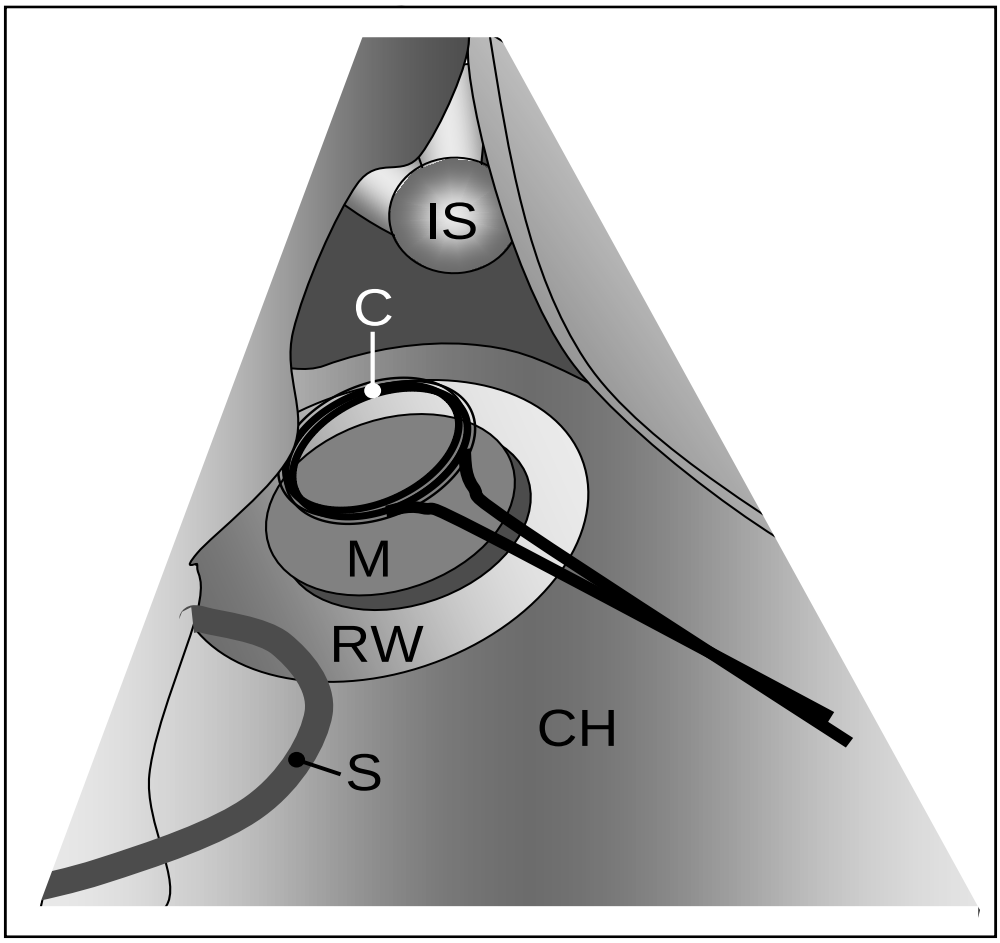

Figure 2.1 Schematic view of the guinea pig cochlea through a lateral opening in the temporal bone. M indicates a neodymium iron boron disk magnet (diameter 0.6mm, thickness 0.2mm) placed on the surface of the RW. C labels a miniature coil situated above the magnet. S denotes a Teflon-coated silver wire used for recording of activity of the auditory nerve. IS indicates incostapedial joint.

A floating mass transducer (FMT), a neodymium iron boron disk magnet (M in Figure 2.1) (diameter 0.6 mm, thickness 0.2 mm), was placed on the RW membrane to stimulate the cochlea through the RW. The magnet covered approximately one fourth of the RW surface of total area of 1.18 mm^2 (Ghiz et al., 2001). A miniature coil (C in Figure 2.1) made of two turns of copper wire (0.15 mm in diameter) was placed above the magnet. The magnet was driven with a magnetic field created by an alternating current (AC) applied to the coil. Stimulating current through the coil was generated by programs written in TestPoint (CEC, MA, USA) and delivered via a DT3010/32 (Data Translation) data acquisition board at a rate of 250 kHz, attenuated and fed to the coil through a current buffer. Maximum voltage applied to the coil in

this study was 10 V, which corresponded to 0 dB attenuation. Displacements of the magnet and the stapes were measured using a laser diode interferometer (Lukashkin et al., 2005)(see Chapter 2.2.3.2 for more information).

For experiments involving fixation of the ossicules the stapes was immobilised by filling the ear canal with superglue. Following this, to confirm stapes fixation, laser interferometer recordings were taken from the stapes during RW stimulation across a range of frequencies (1-30) and at the maximum voltage of the coil (10V). Stapes fixation was confirmed when no stapes displacements, above the noise floor of the interferometer, were recorded for any frequencies tested at the maximum voltages used in this study.

All stimuli were shaped with raised cosines of 0.5 ms duration at the beginning and end of stimulation to avoid clicks of the speaker. White noise for acoustical calibration and tone sequences for auditory and mechanical stimulation were synthesised by a DT 3010/32 board at a rate of 200 kHz and delivered either to the microphones or to the coil through low-pass filters (100 kHz cut-off frequency). Signals from the acoustic measuring amplifier were digitised at a rate of 200 kHz using the same data acquisition board and were averaged in the time domain. Experimental control, data acquisition and data analysis were performed using a PC with programmes written in TestPoint (CEC, MA, USA). Electronic equipment was arranged as shown in Figure 2.2.

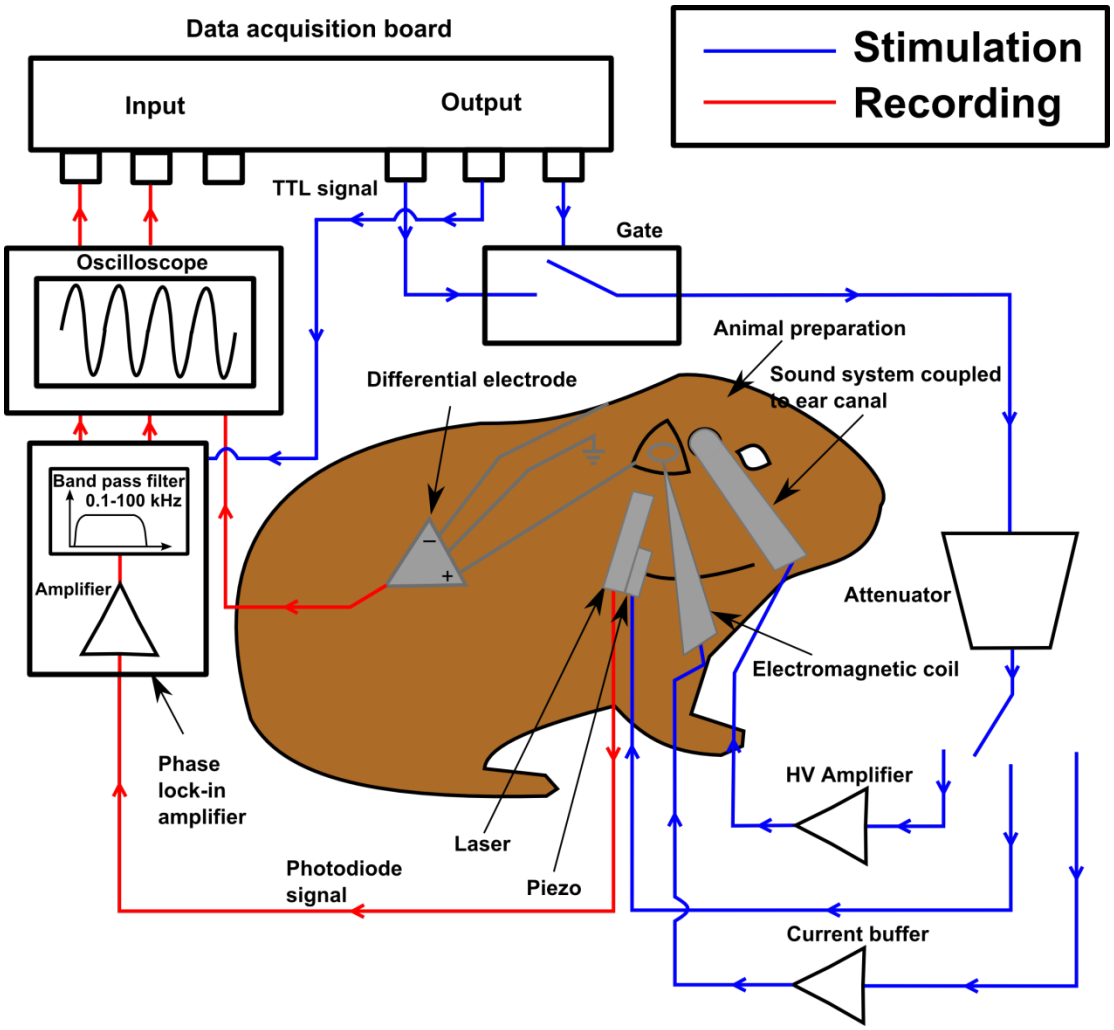

Figure 2.2 Schematic of the electronic equipment used in the guinea pig preparation. Stimulus delivery and signal recording were controlled by a PC via a DT3010/32 data acquisition board. TTL in schematic stands for transitor transitor logic.

2.2.2 Mouse physiological experiments

The physiological effects of a number of different mutations on the peripheral auditory system were investigated in two separate sets of experiments using mice.

In the first set of experiments, the role of the protein prestin in the cochlea was investigated using prestin knock-out (KO), homozygous prestin 499 and wild-type (WT) mice. Laser interferometry was used to record displacement from single points on the basilar membrane (BM) and electrical recordings of threshold values during sound stimulation, at numerous frequencies, were used to compare differences in the electrical and mechanical responses of the cochlear in the different mutant strains.

The second set of experiments investigated the physiological effect of a mutation that knocks out the inner-ear-specific protein otoancorin. These experiments compared the physiological differences between otoancorin KO and wild-type mice, using laser interferometry and electrical recordings with the same procedure as used in the prestin experiments. Additionally, these experiments involved acoustic stimulation to evoke distortion product otoacoustic emissions across (DPOAEs) the auditory range of the mouse to establish response thresholds. As with the prestin experiments electrical threshold recordings were made, but also involved a second suppressor tone in order to assess cochlear tuning.

2.2.2.1 Prestin experiments

Experiments were performed on wild-type, homozygous prestin 499, and prestin KO mice, the F4–F8 generations of a mixed 129/SvEv and C57B6/J background. Because this background is susceptible to early-onset, age-related hearing loss, mice used were of 3 and 4 weeks of age as; at this age, the loss of OHCs from the basal turn of the cochlea and the development of high-frequency hearing loss have not yet occurred. Animals were anaesthetized (i.p.) with urethane (ethyl carbamate, 2 mg/g body weight, i.p.). At the end of the experiments, the mice were overdosed with pentobarbital sodium (150 mg/kg body weight, i.p.). Heartbeat was monitored with skin electrodes, and core temperature was maintained at 38˚C. To measure BM displacements, cochlea microphonics (CMs) and CAPs, the right auditory bulla was opened with a ventrolateral approach to gain access to the RW (Figure 2.3). CMs and CAPs were measured from the RW membrane using glass pipettes filled with artificial perilymph (2M NaCl) with tip diameters of 50–100 µm (recording bandwidth > 30 kHz). Signals were amplified with a recording bandwidth of DC – 100 kHz. Thresholds of the N1 peak of the CAP were estimated visually. Animals were sacrificed at the end of experiments with an overdose of pentobarbitone.

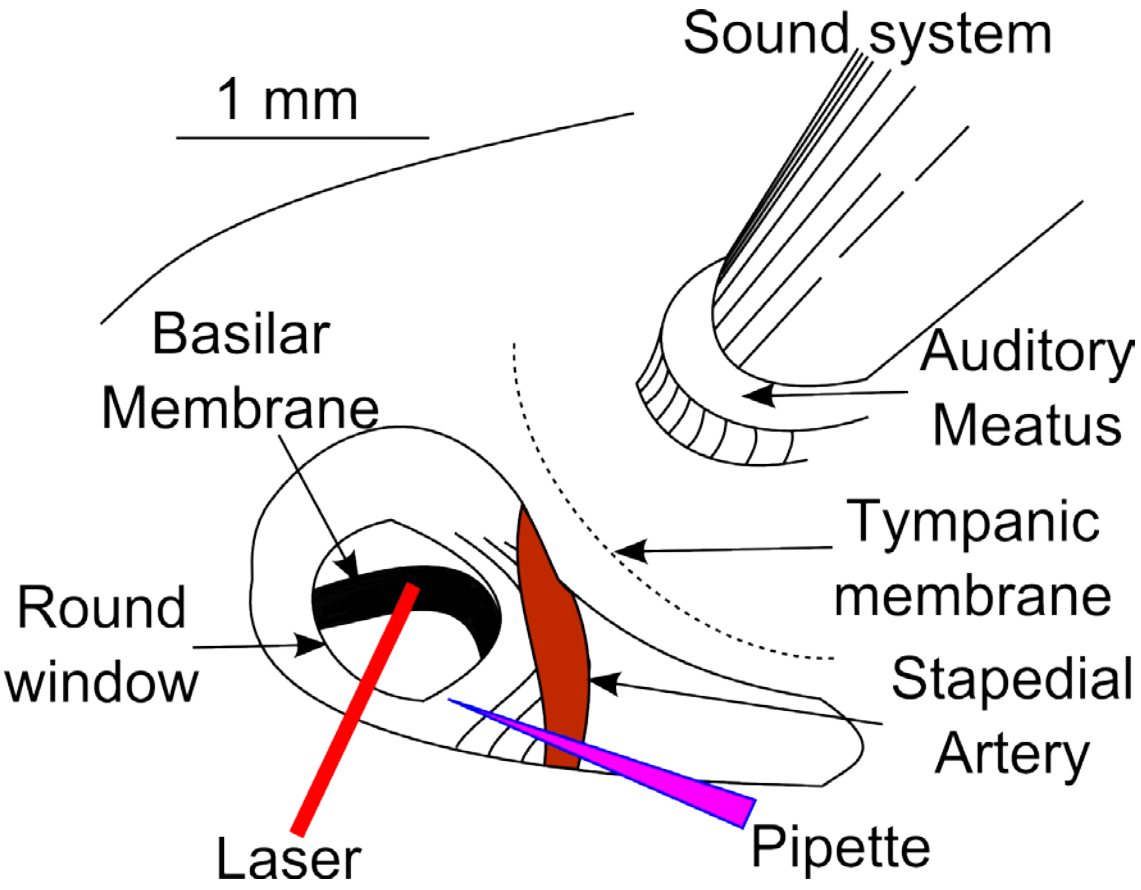

Figure 2.3 Schematic view of the mouse cochlea, ventralateral opening into the right auditory bulla

The right pinna was removed and sound was delivered via a probe with its tip within 1 mm of the tympanic membrane and coupled to a closed acoustic sound system, comprising two MicroTech Gefell 1 inch MK102 microphones for delivering tones and a Bruel & Kjaer 3135 ¼ '' microphone for monitoring sound pressure at the tympanum (Figure 2.3). The sound system was calibrated *in situ* for frequencies between 1-100 kHz using a measuring amplifier and known SPLs were expressed in dB SPL re 2 x 10^{-5} Pa. White noise and tone pulses with rise-fall times of 0.2 ms were synthesized by a DT 3010/32 data acquisition board, attenuated, and used for sound system calibration and the measurement of electrical and acoustical cochlear responses.

BM displacements were measured by focusing a self-mixing laser-diode interferometer through the RW membrane to form a 5 µm spot on the centre of the BM, in the 50–65 kHz region of the cochlea (Figure 2.3). The interferometer was calibrated at each measurement location by vibrating the piezo stack, on which it was mounted, over a known range of displacements (See Chapter 2.2.3.2.4). Tone pulses (with rise-fall times of 1 ms) delivered

during BM measurements were generated by a Phillips PM 5193 programmable synthesizer and attenuated with digitally controlled attenuators. Current changes in the interferometer were converted to voltage, amplified and fed to the data acquisition board. Experimental control, data acquisition, and data analysis were performed with programs written in Matlab 2006b (The MathWorks, Inc.), electronic equipment was arranged as shown in Figure 2.4.

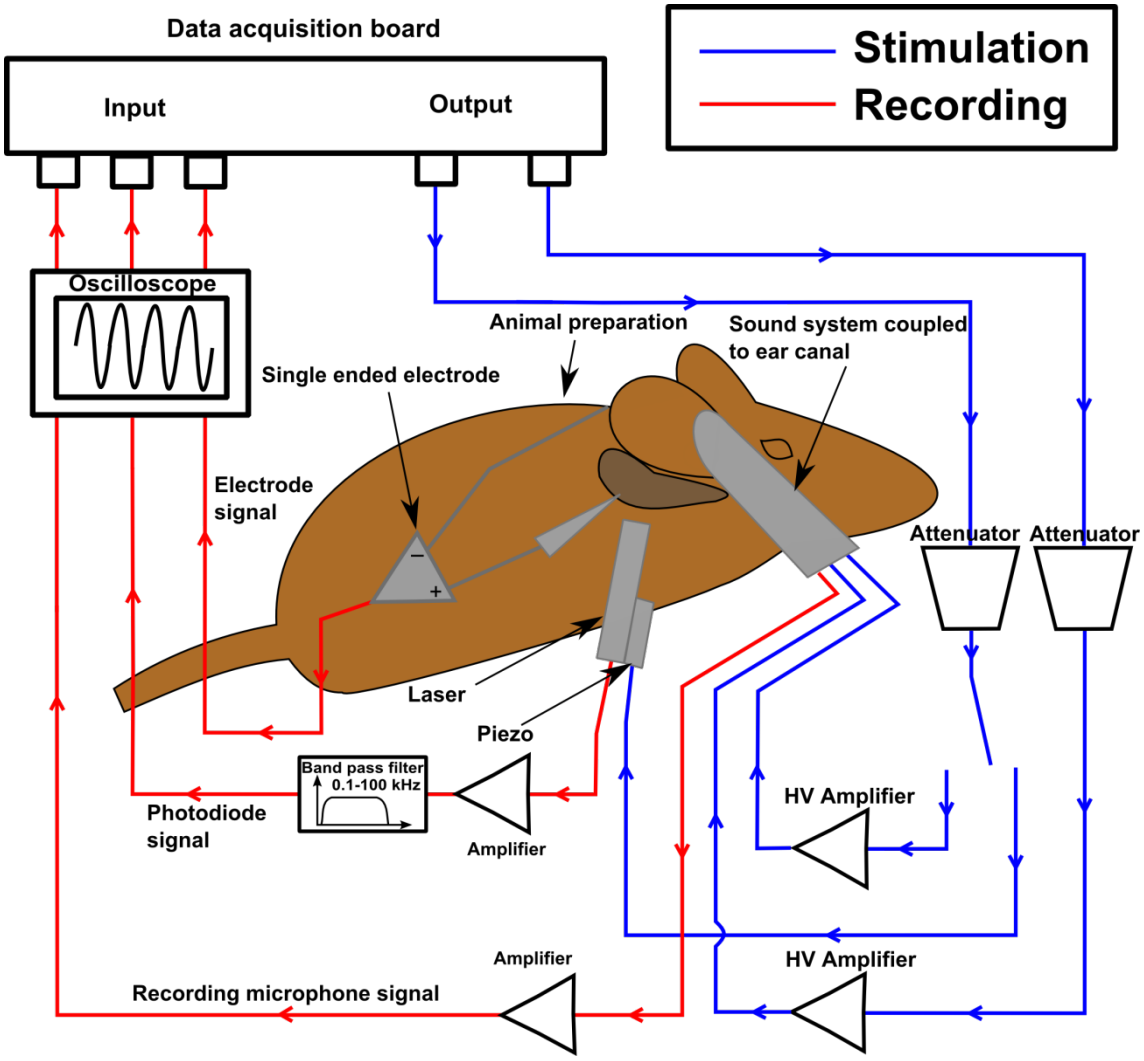

Figure 2.4 Schematic of the electronic equipment used in the mouse preparation. Stimulus delivery and signal recording were controlled by a PC via a DT3010/32 data acquisition board.

2.2.2.2 Ototancorin experiments

Experiments were performed on WT and mutant *Otoa*$^{EGFP/EGFP}$ mice from CBA/Ca and S129 background strains. The mice used were 3 months of age. Sound stimulation and recording, CM, CAP thresholds and BM measurements were performed as in the prestin experiments (Chapter 2.2.2.1).

Measurements of DPOAEs and CAP tuning curves were performed in all mice. To measure DPOAEs, primary tones were set to generate $2f_1$-f_2 distortion products at frequencies between 1-50 kHz. DPOAEs were measured for levels of f_1 ranging from 10-80 dB SPL, with the levels of the f_2 tone set 10 dB below that of the f_1 tone. DPOAE threshold curves were constructed from measurements of the level of the f_2 tone that produced a $2f_1$–f_2 DPOAE with a level of 0 dB SPL where the frequency ratio of f_2:f_1 was 1.23. System distortion during DPOAE measurements was 80 dB below the primary tone levels.

CAP tuning curves were derived from simultaneous tone-on-tone masking (Dallos and Cheatham, 1976), using a 10 ms probe tone centred on a 40 ms masker tone. The probe tone was set to a level where a stable CAP appeared just above the recording noise floor. The frequency of the masker was set and its attenuation adjusted until the probe tone CAP was suppressed. The masker frequency and level was noted, a new masker frequency was set and the process repeated.

The Q10 dB (ratio of the CF to the bandwidth measured 10 dB from the tip) and iso-response BM frequency tuning curves in the *Otoa*$^{EGFP/EGFP}$ and the wild-type mice were analysed statistically to test for significant differences. The Q10 dB from the two types of mice were subjected to two way *t*-tests and the comparisons were judged significant at p=0.05. Iso-response BM frequency tuning curves between the two types of mice were analysed by performing two way *t*-tests at each frequency of the tuning curve. The criteria for significance was set at p=0.001, after a Bonferroni correction of p=0.05 for 35 multiply comparisons.

2.2.3 Techniques

2.2.3.1 Sound stimulation and recording additional information

For both the guinea pig and mouse experiments, sound was delivered to the tympanum by a closed acoustic system. This system, consisted of two speakers and a microphone coupled with small lengths of rubber tubing to a conical probe, with a lab constructed 1 mm tip (Figure 2.5). The exact size and brand of speakers for guinea pigs and mice are as stated in previous Chapters 2.2.1.1 and 2.2.2.1. The probe was manufactured using two plastic yellow tips (Plastibrand, Sigma- Aldrich), shaped to form a distinctively shaped tip (see Figure 2.5) and secured together with Araldite (Huntsman Advanced Materials). The shape of the probe and tip were carefully produced and tested to ensure minimal sound reflections, resonances and anti-resonances within the probe chamber. The entire arrangement was securely clamped on to a micro-manipulator or mounted on a stand.

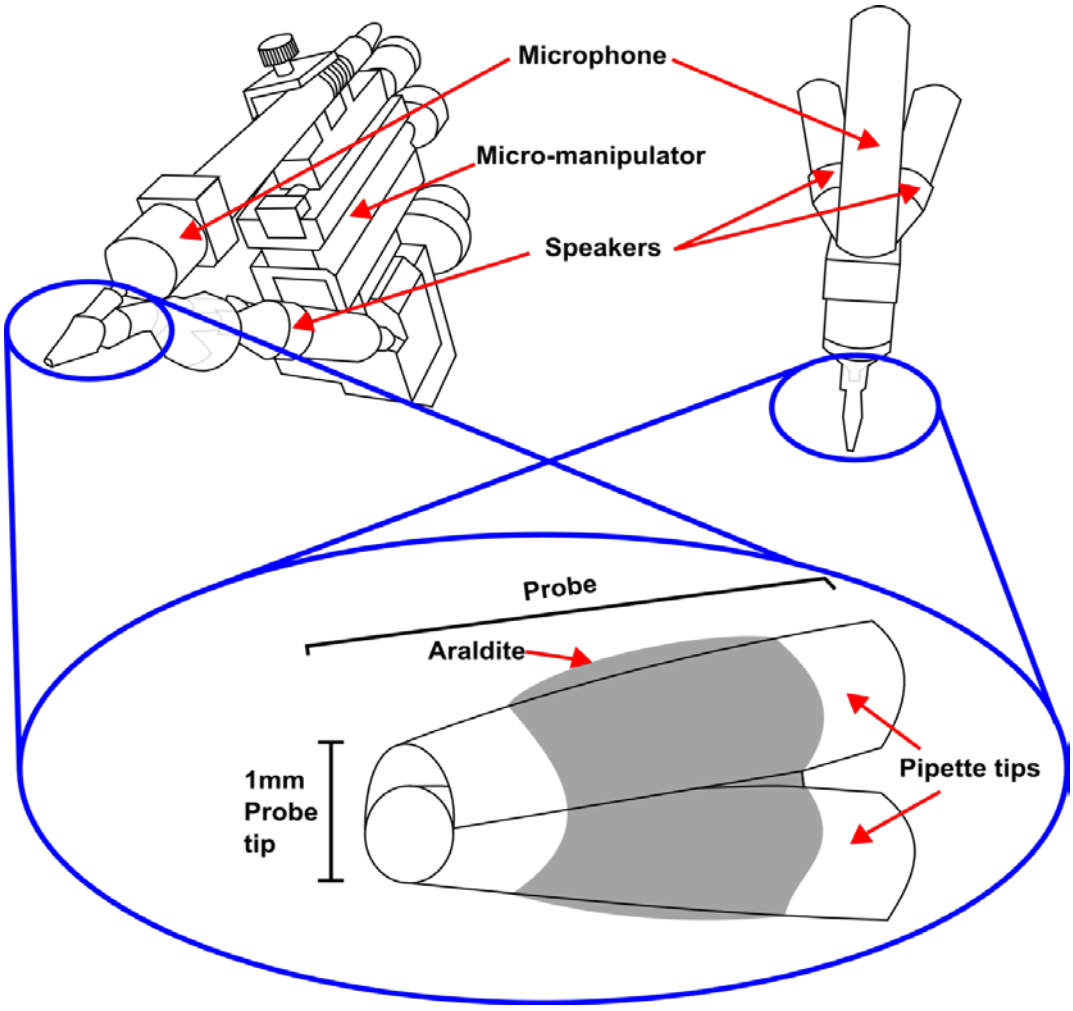

Figure 2.5 Closed acoustic sound delivery system for animal experiments. Upper panel left, side view of sound system mounted on micro-manipulator. Upper panel right, view looking from above of system. Lower panel, probe formed of two carefully shaped pipette tips secured together with araldite

2.2.3.1.1 Condenser microphones and microphone preamplifiers

The condenser microphone consists of a thin metal diaphragm and a rigid back plate, which together make up the electrodes of an air dielectric capacitor (Figure 2.6). A charge can be applied to the capacitor by a direct current (DCurr) voltage, known as the polarisation voltage. Variations in sound pressure cause the thin metal diaphragm to move and cause changes in capacitance, which are transformed into voltage signal variations that can be interpreted as sound. The microphone can be operated in reverse, allowing the condenser microphones to work as speakers for the delivery of sound (Kjaer, 1976).

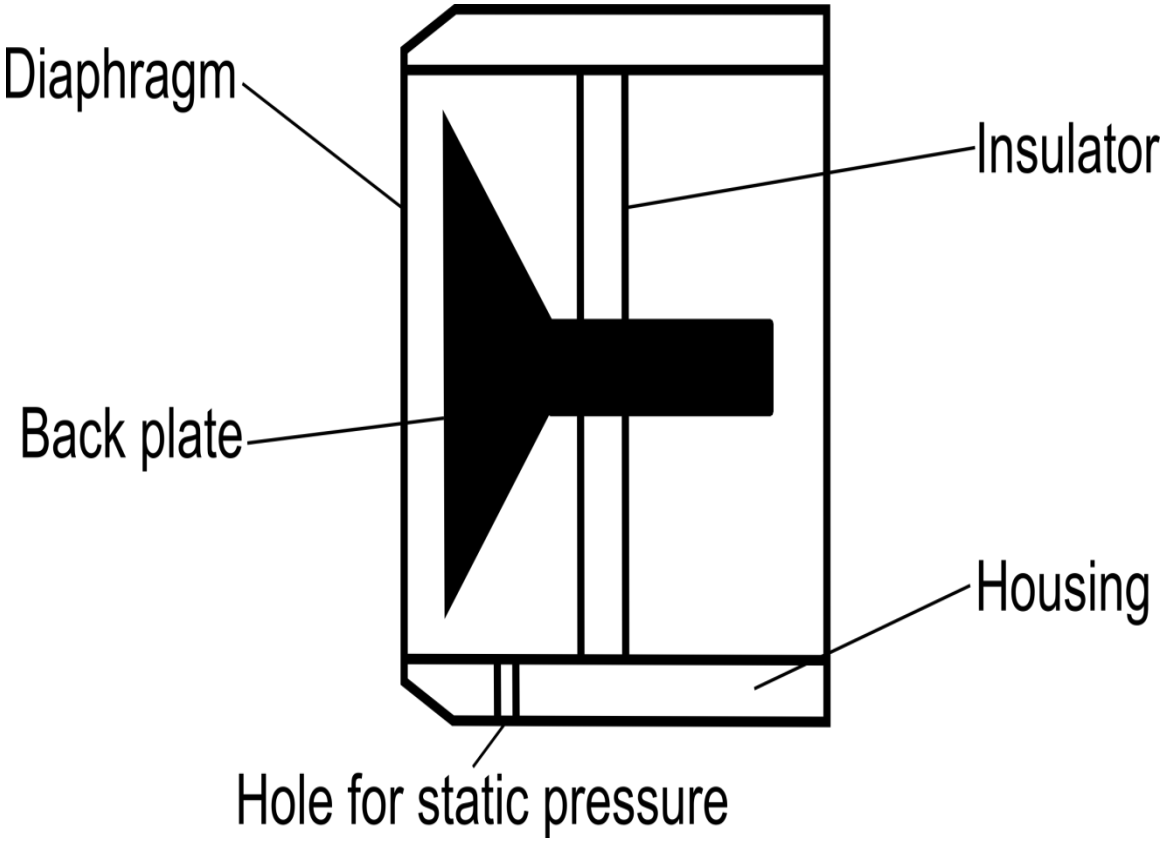

Figure 2.6 Schematic construction of a condenser microphone. Adapted from condenser microphone handbook Kjaer, 1976

The microphone and the preamplifier are placed in close proximity to each other to ensure that stray capacitance of the condenser microphone was kept to a minimum and to increase the relative variation in capacitance, increasing the overall sensitivity of the system.

2.2.3.1.2 Sound calibration

In all animal procedures the closed acoustic system was calibrated *in situ* before the start of experiments. The frequency response in Volts (V) of speaker 1, within the closed system was obtained by a short burst of quasi-white noise (0.1 – 100 kHz) monitored by the recording

microphone. Due to the unique acoustic properties of the closed system the recorded data contains numerous notches (black arrows, Figure 2.7), which are the result of internal reflections, resonances and anti-resonances (Figure 2.7).

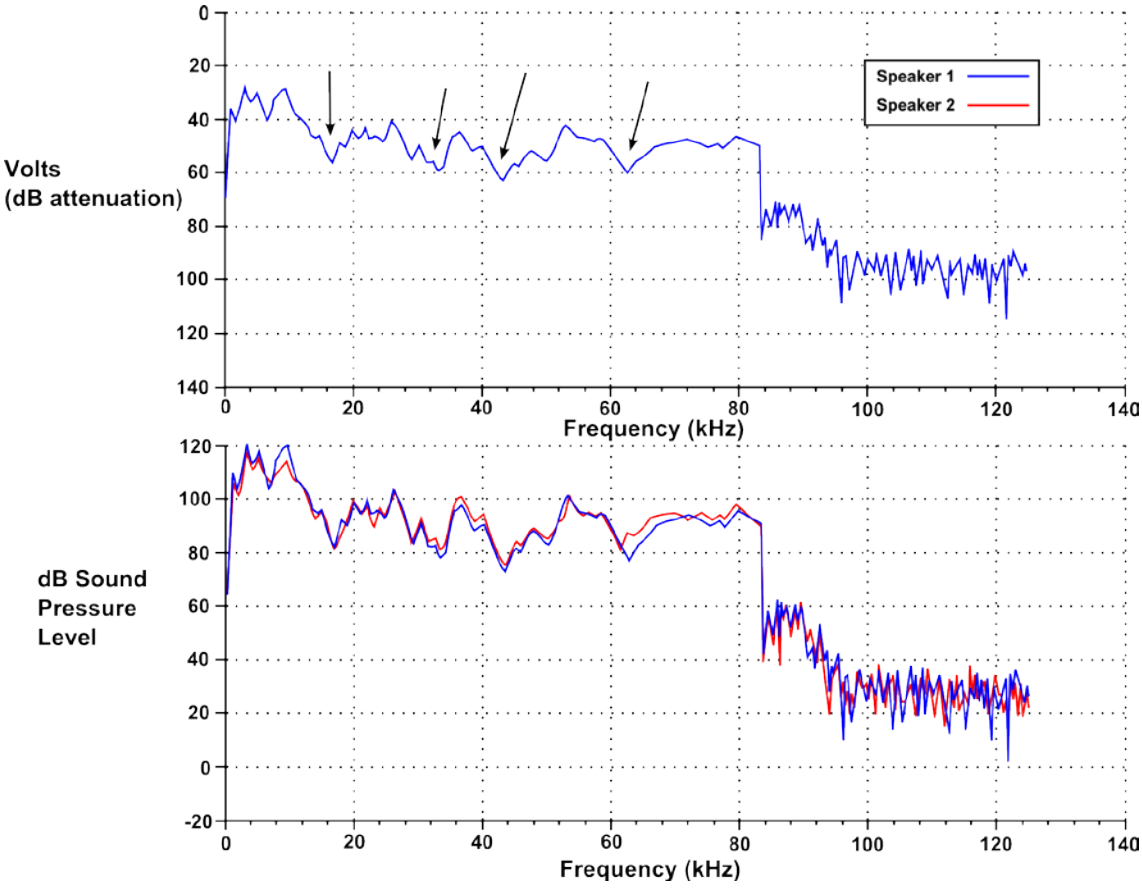

Figure 2.7 Sound calibration, frequency response of speaker 1 and 2 in closed acoustic system

Notch depth was minimised by careful placement of the coupling device within 1 mm of and perpendicular to the tympanum, and by careful shaping of the internal cavity of the sound coupler (Chapter 2.2.3.1).

The voltage response of speaker 1 was used to convert its output to dB SPL re $2x10^{-5}$ Pa. This was achieved by using a 1 kHz sound level calibrator of 94 dB SPL (Sound Level Calibrator Type 4230, Brüel & Kjær) to calibrate the recording microphone before its placement within the closed acoustic system. Speaker 1 was then stimulated to play a short test-tone near to 1 kHz. The frequency response of the recording microphone is known to be linear across all frequencies of interest (0.1-100 kHz). Therefore the test-tone was used to calculate the voltage response of the microphone per dB SPL for the test tone frequency. Once this conversion factor was calculated it was applied across all frequencies to the voltage response curve

previously recorded, to derive a calibration curve in dB SPL re $2x10^{-5}$ Pa. The conversion factor was then applied to speaker 2 in the closed acoustic system after it had been stimulated to play a brief burst of quasi-white noise (0.1-100 kHz). The entire calibration process was automated through programs written in Testpoint (CEC, MA, USA) or Matlab (The MathWorks, Inc.), for the guinea pig and mouse experiments respectively.

2.2.3.2 Laser measurements additional information

A self-mixing laser interferometer was used to make displacement recordings from structures of interest in the guinea pig and mouse preparations (Lukashkin et al., 2005). The laser detects phase and delay dependent changes in intensity of light reflected back from a moving surface in a linear plane. It is highly sensitive to small amounts of back-reflection and so is ideally suited to recordings from poorly reflective surfaces, such as the BM of the mammalian cochlea.

The beam from the laser diode (10 mW, 670 nm) was collimated and was focused on to a 5 μm spot on the structure of interest at a distance of 45 mm (Figure 2.8) with a focal depth of 20 μm. In the guinea pig the laser beam was detected by the integral photodiode and the photocurrent was amplified and converted to voltage for processing with a dual phase lock-in amplifier phase-locked to the driving voltage of the sound system. In the mouse preparation the laser beam was detected by the integral photodiode and the photocurrent was amplified and converted to voltage and the signal fed into the data acquisition board for analysis in Matlab 2006b (The MathWorks, Inc.) The signal from the photodiode was also low-pass-filtered and amplified.

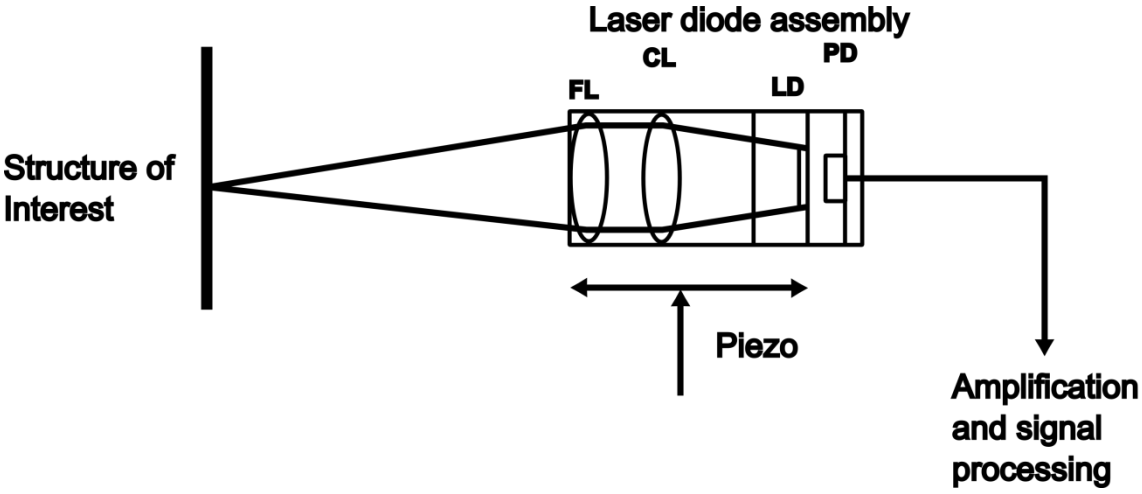

Figure 2.8 Schematic of the self-mixing effect laser interferometer. The laser diode assembly consists of a focusing lens FL, culminating lens CL, laser diode LD and photo-diode PD.

The greatest laser sensitivity is achieved when the operating point is in quadrature at Q1 or Q2 (Figure 2.9, A) . Movements away from these operating points result in a smaller signal being

recorded for the same target displacement (Figure 2.9, B). The wavelength (670 nm) allows a working range of 670/4 = 167 nm around the quadrature points. To improve recording quality and reduce the effect of noise a max-averaging signal processing algorithm was used during data collection. The max-averaging algorithm records the maximum output from the laser interferometer and its phase, upon the assumption that the maximum output is when the laser is set in quadrature (Q1 or Q2), for a number of presentations of the signal (typically *n*=20) at exactly the same moments of time relative to the beginning of the recording. Provided the preparation is in a stable condition and close attention is paid to ensure the laser remains focused in quadrature, then the laser interferometer can record sub-nanometre displacements even with relatively high background noise (Lukashkin et al., 2005).

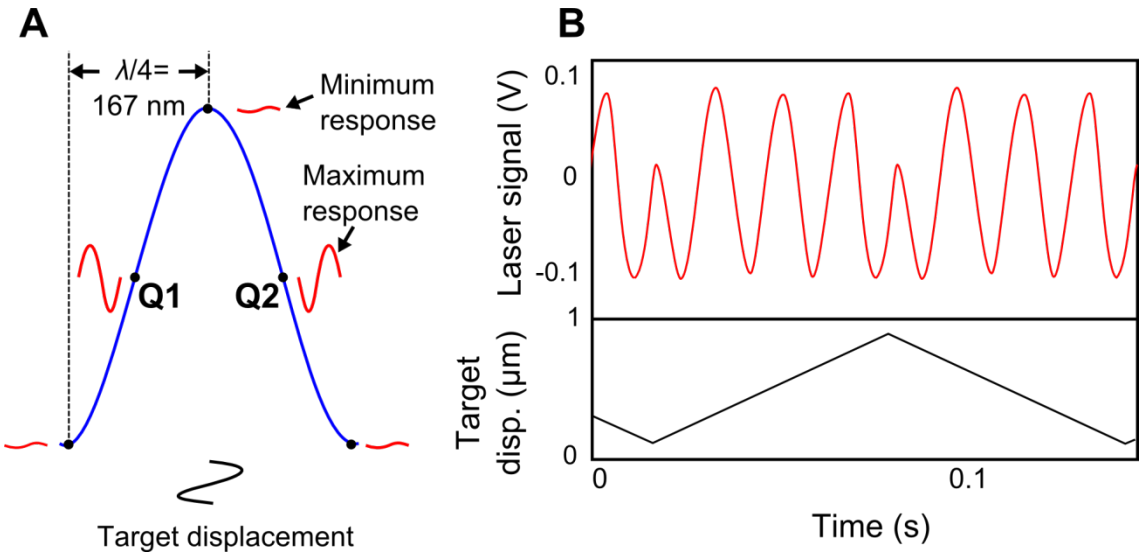

Figure 2.9 Dependence of the interferometer sensitivity on distance to the target. (A) The largest amplitude laser responses are recorded from quadrature points, Q1 and Q2. (B) Movement of the laser relative to the target shifts the operating point and changes signal amplitude. (Adapted from Lukashkin et al., 2005 and Jones, 2012).

2.2.3.2.3 The laser-diode interferometer

The device consists of a laser crystal formed from semiconductor alloys. The alloys have their atomic ratio and impurity concentration varied in order to produce two layers, p-type and n-type layer (Figure 2.10) (Optics, 1993). In a laser diode current flowing across the p-n junction results in light emission due to the recombination of electrical carriers. The process of stimulated emission occurs whereby the emission of a photon of a certain energy, direction and phase results in the emission of a second identical photon, amplifying the signal. The laser crystal consists of two facing mirrors that are coated with a reflective substance to enhance reflectivity (Figure 2.10).

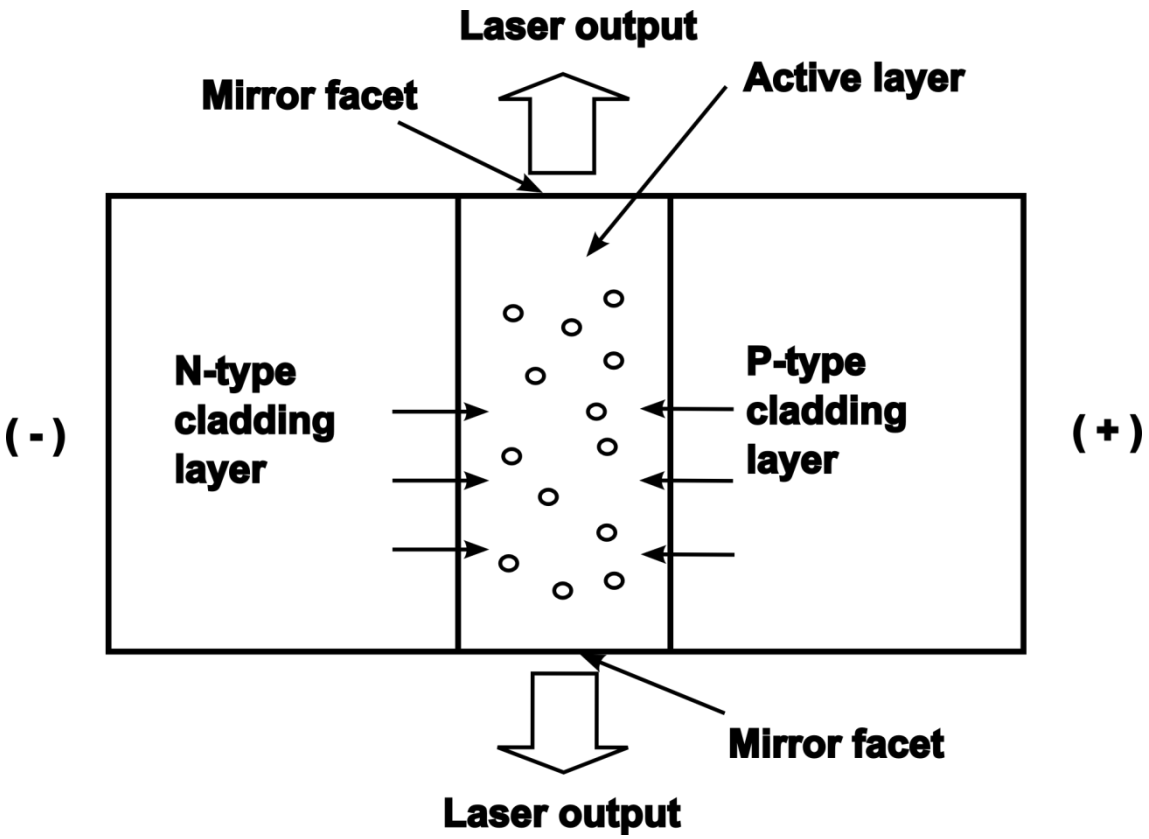

Figure 2.10 Schematic cross-section of the laser diode chip (Optics, 1993).

The mirrors cause light travelling parallel to the optic axis to be reflected between the two surfaces. Further stimulated emission occurs as the light passes over the semi-conductor material. A proportion of the light will be transmitted through the reflective surface at each reflection.

Light is emitted through both facets of the laser crystal (Figure 2.10 and Figure 2.11). The light from the rear facet is emitted onto the photodiode (Figure 2.11). Light from the front facet can be focused onto a target such as the ossicules or the BM. A small amount of this light, approximately 0.01%, is focused back into the laser. When this occurs an external cavity is formed between the target and the rear facet of the laser crystal. If this external cavity is not an exact multiple of $\lambda/2$ in length, the light re-entering the internal cavity will have phase shifted with respect to light being generated, resulting in reduced laser intensity. This reduced intensity is monitored by the photodiode which is calibrated under control conditions. The calibration involves monitoring the output of the photodiode when no light is reflected back into the cavity and the photodiode only receives light from the rear facet. This gives a baseline for reference and allows gain to be increased so that any changes in the current generated by light emitted through the rear facet of the laser crystal will be magnified. These changes occur

when the distance between the target and laser-diode are altered. The changes in coherence enable the laser to detect extremely small displacements of structures in the peripheral hearing system in the order of nm.

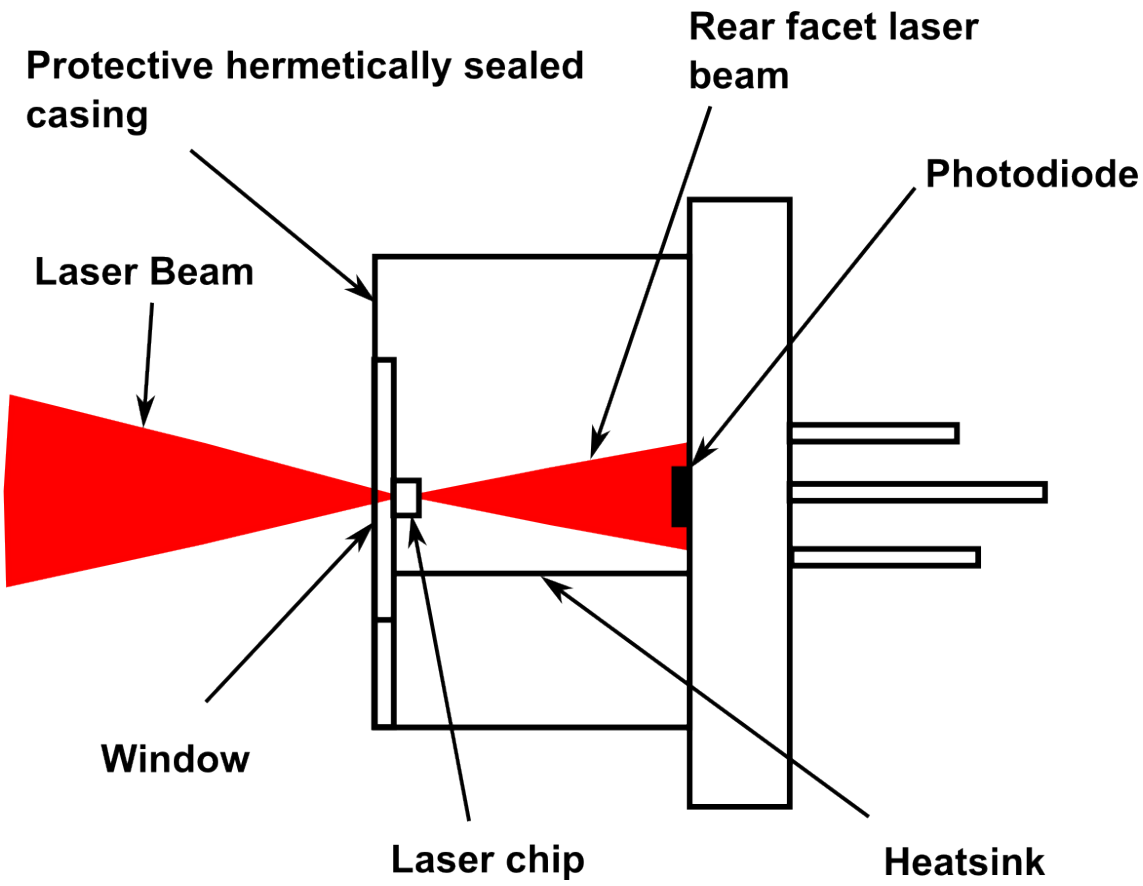

Figure 2.11 Schematic cross-section of a laser-diode interferometer (Optics, 1993).

2.2.3.2.4 Calibration of the laser-diode interfermoter

Measurement of the displacement of structures such as that of the ossicules, BM and magnet using the laser interferometer required frequent calibration to control for any changes in reflectance or shifts of position during the course of experiments. To calibrate, the laser interferometer was vibrated with a piezo with known amplitude, stimulated with 1kHz sinusoid of increasing levels (therefore increasing displacement). This procedure was performed 5 times for each calibration. Knowing the operating range of the laser (167 nm), around its centre position when in quadrature, the largest mixing signal from the laser should be obtained when the target moves 84nm through its linear range from its centre position (Figure 2.12). The peak response (in Volts) should therefore correspond to 84 nm. This value is used to calculate a coefficient in nm/V of the laser sensitivity for each experimental focus

point. During the course of experiments these calibration runs were saved on the computer for use in future analysis.

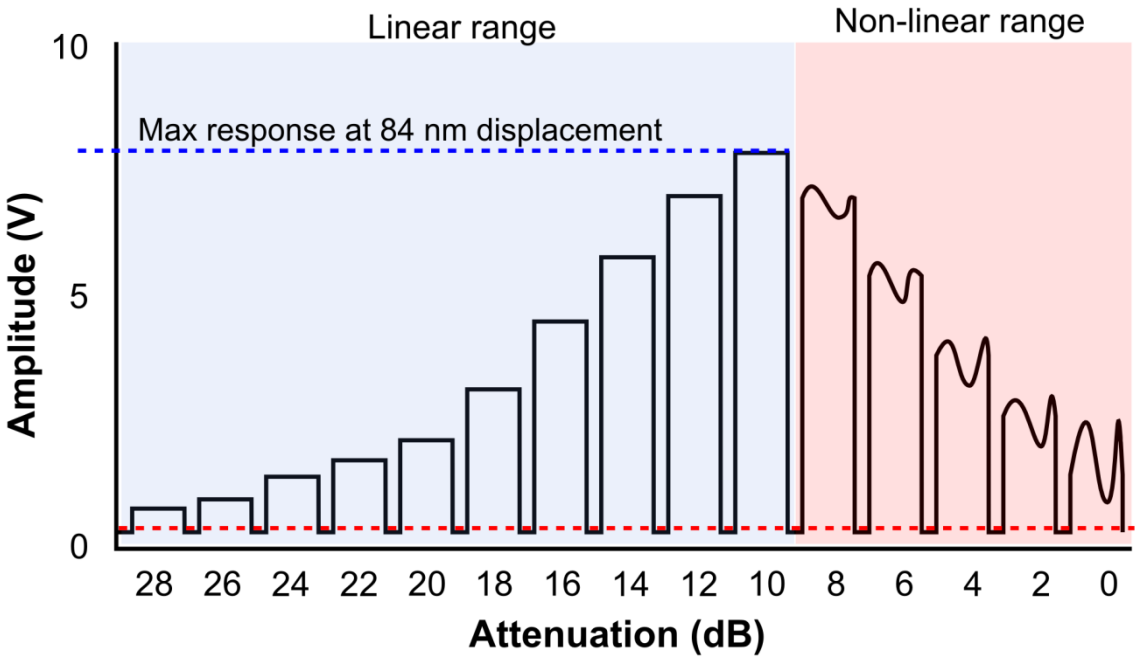

Figure 2.12 Calibration of the self-mixing laser interferometer Increasing the voltage to the piezo driver increases the amplitude of radial displacement of the piezo, upon which the laser is mounted and increases the amplitude (V) from the laser. When the laser is moved by a distance greater than its operating range (167 nm) the response becomes non-linear and unpredictable, and drops in amplitude. The point before this change to a non-linear regime which is measured in the figure with a blue broken line is taken to correspond to half the operating range (84 nm) (adapted from Jones, 2012).

2.2.3.2.5 Laser data analysis

Analysis of raw data was performed after completion of experiments. Magnet displacement in a single plane using the laser interferometer was calculated by calibrating the laser *in situ* as described in Chapter 2.2.3.2.4 and using the resultant coefficient calculated. Under certain conditions such as the experiments involving RW stimulation, or deriving of a iso-displacement frequency tuning curve further data analysis was required. The properties of the laser interferometer result in phase data that requires further data analysis also.

2.2.3.2.5.1 Round window magnet displacement

In the experiments on RW stimulation of the guinea pig cochlea, the displacement of the magnet in a plane perpendicular to the round window was investigated. The surgical approach through a lateral opening in the temporal bone did not allow for laser positioning that resulted in the laser being perpendicular to the magnets surface (Figure 2.13) and what would be a simple laser intensity calculation converting into displacement.

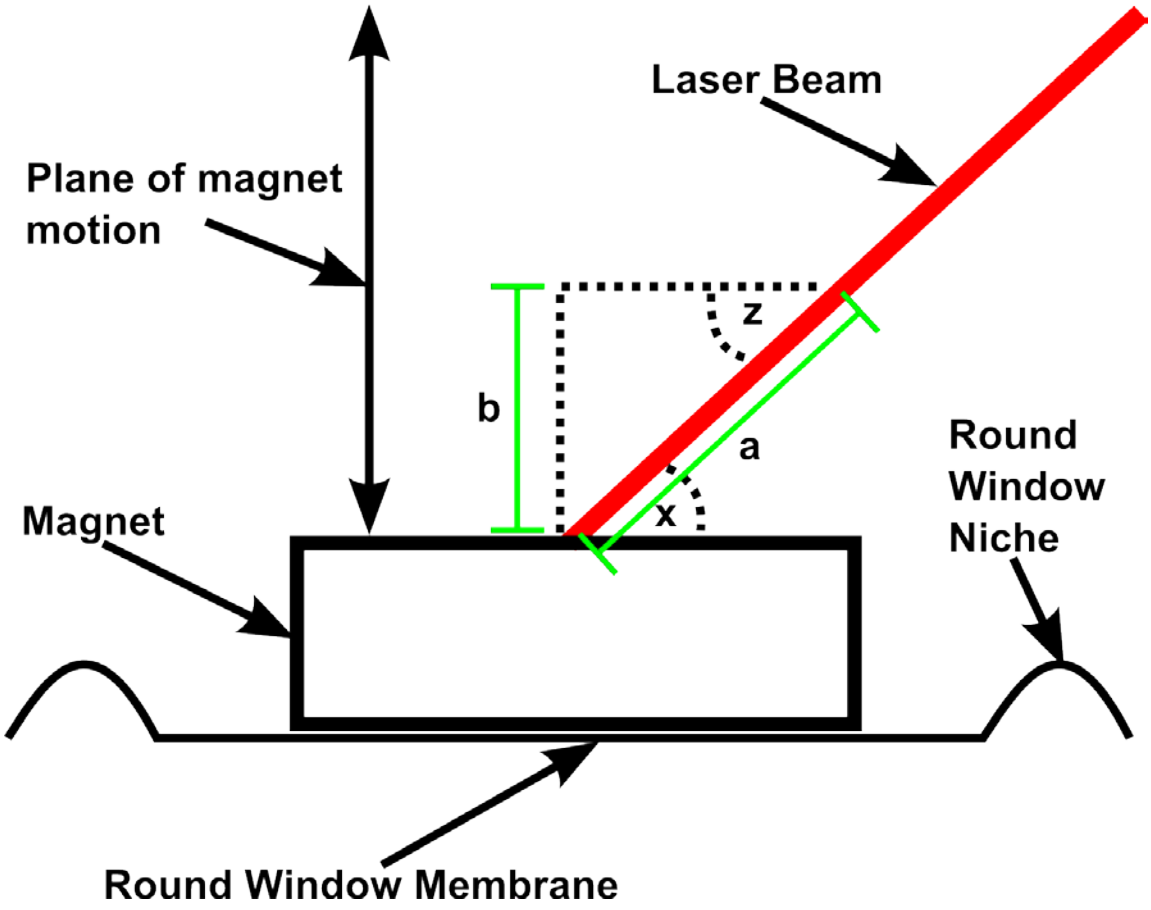

Figure 2.13 Schematic of round window stimulation experiments demonstrating laser recordings of displacement of the magnet. The laser interferometer is focused on the centre of the magnet at an angle from the horizontal x. Magnet movement on stimulation is perpendicular to the round window Membrane, the desired displacement value is in this plane and corresponds to value b. During recordings with the laser at angle x the displacement measurements record the distance a. Knowing angle x (which is equal to angle z) and displacement basic trigonometry can be used to ascertain the value of displacement at b during round window stimulation.

Movements of the magnet in the perpendicular plane to the RW were therefore calculated using trigonometry **(sinx = a/b, where angle x is equal to angle z, a is the hypotenuse and b is the opporsite)**

2.2.3.2.5.2 Iso-displacement frequency tuning curves from the BM of transgenic mice

Iso-displacement frequency tuning curves from the BM in mice were derived through acoustic stimulation of the mouse peripheral auditory system across a range of frequencies (10-80 kHz). During experiments, a single pure tone was presented at a low level (e.g 20 dB SPL) and the response during the stimulus period was recorded by the laser interferometer. The level of this stimulation was increased in 5 dB steps from approximately 20 to 90 dB SPL. The frequency

was then increased by 1 kHz and previous increase in sound intensity repeated. The procedure was carried out across the range of frequencies from 10 – 80 kHz. The resultant voltage response of the laser was converted to displacement (m). An iso-displacement frequency tuning curve is derived by setting a threshold value, if at a certain frequency and intensity of sound stimulation the BM displacement reached this value then that intensity of sound stimulation was recorded as the threshold for that frequency. The process was repeated across all frequencies and the resultant values graphed (see Figure 6.3). In the mouse experiments previous investigations have demonstrated that a threshold criteria of 0.2 nm coincides well with recordings of CAP and so is used to derive curves (Mellado Lagarde et al., 2008).

2.2.3.2.5.3 Laser interferometer phase

Recordings of phase by the laser interferometer required careful data analysis due to its inherent 180˚ phase ambiguity. This was achieved by analysing raw data and using a region where no phase jump occurred (Figure 2.14), which usually corresponded to the maximum amplitude of the response.

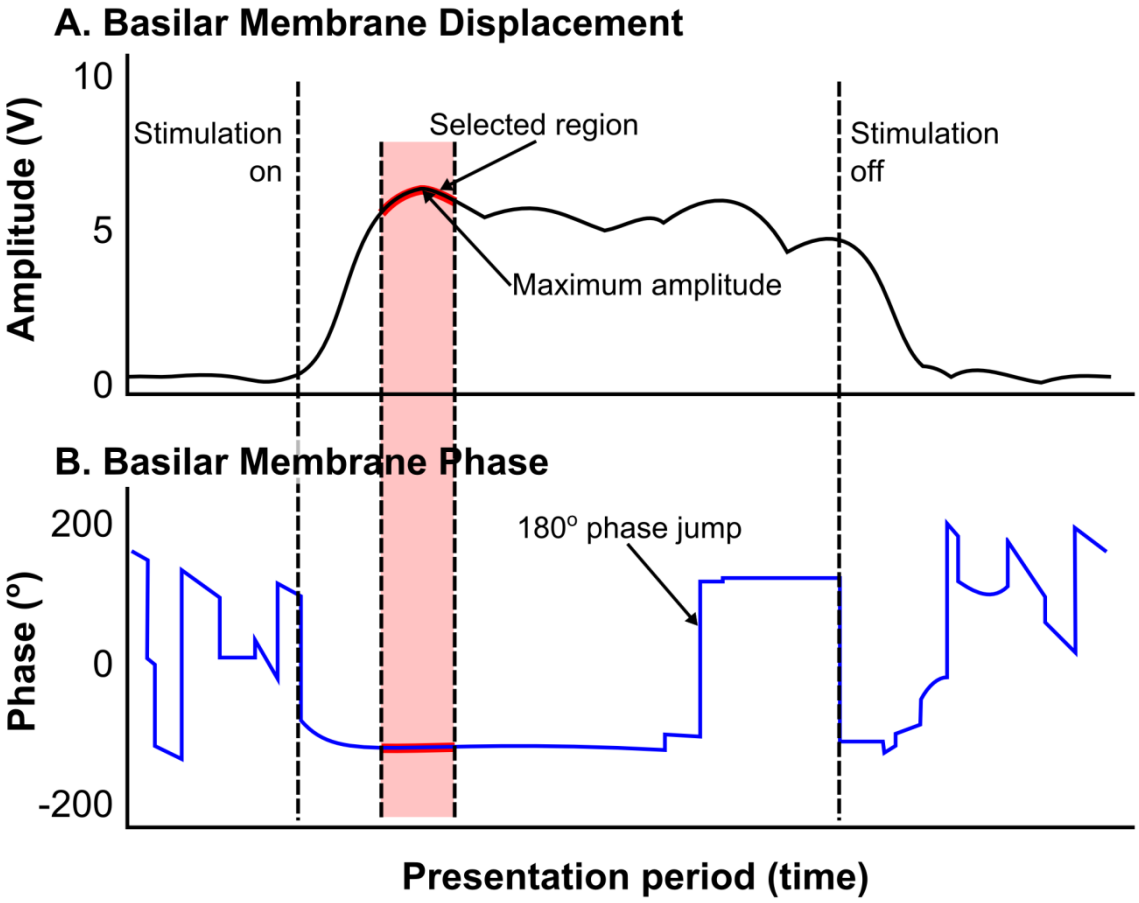

Figure 2.14 Raw data from BM recording, amplitude and phase. Single stimulus presentation showing how the automated Matlab 2006b script samples data from the section with the maximum amplitude and no 180˚ phase jump (adapted Jones, 2012).

In mouse BM recordings, phase was extracted for each frequency at a level of 80 dB SPL from a single point on the BM for each *n* (3-5) by an automated script running in Matlab 2006b. The data was averaged across *n,* ensuring that no phase data overlapped the 180˚ phase ambiguity. For instance, in a scenario where *n=3*, one phase reading could be +180˚ and the remaining two 0˚ resulting in a mean of 60˚, which would not represent the true phase. This problem was avoided by manually sorting through the data and correcting any outliers to the most found phase recording (e.g modal)(Figure 2.15, panel A). The outliers were then corrected by ±180˚ to bring them closer in value to the modal group. After this initial correction of the 180˚ phase ambiguity the mean of the points were plotted at each frequency (Figure 2.15, panel B).

Phase data was unwrapped at each frequency for the single spot recording from the mouse BM. The unwrapping accounts for phase ambiguity due to recording values greater than +180 to -180˚. The ambiguity is corrected by adding or subtracting 360˚relative to the rest of the data (see graph). The result of this analysis is presented in Figure 6.7 in Chapter 6 which is phase lag as a function of frequency from a single location on the mouse BM in one single preparation.

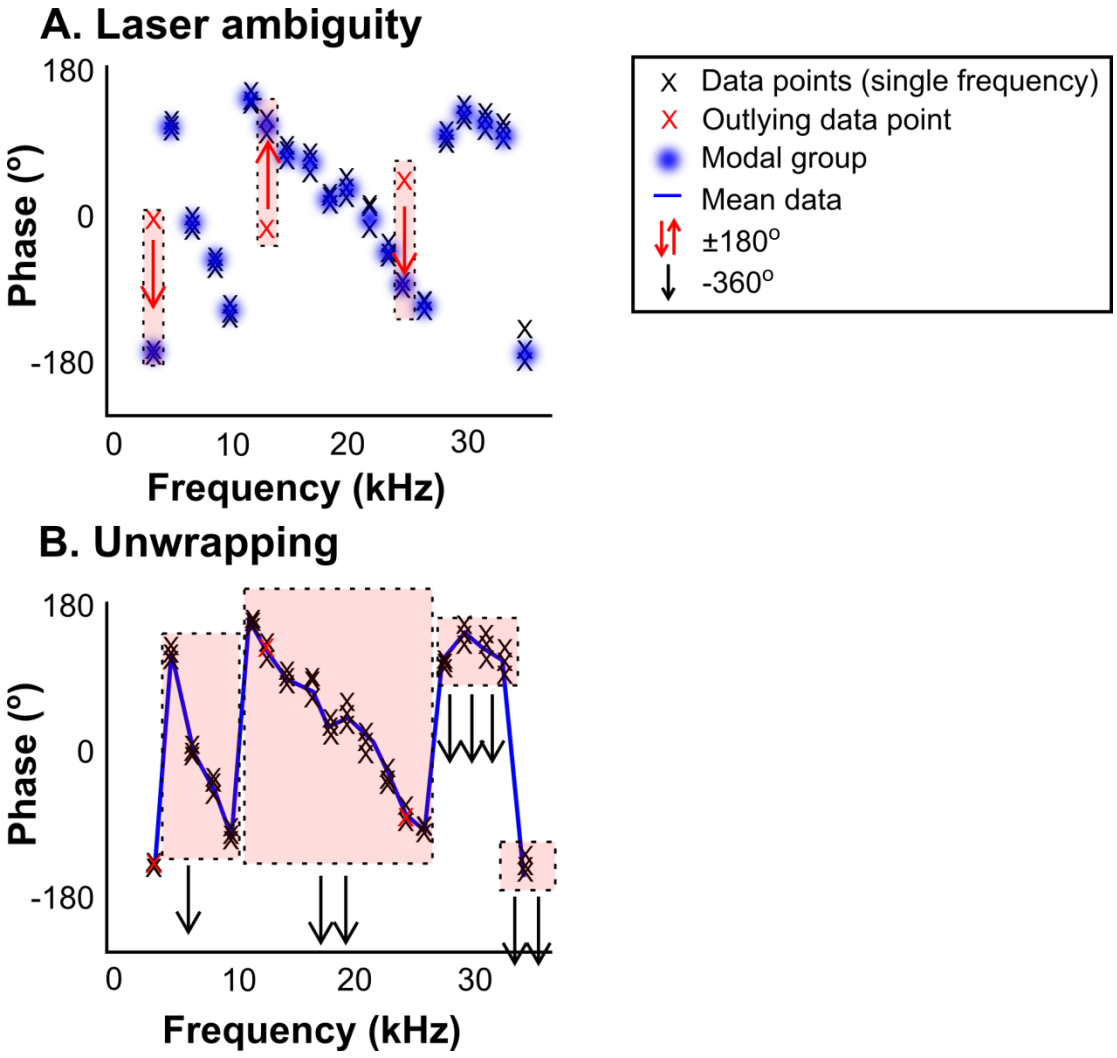

Figure 2.15 Laser interferometer, phase data analysis. Phase lag as a function of frequency calculated for a single point recording from the basal end of the mouse cochlea. A. The laser's inherent 180˚ phase ambiguity was corrected for by assigning the modal groups and adjusting any outliers by ±180˚. B. The mean for each frequency was calculated and unwrapped (adapted from Jones, 2012).

2.3 Human Experiments

In order to investigate differences between DPOAE generation mechanisms in humans and rodents, low-frequency biased cubic DPOAEs (DPOAE modulation patterns) were recorded in human subjects and the results compared with a previous study on guinea pigs (Lukashkin and Russell, 2005b). The methods of data collection for the guinea pig study can be found in appendix 2. In the present study the guinea pig DPOAE data was re-analysed using the same technique as used for analysis of the human data (see below). The data was used to estimate the transfer functions underlying the modulation patterns in the two species.

Low-frequency biased DPOAEs were recorded in 18 human subjects with normal hearing (10 females, and 8 males, with a mean age of 27). Normal hearing was defined as subjects having no history of chronic middle or inner ear diseases, hearing thresholds of less than 10 dB hearing loss (HL) in all tested frequencies (250 -8000 Hz) and tympanometric results considered to be normal (peak admittance between -150-+100 daPa with a peak amplitude of 0.2–2.5 milliohms). Prior to any DPOAE measurements, an ear nose and throat (ENT) specialist performed an otomicroscopy on all subjects to check for and remove if present, any cerumen in the ear canal. No pathological signs were observed on visual inspection of the ear canal in any subject.

2.3.1 Human experimental procedure

During measurements all subjects were seated in a comfortable recliner and requested to remain quiet and motionless, in order to reduce noise. Otoacoustic emissions (OAEs) were recorded with an ER-10C DPOAE probe system (Etymōtic Research Inc., Elk Grove Village, IL, USA). Signal generation and data acquisition was carried out with a RME Fireface UC 24-bit external sound card (RME, Audio AG, Haimhausen, Germany), operated with a sampling rate of 44.1 kHz and a buffer size of 512 bits. The recorded signal was amplified by 30 dB by the preamplifier of the external soundcard; the built-in microphone preamplifier of the ER-10C probe system was set to a gain of 0 as it provides only two gain settings and lacks an overload indicator. The external sound card was controlled by scripts written in MatLab 7.5 (MathWorks, Natick, MA, USA). Sound was coupled to the ear canal using a closed acoustic system consisting of the probe system, a foam ear tip coupler (Etymōtic Research Inc., Elk Grove Village, IL, USA) and a 50 cm long polyethylene tube (inner diameter 1mm) inserted through the foam ear tip coupler for the biasing tone. The biasing tone was produced by an NSW1-205-8A 1” loudspeaker (Aura Sound Inc., Santa Fe Springs, CA, USA) and driven by a RB-960BX stereo power amplifier (Rotel, Worthing, UK). Noise in the system was substantially reduced by suspending all leads into the probe set-up from the ceiling of the booth. During

measurements, data were analysed in pseudo-real time and offline after the experiments in programs written in Matlab (Figure 2.16).

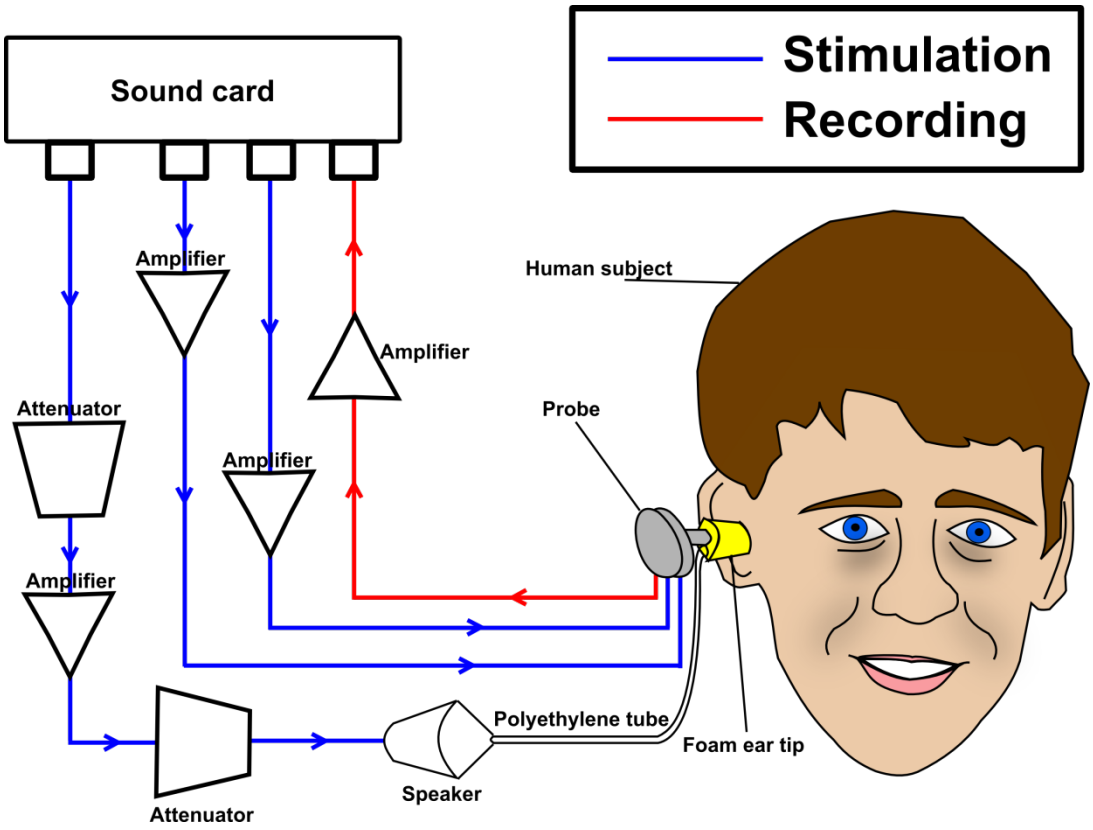

Figure 2.16 Schematic of the electronic equipment used in the human setup. Stimulus delivery and signal recording were controlled by a PC via a RME Fireface UC 24-bit external sound card.

All stimuli were shaped with raised cosines of 0.2 ms duration at the beginning and end of stimulation. The stimuli were presented with durations of 0.5 s or 9 s and a repetition rate of 1.5 Hz and 0.1 Hz, respectively. Primary tones were set to frequencies of 1690 or 2000 Hz and levels varied from 31 to 65 dB SPL. A low-frequency tone of 30 Hz and a level of 120 dB SPL was used to bias the cochlear partition. The stimulus was presented 16 times but would reject a recording if the mean noise floor near to the corresponding spectral line for the CDPOAE exceeded a sound pressure of -5 dB SPL. The recording was set not to stop until 16 valid recordings had been obtained or 32 valid or invalid repetitions were recorded. To reduce contamination of the recorded signal from noise created by, for example, the subject swallowing and coughing, data points would only be accepted if, after 16 valid repetitions, the signal-to-noise-ratio (SNR) was at least 6 dB. Recorded signals were averaged in the time domain to reduce random noise and were windowed with a Hann window (window length equal to signal length) before spectral analysis.

2.3.1.1 Recording protocol

To assess the integrity of the inner ear, a DPOAE-gram was recorded: With a fixed f_2/f_1 ratio of 1.22, CDPOAEs, $2f_1 - f_2$, were evoked with f_2 frequencies set between 1-8 kHz with harmonic increments of 300 Cents and with L_1 = 60 dB SPL, L_2 = 50 dB SPL.

Cubic distortions were recorded while f_2 was held constant at 1690 Hz or 2000 Hz and f_1 was changed so that the f_2/f_1 ratio changed from 1.1 to 1.6 with increments of 0.04 (f_1-Run). The f_2/f_1 ratio resulting in largest $2f_1 - f_2$ magnitudes was adopted as the 'best ratio' and was later used for evoking CDPOAEs during low-frequency biasing.

Low-frequency biased DPOAEs growth functions were evoked with f_2 = 1.690 kHz or 2 kHz depending on which f_2 frequency produced larger DPOAE levels and a f_2/f_1 ratio dependent on the optimal value obtained during the f_1-run. L_1 and L_2 were set according to the scissor relationship L_1=0.4*l2+39 (Kummer et al., 1998). Biasing tone frequency and level were 30 Hz and 120 dB SPL respectively in all experiments.

2.3.2 Calibration

The system was calibrated *in situ* in the closed acoustic system, which resulted in the obvious drawback that the system was calibrated for constant sound pressure at the probe tip and not the tympanum, as would be desirable. The drawback of this method of calibration is that sound pressure deviates between the tympanum and probe tip due to quarter wave length standing waves at frequencies higher than about 3 kHz (Siegel and Hirohata, 1994). Due to the lack of an alternative this remains the most widely used method for calibration but does have the drawback of underestimating the stimulus levels of frequencies higher than 3 kHz.

A chirp of 3 s duration and spanning a frequency range that incorporated all frequencies required for this study, 1-9 kHz, was used for calibration. The frequency response of the speakers was tested *in situ* in the closed acoustic system with the recording microphone of the probe. As the frequency response of the microphone is effectively linear (+/- 1 dB) across the frequency range in question, (1-9 kHz), an impulse response was calculated by cross-correlating input and output of the sound system. By comparing the impulse response with a synthesized impulse response, representing a linear spectrum, the two impulse responses were compared and a compensational response generated, which when convolved with the actual stimuli gave a linear frequency response. This procedure was repeated for each speaker as well as before each test run during the experimental procedure. This, in theory gave a linear spectrum for the calibrated frequency range. If this linear response across frequencies was not achieved, the probe was removed and checked for clogging of the speaker or microphone

channels or the fit re-adjusted and the calibration procedure repeated. Further checks made to ensure accurate calibration of the closed system included a probe fit check, whereby a stop-band noise consisting of a low and a high frequency band was presented and recorded with the recording microphone. A Fourier transform (FT) was performed on the microphone response. If responses before and after recordings were found to be significantly different or the ear responses to low- and high-frequency bands were not approximately similar then the recordings were rejected and repeated.

Calibration of the low frequency biasing tone was required as the amplitude and phase response of the recording pathway may have differed from that found in the normal frequency range. The method used to test for this was based on that used by Marquardt et al., 2007a. The probe was connected to an artificial ear (B&K 4157, Brüel & Kjær Sound & Vibration Measurement A/S, Denmark) and stimulated with a high frequency signal (2 kHz, 80 dB SPL) and a low frequency signal (30 Hz, 120 dB SPL) simultaneously. By driving the microphone into its non-linear range, the low-frequency signal causes very small amplitude modulations of the high frequency tone, which are observable as sidebands in the frequency spectrum. By using the method of data analysis as described in the analysis section the modulation pattern can be extracted that is in phase with the low frequency tone if the phase response of the recording pathway was linear in the low-frequency region. Tests demonstrated that the difference between the recorded low-frequency signal and the modulation pattern amounted to approximately 10˚ which was compensated for. The amplitude response of the probe microphone at low frequencies was compared with the amplitude response of the measuring microphone of the artificial ear (which is linear even at low frequencies) and was corrected accordingly.

2.3.3 Analysis

For consistency of data analysis, the guinea pig data and the human data were analysed using identical methods. The analysis involved using modulation sidebands of the DPOAE frequency (see below), which differed from that originally performed in the published article which used a time windowing technique (Lukashkin and Russell, 2005b). Theoretically the two techniques will produce the same results. This was tested by analysing the original guinea pig data with the modulation sideband technique and then comparing it to the results from the published article. Both sets of analysed data were, as expected, qualitatively and quantitatively almost identical.

For analysis, the recorded and averaged time domain signals were high-pass filtered with a digital filter (corner frequency 500 Hz). A subsequent FT analysis, where the FT size was equal to the length of the recorded signal, transformed the signal from the time domain into the frequency domain. The spectral magnitudes of the CDPOAE, $2f_1 - f_2$ were then extracted from the positive frequency half of the spectrum.

The low-frequency biased DPOAE is a non-linearly amplitude-modulated signal. Therefore, the DPOAE frequency can be regarded as the carrier frequency of this signal, flanked by modulation sidebands at the DPOAE frequency ± integer multiples of the bias frequency. The upper and lower three sidebands and the CDPOAE spectral line were extracted from the positive frequency half of the complex spectrum resulting from an FT. The inclusion of higher sidebands yielded no additional information and added only noise to the signal. Inverse Fourier transformation and a subsequent Hilbert Transform resulted in the time-variant amplitude of the DPOAE as a function of the biasing tone phase (Bian et al., 2007; Hensel et al., 2007; Marquardt et al., 2007)

To correlate the resulting DPOAE modulation pattern with the phase of the low-frequency BT, the unfiltered time-domain signal containing the low-frequency biasing tone was low-pass filtered with a digital filter (corner frequency: 50 Hz) to extract the BT.

For estimates of the transfer functions underlying the modulation patterns in both species, the absolute value of the third derivative of a two-exponential Boltzmann function was fitted to the parts of the modulation patterns corresponding to a rising and a falling half cycle of the biasing tone with a Levenberg-Marquardt algorithm for non-linear regression.

Boltzmann function:

$$t = \frac{A}{[(1 + exp^{b*(x*f-c)}) * (1 + exp^{d*(x*f-e)})]}$$

where *t* is the output of the system, *x* is the displacement represented by bias, *A* is the output scaling factor, *b* and *d* are parameters relating to the slope of the transducer curve, *d* and *e* are constants setting the operating point and *f* is a scaling factor for the input.

With the fitted parameters, the Boltzmann function representing an estimate of the underlying sigmoidal transfer function could be reconstructed. The estimated transfer functions were used to synthesise the corresponding I/O functions to check if the unbiased transfer functions can produce a level-dependent notch.

3 COMPARISON OF LOW-FREQUENCY ACOUSTICAL BIASING OF DISTORION PRODUCT OTOACOUSTIC EMISSIONS IN HUMANS AND GUINEA PIGS

3.1 Abstract

Distortion product otoacoustic emissions (DPOAEs) were recorded from humans over a range of primary tone levels in the presence of a low-frequency biasing tone of 30 Hz at 120 dB SPL. The resultant modulated $2f_1$-f_2 patterns observed were compared with a similar study in guinea pigs and both sets of results used to derive, through non-linear fitting based on the Boltzmann model, the underlying transfer function and resting operating point (OP) for both species. The results obtained suggest that for the parameters used in this study DPOAE generation in both species can be predicted by a single saturating non-linearity that is spatially localised. Any differences found in input/output growth functions between species can be predicted by such a model whereby guinea pig and humans have different operating points or non-linearity shape. Therefore the study supports the transferability of DPOAE findings between humans and rodents.

3.2 Introduction

Otoacoustic emissions (OAEs) are sounds produced by the mammalian inner ear. They result from the cochlea's active, non-linear processes and appear spontaneously or can be evoked with acoustic or electrical stimulation (Shera, 2004).

Although OAEs are found in humans and commonly used rodent laboratory animals, their manifestation is not uniform across the two groups (Avan et al., 1990). Rodents usually present with less frequent and smaller spontaneous otoacoustic emissions (SOAEs), larger distortion product otoacoustic emissions (DPOAEs) and smaller stimulus frequency otoacoustic emissions (SFOAEs) (Avan et al., 1990). Differences in cochlear morphology, levels of cochlea gain or dampening are often hypothesized to account for the observed species differences but not fundamentally different mechanism of OAE generation (Avan et al., 1990). However, there are indications that different mechanisms may generate rodent and human DPOAEs. When the primary tones' levels used to evoke DPOAES, *L1* and *L2*, are increased monotonically the resultant cubic DPOAE, $2f_1\text{-}f_2$, input-output function (growth function) displays a distinctive and highly consistent growth pattern in rodents, with a local minimum (notch) when the primaries are approximately between 60-70 dB SPL. In conjunction with the notch a rapid phase change of approximately 180 degrees occurs (Lukashkin et al., 2005). The appearance of notches in human DPOAEs is variable between and within subjects and is inconsistent, even under specific stimulus level parameters (Whitehead, 1998). These differences could result from different mechanisms of DPOAE generation in rodents and humans, casting doubt on the validity of extrapolating DPOAE data from rodent models to humans (Whitehead, 1998).

It has been hypothesized that the shape of the rodent growth function is due to the interaction between an active, 'low-level' component and a passive, 'high-level' component of DPOAEs that are localized to different sources of non-linearity within the cochlea and dominate at different levels of the primary tones (Mills, 1997; Whitehead, 1998; Shera, 2004; Rhode, 2007). Under this regime it was suggested that the mechanistic basis for the low-level component would be the cochlear amplification process and for the high level component would be the non-linear macromechanical properties of the cochlear partition. The phase difference between the two components would lead to the distinctive notch through phase cancellation and a rapid phase change as the passive component of the DPOAE dominates at high levels. Evidence for the active/passive model of DPOAE generation is indicated through experimental manipulations of the cochlea. Different levels of DPOAEs have differing vulnerabilities to acoustic trauma. In rodents, DPOAEs which are considered to be low-level, those elicited by

primary tones below 60-70 dB SPL, are significantly more susceptible to hypoxia and post-mortem (Kemp and Brown, 1984; Whitehead et al., 1992 Mills et al., 1993; Mills and Rubel, 1994; Frolenkov et al., 1998). Studies using gentamicin-treatment (Brown et al., 1989), high-level noise (Zurek and Leshowitz, 1976) and those in which the level of the endocochlear potential is reduced produce a similar effect; low-level DPOAEs are severely compromised whilst high-level DPOAEs remain relatively stable.

Despite the apparent differences in vulnerability between the 'high-level' component and 'low-level' component, the 'high-level' component is susceptible to cochlea manipulations under certain conditions. Some acoustic traumas can affect the 'high-level' component (Wiederhold and Mahoney, 1985; Whitehead et al., 1992), as can treatments with a combination of aminoglycosides and ethacrinic acid (Whitehead et al., 1992). Blocking OHC electromotility also suppresses the 'high-level' component (Frolenkov et al., 1998) leading to speculation that it is generated partially as a consequence of OHC motility. In this case the difference in the susceptibilities of the two components would be a natural consequence of the differences in the way the cochlear operates at low and high sound pressure levels. At very low levels the response of the cochlear is increased through active amplification and as a result, attenuating this process will have greater consequences on DPOAEs. The contribution of the active process is relatively small at high levels and so its loss has less of an impact on the levels of DPOAEs potentially mediated by OHCs and their mechanical effects (Lukashkin et al., 2002).

Theoretical studies have demonstrated that the distinctive amplitude and phase patterns of DPOAEs can be approximated with a single saturating non-linearity (Lukashkin and Russell, 1998b), such as the MET transfer function of the hair cells and can be approximated by a two-exponential Boltzmann function (Chapter 2.3.3, for Boltzmann equation)(Crawford et al., 1989; Frank and Kossl, 1996; Frank and Kossl, 1997; Lukashkin and Russell, 1998a; Lukashkin and Russell, 2005a). The MET transfer function is often considered as the dominant non-linearity, being the strongest non-linearity in the periphery of the auditory system (Patuzzi et al., 1989b; Santos-Sacchi, 1993), although in a system as non-linear as the cochlea it must be remembered that other sources of non-linearity will contribute. However if we consider DPOAE generation at the output of a single-saturating non-linearity then we can describe it mathematically. Under conditions where the input signals *L1* and *L2* with frequencies f_1 and f_2 are small enough, the output signal , N(x), can be approximated by a Taylor series at x = 0 (Lukashkin and Russell, 2005b).

$$N(x) = \sum_{n=0}^{\infty} \frac{1}{n} \cdot \frac{d^n N\,(x)}{dx^n}_{x=0} \cdot [L_1 \sin(2\pi f_1 t) + L_2 \sin(2\pi f_2 t)]^n$$

$d^nN(x)/d^xn\,|_{x=0}$ is the nth derivative of N(x) at the point x = 0. Absolute values of the first few derivatives of the MET transfer function are illustrated in (Figure 3.1). The function is taken from experimental data of the MET transfer function and has additionally been modified to have approximately 50% of transducer conductance activated at rest (N(0)~0.5). This level of conductance is believed to reflect *in vivo* conditions of OHCs (Russell et al., 1992; Legan et al., 2000).

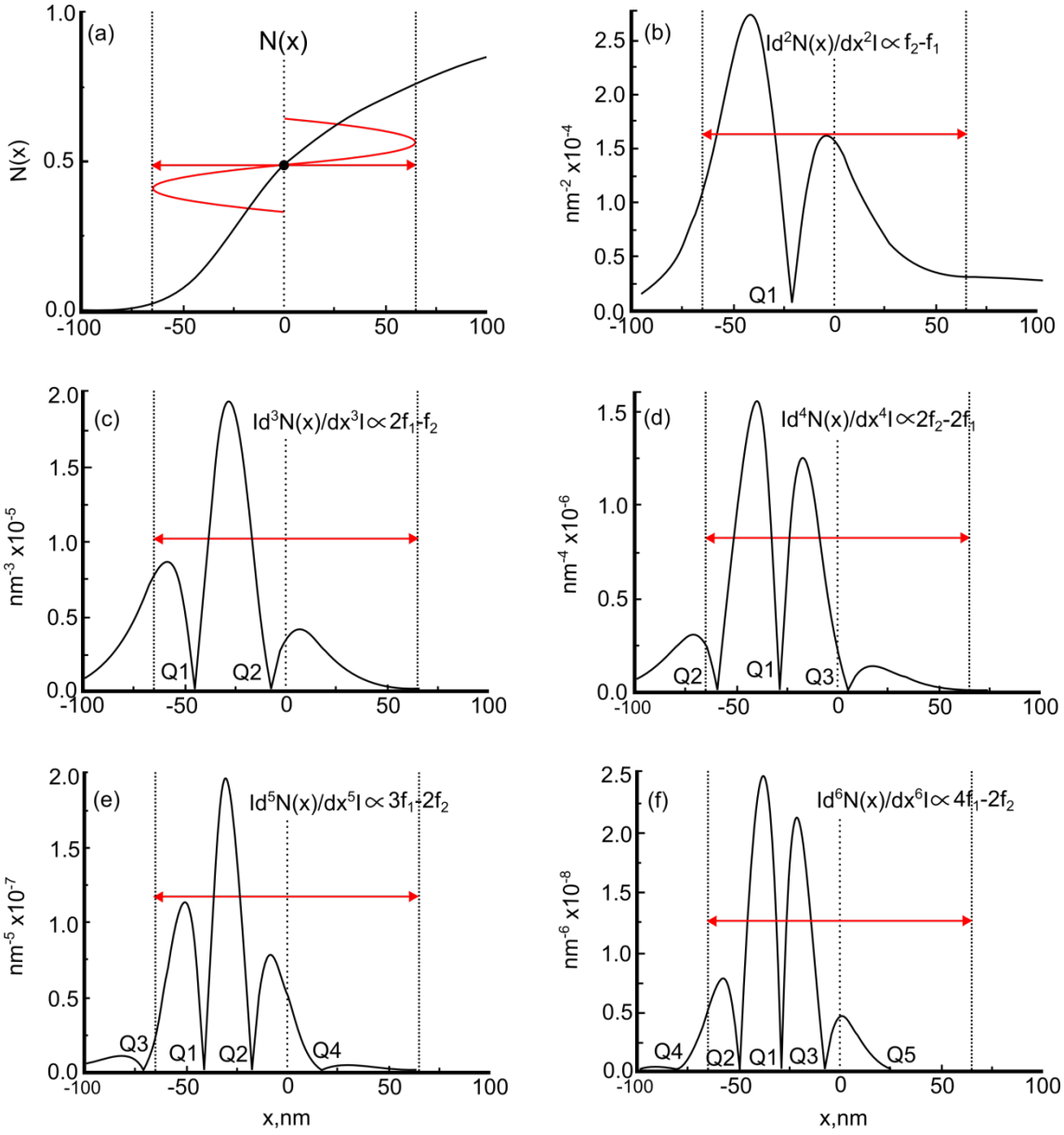

Figure 3.1 Absolute value of the first few derivatives (b-f) of a normalised non-linear I/O function of N(x) of the OHC MET function (a). *N(x)* is obtained by $N(x)=1/\{1+exp(a_2[x_2-x_0-x])[1 + exp(a_1[x_1-x_0-x])]\}$, *x* is bundle displacement in nm. The constant x_0 ~ 49nm is used to set the resting OP to 50% of transducer conductance with given constants obtained from experimental measurements a_1 = 0.065 nm^{-1}, a^2 = 0.016nm^{-1}, x^1 = 24 nm, x^2 = 41 nm (Géléoc et al., 1997). Shown within each panel is the derivative and the distortion product it is proportional to. Red double ended arrow shows schematically the modulation resultant form a low frequency tone, one cycle of which is shown in panel (a). Labels Q indicate the minima (notches) found at certain points within each of the derivatives (Adapted from Lukashkin and Russell, 2005b)

The Boltzmann model can predict the amplitude of distortion products as a function of the operating point (OP) position on the transfer function. The OP is a location on this function where the input is applied. It is important to note that Figure 3.1 shows absolute values of the derivatives of the MET transfer function and that distortion products amplitude will be proportional to the absolute value of the derivative. As the absolute value of the derivative

becomes zero at the points where it changes its sign, so too does the amplitude of the distortion product become zero (notches), labelled Q in Figure 3.1. At the points Q the phase angle of the distortion product flips by 180˚, which corresponds with an inversion in the sign of the derivative. The figure illustrates that by shifting the position of the OP of the non-linear transfer function that underlies the DPOAE it should be possible to observe distinctive maxima and minima (notches) in DPOAE amplitude. These maxima and minima would be proportional to the absolute values of the derivatives of the non-linear transfer function (Lukashkin and Russell, 2005b). Experimental studies have demonstrated by using a low frequency biasing tone, to shift the OP of the transducer, that DPOAEs amplitudes can be predicted by the Boltzmann model (Frank and Kossl, 1996; Frank and Kossl, 1997; Lukashkin and Russell, 2005b). Further studies have demonstrated that by fitting the CDPOAE, $2f_1$-f_2, which has been modulated by a low-frequency, high level tone, with the third derivative of the transducer function the underlying non-linear transducer function can be derived (Bian et al., 2002; Bian et al., 2004; Bian and Scherrer, 2007).

The dependence of cubic DPOAE (CDPOAE), $2f_1$-f_2, amplitude on the OP resting position could account for the different characteristics described earlier in rodent and human DPOAE growth functions whilst maintaining that their mechanistic origin is the same (Lukashkin and Russell, 2005b). Assuming that the resting OP is situated close to the point of inflection of the human transfer function, then it would not be possible to see notches in the DPOAE growth function and differences between human and rodent growth-functions could simply be explained by differences in the resting OP (Lukashkin and Russell, 1999). Another significant influence in this model is the shape of the underlying transfer function, it is demonstrated in Figure 3.2 how this shape can influence the third derivative of the two transfer functions. A number of studies have demonstrated that the pattern of the CDPOAE $2f_1$-f_2 during acoustical biasing using a low frequency tone can be modelled on this derivative (Bian et al., 2002; Lukashkin and Russell, 2005b). Therefore it is possible that the OP in two systems can remain relatively similar but due to differences in the transfer function underlying the DPOAEs different responses can be obtained under certain stimulation conditions. Lukashkin and Russell (1999) demonstrated using differences in gain in the non-linear I/O function of the MET channel transfer function the resultant changes in the third derivative (Figure 3.2).

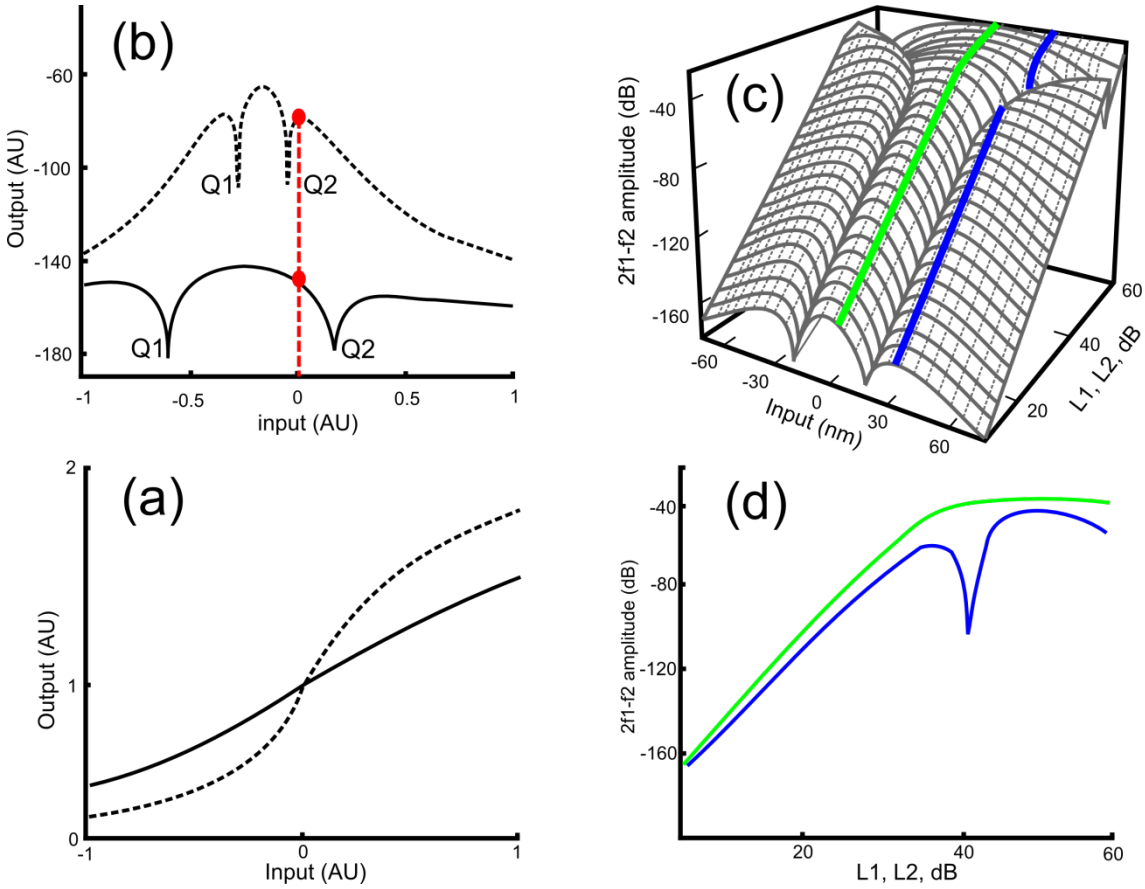

Figure 3.2 Figure 3.2 Boltzmann model of 2f1-f2 CDPOAE generation dependent on OP position, predictions in humans (green) and guinea pigs (blue). (a). Second order Boltzmann function curves with differing shapes. (b). Third derivatives of Boltzmann curves shown in fig.(a) and resting OP (red, dots and broken line), notches labelled Q1 and Q2. (c). Modelled third derivative with increasing levels, notches Q1 and Q2 deviate at higher levels of primaries. (c) and (d) theoretically differing OP positions in humans and guinea pigs could account for characteristic notch in guinea pig I/O function (Lukashkin and Russell, 1999).

In this chapter, we reconstruct the underlying transfer functions for the two species by analysing low frequency biased CDPOAEs and demonstrate that human and guinea pig DPOAEs modulation patterns can both be predicted theoretically as being due to the output of a single saturating non-linearity, under conditions where each species resting OP is different, or the underlying non-linearity has a different shape.

3.3 Results

Amplitude contour plots for CDPOAEs levels, recorded from a single guinea pig and human subject, during one and a half cycles of the low frequency biasing tone (horizontal axis) (30 Hz, 120 dB SPL) and increasing levels of the primaries (vertical axis) are shown in Figure 3.3 (guinea pig left panel, human right panel). The graphs are representative examples of recordings from 6 guinea pigs and 18 human subjects which all demonstrate similar modulation pattern to their respective representative examples in Figure 3.3. When compared, the contour plots of the two species reveal a number of similarities and differences in the modulation of CDPOAEs. Both plots consist of maxima and minima (notches,) over the period of the biasing tone, as previously reported in the study by Lukashkin and Russell (2005b) on guinea pigs and in other studies on humans (Bian and Scherrer 2007). Both patterns are predicted by the third derivative of a two-exponential Boltzmann function particularly at lower levels of the primary tones. Minima are indicated with white arrows in the figure and labelled Q1 or Q2 as they correspond with the two minima found in the third derivative (Figure 3.1 for model).

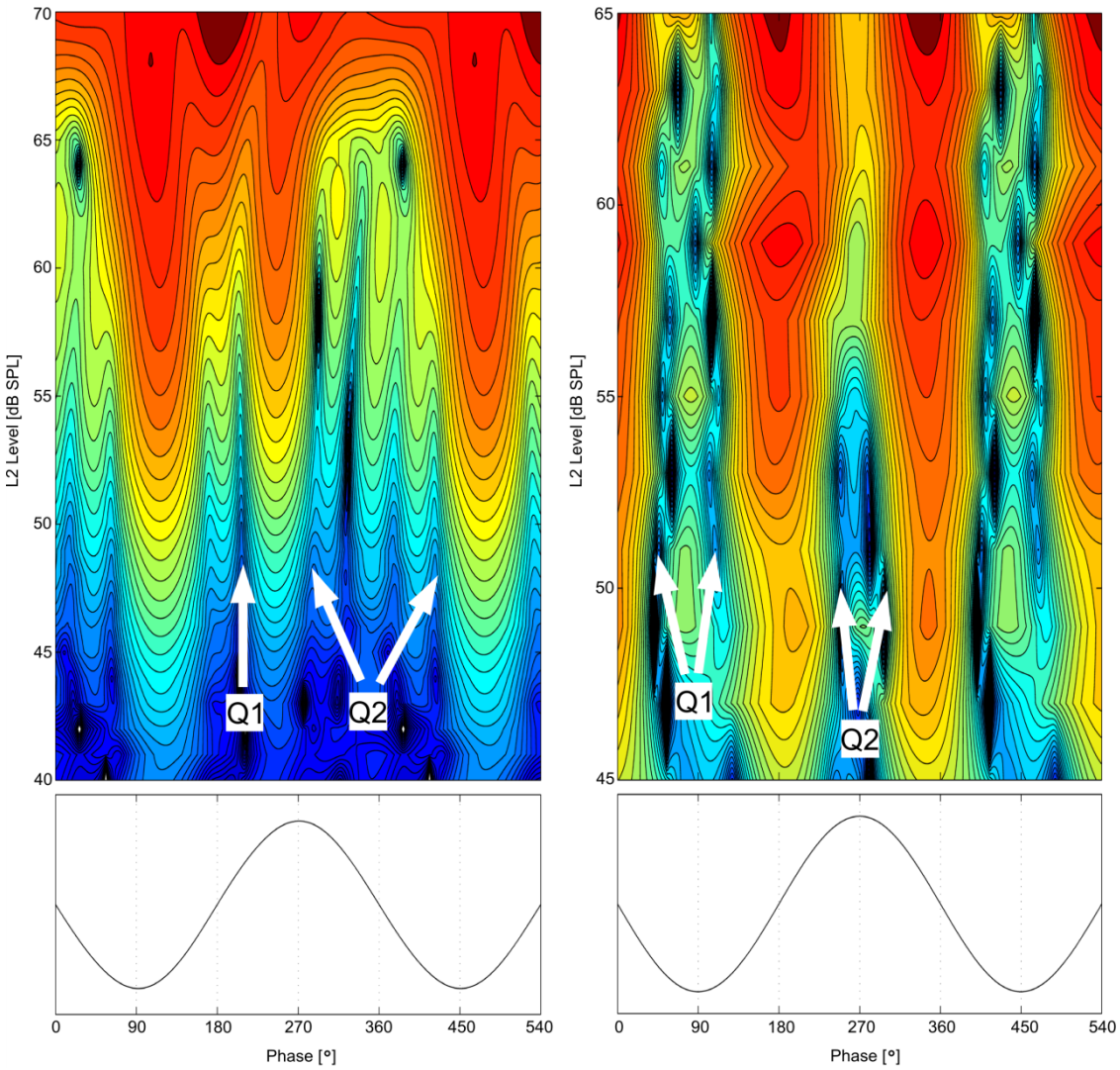

Figure 3.3 $2f_1$- f_2 Contour plots from DPOAE modulated over 1.5 cycles by a 30 Hz 120 dB SPL tone (horizontal axis and lower panels) over a range of primary tone levels (vertical axis) in a single guinea pig (left panel) and a single human (right panel). White arrows with labels show amplitude notches. f_2 is 2 kHz for human subject and 22 kHz for guinea pig subjects. f_2 / f_1 ratio is 1.22 in human and 1.22 in guinea pig. Maximum contour levels are 10 for panel Human and 40 for guinea pig. Contour intervals are 2 dB for human and 1.5 dB for guinea pigs.

The relationship between the modulated CDPOAE-level pattern and the biasing tone phase is different between the two species. As previously described in the guinea pig (Lukashkin and Russell 2005b) the third derivative of the Boltzman function predicts CDPOAE level minima (notches) Q1 or Q2 to correspond to maximum negative and positive biasing tone displacement respectively, with maximum CDPOAE amplitudes being found when the biasing tone induced BM displacement was zero (i.e at the zero-crossing of the biasing tone). In the guinea pig the experimentally derived contour plots lag the biasing tone by about 90˚ which is suggested to result from the cut off frequency of the helicotrema high pass filter (Lukashkin

and Russell 2005b). This lag is either not observed in the human data or corresponds to a lag of 180˚. The contour plots both show significant asymmetry during the rising and falling phase of the biasing tone. This hysteresis has been previously observed in guinea pig, gerbil and human CDPOAEs (Lukashkin and Russell 2005b; Bian and Scherrer 2007; Bian et al. 2004).

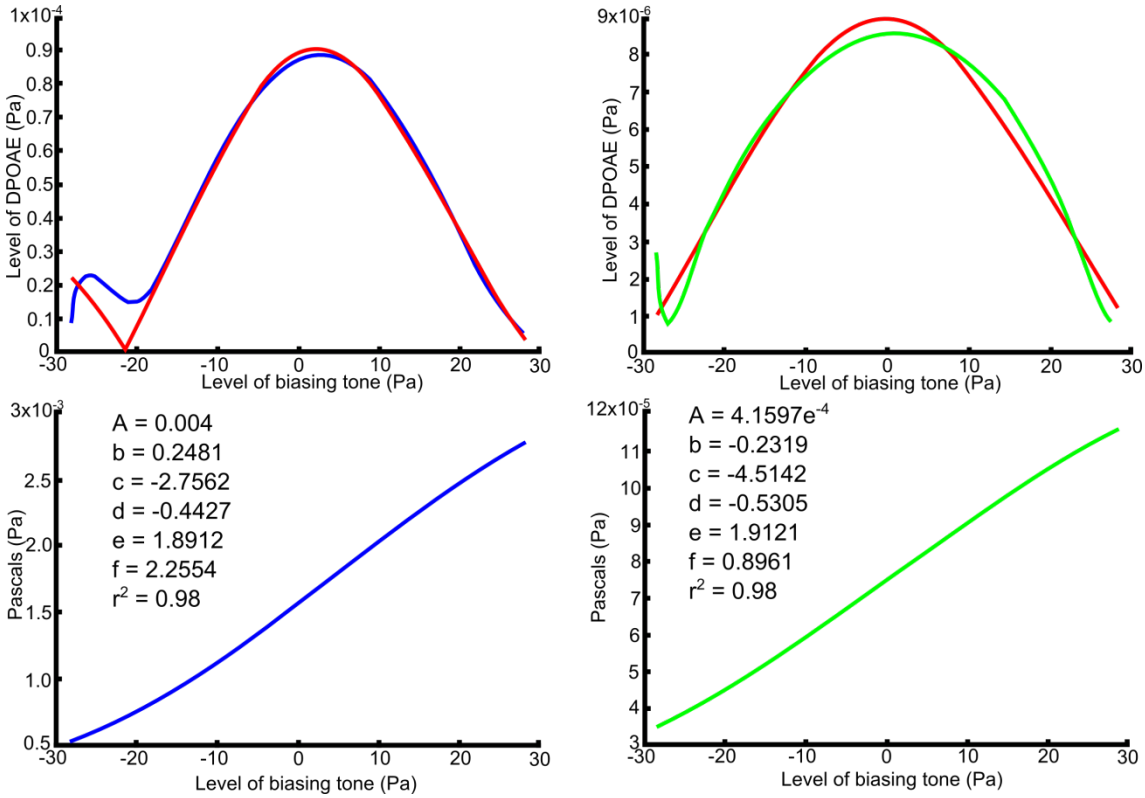

Figure 3.4 Underlying transfer function for modulation patterns (bottom panels) derived through fitting first half cycle (top panel) of selected modulation pattern with absolute value of the third derivative of a two-exponential Boltzmann function (red) in human (right, green) and guinea pig (left, blue). Bottom panels show correlation coefficient (r^2) and Boltzmann parameters for each fitted pattern (inset).

Individual CDPOAE modulation patterns at selected levels of the primaries were fitted with non-linear regression for the first half cycle and the second half cycle of the biasing tone in order to derive the theoretical underlying cochlear transfer function for guinea pigs (left panels) and humans (right panels), shown in Figure 3.4. The first half and second half cycles were fitted separately due to the strong asymmetry previously described. Similar fitting was performed across a range of *L2* values in both animals with the sampling range chosen on the basis that modelling of CDPOAE as the third derivative of the output of a single saturating non-linearity is only consistent at low levels of the primary tones (Lukashkin and Russell 2005b; Bian and Scherrer 2007). Therefore in all animals contour plots were inspected visually to establish sampling levels that were suitable, with CDPOAEs that were high enough to be above the noise floor but of sufficiently low level not to deviate from the proposed model, which was

indicated by the notches starting to deviate at higher levels. The fits obtained via this sampling were relatively good, all with a correlation coefficient (r^2) value between 0.80 and 0.99 (mean 0.94, ±0.01)(Table 3-1, Table 3-2, Table 3-3, Table 3-4).

Table 3-1 Curve fitting results in guinea pigs, rising half cycle of biasing tone. Fit parameters of a second-order Boltzmann function whose third derivative was fit to the data for individuals over a range of selected frequencies (kHz) and levels (L_2), over the rising half cycle of the biasing tone. Correlation coefficients (r^2) of the fits for the different primary frequencies and levels are listed, as are the resting operating point (OP), in pascals (Pa) and if the synthesised I/O function produced by supplying the sum of two sinusoids to the derived transfer function produced a notch.

Subject and f_1 (kHz)	L_2 (dB SPL)	A,b,c,d,e,f	r^2	Resting OP	Notch
GP 53, 22	45	0.0027, -0.1910, -0.8271, -0.3801, 0.6116, 3.0935	0.99	1.81	Y
	46	6.5899e-004, -0.3589, -3.8852, -0.4583, 2.9351, 2.0484	0.99	0.48	Y
	47	0.00077968, -0.3801, -3.9972, -0.4617, 3.1896, 1.9574	0.99	0.44	Y
	48	0.0011, -0.3639, -3.9042, -0.4625, 2.9611, 2.0355	0.99	0.44	Y
	49	0.0015, -0.3646, -3.9204, -0.4627, 2.9552, 2.0288	0.99	0.36	Y
	50	0.0018, -0.3907, -4.0892, -0.4659, 3.2903, 1.9412	0.99	0.25	Y
	51	0.0018, -0.3907, -4.0892, -0.4659, 3.2903, 1.9412	0.99	1.635	Y
GP 53, 28	44	3.5019e-004, -0.3811, -4.1985, -0.4999, 3.5255, 1.7294	0.99	2.2	Y
	45	5.1919e-004, -0.3789, -4.2482, -0.4953, 3.4659, 1.7682	0.99	1.68	Y
	46	6.8865e-004, -0.3813, -4.3543, -0.5046, 3.5296, 1.7452	0.99	1.76	Y
	47	0.0011, -0.3704, -3.9846, -0.4821, 3.2488, 1.8463	0.99	1.61	Y
	48	0.0011, -0.3878, -4.3566, -0.5048, 3.5332, 1.7481	0.99	1.51	Y
	49	0.0017, -0.3698, -3.9861, -0.4833, 3.2323, 1.8414	0.99	1.59	Y
GP 56, 22	50	0.0020, -0.2433, -2.9844, -0.4500, 1.7328, 2.5344	0.98	1.42	Y
	51	0.0030, -0.2322, -2.9371, -0.4527, 1.5945, 2.5989	0.98	1.34	Y
	52	0.0032, -0.2661, -3.2431, -0.4550, 1.8483, 2.4707	0.98	0.7	Y
	53	0.0050, -0.2399, -3.1122, -0.4582, 1.6141, 2.5694	0.98	0.7	Y
	54	0.0070, -0.2244, -3.0692, -0.4635, 1.4695, 2.6300	0.98	0.53	Y

	55	0.0089, -0.2227, -3.1191, -0.4638, 1.4422, 2.6530	0.98	0.36	Y
	56	0.0090, -0.2506, -3.3938, -0.4630, 1.6259, 2.5327	0.98	0.03	Y
GP 56, 26	52	9.8623e-004, -0.3156, -3.3541, -0.4474, 2.8745, 2.1558	0.92	2.6	Y
	53	0.0013, -0.3236, -3.3634, -0.4502, 2.8187, 2.0762	0.95	2.56	Y
	54	0.0024, -0.2831, -2.9213, -0.4388, 2.2585, 2.2864	0.97	1.65	Y
	55	0.0040, 0.2481, -2.7562, -0.4427, 1.8912, 2.4330	0.98	2.27	Y
	56	0.0093, -0.2158, -1.4619, -0.4012, 1.1640, 2.8433	0.98	1.96	Y
GP 56, 29	46	0.0023, -0.2729, -2.6760, -0.4332, 2.1935, 2.4605	0.97	2.97	Y
	47	0.0057, -0.2240, -1.4966, -0.3990, 1.3179, 2.9516	0.97	2.84	Y
	48	2.9516, -0.2121, -1.2735, -0.3989, 1.1688, 3.0373	0.98	2.71	Y
	49	0.0132, -0.2332, -0.5138, -0.3593, 0.4112, 3.3122,	0.98	2.67	Y
	50	0.0190, -0.2103, 0.0070, -0.3708, 0.1950, 3.3578	0.98	2.63	Y

Table 3-2 Curve fitting results in guinea pigs, falling half cycle of biasing tone. Fit parameters of a second-order Boltzmann function whose third derivative was fit to the data for individuals over a range of selected frequencies (kHz) and levels (L_2), over the falling half cycle of the biasing tone. Correlation coefficients (r^2) of the fits for the different primary frequencies and levels are listed, as are the resting operating point (OP), in pascals (Pa) and if the synthesised I/O function, produced by supplying the sum of two sinusoids to the derived transfer function, produced a notch.

Subject and f_1 (kHz)	L_2 (dB SPL)	A,b,c,d,e,f	r^2	Resting OP	Notch
GP53, 22	48	6.8833e-004, -0.5655, -0.7509, -0.8433, -3.5232, 3.8588	0.93	5.74	Y
	49	0.0012, -0.5113, -0.5690, -0.7750, -3.4876, 3.8968	0.93	4.88	Y
	50	0.0017, -0.5074, -0.5507, -0.7650, -3.3761, 3.8281	0.94	4.98	Y
	51	4.2799e-005, -0.7039, -7.6324, -0.7386, 7.8870, 1.4966	0.95	4.81	Y
	52	0.0032, -0.4890, -0.5180, -0.7380, -3.2720, 3.7819	0.95	4.80	Y
	53	0.0023, -0.5056, -0.5779, -0.7608, -3.3521, 3.8141	0.94	5.04	Y
GP53, 28	46	4.1203e-004, -0.5757, -0.9115, -0.7918, -3.8265, 3.9043	0.84	6.2	Y
	47	5.6301e-004, -0.5926, -1.0381, -0.8128, -3.9183, 3.8990	0.87	6.87	Y
	48	7.9722e-004, -0.5764, -1.0112, -0.7831, -	0.87	6.66	Y

		3.9112, 3.8871			
	49	5.4935e-004, -0.4791, -4.5476, -0.3451, 3.5636, 2.5231	0.87	7	Y
	50	0.0011, -0.4324, -4.0721, -0.3041, 2.3003, 2.8900	0.84	7.05	Y
	51	0.0018, -0.3719, -3.8886, -0.3373, 0.9908, 3.0569	0.87	6.92	Y
GP56, 22	51	0.0046, -0.2530, 2.3135, -0.4737, -1.0636, 3.5493	0.88	4.05	Y
	52	0.0046, -0.2530, 2.3135, -0.4737, -1.0636,3.5493	0.88	4.05	Y
	53	0.0084, -0.1372, 1.9346, -0.4135, 0.2728, 4.2769	0.9	2.23	Y
	54	0.0114, -0.1332, 1.0659, -0.3921, 0.4290, 4.4716	0.91	1.89	Y
	55	0.0144, -0.1473, 0.3622, -0.3797, 0.3256, 4.5605	0.92	1.55	Y
	56	0.0176, -0.1599, 0.0662, -0.3724, 0.1917, 4.7279	0.93	1.31	Y
GP56, 26	54	0.0011, -0.5743, 0.2609, -0.9150, -3.1369, 3.7038	0.87	0.15	Y
	55	0.0012, -0.5776, 0.2068, -0.8743, -3.0273, 3.5015	0.88	0.5	Y
	56	0.0017, -0.5597, 0.1067, -0.8417, -3.0652, 3.6177	0.88	1.18	Y
	57	0.0022, -0.5601, -0.0241, -0.8302, -3.0852, 3.6164	0.89	1.9	Y
	58	0.0028, -0.5515, -0.0873, -0.8065, -3.1423, 3.6832	0.89	2.22	Y
GP56, 29	49	0.0016, -0.6174, 0.3013, -1.0288, -2.9733, 3.6486	0.8	0.27	Y
	50	0.0020, -0.6112, 0.2121, -0.9751, -3.0157, 3.6531	0.83	0.28	Y
	51	0.0026, -0.6005, 0.1185, -0.9147, -3.0375, 3.6950	0.86	0.88	Y
	52	0.0032, -0.5994, 0.0663, -0.8972, -3.0594, 3.7567	0.86	0.86	Y
	53	0.0038, -0.6017, 0.0378, -0.8878, -3.0150, 3.7902	0.86	0.86	Y

Table 3-3 Curve fitting results in humans, rising half cycle of biasing tone. Fit parameters of a second-order Boltzmann function whose third derivative was fit to the data for individuals over a range of selected frequencies (kHz) and levels (L_2)**.** Correlation coefficients (r^2) of the fits for the different primary frequencies and levels are listed, as are the resting operating point (OP) and if the synthesised I/O function produced by supplying the sum of two sinusoids to the derived transfer function produced a notch.

Subject and f_1 (kHz)	L_2 (dB SPL)	A,b,c,d,e,f	r^2	Resting OP	Notch
Connie, 2	37	2.9563e-004, -0.2840, -5.0450, -0.5643, 2.9186, 0.8904	0.96	2.28	N
	39	1.3222e-004, -0.3713, -6.8840, -0.6975, 3.8628, 0.6487	0.98	1.56	N
	41	2.3882e-004, -0.3293, -6.5783, -0.6558, 3.5648, 0.7274	0.98	1.87	N
	43	2.3392e-004, -0.3665, -6.9866, -0.6991, 3.9243, 0.6314	0.99	1.94	N
Elena, 2	47	1.3414e-004, -0.3364, -5.1679, -0.5143, 3.2841, 0.7074	0.97	0.23	N
	49	-5.6144e-005, -0.4035, -7.1554, -0.7053, 4.2739, 0.5061	0.81	1.2	N
	51	1.6408e-004, -0.3095, -5.0508, -0.5231, 2.9647, 0.7452	0.96	0.2533	N
	53	4.1597e-004, -0.2319, -4.5142, -0.5305, 1.9121, 0.8961	0.98	0.0404	N
	55	3.4504e-004, -0.3038, -4.9919, -0.5187, 2.9215, 0.7898	0.98	0.74	N
	57	0.0025, -0.1733, -2.2488, -0.3371, 1.1715, 1.3744	0.97	1.0025	N
Micha, 1.690	37	7.5112e-005, -0.4562, -6.7336, -0.7951, 4.1219, 0.5740	0.98	2.29	N
	39	2.6936e-004, -0.3157, -6.2668, -0.6348, 3.4039, 0.7662	0.97	1.99	N
	41	1.7882e-004, -0.3712, -6.5951, -0.6920, 3.7653, 0.6940	0.98	1.79	N
Sabina, 1.690	41	2.3923e-004, -0.2858, -6.2714, -0.6211, 3.6436, 0.6389	0.95	4.5	N
	43	2.2679e-004, -0.3085, -6.5271, -0.6416, 3.7142, 0.6107	0.97	3.6	N
	45	2.1256e-004, -0.3051, -5.8546, -0.6534, 3.4732, 0.7178	0.92	4.7	N
	47	2.3272e-004, -0.3155, -6.2478, -0.6510, 3.5175, 0.6745	0.95	3.2	N
Tom, 1.690	47	6.2605e-005, -0.4349, -6.2396, -0.7758, 4.0876, 0.5328	0.97	5.6	N
	49	0.00010412, -0.3910, -6.5038, -0.7592, 4.0288, 0.5713	0.94	5.77	N
	51	1.5219e-004, -0.3605, -6.6809, -0.7283, 4.0775, 0.5760	0.98	5.2	N

Table 3-4 Curve fitting results in humans, falling half cycle of biasing tone. Fit parameters of a second-order Boltzmann function whose third derivative was fit to the data for individuals over a range of selected frequencies (kHz) and levels (L2). Correlation coefficients (r2) of the fits for the different primary frequencies and levels are listed, as are the resting operating point (OP) and if the synthesised I/O function produced by supplying the sum of two sinusoids to the derived transfer function produced a notch.

Subject and f_1 (kHz)	L_2 (dB SPL)	A,b,c,d,e,f	r^2	Resting OP	Notch
Connie, 2	37	1.2765e-004, -0.3074, -5.5442, -0.6438, 3.3685, 0.7531	0.92	4.45	N
	39	0.000075924, -0.3892, -6.4746, -0.7507, 3.9151, 0.5861	0.93	4.09	N
	41	0.000091938, -0.4055, -6.3893, -0.7574, 4.0372, 0.5565	0.91	4.5	N
	43	0.00015786, -0.362, -6.5764, -0.7202, 4.0246, 0.5741	0.93	4.91	N
Elena, 2	47	0.000060497, -0.3962, -6.1818, -0.7242, 3.8018, 0.5992	0.96	3.04	N
	49	0.00024884, -0.2796, -4.319, -0.5586, 2.7425, 0.9715	0.96	3.06	N
	51	0.00022621, -0.2783, -4.7792, -0.5709, 2.8374, 0.9247	0.93	2.8	N
	53	0.00021334, -0.3003, -5.4906, -0.5863, 3.1037, 0.7805	0.98	1.79	N
	55	0.00032182, -0.2711, -4.8914, -0.5758, 2.8782, 0.8625	0.97	3.32	N
	57	3.5457e-004, -0.2645, -5.6112, -0.5742, 3.1708, 0.7484	0.97	3.04	N
Micha, 1.690	37	2.2081e-005, -0.6018, -6.3979, -0.9830, 5.0064, 0.6301	0.91	9.54	N
	39	2.9721e-005, -0.5734, -6.0421, -0.9975, 4.7011, 0.7313	0.83	10.4	N
	41	0.00006055, -0.4473, -6.8949, -0.8124, 4.6385, 0.5283	0.89	6.4	N
Sabina, 1.690	41	3.4141e-004, -0.2905, -5.0662, -0.5324, 3.0402, 0.7197	0.99	1.68	N
	43	2.0378e-004, -0.3369, -5.7143, -0.5954, 3.6197, 0.5824	0.96	2.35	N
	45	0.0017, -0.1756, -3.1819, -0.3985, 1.7522, 1.1472	0.95	1.56	N
	47	4.7510e-004, -0.2713, -4.8167, -0.5282, 2.7971, 0.8366	0.99	1.88	N
Tom, 1.690	47	1.5170e-004, -0.3270, -5.9149, -0.6296, 3.2909, 0.7555	0.98	1.49	N
	49	2.6411e-004, -0.2937, -5.8721, -0.6134, 3.2418, 0.7331	0.97	2.58	N
	51	4.9345e-004, -0.2639, -5.0659, -0.5518, 3.1525, 0.7348	0.97	3.69	N

The resting OP is taken as the resting position of the organ of Corti or its position during zero crossing of the sinusoidal input. A measure of the resting OP of each derived transfer function was obtained within the analysis program by calculating the distance in pascals of the 0 crossing point from the point of inflection (Table 3-1Table 3-3). Mean of human resting OP 2.49 ± 1.83 Pa, mean of guinea pig resting OP 1.52 ± 0.91 Pa.

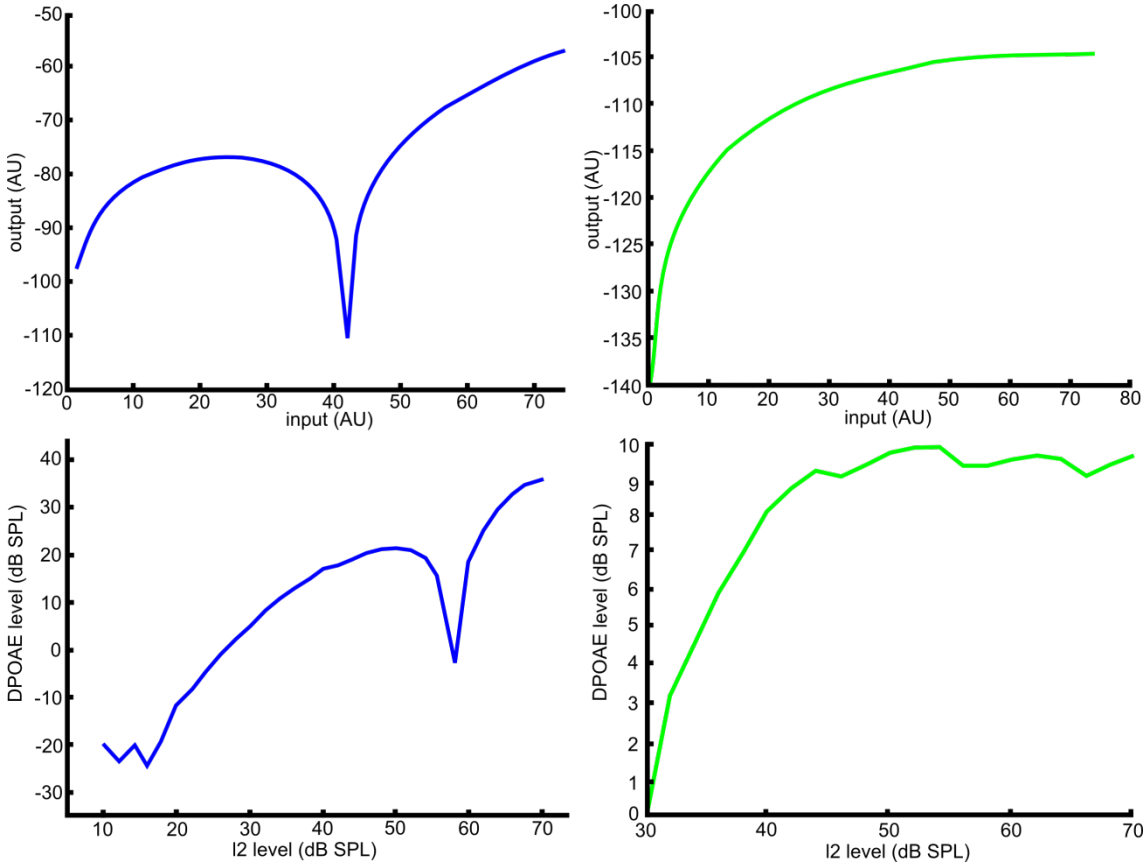

Figure 3.5 Reconstructed level function (top panels) derived through supplying predicted transfer function for guinea pig (left, blue) and human (right, green) previously obtained in Figure 3.4 with two sinusoidal inputs, all units in top panels are arbitrary. Experimentally obtained I/O functions (bottom panel) from human (right, green) and guinea pig (left, blue) are shown for comparison.

Reconstructed I/O functions created by supplying the derived transfer function for human and guinea pig subject, shown in Figure 3.4, with an input to produce predicted CDPOAE I/O level function is shown in the top two panels in Figure 3.5 (Guinea pig left panel, human right panel). For comparison the bottom two panels show experimental DPOAE level function results (guinea pig bottom left panel, human bottom right panel). Modelled CDPOAE level functions are qualitatively similar to those found experimentally, at low levels of the primary tones the initial growth of the CDPOAE of both species is monotonic. In humans this growth slows and eventually saturates at higher levels, in guinea pigs the growth becomes non-monotonic, a minima occurs at higher levels before returning to growth and then saturation.

All synthesised I/O functions displayed a clear notch for guinea pigs and no notch for humans (Table 3-1, Table 3-3). Results were consistent for both species and synthesised CDPOAE level functions are representative of all remodelling performed.

3.4 Discussion

The present study demonstrates through a combination of experimental investigation and modeling that CDPOAE amplitude growth functions can be predicted by the third derivative of the output of a single saturating nonlinearity in both humans and rodents. CDPOAE contour plots for guinea pigs and humans (Figure 3.3) show a series of maxima and minima during the time course of a biasing tone that are predicted when using the third derivative model for CDPOAE generation. Differences in CDPOAE growth funtions, such as the characteristic and consistent notch and phase shift observed in guinea pigs but not in humans, are accounted for within this model through differences in the resting OP of the two species or in the shape of the underlying transfer function. For example in humans this resting OP would be located centrally on the transfer function at or around its steepest point whereas in guinea pigs the resting OP would be biased to the more positive end of the transfer function. Alternatively or possibly in conjunction with a resting OP difference between species the non-linearity underlying the third derivative could have a different shape and so in guinea pigs for example, its resting OP may be located on one of the side lobes of the third derivative whereas in human it would be positioned on the central lobe (see Figure 3.2). The characteristic notch found in rodents is due to minima found in the third derivative deviating at high SPLs and intersecting the guinea pig growth function (Figure 3.2), the resting OP of humans mean that under normal circumstances its growth function never intersects this notch. The results from this study support differences in non-linearity shape underlying the position of the resting OP on the third derivative as both guinea pig and human resting OPs are close to the point of inflection. The finding that both species have resting OPs close to the point of inflection is not surprising as this positioning in the MET transfer function, reflected in CM recordings, has been predicted to increase the sensitivity of the OHCs (Russell and Sellick, 1978). It is not possible to make a direct comparison of the resting OP between guinea and human as with the current measure quantifying resting OP position does not account for species differences in suseptability to bias (Marquardt et al., 2007b). It has been demonstrated theoretically that changes in the underlying gain of the cochlear amplifier could lead to changes in the shape of the MET transfer function (Lukashkin and Russell, 2005b). This could account for why, despite both guinea pig and humans not having particularly biased reconstructed transfer functions, their resting OPs could lead to very different I/O growth functions (Figure 3.2). There are certainly differences in sensitivity between humans and rodents, the CAP threshold curves in guinea pigs can be up to 20 dB more sensitive than psychoacoustic measures from humans and it has been shown experimentally that changing the gain of the cochlear amplifier in rodents can

affect DPOAE components consistent with changes in the transfer function and resultant changes in third derivative shape (Frank and Kossl, 1996). Reconstructing the underlying transfer functions from the experimentally obtained data for the two species (Figure 3.4) shows human's and rodent's data are as predicted under the Boltzmann model. When these transfer functions are remodelled to produce a CDPOAE growth function, the results are qualitatively similar to those obtained experimentally from rodents and humans (Figure 3.5). Taken together the results from this study provide strong support for the comparability between human and rodent DPOAEs under low levels of the primaries and with the correct understanding of a difference in the species operating points. The study does not support the 'active'/ 'passive' model of DPOAE generation or a distinct difference in DPOAE generation mechanism between humans and rodents at least at low levels of the primaries (Mills, 1997; Whitehead, 1998; Avan et al., 2003; Shera, 2004; Rhode, 2007).

It is predicted from the experimentally obtained CDPOAE contour plots (Figure 3.3), fitting and re-modelling results (Figure 3.4, Figure 3.5) from this study that the non-linearity largely responsible for generating CDPOAEs in humans and rodents can be predicted by the output of a single sigmoidal non-linearity and is spatially localised. We can only speculate as to the identity of the sigmoidal non-linearity or indeed non-linearity's. As a dominant non-linearity in the hearing periphery one strong candidate is the MET transfer function, however findings of its strong symmetrical appearance from *in vivo* recordings in guinea pigs (Russell and Sellick, 1983) and reflected in CM recordings would at first glance seem to rule out it completely underlying what we have found as an asymmetrical transfer function in CDPOAEs in guinea pigs and humans. However, shifts of only a few nanometres for a system with positive feedback could have profound effects on the transfer level functions of humans and guinea pigs that fit with the findings of this study and the observation of both species having resting OPs slightly biased in the positive direction has been observed experimentally with both CM recordings (Dallos, 1986; Cody and Russell, 1987; Dallos and Cheatham, 1989) and in DPOAE experiments where the OP was shifted by electrical and acoustic biasing (Frank and Kossl, 1996; Frank and Kossl, 1997). Our findings cannot rule out the contribution of other non-linearities to CDPOAE generation found in the peripheral hearing system. For instance, a recent study on stereocillin knock-out mice suggested non-linear stereociliary hair bundle stiffness could contribute to DPOAE generation. It is also widely recognized that in humans a second source of DPOAE generation (place fixed) at the CF contributes to the overall emission and is believed to account for the inconsistent notches found in human CDPOAE level functions through a phase cancellation mechanism. This second source of emission is less prominent in

rodents which is believed to be due to anatomical differences between species (Shera, 2004). It is also the case that the Boltzmann model predicts a 'perfect' point like non-linearity whereas in reality *in vivo* the DPOAEs are generated over an extended region of the cochlear partition with some phase gradients along this region (Russell and Nilsen, 1997). We attempted to mitigate this affect in this study by using low level DPOAEs that would be generated from a relatively spatially localised region and by optimising the wave ratios for wave fixed generation. Despite other potential sources of non-linearity we find that at the stimulation parameters used in this investigation, CDPOAE amplitude is predicted to be mostly generated by a single saturating non-linearity that is spatially localized, as any significant extra non-linearity's at other places would likely interact and not be predicted by the Boltzmann model.

The hysteresis observed in the contour plots (Figure 3.3) in this investigation and others across all species studied does not entirely fit the simple Boltzmann model of DPOAE generation and was why each half cycle of the biasing tone was fitted separately to derive the transfer functions. The origin of this hysteresis is still unknown but there are currently two promising candidates, one is that it is the result of negative dampening the result of active amplification within the cochlear, the other could be based on hair cell adaptation keeping the OP of the MET transfer function biased towards a specific point during sound simulation (Lukashkin and Russell, 2005b; Bian and Scherrer, 2007).

The phase relationship between the low-frequency biasing tone and modulation pattern is different between humans and guinea pigs. In guinea pigs the modulation pattern lags the biasing tone by approximately 90˚, which was previously observed by Lukashkin and Russell (2005b) whereas the human pattern shows either no phase lag or a lag of 180˚ that if present is difficult to identify because CDPOAE resultant from any shift would appear at least to correspond to correct maxima and minima for biasing of the CDPOAEs (Figure 3.3). The phase correspondance in humans is similar to that obtained in previous reports and has led to the suggestion that positive and negative biasing tone pressure results in a movement of the BM towards the Scala vestibuli and Scala Tympani respectively, at the CDPOAE generation location (Bian and Scherrer, 2007). This 180˚ phase lag is predicted from psychoacoustic investigations and animal experiments in species with similar cochlea anatomy to humans. Human psyschoacoustic investigations observing masking period patterns of low-frequency maskers found that below 40 Hz the second derivative of the sound pressure at the eardrum is responsible for the masking period pattern found which corresponds to a 180˚ phase difference between tympanic membrane displacement and BM movement (Zwicker, 1977).

Acoustic investigations in humans and guinea pigs (Marquardt et al., 2007b) and CM recordings in a number of mammalian species with differing cochlear morphologies (Dallos, 1970) have all predicted BM phase shifts of 180˚ in humans. This phase lag difference between humans and guinea pigs is predicted to result from the different anatomies of the cochlea in the two species, particulary the relative sizes of their helicotremas and the resultant differences in cut-off frequencies due to this. Based on the phase correspondance between modulation pattern and biasing tone found in this investigation combined with experimental results in humans we postulate that when using a low-frequency biasing tone below 40 Hz to modulate CDPOAEs positive and negative biasing tone pressures correspond to a movement of the BM towards the SV and ST respectively, agreeing with previous studies (Zwicker, 1977; Marquardt et al., 2007b).

4 EFFECTIVE, SIMULTANEOUS COCHLEAR STIMULATION AND PRESSURE RELIEF THROUGH THE ROUND WINDOW IN GUINEA PIGS

4.1 Abstract

The round window (RW) membrane functions as a pressure relief valve in conventional hearing allowing structures of the middle ear to move. Investigations in recent years have shown that active middle ear prosthesis can be used to stimulate the cochlea via the RW. This technique has been used occasionally in clinical applications but more thorough theoretical and empirical studies are required in order to make it more effective. Guinea pigs were used as test subjects to investigate the physiological effects of RW stimulation using a simulation of an active middle ear prosthesis, namely a cylindrical neodymium iron boron disk magnet placed upon the RW, which can be stimulated by an electromagnetic coil positioned in close proximity to the magnet. The cochlear neural threshold did not change after placement of the magnet on the RW. The coil voltage - magnet displacement relationship was linear. Magnet displacement threshold curves revealed the high sensitivity of the cochlea to RW stimulation in the sub-nanometre range. When the cochlea was driven with an active middle ear prosthesis through the RW, ossicular movement was observed only at low frequencies <7 kHz and high stimulation amplitudes. Mobility of the stapes was not necessary for successful cochlear stimulation through the partially occluded RW and neural thresholds to the RW stimulation remained unchanged after immobilisation of the ossicular chain. The relatively high impedance of the ossicles as seen from the cochlea and the fact that the magnet did not entirely cover the RW, enabled that part of the RW not covered by the magnet to function as a pressure shunt during RW stimulation. We propose that the basilar membrane (BM) in these experiments was driven directly via near-field pressure variations generated in the vicinity of the RW by vibrations of the magnet.

4.2 Introduction

The RW membrane of the cochlea acts as a pressure relief valve for the incompressible cochlear fluids, making movement of the stapes and, as a consequence, movement of the structures of the inner ear possible. It has been known for some time (e.g. see Culler et al., 1935) that the efficiency of cochlear function is impaired when the RW membrane is immobilised or simply thickened. Hearing performance is also affected as a consequence of conductive or mixed hearing loss when the RW is congenitally malformed or absent (Martin et al., 2002; Linder et al., 2003; Borrmann and Arnold, 2007). Clinical observations reveal not only the physiological importance of the RW membrane for the hearing process but also its high vulnerability and the necessity to retain it during surgical manipulations within the middle and inner ear (e.g. during insertion of cochlear implants using the scala tympani approach) (Roland and Wright, 2006). Traumatic damage or rupture of the RW membrane causes, in some cases, high-grade sensorineural hearing loss and deafness (Goodhill, 1971; Mertens, 1991; Rozsasi et al., 2003; Gedlicka et al., 2009).

It has been established however that, while normal function of the RW is important for effective stimulation of the cochlear through the conventional route, the cochlea can be stimulated successfully in non-conventional ways (through bone conduction, through the RW, and through perforations in the cochlea's apical turn, for example). Sensitivity and excitation patterns of the cochlea are similar through all of the above modes of excitation, at least in a linear (passive) regime (Wever et al., 1954; Békésy, 1960; Voss et al., 1996b). In recent years it has been shown that active middle ear implants can be used beneficially to stimulate the cochlea through the RW with significant recovery of the hearing thresholds (Colletti et al., 2006; Kiefer et al., 2006; Wollenberg et al., 2007; Koka et al., 2010). The RW approach could be an effective and preferable option for hearing rehabilitation in some cases of sensorineural and mixed hearing loss where conventional hearing aids cannot be used satisfactorily. This may include patients with chronic inflammatory middle ear diseases after multiple re-operations, or recurrent cholesteatoma, when the anatomy of the middle ear is highly distorted (Colletti et al., 2006). The RW approach for the cochlear stimulation may be indicated for patients with congenital malformations of the outer and middle ear. In this situation dysplasia and immobilisation of the ossicles, often in combination with malformations of the oval window, can make hearing reconstruction through the natural way impossible (i.e. through the oval window). Recent successful attempts to combine the outer and middle ear reconstruction with implantation of the active middle ear prostheses on the RW (Kiefer et al., 2006; Wollenberg et al., 2007) demonstrated the feasibility of the RW approach for these

difficult to cure disorders, as well as for some other conditions when the oval window is inaccessible. While successful in many cases, implementation of middle ear prostheses for RW stimulation has been based on trial and error without thorough theoretical and empirical studies which could make the outcome of this technique more predictable and effective in the clinical environment.

One of these uncertainties is related to the mechanisms of BM excitation using probes covering just a relatively small part of the RW membrane. The area of the RW not covered by the probe provides an effective pressure shunt in this case (Békésy, 1960). This might make excitation of the cochlea problematic because, as a consequence of the shunt, pressure variations that excite the BM might be expected to be small. It is also likely that mobility of the stapes is not essential for successful cochlear excitation through the RW if most of the pressure relief is provided by the exposed area of the RW. In this work we investigate the mechanisms of cochlear excitation and the importance of stapes mobility for successful cochlear excitation with a probe that partially covers the RW.

4.3 Results

The cochlear neural threshold to acoustic stimulation measured as a threshold for the N1 peak of the compound action potential (CAP) did not change after placement of the magnet on the RW and during the entire experiment (up to 3 hours after magnet placement) (Figure 4.1). Increases in the impedance of the RW leads to elevation of the hearing threshold (e.g. see Culler et al., 1935); thus the observed stability of the CAP thresholds after the magnet placement revealed that the area of the RW not covered by the magnet could provide effective pressure relief at acoustic frequencies when the cochlea is stimulated conventionally. This finding is not surprising when taking into account the small volume displacements of the cochlear fluid at the acoustic frequencies (Békésy, 1960). The exposed area of the RW might also be expected to provide an effective pressure shunt during RW stimulation (Békésy, 1960).

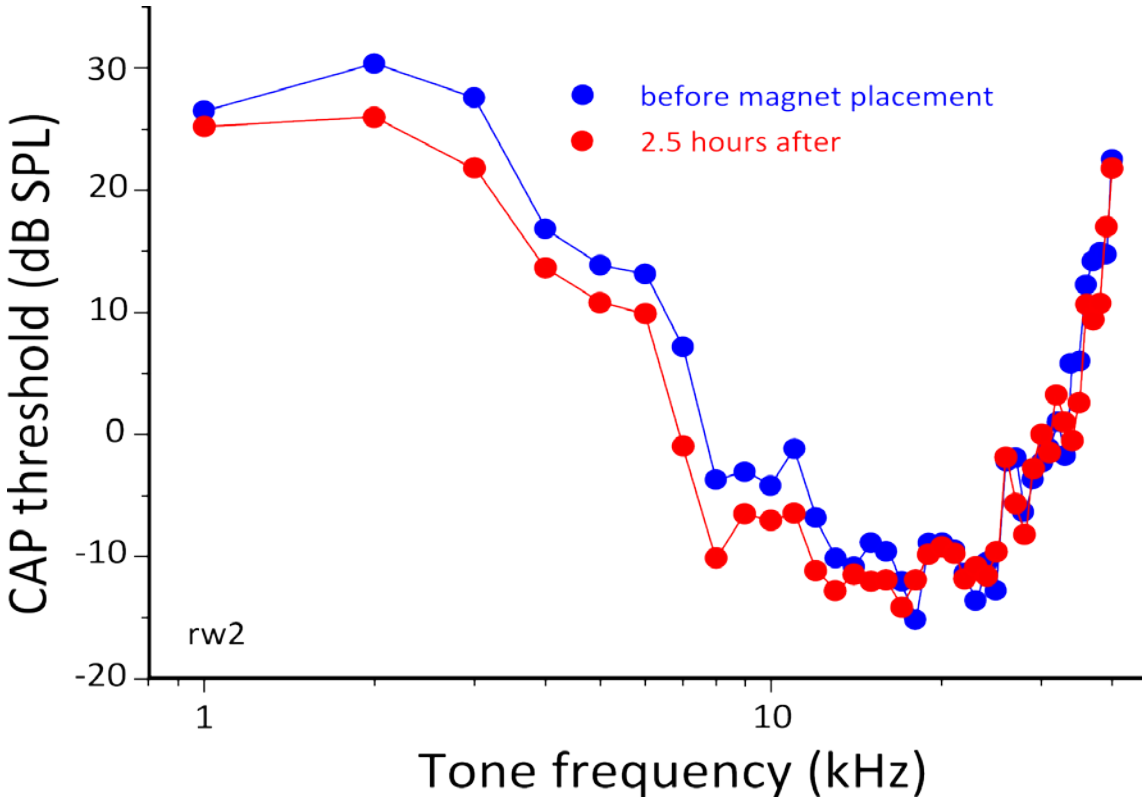

Figure 4.1 Thresholds for N1 peak of the CAP of the auditory nerve measured before (blue) and 2.5 hours after (red) placement of the magnet on the round window.

The coil voltage - magnet displacement relationship was linear in all preparations where this characteristic was studied (Figure 4.2).

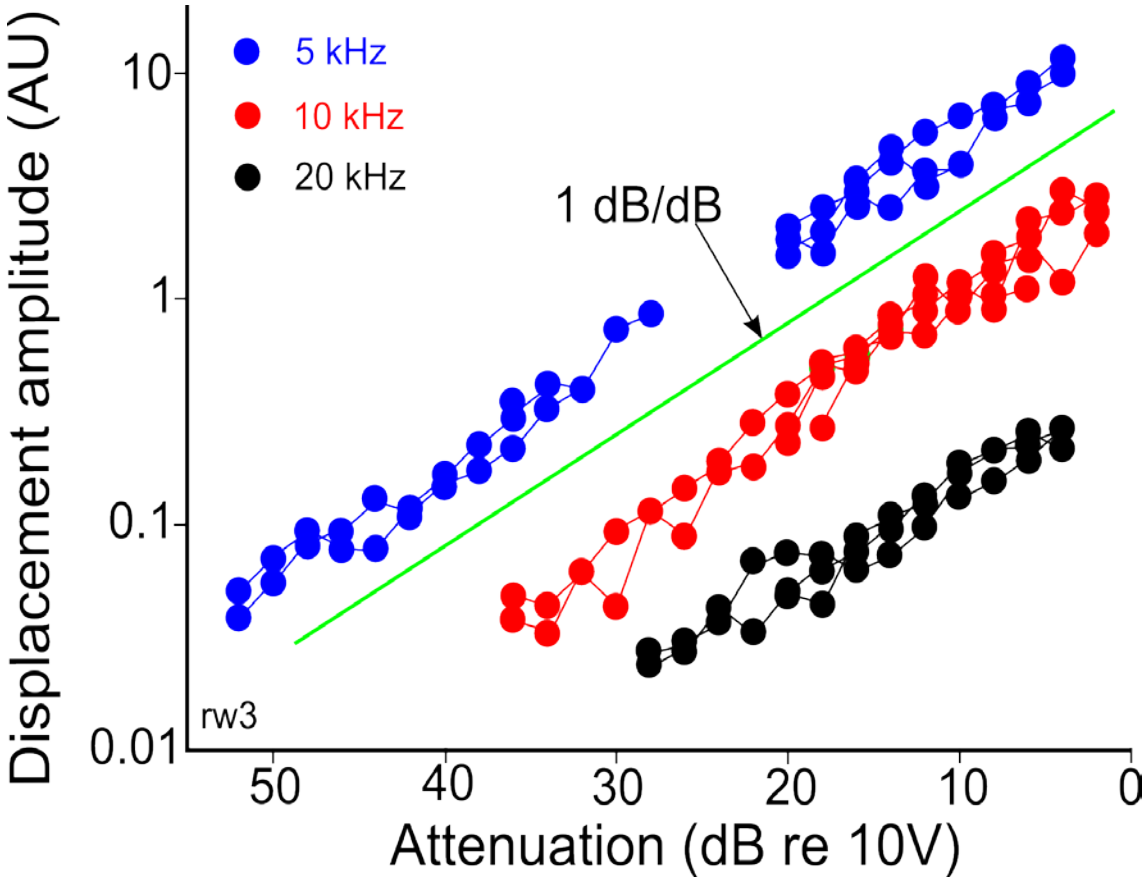

Figure 4.2 Magnet displacement as a function of voltage applied to the coil for three different frequencies of the stimulation (5, 10 and 20 kHz) recorded in one preparation.

In all preparations, frequency dependence of the magnet displacement resembled a low-pass filter characteristic with the high-frequency slope being between 12 - 18 dB/octave (Figure 4.3).

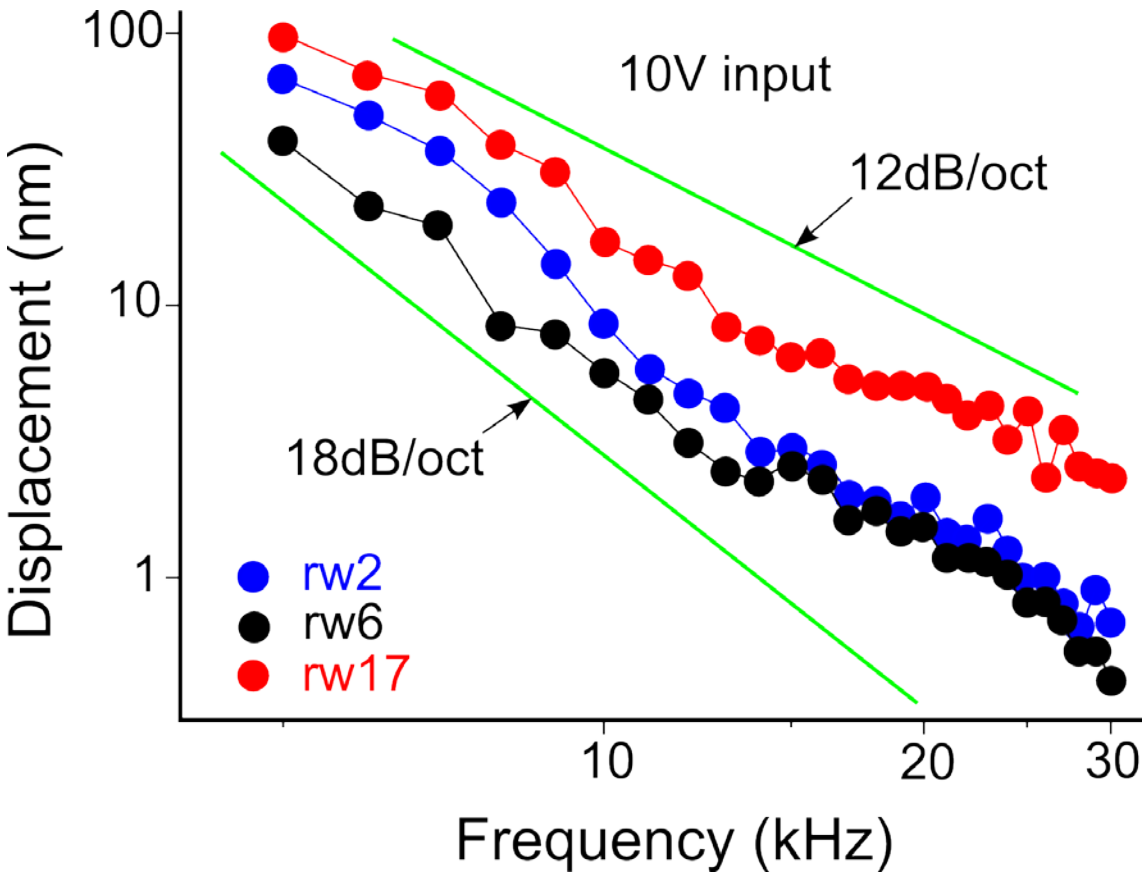

Figure 4.3 Magnet displacement as a function of the stimulation frequency at constant voltage (10 V) applied to the coil for three representative preparations.

Taking into account the small electrical impedance of the coil, it is unlikely that this relatively steep slope originates in the electrical properties of the stimulating system. More likely, it reflects the multiple degrees of freedom of the mechanical system formed by the inductively coupled coil and the magnet, together with the RW and the cochlear fluid. The frequency dependence of the coil voltage required to generate threshold CAP during RW stimulation varied slightly for different preparations (Figure 4.4), which was attributable to variation in the relative position of the magnet and the coil and to slightly different locations of the magnet on the RW. The most effective stimulation was observed for frequencies between 10-11 kHz, with the smallest voltage required at these frequencies to generate the threshold CAP.

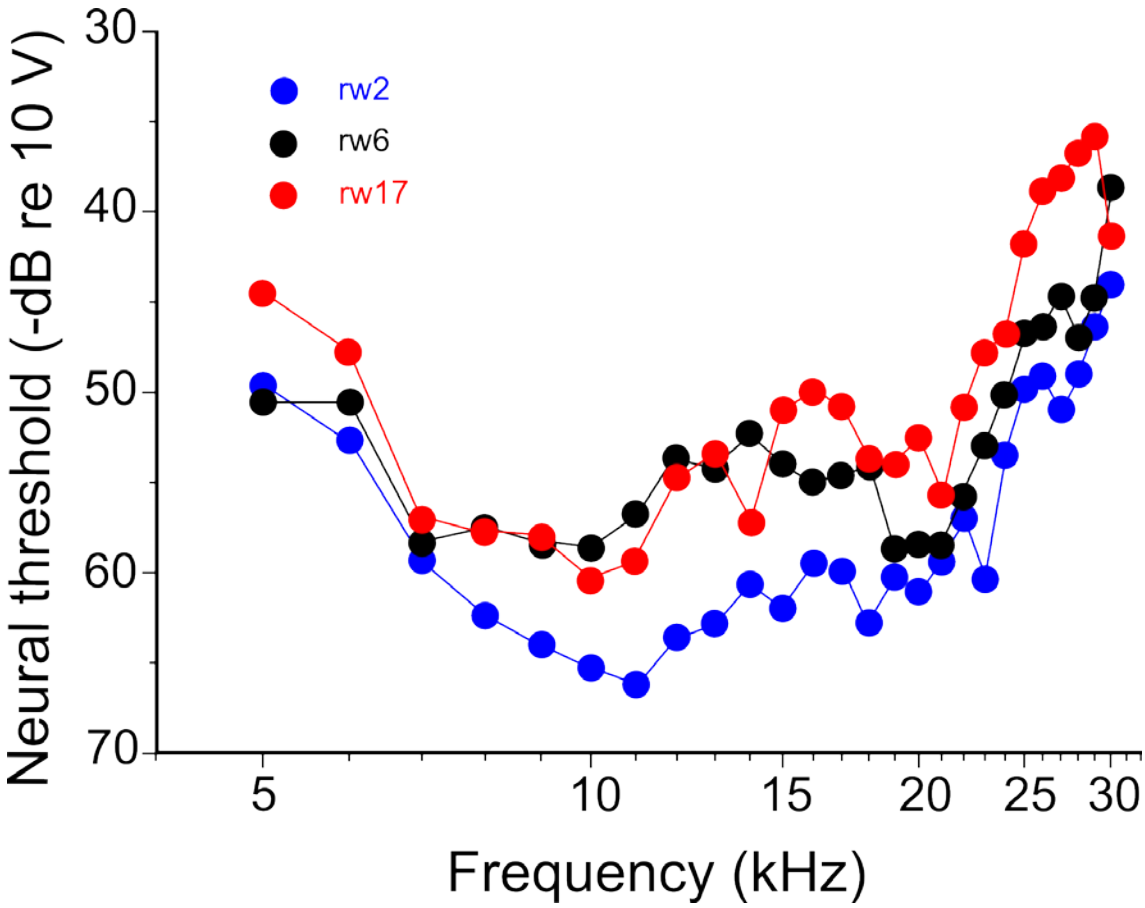

Figure 4.4 Dependence of the coil voltage to generate threshold CAP during the round window stimulation on frequency of the stimulation for three preparations shown in Figure 4.3

Taking into account the linearity of the magnet displacement (Figure 4.2), the corresponding magnet displacements for the threshold coil voltage could be readily derived from the iso-voltage response curves at 10 V (Figure 4.3) and the CAP threshold curves (Figure 4.4) using the following equation:

displacement at threshold = displacement at 10 V / 10^(attenuation at threshold/20)

The derived magnet displacement threshold curves (Figure 4.5) demonstrate the extremely high sensitivity of the guinea pig cochlea to RW stimulation in the sub-nanometre range. Maximum sensitivity, which corresponds to the smallest magnet displacements at the threshold, was observed at around 20 kHz, which is similar to the frequency of maximum sensitivity for acoustic stimulation (Figure 4.1).

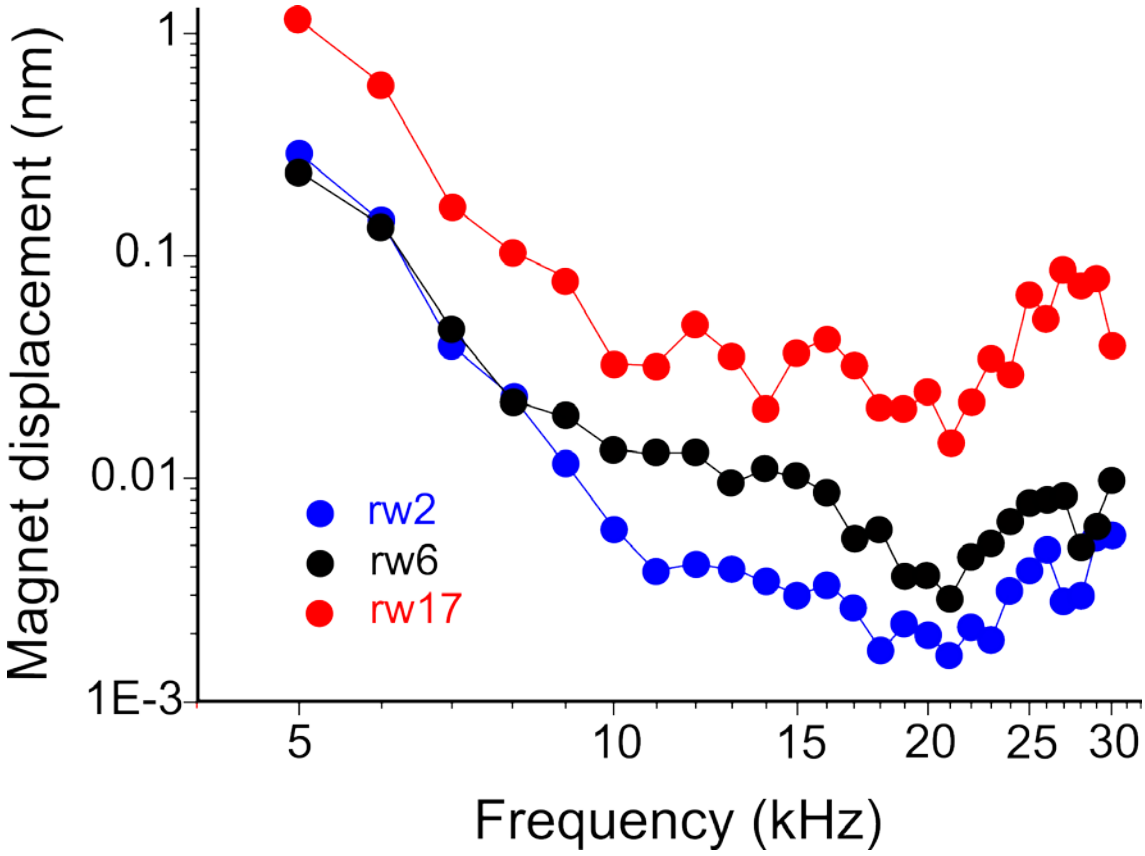

Figure 4.5 Magnet displacement at the CAP threshold calculated for three preparations shown in Figure 4.4

The absolute sensitivity of the magnet displacement threshold curves varied between preparations (Figure 4.5), which also reflects variations between preparations in the frequency dependence of the magnet displacement (Figure 4.3) and the coil voltage required to generate threshold CAP (Figure 4.4Figure 4.5). These variations were attributed to different relative positions of the magnet on the RW and the magnet to the coil.

Due to the relatively high impedance of the ossicles, as seen from the cochlea and the fact that the magnet did not entirely cover the RW, that region of the RW not covered by the magnet, would be available to function as a pressure shunt during RW stimulation, with consequent poor hydromechanical coupling between the magnet vibration and the oval window. Indeed, when the cochlea was excited through the RW, movements of the stapes at the frequency of stimulation were observed above the noise floor of the interferometer only at low frequencies <7 kHz and high stimulation amplitudes. This observation suggests that stapes mobility is not required for effective excitation of the cochlea through the RW (Figure 4.6).

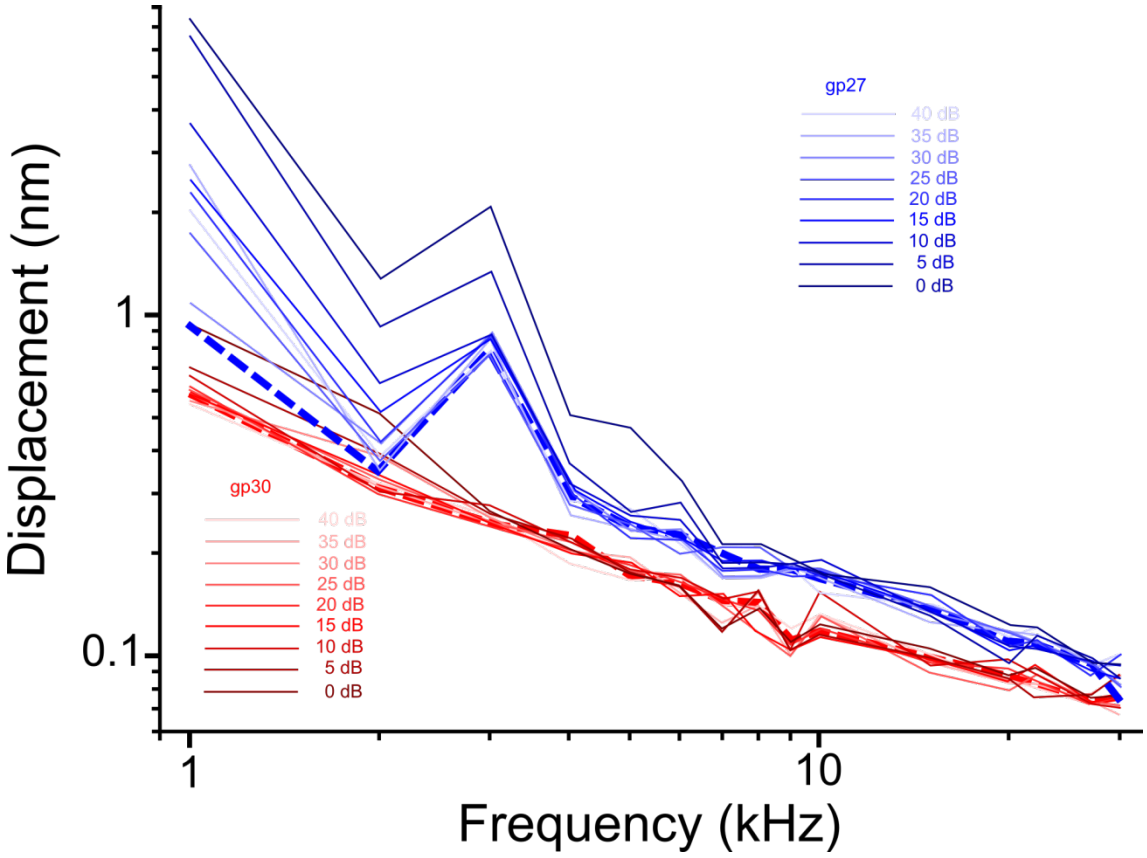

Figure 4.6 Ossicular displacement, measured from inco-stapedial joint, during RW stimulation over a range of frequencies (1-30khz) and levels (40dB – 0 dB attenuation regarding 10V) for two guinea pig preparations (red and blue scales). Red and blue broken lines indicate noise for each preparation.

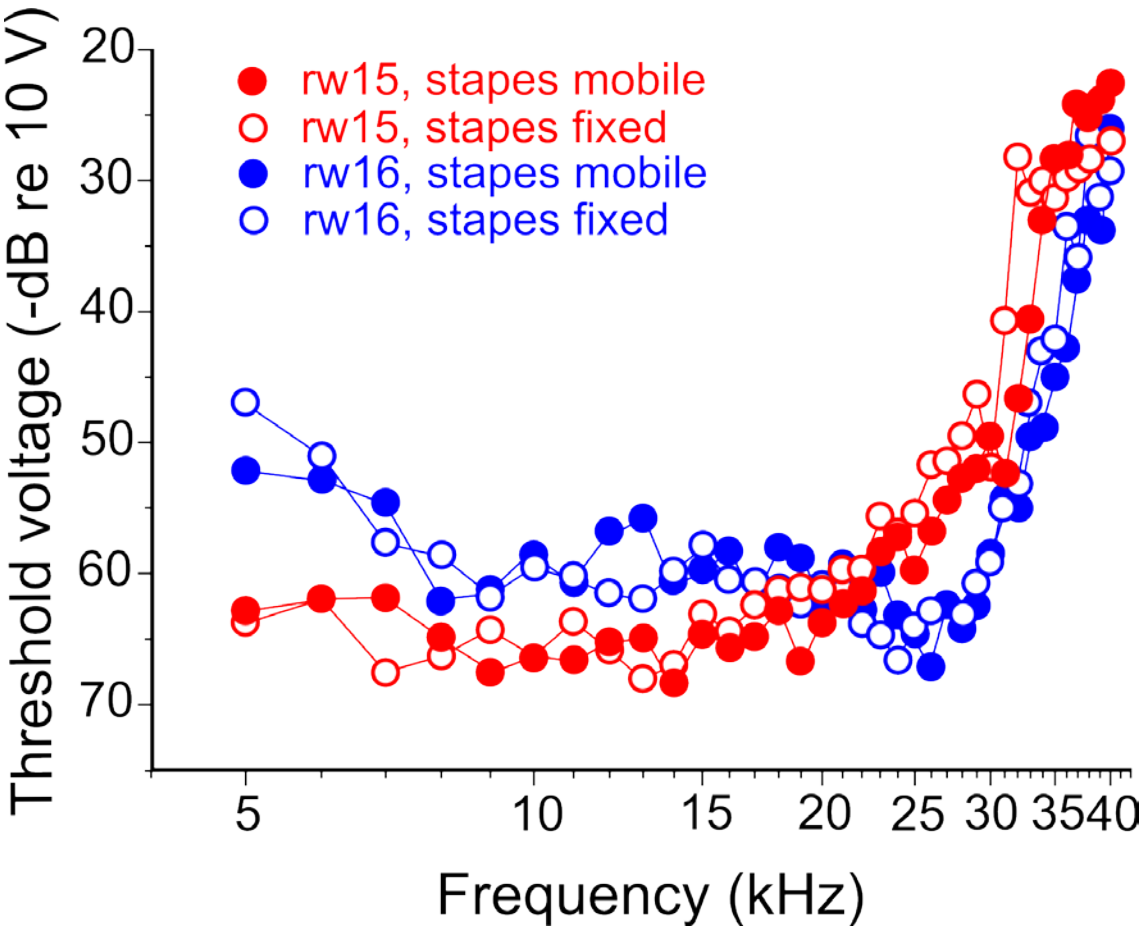

Figure 4.7 Threshold CAP during the round window stimulation before (solid symbols) and after (open symbols) immobilisation of the stapes for two preparations (circles and triangles).

This suggestion was confirmed by observing that thresholds of RW elicited CAPs before and after immobilisation of the stapes were similar (Figure 4.7). The stapes was immobilised by filling the ear canal with superglue. Following this, no stapes displacements above the noise floor of the interferometer were recorded after that for any frequencies tested at the maximum voltages used in this study.

4.4 Discussion

Across a wide acoustic frequency range, the guinea pig cochlea is extremely sensitive to mechanical stimulation of the RW, as demonstrated through recording of the CAP thresholds (Figure 4.4 and Figure 4.5). The CAP data show the viability of RW stimulation as an effective route for exciting the mammalian cochlea, with a guinea pig model, building upon the historical mechanical studies of the cochlea as well as recent work surrounding this form of implantable hearing device (Zennaro et al., 1992; Spindel et al., 1995; Lupo et al., 2009; Koka et al., 2010). The study has quantified the displacement of a transducer required for effective cochlear stimulation and demonstrated it to be in the sub-nm range and dependent on frequency (Figure 4.5). The small size of the magnet displacement required for cochlear stimulation is not surprising, considering the equally small magnitude of stapes displacement at the threshold of cochlear stimulation through the 'normal' ossicular route (Békésy, 1960). Quantification of the RW transducer displacement gives valuable information for design parameters for future devices. These parameters, however, vary within individuals (Figure 4.4 and Figure 4.5). The shape of the transducer and the area of the RW it covers are other factors that may be important in a usable device. Most significant is whether the transducer completely covers the RW, as demonstrated by other groups (Nakajima et al., 2010a; Nakajima et al., 2010b; Tringali et al., 2010; Schraven et al., 2011; Schraven et al., 2012) or leaves an area of the RW partially free (Lupo et al., 2009). These experiments show that partial coverage of the RW does not affect RW impedance sufficiently to affect cochlea stimulation and provides evidence that the exposed portion of the RW membrane acts as a pressure shunt (Figure 4.1). Complete coverage is likely to remove this shunt and may result in a different mechanism of BM stimulation (Arnold et al., 2010; Nakajima et al., 2010b).

The experiments in this study demonstrate that middle ear prostheses that partially cover the RW can be used effectively for simultaneous cochlear stimulation and pressure relief through the RW. The existence of a 'third window' (an additional pressure shunt) in the cochlea has been postulated to account for the efficiency of RW stimulation because of the relatively high impedance, as seen from the cochlea, presented by the ossicles (Lupo et al., 2009). The identity of the 'third window' ranges from the vasculature of the cochlea to the cochlea and vestibular aqueducts (Lupo et al., 2009; Koka et al., 2010) and its existence and ability to shunt pressure is evidenced from experiments in which the RW membrane is completely blocked during normal acoustic stimulation, and where the stapes is immobilised and the cochlea stimulated through the RW route. Despite blockage or fixation, the air conduction thresholds are raised only by between 20-50 dB, depending on the study cited (Wever et al., 1954;

Tonndorf and Tabor, 1962; Linder et al., 2003; de Alarcon et al., 2008; Lupo et al., 2009). However, even the comparatively low experimental value of a 20 dB rise in threshold level is significant when compared to the current study (Figure 4.7). Additionally, it is unlikely that a hypothetical 'third window' is responsible and, indeed, required for pressure relief in our experiments. We observed poor transmission of pressure into the cochlear fluid, which was confirmed by reduced hydromechanical coupling between the transducer and the stapes with consecutive lack of any stapes movement at higher frequencies of stimulation. Von Békésy (1960) demonstrated the need for the stapes footplate to be closely matched to the size of the oval window to avoid pressure being shunted through the uncovered area of the oval window. A recent study by Schraven et al, (2012) testing different sized actuator tips and coupling, it was demonstrated that actuators with reduced tip size led to reduced stapedial movements compared with those coupled to the size of the RW during stimulation, a result which was accounted for by the free area of the RW acting as a pressure shunt. We propose that in our experiments a similar mechanism of shunting occurs when the cochlea is stimulated through the partially covered RW. This does not discount other 'windows' contributing to pressure relief but it is clear that, in our case and regardless of their identity, their contribution appears to be negligible because pressure is transmitted poorly through the extent of the cochlea.

When, as in our experiments, stimulation is delivered via a magnet stimulated by an electric coil through a partially occluded RW, energy flow in the cochlea is not significantly affected by stapes mobility. We found that CAP thresholds before and after stapes fixation (Figure 4.7) remained remarkably similar and did not show a threshold elevation after stapes fixation, as was evident in earlier studies using RW stimulation through a partially blocked RW (Lupo et al., 2009). It is worth noting that, in contrast to our findings, where RW stimulation through the partially occluded RW elicited stapes displacements only at high intensities below 7 kHz, under similar stimulus conditions, Lupo et al (2009) observed stapes movement in chinchillas across a wider frequency range of 0.25 - 16 kHz. Better hydromechanical coupling between the RW transducer and the stapes, and consequent changes in the cochlear hydromechanical properties after stapes immobilisation, may account for elevation of the CAP thresholds after stapes fixation these authors observed. Correspondingly, differences in transducer shape, pre-tensing of the actuator tip and the proportion of the RW covered, may potentially account for differences in the transducer-stapes hydromechanical coupling reported both in this study and that of Lupo et al (2009). It is apparent from differences between Lupo et al's (2009) and our studies that the choice of both the size and shape of the transducer are important if mobility of the ossicular chain is to become irrelevant, thereby negating the need for additional

intrusive procedures that have the potential to cause sensorineural hearing loss. Additionally pretension of the transducer is important for effective transfer of vibrational energy (Schraven et al., 2011).

Since in our experiments both cochlear stimulation and pressure relief were through the RW, we conclude that the mode of cochlear excitation through the RW is different from that observed during conventional, acoustical cochlear stimulation or RW stimulation which does not allow pressure relief through the RW (Nakajima et al., 2010b; Tringali et al., 2010). We propose that during RW stimulation through the partially occluded RW, the BM is driven via bulk fluid movement and near-field pressure variations generated in the vicinity of the RW, which, result in the generation of conventional travelling waves along the cochlear partition. We reach this conclusion because the 20 kHz region of the cochlea, which is most sensitive to RW magnet stimulation (Figure 4.5), is located in the middle of the basal turn of the cochlea and cannot be observed through the RW. Indeed, CAP threshold tuning curves derived through acoustic (Figure 4.1) and RW magnet (Figure 4.5) stimulations are very similar in shape, indicating that cochlear excitation due to RW stimulation travels to the apex of the cochlea.

Our results indicate that the transducer displacement is not able to cause a pressure difference between the cochlear scalae in the conventional way (Voss et al., 1996b) when using a transducer that leaves the RW partially exposed. This is likely to be due to the high impedance of the ossicular chain, as seen from the cochlea (Nakajima et al., 2010a) and pressure backflow around the transducer (Békésy, 1960). Due to the incompressibility of the cochlear fluid, the near-field pressure variations which, according to the results of our experiments excite the BM, should be limited to vicinity of the RW membrane. However, the relatively small distances between the RW and the BM and the small displacements of the BM required to generate a travelling wave make excitation of the BM by these local pressure variations possible. Once the BM is displaced, localised (Olson et al., 1998) pressure differences between the scalae are generated and the travelling wave is able to propagate to its characteristic frequency, as evidenced in out CAP recordings (Figure 4.5). It is worth noting that excitation of the cochlea in our experiments was due to energy propagation into the cochlear fluids and not through bone conduction, as demonstrated by experiments where the cochlea was stimulated through the completely or partially covered RW (Arnold et al., 2010).

By investigating the mechanisms underlying cochlea stimulation through the RW using a transducer that partially covers the RW membrane this study has important significance for future clinical use of such devices. In general, a number of clinical conditions that affect sound

conduction through the middle ear, including otosclerosis, chronic otitis media and congenital malformations of the outer and middle ear, can be treated successfully using RW stimulation. The traditional treatments applicable in, for example, otosclerosis, such as stapedectomy, sometimes require revision surgery that can result in sensorineural hearing loss (Gros et al. 2005). Other sound conduction pathologies that can be treated with active middle ear prostheses, which deliver vibrational energy to the ossicles directly, may become untreatable on further progression of the disease such as in severe otosclerosis or unsuccessful reconstructions of the ossicular chain. In such cases the only alternative traditionally has been the bone-anchored hearing aid device that delivers sound energy through bone conduction. RW stimulation with a floating mass transducer is not compromised by any of these complications and does not require mobility of the ossicular chain to provide input to the cochlea that is similar to that obtained acoustically in a 'normal' ear.

5 A MOUSE MODEL FOR HUMAN DEAFNESS DFNB22 REVEALS THAT HEARING IMPAIRMENT IS DUE TO LOSS OF INNER HAIR CELL EXCITATION

5.1 Abstract

Mutations at the DFNB22 locus encoding the 120 kDa inner-ear specific protein otoancorin, that is expressed on the surface of the spiral limbus of the cochlea, cause recessive nonsyndromic hearing impairment in humans. Gene targeting in embryonic stem cells was used to create an EGFP knock in, otoancorin (*Otoa*$^{EGFP/EGFP}$) knock-out (KO) mouse. In the *Otoa*$^{EGFP/EGFP}$ mouse the tectorial membrane, a ribbon-like strip of extracellular matrix that is normally anchored by one edge to the spiral limbus and lies over the organ of Corti, retains its general form and remains in close proximity to Corti's organ, but is detached from the limbal surface. Electrophysiological and mechanical recordings from the *Otoa*$^{EGFP/EGFP}$ mouse including measurements of cochlear microphonic (CM) potentials, distortion product otoacoustic emissions (DPOAEs) and basilar membrane (BM) motion indicate the tectorial membrane (TM) remains functionally attached to the electromotile, sensorimotor outer hair cells (OHCs) of the organ of Corti and that the amplification and frequency tuning of the basilar membrane responses to sounds are almost normal. The compound action potential (CAP) masker tuning curves, a measure of the tuning of the sensory inner hair cells (IHCs), are also sharply tuned but the thresholds of the CAP, a measure of inner hair cell sensitivity, are significantly elevated. These results indicate that the hearing loss in DFNB22 patients is due to a defect in IHC stimulation, and reveal the limbal attachment of the tectorial membrane plays a critical role in this process.

5.2 Introduction

The sensory epithelium of the cochlea, the organ of Corti (Figure 5.1), contains two types of hair cell: the purely sensory IHCs and the electromotile, sensori-motor OHCs. These cells are critically positioned between two strips of extracellular matrix, the BM and the TM respectively (see chapter 1.2.3).

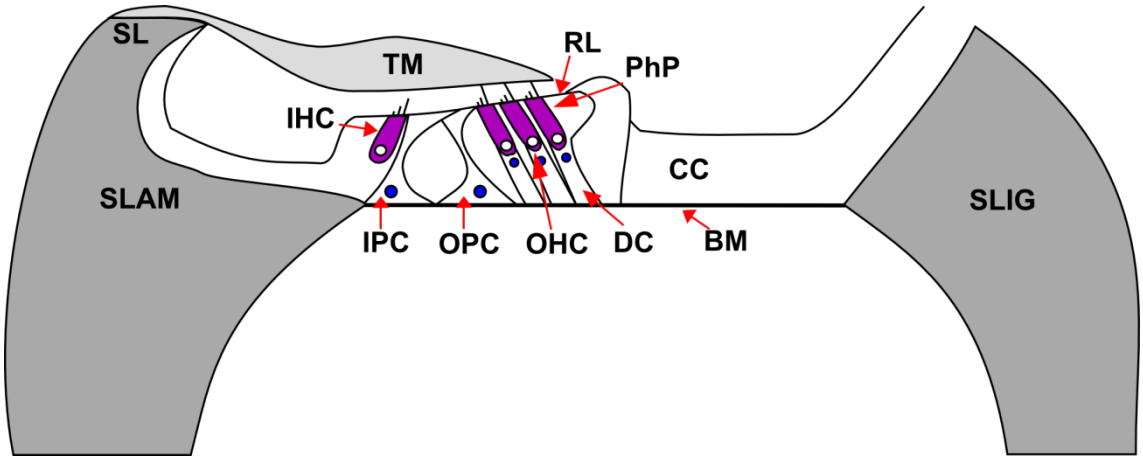

Figure 5.1 Schematic cross-section of the wild-type cochlea. Spiral lamina (SLAM), spiral ligament SLIG) inner pillar cells (IPC), outer pillar cells (OPC), Deiters' cells (DC), phalangeal process of DC (PhP) Claudius cells (CC), outer hair cell (OHC), inner hair cell (IHC), reticular laminar (RL and major non-cellular elements (basilar membrane (BM) and tectorial membrane (TM))

Signal processing in the cochlea is initiated when sound-induced changes in fluid pressure displace the BM in the transverse direction, causing radial shearing displacements between the surface of the organ of Corti and the overlying TM (Davis, 1965). The radial shear is detected by the hair bundles of both the IHCs and the OHCs (Sellick and Russell, 1980), with the stereocilia of the OHC hair bundles forming an elastic link between the organ of Corti and the overlying TM (Kimura, 1966). Deflection of the stereocilia gates the hair cells' mechanoelectrical transducer (MET) channels, thereby initiating a MET current (Hudspeth and Corey, 1977). The MET current promotes active mechanical force production by the OHCs which, in turn, influences mechanical interactions between the TM and the BM (Allen, 1980; Zwislocki, 1980). This nonlinear frequency dependent enhancement process, which boosts the sensitivity of cochlear responses to low level sounds and compresses them at high levels, is known as the cochlear amplifier (Davis, 1983) and enables the dynamic response range of the cochlea to extend over six orders of magnitude of sound pressure (Yates, 1990).

Whilst the hair bundles of the OHCs are imbedded into the TM and therefore directly excited by relative displacement of the under surface of the TM and the RL, those of the IHCs are not

in direct contact with the TM. The mechanism by which organ of Corti motion results in IHC excitation is not understood and may be complicated by multiple mechanisms that dominate at different frequencies and levels (Guinan Jr, 2012). Classically, IHC excitation has been hypothesised to result indirectly from organ of Corti motion due to the radial shear between the RL and TM. Under this regime IHC excitation would occur due to viscous drag displacing IHC hair bundles. Intracellular recordings of the receptor potentials in IHCs indicate the bundles are velocity coupled (to fluid flow) at low frequencies of stimulation, and displacement coupled at higher frequencies of stimulation (Dallos et al., 1972; Sellick and Russell, 1980; Patuzzi and Yates, 1987). Direct measurements of the motion of the RL and the lower surface of the TM in an *ex vivo* preparation of the guinea pig cochlea provide evidence that, at frequencies below 3 kHz, counterphase transverse movements of the two surfaces generate pulsatile fluid movements in the sub-tectorial space that could potentially drive the hair bundles of the IHCs (Nowotny and Gummer, 2006). At higher frequencies the two surfaces move in phase and radial shear alone is thought to dominate. Theoretical studies (Freeman and Weiss, 1990) reveal that the boundary layers will be vanishingly thin at high frequencies, that the fluid in the gap between the TM and the reticular lamina will be in viscid, and that the hydrodynamic forces on the hair bundle will be inertial. Whilst an overlying TM that is not directly attached to a hair bundle does not apply direct torque to the bundle (Freeman and Weiss, 1990), the inertial force of the fluid driving the bundle depends on its mass and therefore the size of the gap between the reticular lamina and the TM (Freeman and Weiss, 1990).

Mutations in many different genes are now known to cause human hereditary hearing loss and mutant mice (either spontaneous, induced or engineered) have provided considerable insight into our understanding of the roles of various structures within the organ of Corti (for reviews see Richardson et al., 2011, Brown et al., 2008). One such structure is the TM, a spiralling ribbon composed of radially arrayed collagen fibrils that are imbedded in a non-collagenous matrix composed of a number of different glycoproteins including Tecta, Tectb, otogelin, otolin and Ceacam 16 (Cohen-Salmon et al., 1997; Legan et al., 1997; Deans et al., 2010; Zheng et al., 2011). Mutations in Tecta cause recessive (DFNB21) and dominant (DFNA8/12) forms of human hereditary deafness (Verhoeven et al., 1998; Mustapha et al., 1999; Alasti et al., 2008) and a dominant missense mutation in Ceacam 16 (DFNA4) has been identified recently as a cause of late onset progressive hearing loss in an American family (Zheng et al., 2011). Mutations in Tecta are one of the most common causes of autosomal dominant, non-syndromic hereditary hearing loss (Hildebrand et al., 2011). Mouse models for both the

recessive (Legan et al., 2000) and dominant (Legan et al., 2005) forms of deafness arising from mutations in Tecta have been created and, together with data from a Tectb null mutant mouse (Russell et al., 2007), have provided evidence that the TM plays multiple roles in hearing. The α-tectorin mouse in which the tectorial membrane is completely detached from the cochlear epithelium indicates the importance of the TM in determining the gain and timing of cochlear feedback (Legan et al., 2000). Another α-tectorin mutant, $Tecta^{Y1870C/+}$, which has a missense mutation in TECTA, which result in structural changes in its tectorial membrane that do not affect BM sensitivity but do affect neural tuning, demonstrates the TMs role in ensuring that the hair bundles of the IHCs are driven optimally at their best frequency (Legan et al., 2005). The Tectb null mutant mouse which possesses a disrupted striated sheet matrix (see chapter 1.2.3.4), has enhanced BM and frequency tuning and little loss in sensitivity in its high frequency region and indicates a role for Tectb in coupling individual elements along the length of the cochlea (Russell et al., 2007). Although as indicated above much is known about the structure of the TM, an extracellular matrix that is unique to the cochlea, relatively little is known about how it attaches to the apical surface of the cochlear epithelium. Otoancorin, a product of the DFNB22 locus, is expressed on the apical surface of the spiral limbus and has been suggested to mediate TM attachment to this region of the cochlear epithelium. In this investigation a mouse model for DFNB22 was examined, revealing a loss of IHC sensitivity as the primary cause of deafness, and isolates a specific role for the limbal attachment of the TM in driving the hair bundles of the IHCs.

5.3 Results

The *Otoa*$^{EGFP/EGFP}$ mouse cochlea was characterised in terms of its morphology and otoancorin expression by the Richardson Laboratory of the University of Sussex Life Sciences department. The results of these analyses can be found as part of a copy of the full published paper in Appendix 3. The Richardson laboratory analysis found the *Otoa*$^{EGFP/EGFP}$ mouse to be an otoancorin null mutant, that the TM in the *Otoa*$^{EGFP/EGFP}$ mouse is detached from the spiral limbus but remains attached via the OHC stereocilia to the OHCs and that the morphology of the TM is grossly normal in structure with minor alterations, such as no Henson's stripe, compared to WTs.

The CM potentials recorded from the round window of *Otoa*$^{EGFP/EGFP}$ mice are symmetric and similar to those recorded from wild-type (WT) mice, being symmetric at low to moderate sound levels, becoming negatively and then positively asymmetrical with increasing sound levels above 80 dB sound pressure level (SPL) (Russell et al., 1986). (representative example Figure 5.2, means of DC offset Figure 5.3). These data provide functional evidence that the hair bundles of OHCs are attached to the TM in the homozygous mutants, which supports the morphological findings of the presence of hair bundle imprints (See appendix 3).

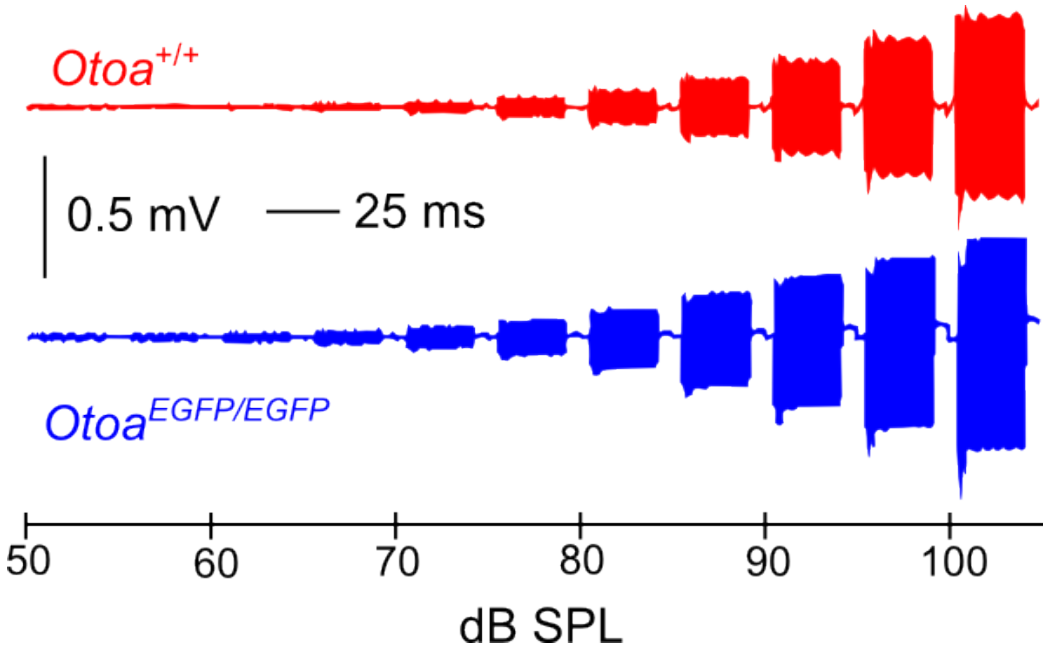

Figure 5.2 CM potentials recorded from WT (red) and *Otoa*$^{EGFP/EGFP}$ (blue) mice, from the round window in response to 10 kHz tones of increasing levels (low-pass filtered at 12 kHz) representative example from single individuals.

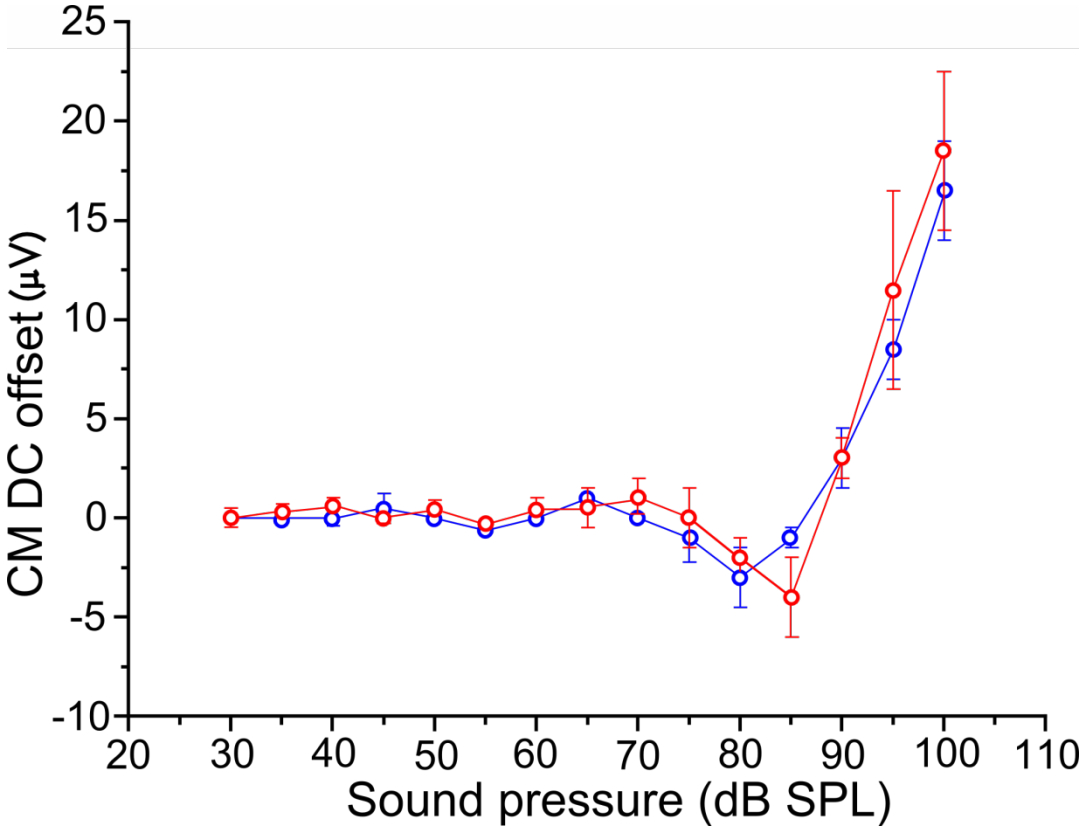

Figure 5.3 CM potentials recorded from round window in response to 10 kHz tones of increasing levels (low-pass filtered at 12 kHz) mean values. DCurr component of the CM (mean +/- standard deviation, *n* = 10 preparations each for WT and *Otoa*$^{EGFP/EGFP}$ mice).

A 10-35 dB elevation in threshold is observed for DPOAEs in the 8-65 kHz, low-threshold region of the cochlea (Müller et al., 2005) in *Otoa*$^{EGFP/EGFP}$ mice (Figure 5.4) with the difference being restricted to ≤ 20 dB in the basal region where we are able to measure basilar membrane responses. If it is assumed that these changes in DPOAE threshold reflect changes in the gain of the cochlear amplifier, and that the amplifier provides a gain of 60 dB in the low-threshold region of the mammalian cochlea, then the feedback efficiency from the OHCs in the 8-65 kHz region of the cochlea in *Otoa*$^{EGFP/EGFP}$ mice is only decreased by about 3%.

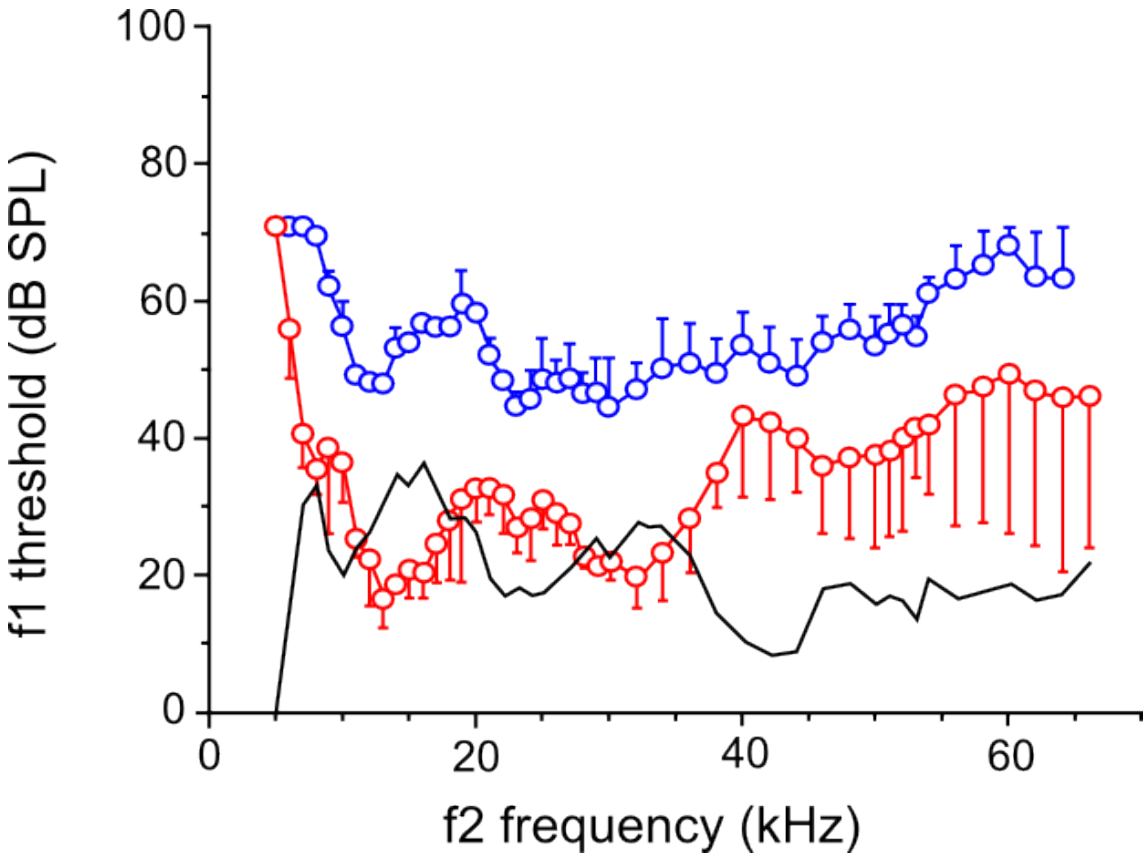

Figure 5.4 Distortion product otoacoustic emission from WT (red) and *Otoa*$^{EGFP/EGFP}$ (blue) mice, ($2f_1 - f_2$, 0 dB SPL, criterion mean +/- standard deviation) as a function of the f_2 frequency (f_2/f_1 ratio = 1.23). Black line: mean difference between measurements from n = 4 WT and n = 4 *Otoa*$^{EGFP/EGFP}$.

Measurements of the BM responses from the 55-65 kHz, high-frequency end of the cochlea in *Otoa*$^{EGFP/EGFP}$ mice provide direct confirmation that cochlear amplification remains close to normal when the TM is detached from the spiral limbus (Figure 5.5, Figure 5.6). The sensitivity and sharpness of tuning given by the Q10 dB (ratio of the CF to the bandwidth measured 10 dB from the tip) in the *Otoa*$^{EGFP/EGFP}$ and the wild-type mice do not differ significantly (P≤0.05, Table 5-1, see chapter 2.2.2.2 for statistical methods). The low-frequency shoulder of the BM tuning curves is, however, modified at frequencies between 44 and 48 kHz, sensitivities are significantly different (p≤0.001, see chapter 2.2.2.2 for statistical methods) and the threshold minimum observed in the tuning curve of WT mice (red star in Figure 5.5) and in previous investigations of mouse BM mechanics (Legan et al., 2000; Mellado Lagarde, 2008) is absent in the *Otoa*$^{EGFP/EGFP}$ mice.

Table 5-1. Parameters of the BM tuning curves for WT and *Otoa*$^{EGFP/EGFP}$ mice.

Genotype	CF (kHz)	Q10dB	Threshold (dB SPL)	Gain re post mortem (dB)	Number of animals
Wild-type *Otoa*$^{+/+}$	55 – 68	9.3±1.50	27 ± 7	33±7	5
Otoa$^{EGFP/EGFP}$	55 – 65	8.2±1.0	29 ± 4	30±6	8

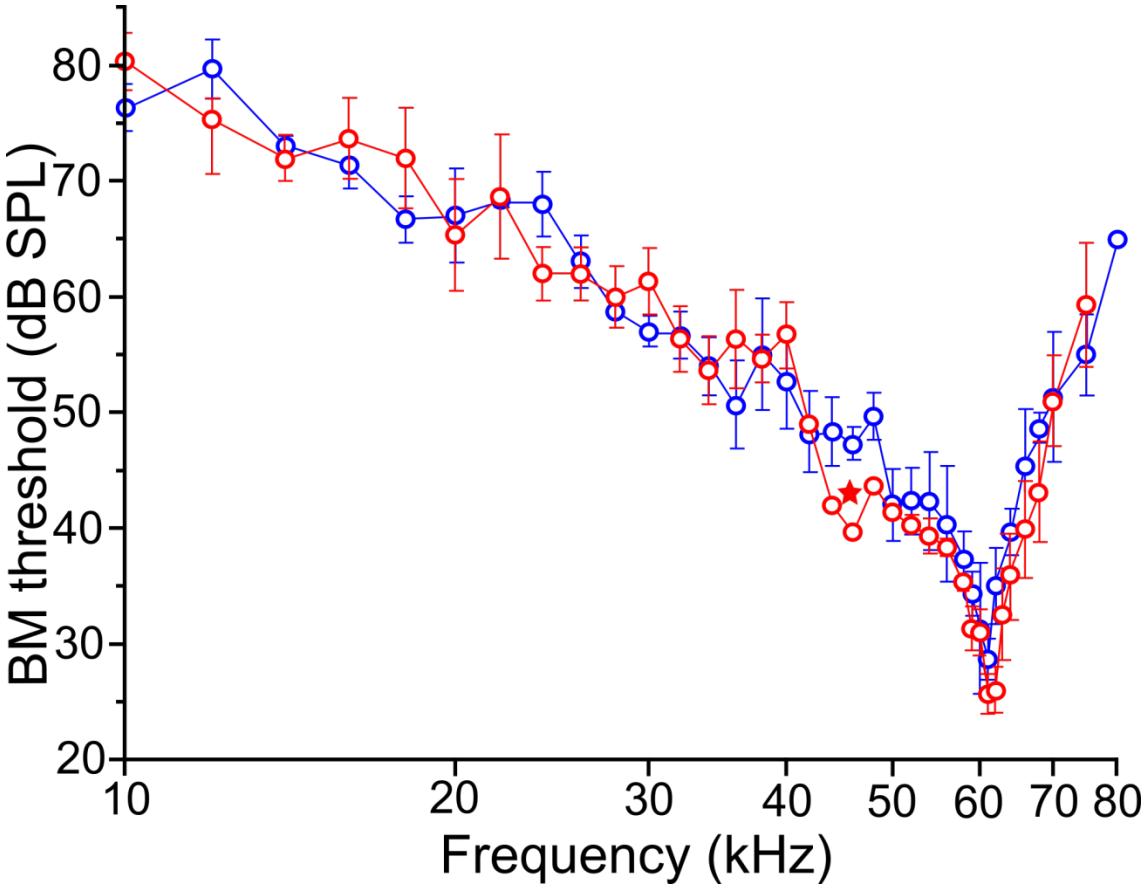

Figure 5.5 Iso-response BM frequency tuning curves (0.2 nm criterion) (mean +/- standard deviation, n = 4 WT (blue curve) and n = 4 *Otoa*$^{EGFP/EGFP}$ (red curve) mice with CFs between 59 kHz – 61 kHz). Red star is maximum of sensitivity associated with the TM resonance for WT.

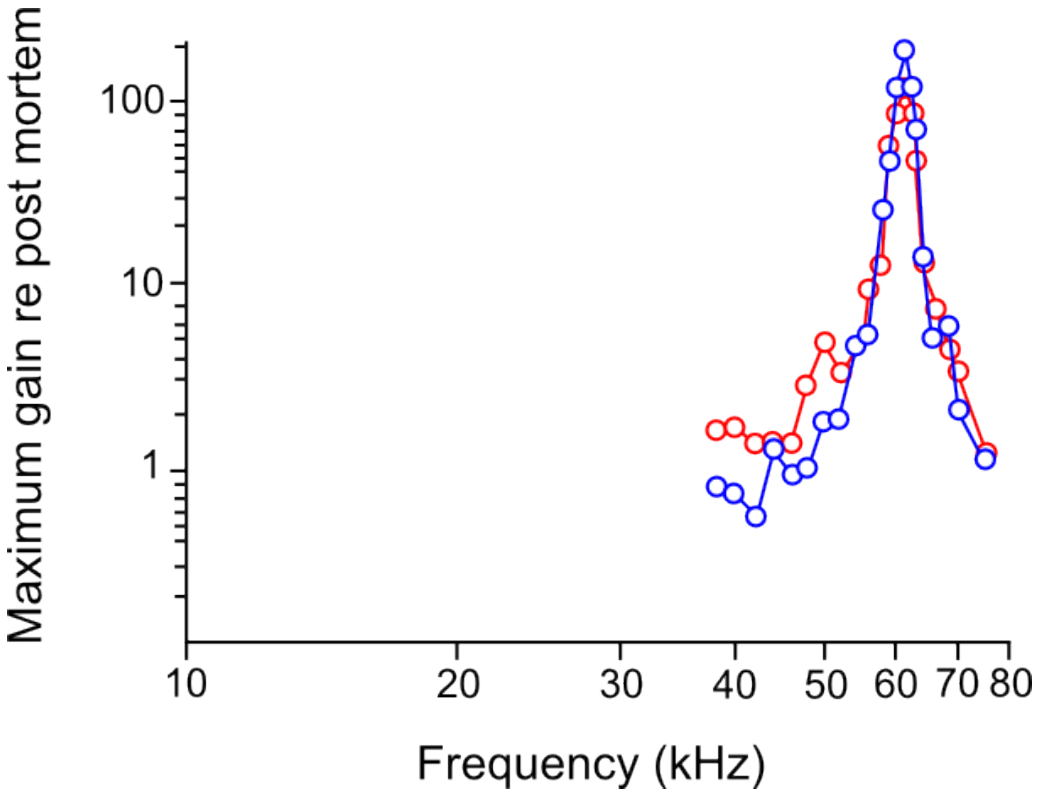

Figure 5.6 Maximum gain in WT (red) and *Otoa*$^{EGFP/EGFP}$ (blue) mice, measured as difference in alive with respect to (re) post mortem, representative animal shown.

The compound action potential (CAP) is the synchronised activity of the auditory nerve fibres that is measured at the beginning of pure-tone stimulation. The thresholds for these potentials are elevated by 35-55 dB in the 8-70 kHz range in the *Otoa*$^{EGFP/EGFP}$ mice (Figure 5.7).

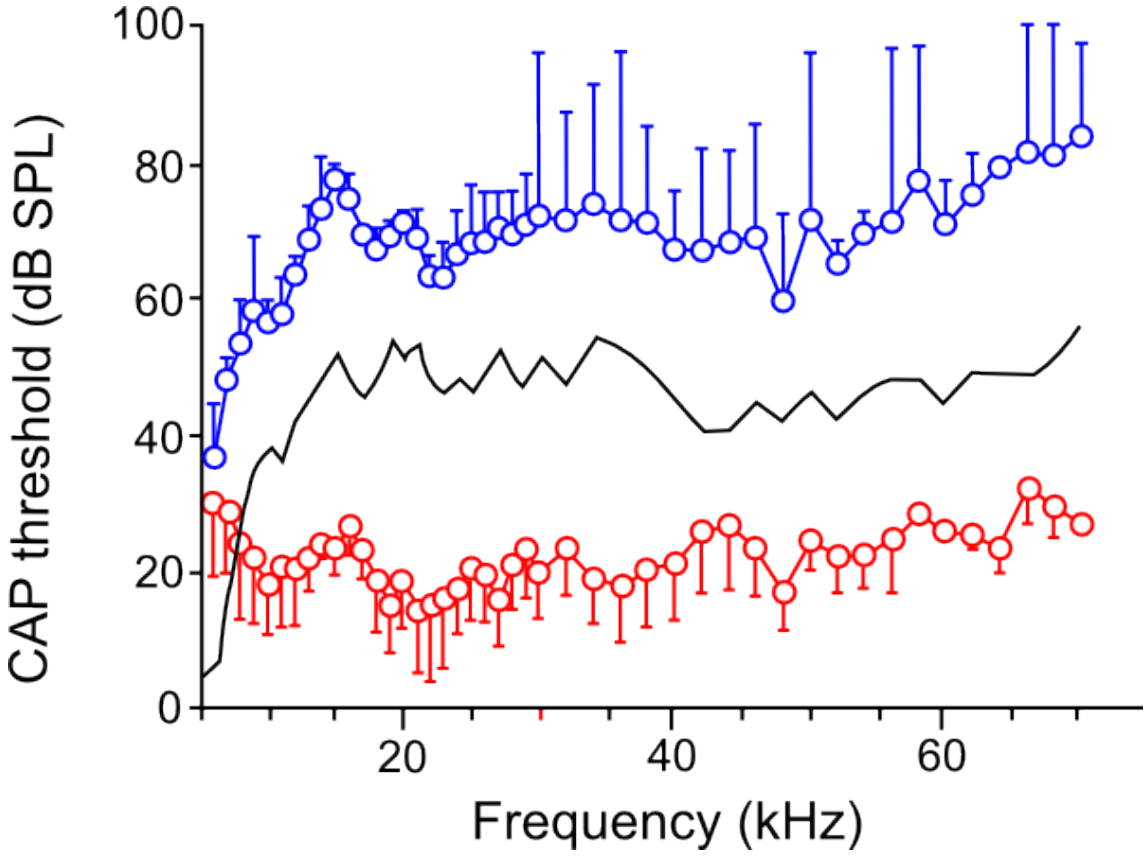

Figure 5.7 Auditory nerve, CAP threshold-curves as a function of stimulus tone frequency (mean +/- standard deviation) in WT (red) *and* *Otoa*$^{EGFP/EGFP}$ (blue) mice. Black line: mean difference between n = 5 WT and n = 4 *Otoa*$^{EGFP/EGFP}$ mice.

Derived simultaneous masking neural tuning curves closely resemble the tuning of single auditory nerve fibres (Dallos and Cheatham, 1976) and are known to become less sharp when cochlear amplification is compromised (Harrison and Prijs, 1984). Although the CAP thresholds of *Otoa*$^{EGFP/EGFP}$ mice are elevated, the CAP masking tuning curves derived from simultaneous tone-on-tone masking (Dallos and Cheatham, 1976) remain sharp in the *Otoa*$^{EGFP/EGFP}$, which indicates that BM tuning remains similar to that found in WT but the transmission of this response to the IHCs is attenuated (Figure 5.8).

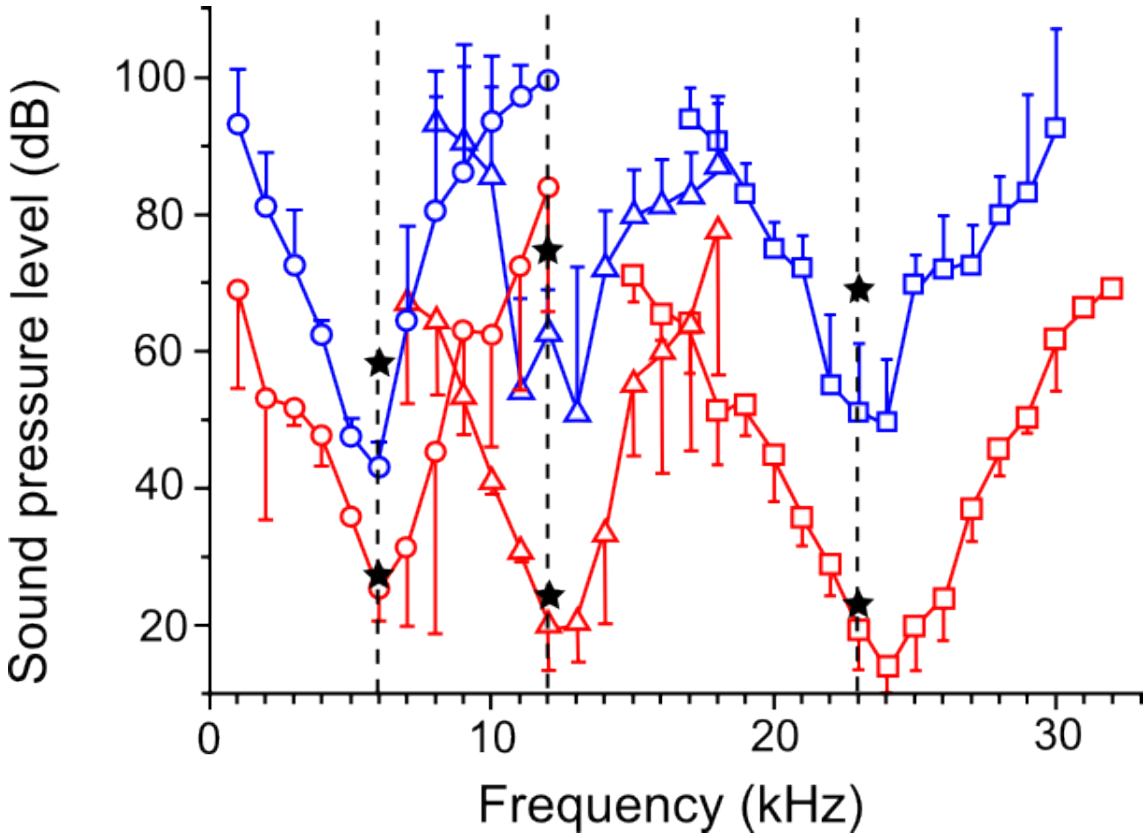

Figure 5.8 Masking tuning curves (mean +/- standard deviation, *n* = 10 preparations) for auditory nerve CAP from WT (red) and *Otoa*$^{EGFP/EGFP}$ (probe tone frequencies indicated by vertical dashed lines; levels are indicated by black stars; lower stars: probe level for the WT mice; upper stars:level for *Otoa*$^{EGFP/EGFP}$. Q10dB (bandwidth measured 10dB above tip / probe tone frequency) at the probe tone frequencies of 6, 12 and 23 kHz are 2.3±0.4, 4.6±0.5 and 7.2±0.7 for WT; and 3.2±0.2, 7.5±0.5 and 12.1±3.8 for *Otoa*$^{EGFP/EGFP}$ mice respectively.

Two characteristics of the CAP masker tuning curves recorded from *Otoa*$^{EGFP/EGFP}$ mice further indicate cochlear amplification is not compromised and that non-linear suppression (the basis for the tuning curves) is already manifested in the mechanical responses of the cochlear partition before the latter elicit neural excitation. First, the masker levels used are about 20 dB below the relatively high probe tone levels (upper black stars in Figure 5.8) necessary to elicit a measurable neural response for frequencies around the probe frequency. Second, the tuning curves are significantly sharper than those of WT mice (Figure 5.8), as has been observed previously for probe tone levels well above the mechanical threshold in sensitive, WT cochleae (Legan et al., 2005). These observations provide further evidence that the threshold of the mechanical responses is not significantly changed in the *Otoa*$^{EGFP/EGFP}$ mice, but that it is the transmission of these responses to the IHCs that is attenuated.

5.4 Discussion

Despite the loss of the limbal attachment of the TM and the abnormalities in structure described by the Richardson laboratory (Appendix 3) there is relatively little affect on the tuning and sensitivity of the BM response in the *Otoa*$^{EGFP/EGFP}$ mouse compared to WT, and only a mild (approximately 20 dB) reduction in the threshold of the DPOAEs. However these findings are in stark contrast to neural responses, which show a substantial (50 dB) increase in the threshold of the neural tuning curves, although the neural responses remain sharply tuned, and a similar rise in the threshold of the CAP threshold curves. From these results we can conclude that the limbal attachment of the TM is not necessary for cochlear amplification and tuning but is vital to ensure that the response of the BM and the reticular lamina are transmitted to the hair bundles of the IHCs without loss of sensitivity. Increased neural thresholds with preserved BM sensitivity have been described previously for the *Tecta*$^{Y1870C/+}$ mouse in which the TM remains attached to the spiral limbus but the subtectorial space in the vicinity of the IHCs is much increased, but are accompanied by a broadening of the neural tuning curves despite the BM remaining sharply tuned. It is not possible to ascertain from our results the exact underlying mechanism for the increase in neural threshold observed in this case, as the processes of fixation and dehydration likely cause changes in the relative positions of the TM and the hair cells which make quantification of any changes, if any, in the subtectorial space of *Otoa*$^{EGFP/EGFP}$ mice impossible. Nonetheless, modelling studies indicate only a small change (2 fold, from 5-10 microns) in the dimensions of this space would severely reduce hydrodynamic input to the IHC bundle. Loss of limbal attachment may be sufficient to cause such a change, or reduce the pressure difference between the inner sulcus and the hair bundles of the OHCs (Steele, 2005) caused by organ of Corti motion, and therefore reduce the sensitivity of the IHCs without affecting neural tuning. Pulsatile fluid motion resultant from rocking of the RL (Nowotny and Gummer, 2006) has been demonstrated in an *ex vivo* preparation as being able to stimulate IHCs and other hypothetical IHC excitation mechanisms have been postulated based around fluid flow (Guinan Jr, 2012). However, attenuation of the pulsatile fluid motion IHC stimulation mechanism and other fluid flow mechanisms seem unlikely given that they only operate at low frequencies below 3 kHz, well below the frequencies used in this study and the frequency range of the mouse cochlea (5-80 kHz). Likewise it seems unlikely that the absence of Hensen's stripe leads to a loss in neural sensitivity, as it is only a prominent feature in the basal, high-frequency half of the murine

cochlea and cannot be responsible for sensitivity in the low-frequency region of the CAP audiogram in the mouse.

It may also appear surprising that the loss of the limbal attachment of the TM has little effect on BM sensitivity and tuning. This finding is predicted by a lever and springs model of the cochlea (Dallos, 2003). As the radial motion of the reticular lamina is largely controlled by the displacement of its attachment point at the pillar head and its rotation of secondary importance, changes in the angular rotation of the RL will be predicted to have little effect on the radial shear of the OHC hair bundles. It will result in increases in amplification of BM motion by a factor of 1.5 at most, i.e, 3 dB or less, an outcome supported by our findings.

The CM observed in the *Otoa*$^{EGFP/EGFP}$ mice is symmetrical across all animals and implies that the OHCs are working, as in WT mice around the most sensitive point on their MET input-output function, the point of inflection, which allows maximal gain of BM amplification (Legan et al., 2000). Previous studies have suggested that the setting of this sensitive point, or operating point (OP), was governed by the OHCs acting against the radial stiffness of the TM provided by its attachment to the spiral limbus (Russell et al., 1986; Geisler and Sang, 1995; Legan et al., 2000). Unless there is some kind of otoancorin independent attachment to a structure lateral to the OHCs, for which there is no evidence in this study although other studies have indicated an attachment to the Hensen's cells (Kronester-Frei, 1978), then the limbal attachment is not required for setting the OP of the OHCs. The OP is therefore more likely to be set by the resting open probability of the MET channels, which is close to 50% in artificial endolymph containing low (0.02 mM) calcium, (Johnson et al., 2011). This raises the interesting possibility that the TM may passively regulate the local calcium ionic environment in the close vicinity of the MET channels (Heinrich et al., 1998), and may also explain why the CM recorded from the organ of Corti of *Tecta*$^{\Delta ENT/\Delta ENT}$ mice, where the TM is completely detached from the organ of Corti, is typically asymmetrical in form (Legan et al., 2000).

Cochlear amplification relies upon the effective movements of the structures of the cochlear partition and the timings of these movements. Of particular importance are the timings of feedback by the amplification forces located in the OHCs (Kronester-Frei, 1978; Geisler and Sang, 1995; Hildebrand et al., 2011; Johnson et al., 2011) which depend on whether the OHC hair bundles are driven by the elastic or inertial forces delivered by the TM (Gummer et al., 1996). Well below the CF the TM imposes an elastic load on the OHC bundles and they are displaced maximally in the excitatory direction during maximum displacement of the cochlear partition towards scala vestibule (Davis, 1965; Mammano and Nobili, 1993; Russell and Nilsen,

1997; Heinrich et al., 1998; Yu and Zhao, 2009b). However at and around the CF it has been been proposed that the hair bundles of the OHCs are excited by the inertial force imposed by the TM (Russell et al., 2007). The results of this study provide an opportunity to test this proposal. The *Otoa*$^{EGFP/EGFP}$ mouse lacks the elasticity of the TM attachment to the spiral limbus and as the sensitivity and sharpness of BM tuning remain the same this must not be a crucial factor in exciting the OHCs at CF. It is therefore likely that the OHCs must react against the inertial load of the TM at CF (Legan et al., 2005). Potentially this has profound implications for the ongoing debate concerning the identity of the cochlear amplifier and is discussed in more detail in a further discussion in chapter 7.3.2.

A second resonance has been observed approximately half an octave below the tip of the BM tuning curve in measurements obtained from the basal, high-frequency end of the murine cochlea (Legan et al., 2000; Hildebrand et al., 2011). This feature of BM tuning curves has been previously attributed to the TM resonance (Russell et al., 2007; Hildebrand et al., 2011) and is thought to result from a reduction in the load imposed by the TM at its resonance frequency. Indirect evidence of this second resonance has also been observed in recordings from auditory afferent nerve fibres across a range of species in the form of a notch of insensitivity especially prominent in the high frequency region (Liberman, 1978; Allen, 1980; Taberner and Liberman, 2005; Temchin et al., 2008). The notch of insensitivity is believed to result from a decrease in excitation of the IHCs as at this frequency the load of the TM on OHC hair bundles decreases. The consequence of this drop in impedance is that the OHC hair bundles entrain the TM and decrease the relative displacement between TM and RL. Neural suppression tuning curves also display this notch of insensitivity (Lukashkin et al., 2007a; Russell et al., 2007). Whilst the TM's role as both an inertial mass and a source of the second resonance had been deduced from previous studies of the *Tecta*$^{\Delta ENT/\Delta ENT}$ mouse, it was not possible to isolate a specific role for the elasticity of the limbal attachment region as the residual TM is completely detached from both the spiral limbus and the surface of the organ of Corti in the *Tecta*$^{\Delta ENT/\Delta ENT}$ mouse. The absence of a second resonance in the BM tuning curves of *Otoa*$^{EGFP/EGFP}$ mouse in which the TM is detached from the spiral limbus now provides evidence that this resonance derives specifically from the elasticity of the TM's attachment to the spiral limbus, combined with its effective mass.

Whilst the sensitivities of the BM responses recorded from WT and *Otoa*$^{EGFP/EGFP}$ mice are similar, DPOAEs recorded at similar frequencies differ by about 20 dB. Slight changes in the motion of the RL due to changes in loading of the cochlear partition by the modified TM of the *Otoa*$^{EGFP/EGFP}$ mouse might cause this increase in DPOAE thresholds. The RL is, however, coupled

compliantly to the BM via the OHC-Deiter's cell complex (Mammano and Nobili, 1993; Russell and Nilsen, 1997; Yu and Zhao, 2009a; Chen et al., 2011), so any change in the load on the cochlear partition would be expected to affect amplification of BM motion and be reflected in the vibrations of the BM. It is therefore more likely that this mild loss in the sensitivity of the DPOAEs in *Otoa*$^{EGFP/EGFP}$ mice is due to the detachment of the TM from the spiral limbus altering the transmission pathway between the source of the DPOAEs and the point of measurement at the eardrum.

The results also inform as to the cause of deafness in DFNB22 families. Three different recessive mutations in OTOA, a splice site mutation, a missense mutation and a large genomic deletion, have been identified in Palestinian families as the cause of prelingual, sensorineural deafness (Zwaenepoel, 2002). The degree of deafness of the affected individuals in two of these three families has been reported and has been described as being moderate-to-severe, i.e., similar or slightly more severe than the 35-55 dB hearing loss found in the Otoa$^{EGFP/EGFP}$ mouse over the 8-55 kHz range. Whilst the exact consequences of the splice site and missense mutation are unknown, both are recessive and therefore likely to cause loss of function, as is also expected for the deletion, which encompasses the first 19 of the 28 coding exons. The *Otoa*$^{EGFP/EGFP}$ mouse lacks expression of otoancorin and should be a faithful model for the recessive human mutations that have been identified thus far. The hearing loss in patients with recessive loss-of-function mutations in OTOA is therefore predicted to be due to a failure in the excitation of the IHCs, and not due to a loss of cochlear amplification.

6 PRESTIN LINKS EXTRINSIC TUNING TO NEURAL EXCITATION IN THE MAMMALIAN COCHLEA

Thomas D. Weddell, Marcia Mellado-Lagarde, Victoria A. Lukashkina, Andrei N. Lukashkin, Jian Zuo and Ian J. Russell

6.1 Abstract

Mammalian hearing relies for its sensitivity, dynamic range and frequency selectivity on active power amplification of cochlear responses (Lukashkin et al., 2007b). Power amplification depends on the integrity of the outer hair cells (OHCs) and the presence of the motor protein prestin located in their lateral membranes. Measurements from prestin knockout (KO) mice revealed basilar membrane (BM) motion to be surprisingly as sensitive as in wild-type (WT) mice, but broadly tuned with a characteristic frequency (CF) shifted to lower frequencies. Coupling between BM motion and inner hair cell (IHC) excitation was also lost and neural sensitivity was entirely compromised. We attributed these characteristics to both loss of somatic motility and drastic reduction in OHC axial stiffness. Here we measured the cochlear responses of the prestin 499 knockin mouse, where the OHCs have normal axial stiffness but lack somatic motility. Their BM responses were shifted to lower frequencies, as in the prestin KO mouse, but with reduced sensitivity that closely matched that of the neural responses. Through comparing BM motion and neural responses in prestin KO, 499 and WT mice, we conclude that prestin is the essential molecular element that enables OHCs to act as the amplifying electromechanical element in the feedback loop between themselves and the tuned vibrations of the BM and to transmit the amplified BM vibrations to provide IHC stereocilia with excitatory shear. We suggest that the expression of prestin in their lateral membranes has enabled OHCs to devolve responsibility for frequency tuning to the graded mechanical properties of the BM. Thus the organ of Corti was enabled to exploit the wide frequency range of a mechanically-tuned extracellular matrix to gain the enormous apparent benefit from being able to listen to frequencies beyond the auditory ranges of birds and reptiles (Vater et al., 2004).

6.2 Introduction

The sensory hair cells of amniote hearing organs are usually distributed in tonotopic array from low to high frequencies and are very sensitively and sharply tuned to acoustic stimulation. Frequency tuning and tonotopicity of non-mammalian auditory hair cells is due largely to intrinsic properties of the hair cells (Fettiplace and Hackney, 2006). In non-mammalian hearing organs, at least, amplification is attributed to calcium-mediated hair bundle motion (Fettiplace and Hackney, 2006). Frequency tuning and tonotopic organisation of the mammalian cochlea has an extrinsic basis in the BM; a spiralling ribbon of collagen-rich extracellular matrix that decreases in stiffness from the high-frequency base of the cochlea to the low-frequency apex (Robles and Ruggero, 2001; Ashmore, 2008). Sensitive frequency tuning is due to amplification, which specifically boosts low-level input to the mechanosensitive hair cells at their tonotopic location to overcome viscous damping (Robles and Ruggero, 2001; Fettiplace and Hackney, 2006; Ashmore, 2008). In the mammalian cochlea, amplification is the remit of the sensory-motor OHCs, located within the organ of Corti to exercise maximum mechanical effect on the motion of the BM and transmit cochlear responses to the adjacent sensory IHCs and, consequently, to the auditory nerve (Robles and Ruggero, 2001; Fettiplace and Hackney, 2006; Ashmore, 2008)(Figure 6.1). OHCs behave like piezoelectric actuators, developing forces along their long axis in response to changes in membrane potential (Ashmore, 2008). These forces are due to voltage-dependent conformational changes in the motor molecule prestin, which is densely distributed in the OHC lateral membranes (Ashmore, 2008).

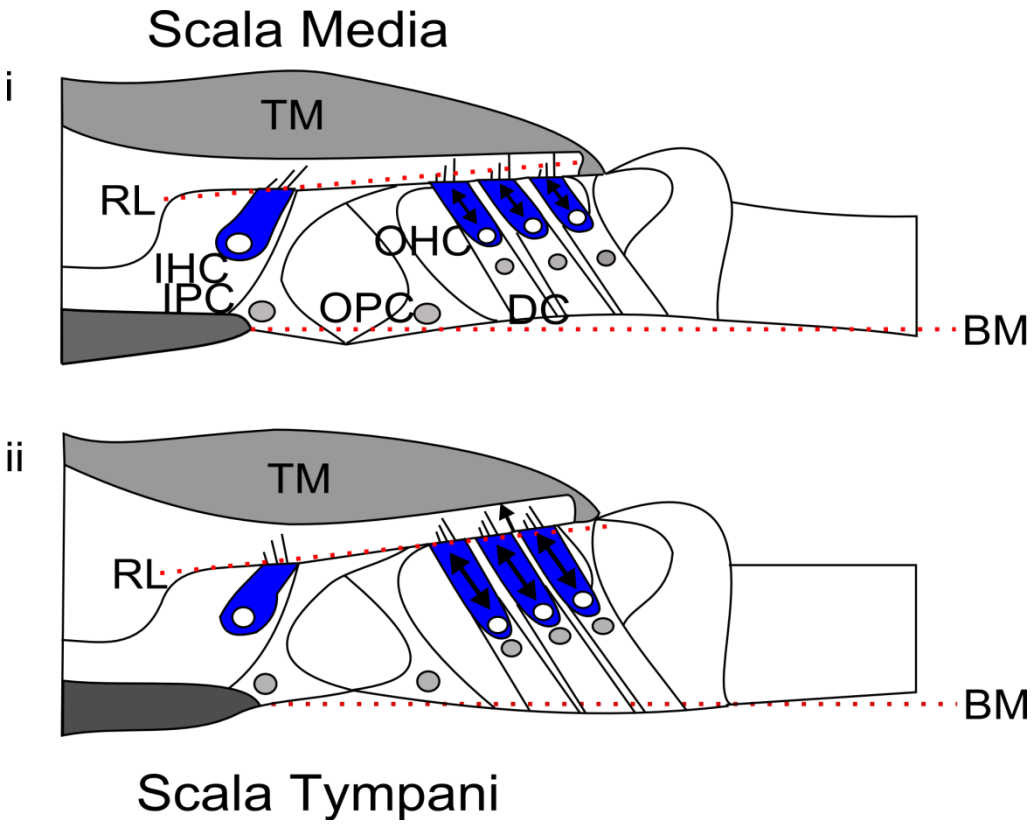

Figure 6.1 Schematic cross-section of the organ of Corti of the cochlea illustrating hypothesised mechanical distortion of the structural supporting cells (inner pillar cells (IPC), outer pillar cells (OPC) and Deiters' cells (DC) and major non-cellular elements (basilar membrane (BM), tectorial membrane (TM) and reticular laminar (RL)) when the outer hair cells (OHC) shorten (i) during maximum BM velocity towards scala media and lengthen (ii) during maximum velocity towards scala tympani. Inner hair cells (IHC).

Here we consider roles for prestin in harnessing the BM as the source of cochlear frequency tuning. The OHCs might be considered as active struts in the complex cellular architecture of the organ of Corti. The tubulin-packed cytoskeletons of the supporting cells behave as structures that are distorted by changes in OHC forces to interactively transmit sound-induced vibrations between the mechanical elements of the cochlear partition (Figure 6.1). For this to happen, the mechanical impedance of the OHCs has to be matched to that of the surrounding mechanical elements of the cochlear partition (Ashmore, 2008). We report measurements from homozygous prestin KO mice, which have compliant OHCs devoid of prestin (Mellado Lagarde et al., 2008), homozygous prestin 499 knockin mice, which have stiff OHCs populated with non-motile prestin (Dallos et al., 2008), and WT mice (stiff, motile OHCs). We have tested the hypothesis that prestin, acting as both a motile and structural element of OHCs, is essential for power amplification (Lukashkin et al., 2007b) and mechanical coupling of BM vibrations to the organ of Corti and, ultimately, for auditory sensation.

6.3 Results

Given that both prestin KO and prestin 499 mice suffer significant loss of OHCs (at least from 28 days post-partum (Dallos et al., 2008; Mellado Lagarde et al., 2008) from the basal turn of the cochlea (the locus of our measurements), we made electrical and mechanical measurements only from 17–21-day-old mice. In these mice OHCs in the basal turn of the cochlea are viable and perform mechano-electrical transduction as indicated by the recording of compound receptor potentials (cochlear microphonic, CM) at the round-window membrane. Round-window CM is dominated by receptor currents from the basal turn OHCs (Patuzzi et al., 1989b). CM as a function of stimulus level is not significantly different between WT and prestin 499 littermates (Figure 6.2) and WT and prestin KO littermates (Mellado Lagarde et al., 2008) in 17–21-day-old mice in response to 10 kHz tones. 10 kHz is about two octaves below the frequency range of basal turn OHCs; the OHC responses were therefore not subject to significant amplification (Patuzzi et al., 1989a).

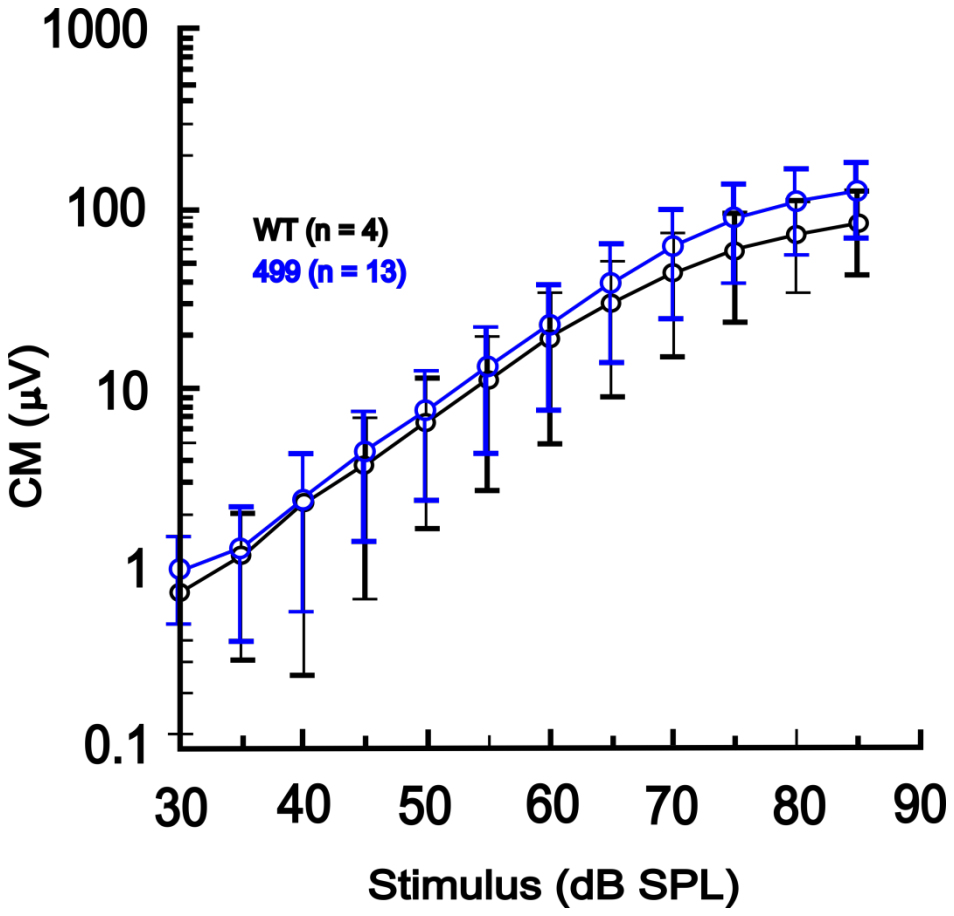

Figure 6.2 CM measured from the round windows of the cochleae of 17–21 day-old WT (black) and prestin 499 (blue) mice in response to 10 kHz tones as functions of stimulus level. Receptor currents from basal turn OHCs dominate round-window CM (Mellado Lagarde, 2008) and 10 kHz is at least two octaves below the frequency range of basal turn OHCs and, therefore, the OHC responses were not subject to amplification (Patuzzi et al., 1989a).

An indication of the roles of prestin in amplifying and relaying mechanical responses between the BM, OHCs, and IHCs was obtained from measurements of BM mechanical responses to acoustic stimulation and compound action potential (CAP) threshold audiograms measured from the round window (chapter 2.1.2, Mouse experimental methods). BM iso-displacement, frequency-tuning curves were obtained from WT mice (Figure 6.3) based on the sound pressure level (SPL) required to cause 0.2 nm displacements of the BM in the ~60 kHz region of the cochlea. The curves were typical with a minimum at the characteristic frequency (CF) of the measurement location. The tuning curve tips became broadened, desensitized by 20–30 dB SPL and moved to lower frequencies post-mortem.

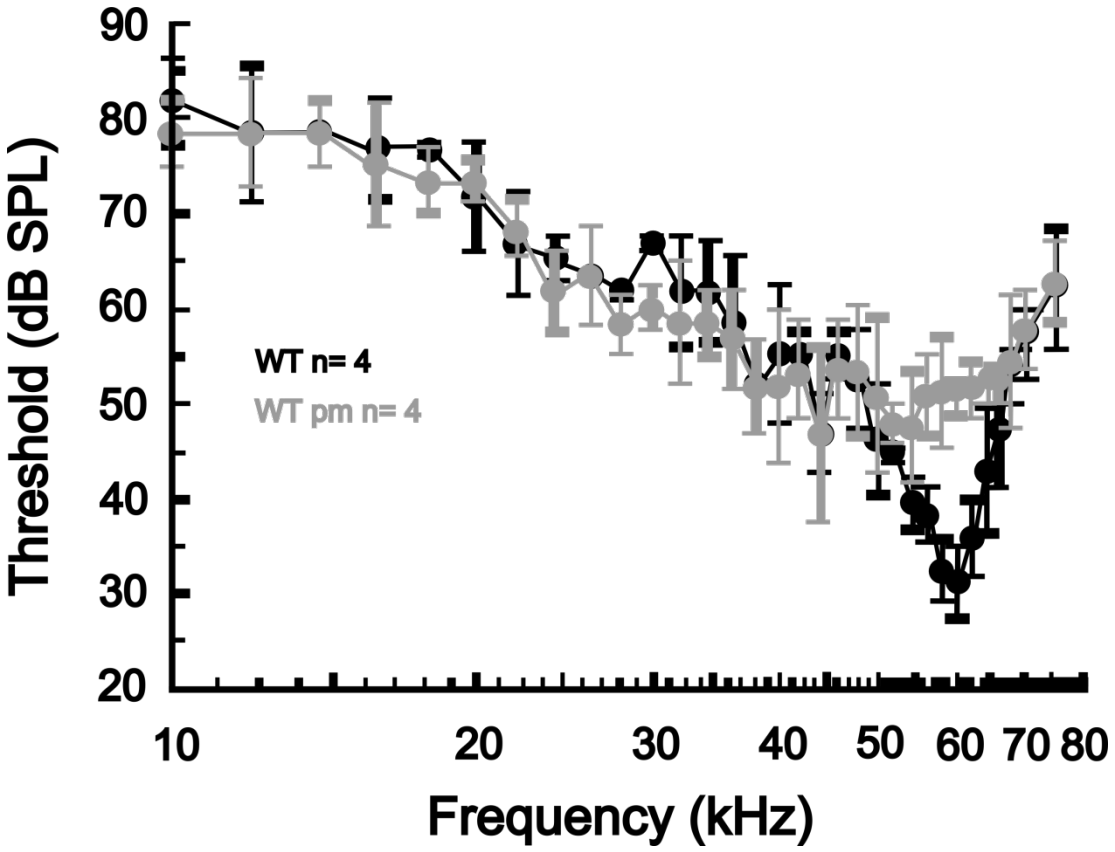

Figure 6.3 Means ± standard deviation of iso-displacement (0.2 nm) frequency tuning curves measured from the basilar membranes in the 60 kHz region of live and post-mortem (pm) wild-type (WT) mice.

BM iso-displacement, frequency-tuning curves recorded from the cochleae of prestin KO and 499 mice, at BM spatial locations similar to those made from WT mice, were very broadly

tuned, with minima shifted by about a half octave to ~45 kHz and did not change significantly after death (Figure 2.1).

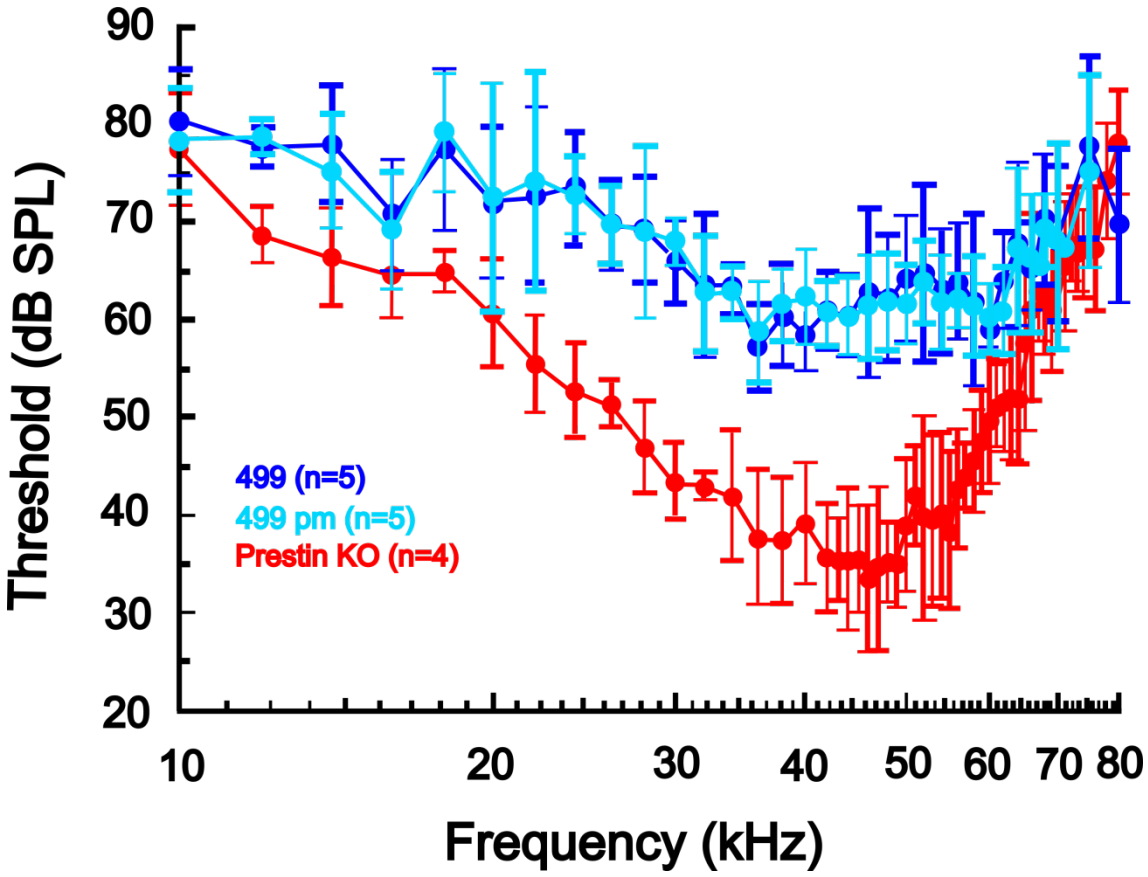

Figure 6.4 Means ± standard deviation of iso-displacement (0.2 nm) frequency tuning curves measured from the BMs in the 60 kHz region of live and post mortem (pm) prestin 499 mice (499) and in live prestin KO mice

The sensitivity of BM tuning curves measured from prestin KO mice, which is similar to that of WT mice, is attributed (Mellado Lagarde et al., 2008) to a reduction in mechanical coupling of the BM to other elements of the cochlear partition as a consequence of the greatly reduced axial stiffness of the OHCs (Dallos et al., 2008). Axial stiffness of OHCs of the prestin 499 mice are indistinguishable from those of WT mice (Dallos et al., 2008) and the sensitivity of the BM tuning curves of these mice is similar to that of the post-mortem tuning curves of WT mice, as might be expected from a critically damped cochlea without amplification (Robles and Ruggero, 2001). The significance of OHC axial stiffness for mechanically coupling the BM to other elements of the cochlear partition can be deduced from the close correspondence between CAP threshold audiograms (Figure 6.5) and BM iso-displacement thresholds for frequencies at the tip of the tuning curve for WT and prestin 499 mice,

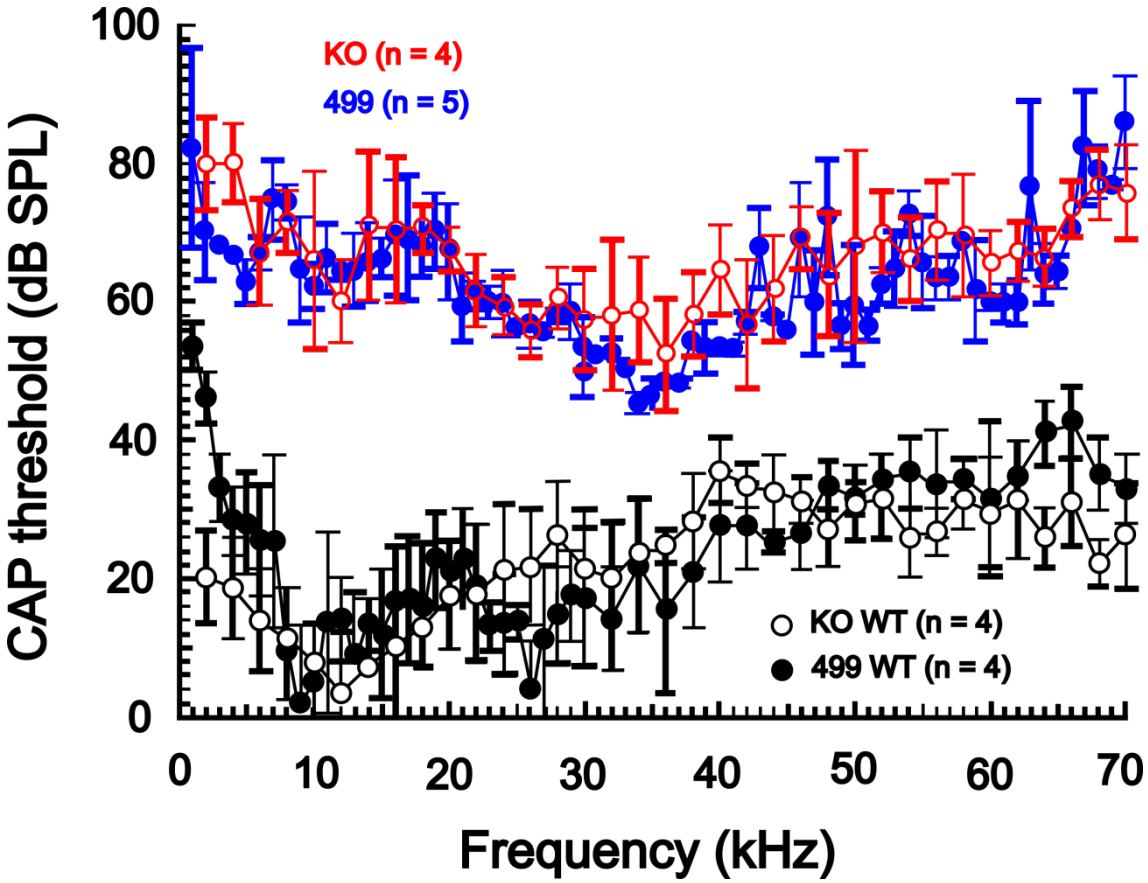

Figure 6.5 CAP threshold measured from the round windows of the cochleae of WT, prestin KO, and prestin 499 littermates as a function of stimulus frequency for the N1 peak of the auditory nerve

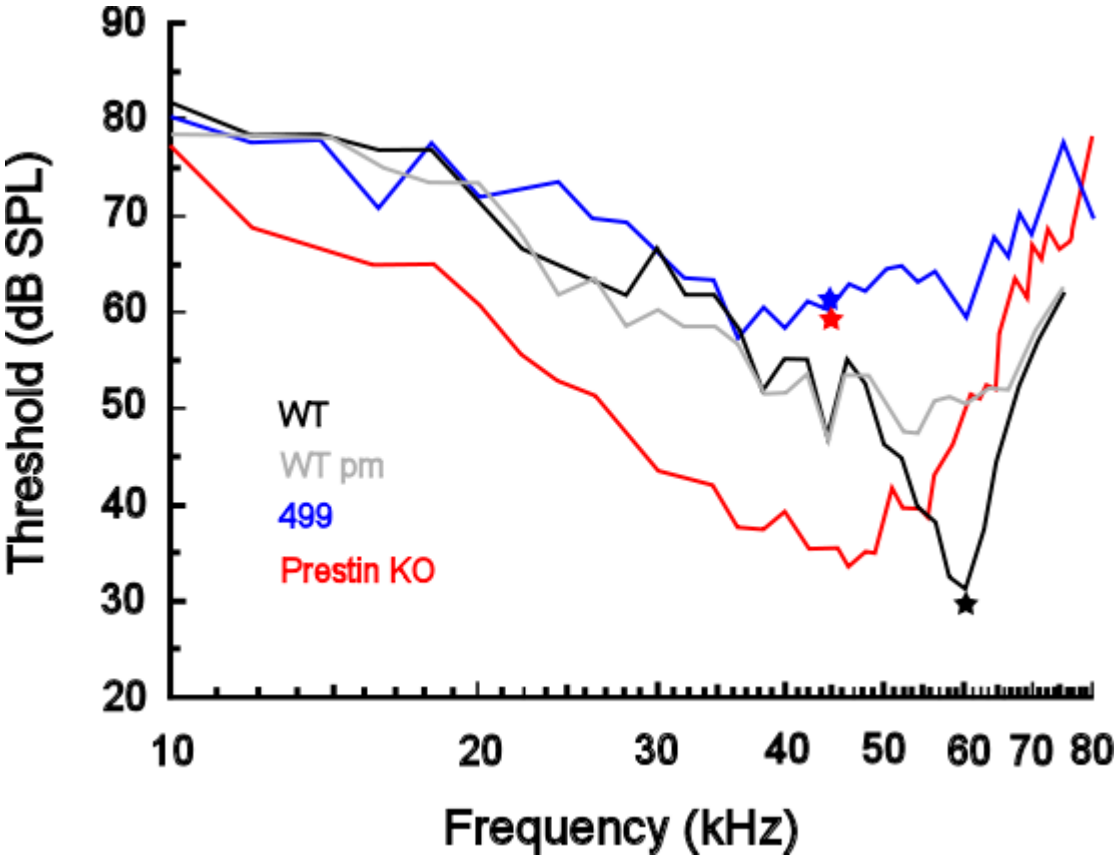

Figure 6.6 Means of iso-displacement (0.2 nm) BM frequency tuning curves measured from the BMs in the 60 kHz region of WT, WT pm, homozygous prestin 499, and prestin KO mice taken from Figure 6.3 and Figure 6.4. Stars represent neural thresholds at the characteristic BM frequency.

but not for prestin KO mice, where coupling between BM vibration and IHC excitation is weak (Mellado Lagarde et al., 2008) (see stars representing CAP threshold at BM characteristic frequencies(Figure 6.6). BM responses to frequencies more than one octave below the CF of the tuning curve, where BM motion is passive (Robles and Ruggero, 2001), are up to 20 dB more sensitive in prestin KO mice than in WT and prestin 499 mice (Figure 6.3 and Figure 6.6); a strong indication that the cochlear partition of prestin KO mice is more compliant. This conclusion is supported by measurements of the phase of BM motion relative to that of the middle ear in response to high-level (80 dB SPL) stimulation, when BM motion is governed by passive forces (Robles and Ruggero, 2001). Travelling waves along the BM in response to tones with frequencies well below the CF are stiffness dominated (Robles and Ruggero, 2001). Changes in the phase angle with increasing frequency are expected to be smaller in this frequency region for faster travelling waves propagating along a stiffer cochlear partition, as indeed is the case for both WT and prestin 499 mice for frequencies between 10 and 30 kHz (Figure 6.7). Over the same frequency range, BM vibrations measured from prestin KO mice lag

by around two cycles (Figure 6.7), providing further indication that the cochlear partition of prestin KO mice is more compliant than that of WT and prestin 499 mice.

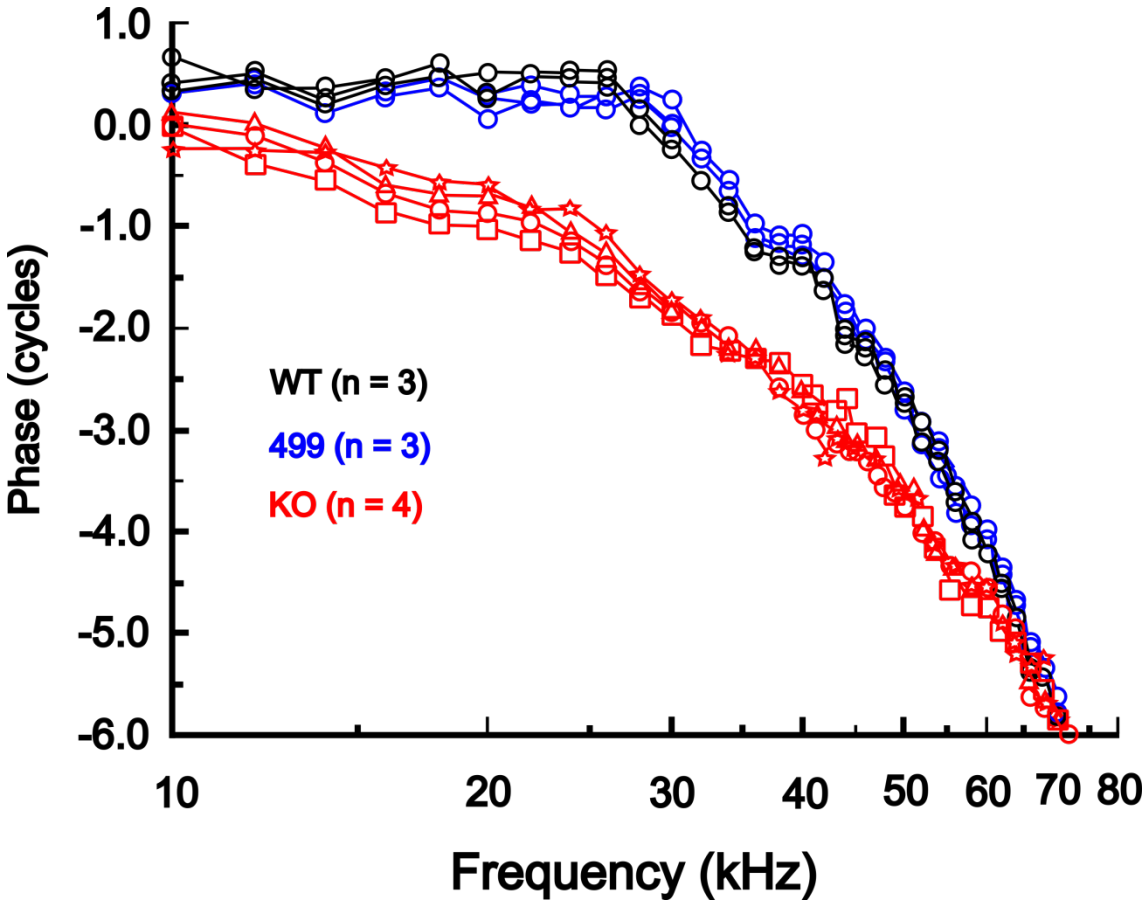

Figure 6.7 Phase of BM motion relative to the malleus as a function of stimulus frequency measured from the BMs in the 60 kHz region of WT, prestin 499, and prestin KO mice at 80 dB SPL.

6.4 Discussion

We conclude that prestin evolved in the mammalian cochlea to provide the basis for the amplified, impedance-matching mechanical link that enabled the OHCs of the organ of Corti to devolve responsibility for frequency tuning to the potentially enormous frequency range of the graded mechanical properties of the BM. In this scenario, prestin provides the rapid, voltage-dependent conformational changes that amplify and closely couple the movements of the BM to those of the OHCs, as part of a mechanosensory feedback loop, and the essential mechanical link between the movements of the BM and the excitatory shear of the IHCs (Mellado Lagarde et al., 2008; Santos-Sacchi, 2008). Prestin is therefore the key molecular element that has enabled the organ of Corti of the mammalian cochlea to exploit a mechanically-tuned extracellular matrix to provide mammals with the enormous apparent benefit of being able to listen to frequencies way beyond the auditory ranges of other amniotes (Vater and Kössl, 2011).

7 GENERAL DISCUSSION

Each of the four results chapters within this thesis further advance knowledge of the mammalian cochleas' physiology and the mechanisms which underpin its ability to amplify sounds and be excited effectively. These results also provide interesting topics for further discussion within their subject fields and the potential for exciting investigations in the future. These ideas and proposals are expanded upon in the following section and certain topics are discussed in more detail to enable greater understanding.

7.1 DPOAE biasing

DPOAEs provide an excellent non-invasive test of cochlear function and have been extensively used in both clinical and research settings.

7.1.1 Hysteresis

It was previously observed in the discussion section of chapter 3 that there exists an asymmetry of the DPOAE amplitude patterns during the low-frequency biasing tone. This hysteresis has been observed previously in gerbils (Bian, 2004) and is observed in our own results that were previously published by Lukashkin and Russell, 2005b for the guinea pig and in the human results presented in this chapter. Bian et al., 2004 have proposed that this asymmetry is the result of negative dampening due to an active feedback mechanism that changes gain at different levels of the primaries. In their investigation they used the Boltzmann model to ascertain the underlying transfer functions of the modulation, during the rising and falling half cycles of the biasing tone separately. The transfer functions for rising and falling phases revealed a hysteresis loop with a counter clockwise traversal. These results were compared to a Botlzmann-function-based model which was able to predict the experimental results. An alternative model has been suggested in which the asymmetry is generated by a feedback process, possibly due to adaptation of the MET channels, which attempts to maintain the OHC MET at its most sensitive point, i.e the point of inflection of the transducer function. In theory both mechanisms may contribute to the asymmetry.

7.1.2 Further experiments

The results presented in chapter 3 provide important insights into the DPOAE generation mechanisms found in human and rodent ears. However the investigation does raise some interesting further questions and avenues of research concerning DPOAEs and the use of low frequency biasing tones.

Mechanisms underlying the DPOAE modulation pattern hysteresis. The commonly observed hysteresis observed in DPOAE modulation patterns has so far been hypothesised to result from one of two mechanisms in the cochlea, either the active amplification of cochlea responses or the adaptation mechanism of the MET channel. In theory changes in biasing tone frequency could provide evidence for two different mechanisms.

Differences in gain between species by investigation of human and guinea pig DPOAEs during a low-frequency high level tone across age ranges. It was speculated in chapter 3 that differences in DPOAE I/O functions between species could result from differences in OP or in the transfer function that underlies the non-linearity such as the MET transfer function. The shape of this transfer function can be affected by changes in the gain of the cochlea and this could be different between species. Investigations could be conducted to see if this is also reflected across age groups by performing the same experiments in younger human subjects, fitting their modulation patterns and deriving their transfer functions.

7.2 RW stimulation

Hearing loss is a highly prevalent condition within human populations, in the UK it is estimated that approximately 10 million people suffer some form of hearing loss, by 2031 it is predicted that this number may rise to 14.5 million, with increases in population and larger proportions of that population being over 60 years of age (RNID website). The problem is not confined to just the UK or even the Western post-industrial countries, similar trends in population are beginning to occur in emerging nations. Use of conventional hearing aids (CHAs) and improvements in the technology that underpin these devices have led to improvements in treatment of hearing loss for many. However, uptake remains remarkably low especially in groups often predicted to benefit the most from these devices, such as those with moderate hearing loss. There is variation as to why usage of CHAs is low but reasons cited by users include: poor quality of sound due to feedback, limited frequency response range, poor binaural and spatial hearing, poor performance in noisy and reverberant environments, ear canal occlusion, pain or irritation and social stigma (Koka et al., 2010). Semi-implantable and implantable hearing devices that provide a direct stimulation of cochlea structures such as the ossicules, are one way of circumventing many of the traditional problems associated with CHAs. These devices come in many forms but are collectively known as active middle ear prostheses (AMEP). In some cases these AMEP are a better treatment option in patients with more profound hearing loss where both CHAs and bone anchored hearing aids (BAHA) (a form of implantable hearing aid devise where vibrations are applied directly to the skull of the patient) are unable to provide benefit. More recently AMEPs have been adapted to provide stimulation via the RW in conditions where conventional stimulation via the ossicules is not feasible (see introduction chapter 4).

7.2.1 Clinical significance

Although the number of AMEPs using the RW approach have increased in recent years the amount of data on parameters for stimulation and how these devices function is surprisingly sparse. Indeed, observations of the surgery to implant these devices and follow up meetings in which they are activated reveal that it is currently a rather qualitative exercise rather than a quantative one (observations at Munich ENT clinic). Some studies have aimed to address this problem by taking measurements from cadaveric temporal bone specimens (Arnold et al., 2010; Nakajima et al., 2010a; Schraven et al., 2011; Schraven et al., 2012). However as in the classic example of Bekesy's use of cadavers when studying the cochlea these experimental approaches can often miss important active features of the system and the most important

feature of all its electrical output. The RW studies performed on human temporal bones are predicated on certain assumptions of how the cochlea functions, i.e that during RW stimulation the mechanics of the ossicules and fluid compartments of the cochlea ducts are working in reverse. In the clinical setting with a large AMEP coupled to the RW membrane with fascia and in the cadaveric studies this reverse cochlea stimulation is most likely the case. Indeed in some studies where areas of the RW membrane are left exposed by the size of the actuator tip or coupling material, efficiency of Stapes motion is indeed reduced compared to experiments where it is entirely covered, most likely due to the RW membrane acting as a pressure shunt (Schraven et al., 2012). What this present study demonstrates is that use of an AMEP that stimulates the RW but does not cover the entirety of its surface area can result in efficient cochlea stimulation in an *in vivo* guinea pig preparation and give physiologically relevant stimulation parameters for this form of excitation. In this scenario we postulate that the area left uncovered by the probe acts as a pressure shunt and therefore the cochlea may not be working in reverse in this scenario and the BM may initially be stimulated by near field particle displacement before generating a travelling wave capable of travelling to its frequency specific CF in the normal fashion. The clinical significance of this finding is that probes could be modified to have a smaller tip in contact with the RW with the potential that less invasive surgery would need to be performed. Currently surgery using devices such as the Med-El floating mass transducer require extensive drilling of the RW niche.

7.2.2 Further experiments

The results presented in chapter 4 provide important information regarding AMEP stimulation via the RW approach. However the results of this chapter do raise further questions about RW stimulation of the cochlea that may refine stimulation parameters for clinical applications and provide further evidence for the RW acting as a pressure shunt, when stimulated with a probe that partially covers its surface area. Proposals for some potential experiments are discussed below.

Measurements of CAP thresholds and mechanical measurements of Stapes displacement during RW stimulation with a AMEP. Theoretical models predict that if excitation of the cochlea is initially occurring through near field particle displacement and the RW acting as a pressure shunt as suggested by Chapter 4, then changes in the size of the probe tip may result in differences in stimulation efficiency (Elliot, 2011). Specifically reduction in the size of the probe tip would be predicted to increase the strength of the near field particle displacement and lead to an increased efficiency of stimulation.

Displacement measurements using laser interferometer, of RW membrane area not covered by the probe during RW stimulation. This experiment may be able to confirm if the area of the RW membrane not covered by the probe is acting as a pressure shunt, in theory this area would show movement 180° out of phase with the movement of the probe although certainly at higher frequencies this may not be the case, with the current 'floating' magnet probe/coil arrangement which has multiple degrees of freedom and a potentially complex movement pattern (which may involve rocking motions of the magnet). This complex motion may necessitate the use of a fixed rod probe. Currently the size of the probe does not allow for these measurement to take place in the confines of the guinea pig middle ear cavity, but with the use of smaller probe tips these experiments should become feasible.

7.3 Otoancorin knockout mouse

The otoancorin knockout mouse model used in this investigation potentially replicates the three different recessive mutations of *OTOA* found in the human population. Targeting of inner ear specific proteins has become an increasingly potent tool for hearing physiologists in recent years (Richardson et al., 2011). These mutations provide opportunities to better understand particular disease pathologies and the normal neural and mechanical function of the cochlea, which will inform clinicians and researchers in disease treatment in the present and provide avenues for its treatment in the future.

7.3.1 Human deafness mutations

The mouse has become a crucial model for studying the genetic pathologies of the human hearing system in recent years, due to its relative ease of genetic manipulation and genetic similarity to humans (mouse genes have are almost 99% orthologous to humans) (Brown et al., 2008). The majority of severe-to-profound early onset forms of deafness are known to be due to genetic defects and are largely isolated to the cochlea. There are currently known to be 135 loci for monogenic forms of human deafness and to date only 55 genes have been identified (Brown et al., 2008; Richardson et al., 2011). Although the most prevalent form of congenital sensorineural deafness so far studied has been ascribed to defects in the gene encoding connexin26 (*GJB2*), which is expressed in the non-sensory cells of the cochlea, early-onset deafness mutations more commonly affect the sensory cells, i.e the outer hair cells (OHCs) and the inner hair cells (IHCs). Mouse models of human deafness genes have the potential to provide a wealth of information clinically.

In this study a model was created of the human deafness DFNB22 mutation first identified by Zwaenepoel, 2002. Currently mutations of the *OTOA* gene have included a splice site mutation, a missense mutation and a large genomic deletion, and were identified in a relatively small number of Palestinian families who underwent screening (Zwaenepoel, 2002; Walsh et al., 2006). Palestinian families are particularly susceptible to recessively inherited phenotypes due to a tendency towards consanguineous marriages within the community (Jaber et al., 2000). In this study we demonstrate that a knockout mutation in the OTOA gene results in the loss of the limbal attachment of the tectorial membrane (TM) but not its attachment to the OHCs via the stereocilia. This loss of attachment prevents effective stimulation of the IHCs at anything but high levels of stimulation of the cochlea, and so fits with the pattern of moderate to severe prelingual hearing loss observed in the Palestinian families tested. The study is very likely to be

an accurate reflection of the pathology found in the human form of the disease, with the potential to inform clinicians in the choice of treatment options. For example, clinically, an audiologist may be informed as to the use of various hearing devices. The fact that in the mouse model investigated here, hearing loss was not due to a loss of OHC function, (indeed the mechanics of the BM were found to be normal), may have implications for the use of a hearing aid. After all overstimulation of the cochlea in these patients may damage the remaining function in the periphery. Although the coupling between the OHCs and the IHCs is greatly reduced in OTOA mutants, this study shows that IHCs remain present and functional as presumably do the afferent fibres that innervate them. This fact may suggest the fitting of cochlea implants is indicated in these patients.

7.3.2 Cochlea mechanics and amplification

The mammalian cochlea relies for its extraordinary sensitivity and vast dynamic range on the an amplification process termed the cochlear amplifier, which amplifies low level sounds and compresses high level sounds. There is a broad consensus within hearing research that the OHCs provide the cellular substrate for cochlear amplification, but the mechanism by which they bring about this amplification is the subject of debate. There are currently two candidate mechanisms for the amplifier: OHC somatic motility, driven by the motor protein prestin that is unique to mammalian OHCs, or active hair-bundle motility, resulting from fast adaptation of the MET channels that are common to all hair cells (for review see (Fettiplace and Hackney, 2006) or introduction), regimes in which both mechanisms contribute have also been suggested. For the OHCs to exert any influence on the cochlear partition and bring about amplification its various structures must interact effectively to allow the correct timings and directions of forces. Theoretical and experimental studies (Allen, 1980; Zwislocki, 1980; Gummer et al., 1996, see introduction) indicate the mass of the TM, suspended by its elastic attachments to the spiral limbus and the OHC hair bundles, forms a resonator that interacts with the local resonance of the BM. The nature and precise role of these elastic attachments remains unknown, the otoancorin mouse model with a TM which is no longer attached to the spiral limbus provides a unique opportunity to test theories concerning the importance of this limbal attachment and the relative contributions of mass and elasticity to excitation of the IHCs and OHCs. The model may also inform as to the relative contributions to cochlea amplification from somatic motility and hair bundle motility.

As described in chapter 5, this study has identified that the TM has to be attached to the limbus in order to drive the hair bundles of the IHCs optimally but that in this mouse model the loss of attachment has little effect on the excitation of the OHCs and resultant mechanical

movements of the cochlea partition. As in the *Otoa*$^{EGFP/EGFP}$ mouse the TM is no longer attached to the spiral limbus but it maintains a sensitive and sharply tuned BM, it would appear that the TM attachment to the spiral limbus is not a crucial factor for exciting the OHCs near their CF. The OHCs must therefore react against, and be excited by, the inertial load provided by the tectorial membrane at CF to effectively boost the mechanical responses of the cochlea. Whether the OHCs at CF are stimulated by mass or stiffness has profound consequences for movements and the timings of those movements of the various structures within the cochlea partition. Below CF it has been demonstrated that the TM imposes an elastic load on the OHC bundles and they are displaced maximally in the excitatory direction (i.e. towards the tallest row of stereocilia) during maximum displacement of the cochlea towards the scala vestibule (Nilsen and Russell, 1999; Fridberger et al., 2004; He et al., 2004) (Fridberger et al., 2004; He et al., 2004; Nowotny and Gummer, 2006) (see introduction 1). However it has been hypothesised that at and around the CF the OHCs are driven by the inertial forces of the TM which result in a 0.5 cycle lag, that means the maximum stereocilia excitation occurs when the cochlea partition is displaced towards the scala tympani (Gummer et al., 1996). This allows, with the addition of a 0.25 cycle delay imposed by the membrane time constant the forces produced by somatic motility to be in phase with the velocity of the cochlear partition at its maximal velocity as it crosses the BM baseline position. Previously one problem with the delay imposed by the membrane time-constant was that it was severely attenuated at high frequencies (Preyer et al., 1996) and therefore would be unable to drive somatic motility. Regimes in which somatic motility was hypothesised to be driven by extracellular potential, which would not be attenuated at high frequencies, would not be suitable as they would not introduce a phase delay for correct timings of forces (Dallos, 1986; Kössl and Russell, 1992). Recent experiments concerning the OHC membrane time constant, in which physiologically relevant levels of calcium in the endolymph were used, have predicted it to track the characteristic frequency of the OHCs up to 8 kHz (Johnson et al., 2011). Therefore the mode of excitation through the mass of the TM allows somatic electromotility to feed energy into the cochlea partition with the correct timings for augmentation of its movements. However, this is not the case if OHC hair bundle motility was the mechanism behind amplification as this motility is due to a fast, sub-millisecond, calcium-current driven force generation by the OHC bundles (Kennedy et al., 2005; Beurg et al., 2008) which do not possess the 0.25 phase lag caused by the membrane time-constant in somatic motility. The active forces resultant from hair bundle displacement in the excitatory direction would be in phase (Meaud and Grosh, 2011) and are predicted to cause the BM to be displaced towards the scala vestibule during movements of the bundles in the excitatory direction (Nowotny and Gummer, 2006).

Therefore the timing of stereociliary motility would cause active hair bundle forces to lag BM velocity by 0.25 -0.5 cycles and would oppose cochlear amplification. The present study provides strong evidence for the identitiy of the cochlear amplifier as being based on somatic motility.

7.3.3 Further experiments

The results presented in Chapter 5 increase our understanding of the role of otoancorin in the mammalian hearing organ and the underlying mechanism behind human deafness DFNB22. However the work does lead to further questions concerning human deafness DFNB22 and how sound energy propagates through various cochlea structures to stimulate the IHCs. Proposals for some further experiments are listed below.

Measurements of auditory brainstem responses (ABR) and psychoacoustic measurements in Palestinian families identified as having DFNB22 deafness. Comprehensive audiological testing has so far not been performed on the Palestinian families found to be affected by mutations in the DFNB22 gene although the hearing loss is described as moderate to severe. It would be interesting to look at upstream indicators of hearing function such as ABR. But also it would be interesting to investigate psychoacoustic indicators such as loudness discomfort level, loudness scaling, gap detection, ability to localise sound or distinguish sounds in noisy environments. This could inform clinicians about treatment strategies in the individuals involved and in a broader sense in conditions where transmission from the periphery to the central nervous system is compromised, such as auditory neuropathy spectrum disorder.

Measurements of ABR and behavioural indices in *Otoa* mutant mice. This could provide a insight into the upstream events of the hearing loss experienced disruption of otoancorin function and inform clinicians as to the best strategies for treatment in humans with DFBN22 deafness and other hearing impairments in which transmission from the periphery to the central hearing areas is compromised.

7.4 Duel roles for Prestin in impedance matching and amplification in the cochlear

The mammalian cochlea has adapted to be highly efficient at processing sound for the myriad of auditory environments inhabited by different species. Von Beskesy (1960) demonstrated that the anisotropic passive properties of the cochlea along its length result in a mechanical frequency analyser. However the properties of this purely passive cochlea was still unable to account fully for the sharpness, sensitivity and enormous dynamic range evident from neural recordings in the cochlea, and it was only 30 years ago that it became clear that an active cellular process supplemented this passive mechanical tuning. Passive mechanical properties, combined with active cellular processes, are two fundamentally important adaptations of the auditory system in mammals. These adaptations seem to have created the conditions where mammals could extend their frequency range to hundreds of kHz, in some cases, with the enormous evolutionary advantages such high frequency hearing could bring.

7.4.1 Cochlea partition mechanics

The cochlea partition is a complex structure of sensory cells, supporting cells and acellular membranes that runs the length of the cochlea duct. Interaction between these diverse elements determines the mechanical impedance of the cochlea partition and the reaction of this partition to sound waves in the periphery. The contribution to the overall impedance of the cochlea partition can be dynamic, or passive, depending on the frequency and level of stimulation used. Numerous attempts have been made to quantify the overall impedance of the cochlea partition, and these have largely consisted of static or quasistatic point stiffness estimates or modelling using BM motions, BM velocity combined with intracochlea pressure measurements have also recently been employed (Dong and Olson, 2009).

Quantifying the relative contributions of the cochlea partition's elements to its overall impedance has always proven difficult, especially *in vivo* due to the various elements' dynamic nature, interdependency and inaccessibility of the cochlea. Various manipulations have been used to elucidate different elements' roles, *in vitro* preparations have been used to demonstrate the contribution of the tip-links and TM to the overall impedance of the cochlea partition by destroying or removing them respectively, as both manipulations resulted in changes in stiffness of the cochlea partition (Chan and Hudspeth, 2005b). OHCs contribute significantly to the impedance of the cochlear partition, changes in OHC stiffness can be induced, for example, through treatment with chlorpromazine and salicylate, which are believed to act on the lipid bilayer of the OHCs (Zheng et al., 2007). It has been demonstrated

that during development the expression of prestin in OHCs is directly related to an increase in their stiffness and the onset of hearing in gerbils (Jensen-Smith and Hallworth, 2007). Alterations in intracellular Cl^- have been shown to reduce the voltage dependent stiffness of apical OHCs (He et al., 2003). Through use of the prestin KO mouse, Mellado Lagarde et al., 2008 showed that prestin contributes to the passive impedance of the cochlea *in vivo,* this present study has confirmed these initial findings by demonstrating that restoration of a non-motile form of prestin increases the mechanical impedance of the basal region of the cochlea in comparison to the prestin KO, shifting its passive resonance towards higher frequencies. The present study confirms that prestin and the resultant impedance matched stiffness increase that it provides by its presence in the lateral membrane of the OHCs is vital in linking the movements of the BM to the neural excitation of the IHCs. Without this impedance matching, this link is devastated as shown in the prestin KO mouse.

7.4.2 Cochlea amplification

The identity of the putative cochlear amplifier (Davis, 1983) has been a source of debate between hearing physiologists for over 30 years. The amplifier is widely accepted to be responsible for the sharp tuning, high sensitivity and large dynamic range of the mammalian cochlea and to be localised to the OHCs (Hudspeth, 2008). Two strong candidate mechanisms have been proposed to be the basis of cochlea amplification, somatic motility based on the motor protein prestin, and hair bundle motility based on the fast adaptation mechanism present in stereocilia MET channels (see chapter 1).

It has been demonstrated that the sound amplification and frequency tuning of cochlear electrical and acoustical responses are lost in mice lacking prestin (Liberman et al., 2002) or in 499 mice where prestin is effectively silenced and devoid of electromotility (Dallos et al., 2008). On the basis of these experiments it was concluded that “prestin-based outer hair cell motility is necessary for mammalian cochlear amplification”. Sharply-tuned, sensitive BM responses, indistinguishable from those measured in response to acoustic and electrical stimulation from wild type mice, were elicited from *Tecta*$^{\Delta ENT/\Delta ENT}$ mice, where OHC stereocilia are detached from the tectorial membrane, in response to levels of electrical stimulation that excluded contributions from the stereocilia (Mellado Lagarde, 2008). Somatic electromotility alone is therefore sufficient to amplify and sharply tune BM motion. This conclusion was also made following measurements from *Tecta*$^{\Delta ENT/\Delta ENT}$ mice of near-threshold otoacoustic emissions and prestin KO mice (Drexl et al., 2008). The results presented here further support the predominant role for prestin as the cochlea amplifier and extend this role to the high frequency region of the mouse cochlea.

It has been suggested that hair-bundle motility, which has been directly observed *in vitro* preparations of the mammalian cochlea in response to electrical and mechanical stimulation, may cooperate with OHC electromotility or indeed be the basis of amplification in the mammalian cochlea. We have observed no evidence for amplification of BM vibrations in the 499 mouse, even though the axial stiffness of the OHCs is apparently identical to that of WT mice, and capable of transmitting BM vibrations without apparent loss to the IHCs, as deduced from the close correspondence between neural and BM isoresponse thresholds. It would therefore be expected that, as a consequence of reciprocity, any calcium-driven active hair bundle motility arising from the transmission of BM vibrations to the OHCs and IHCs would be observed in the vibrations of the BM. However, we did not observe compressive nonlinearity in the BM vibrations recorded from 499 mice or any apparent difference in the vibrations between measurements made from living and post mortem preparations.

Two main sources of argument have been used to dismiss the exclusivity of prestin based motility as the source of the cochlea amplifier in mammals. The first is the membrane time constant which in theory puts a limit on the ability of prestin to act on a cycle-by-cycle basis to feed energy into the cochlea partition and overcome viscous dampening. This is due to the resistance and capacitance properties of the membrane reducing the sensitivity to voltage above a corner frequency of only a few kilohertz. The second is that amplification is observed in numerous auditory organs lacking prestin (Manley, 2000). A number of theories have been proposed to overcome the limitations of the membrane time constant for prestin (for review see Hudspeth, 2008), but none have been demonstrated *in vivo*. However recent experiments may have provided a solution to the limitation of the membrane time constant. By using physiologically relevant calcium concentrations in rats and gerbils (Johnson et al., 2011) demonstrated that the membrane time constant may not in fact place a limit on prestin mediated amplification at higher frequencies, certainly up to approximately 8 kHz. The study proposes that by maintaining OHCs in a state whereby half their MET channels remain open at rest the cochlea is able to reduce the membrane time constant and extend the corner frequency of OHCs to much higher frequencies. Although stereociliary motility has been demonstrated *in vitro* in the IHCs of mammals (Chan and Hudspeth, 2005a) it has as yet not been shown to occur *in vivo* under normal physiological conditions, which opens the possibility that although inducible due to the presence of the mechanisms that underlie other processes such as adaptation, stereociliary amplification is no longer relevant in the mammalian auditory system. It is possible that prestin is required for amplification at and very close to the threshold of hearing and that active hair bundle motility somehow supplements amplification

at higher stimulus levels, although this proposal is not supported by previous measurements (Mellado Lagarde et al., 2008). In recent years as the evidence for prestin based motility of OHCs has gained momentum compromises have been proposed of the two systems working in synergy with one another. For example prestin based motility could act to adjust the operating point of stereociliary based amplification, however work by (Gao et al., 2007) seems to refute this idea, by using a mouse mutant to demonstrate that prestin is not required to adjust the operating point of the stereocilia based amplifier. The present study further supports the predominance of prestin based electromotility as the mechanism underlying cochlea amplification, further building on a weight of evidence from previous investigations in recent years.

7.4.3 Evolutionary perspective

Despite being the last of the paired sense organs in amniotes to undergo formative evolution, the hearing organ of the inner ear shows a vast array of morphologies across reptiles, birds and mammals (Manley, 2000). Standard theory held for a number of years, follows that the major specialisations of the hearing organs of these different groups originated from a single ancestor before the splitting of groups, beginning with the group that would eventually go on to form mammals, synapsids, approximately 320 million years ago. However, although there is evidence that a common ancestor possessed a rudimentary hearing epithelium possessing hair cells, an amplification mechanism and some form of micromechanical tuning, it now appears more likely that the major specialisation, that of a dedicated middle ear, that led to the hearing organs present across the amniotes today, evolved in parallel across groups. The tympanic middle ear across species was vital for allowing the selection pressures to act on the obvious advantages for improved hearing such as sensing danger, communication with conspecifics and warning signals (Manley, 2010). Broadly these selection pressures resulted in papillar elongation, increased numbers of sensory cells, enhanced micromechanical tuning and group specific hair-cell specializations. The resultant range of morphologies across the amniotes is therefore huge, however convergent evolution has often been the result with similar solutions to the demands of hearing, such as the presence of two specialised populations of cells with differing roles in both mammals and birds, (the IHC and OHCs and the tall and short cells respectively) (Manley, 2000), to name one example (for review see Manley, 2000).

Compared to all other amniotes it is mammals that have evolved to become expert high frequency hearing specialists. Even the hearing of their closest relatives, the monotremes, only extends to a maximum of approximately 12 kHz, whereas some mammals (such as bats) can

hear over 100kHz (Vater and Kössl, 2011). A note of caution must be made clear, however, in that when discussing mammalian hearing as a group current knowledge is limited to relatively few species, and mainly cat and rodents, from the nearly 5500 that exist. Although the general morphology of mammalian cochlea's are broadly the same, this has not eradicated morphological differences between species that are plainly the result of adaptations to the vast array of auditory environments in which mammals inhabit. There are examples of extremely high frequency specialists, such as the bat, and extremely low frequency specialists such as the blind mole rat, with cochlea morphologies that differ markedly. However, on the whole, and very specialised cochleae aside, mammals do show a propensity to have good high frequency hearing when compared with other groups of vertebrates (Vater and Kössl, 2011).

A quirk of evolution seems likely to have created the conditions for mammals to become such excellent high frequency specialists. Whilst during the Triassic eras (280-230 MYA), all other lines of amniotes developed a 'single-ossicule' middle ear, which is in fact made up of two components (the *columella=stapes=hyomandibula* and *extracolumella*) (Clack, 2002), the synapsid lineage that eventually led to mammals incorporated the columella=stapes, quadrate (= malleus) and articular (= incus) (Maier, 1989). The result of what might appear at first to be a relatively small difference between species was profound mechanically, the three boned ossicular chain transmits energy far more efficiently than single-ossicule systems and is far better suited to transmission of high frequency sound (Manley, 2010). However, the three ossicule chain was not the driving force behind the development of high frequency hearing in mammals, it merely provided conditions in which it could occur. The most powerful selective pressure appears to have come from sound localisation (Manley, 2010, Heffner et al., 2001). In this study on prestin we demonstrate that it is a key component contributing to the stiffness and overall impedance of the cochlea partition that when removed from the partition results in sensitive but poorly tuned cochlea and that tuning but not sensitivity can be restored by a non-motile form of prestin. The evolutionary importance of prestin to mammalian hearing is indicated by the high positive selective pressure which it underwent in the ancesters of mammals (Liu et al., 2012). It appears that evolution enabled mammals to gain a high frequency advantage, by devolving responsibility for tuning from the hair cell based tuning found in other amniotes to an extracellular matrix, by exploiting the protein prestin as a structural impedance matching link between the organ of Corti and the BM. Under this regime motility would have been required to overcome the dampening caused by the cochlea fluids and to amplify sound. Prestin is therefore the key molecular element that has enabled the organ of Corti of the mammalian cochlea to exploit a mechanically-tuned, extracellular-matrix

to gain the enormous benefit from being able to listen to frequencies way beyond the auditory range of numerous predators.

7.4.4 Further experiments

The results presented in chapter 6 clarify important issues concerning the role of prestin in the mammalian cochlea. However the chapter does ultimately lead to further questions concerning the role of prestin in the cochlea and more specifically its role in the mechanics of the cochlea partition and what role if any the supporting cells have in the partition. Proposals for some potential experiments are discussed below.

Measurements of the stiffness of the cochlea partition in a mouse mutant in the basal (*in vivo* and *in vitro*) regions of the cochlea in mice with mutations that reduced quantities of prestin in the OHCs. Mice of this type currently exist (Mellado Lagarde, 2011) and express reduced quantities of prestin (25% and 50%). *In vitro* techniques using single point stiffness measurements or *in vivo* in the basal end of the cochlea using techniques similar to those employed by (Dong and Olson, 2009). These measurements could help to further understand and quantify the contribution of prestin to the overall impedance of the cochlea partition.

Measurements of BM mechanical and electrophysiological response to acoustic stimulation in the high frequency region of the mouse cochlea in mutant mice with reduced quantities of prestin in OHCs (Mellado Lagarde, 2011). Recordings have already been made in the low-frequency region, below 22kHz, of these mice showing that the response of the cochlea is not compromised despite there only being 25% and 50% of normal prestin levels (Mellado Lagarde, 2011). As current investigations show the cochlea amplifier plays a more prominent role in the base of the cochlear than the apex, these experiments would be very interesting to test the current models of cochear amplification in the basal region.

Measurements of BM mechanical and electrophysiological response to acoustic stimulation in mutant mice with selectively knocked out connexion 26 gap junctions in DCs *in vivo*. Previous work has demonstrated the potential for DCs to have a mechanical role in regulating OHC amplification (Yu and Zhao, 2009a) through their unique interaction with OHCs via the cup of the DC and the pharyngeal process. This investigation may be able to ascertain the role if any of DCs *in vivo* in regulating amplification by the OHCs

REFERENCES

ABNET, C. C. 1998. *Measuring Mechanical Properties of the Tectorial Membrane with a Magnetizable Bead.* phD, Massachusetts Institude of Technology.

ALASTI, F., SANATI, M. H., BEHROUZIFARD, A. H., SADEGHI, A., DE BROUWER, A. P. M., KREMER, H., SMITH, R. J. H. & VAN CAMP, G. 2008. A novel TECTA mutation confirms the recognizable phenotype among autosomal recessive hearing impairment families. *International Journal of Pediatric Otorhinolaryngology,* 72**,** 249-255.

ALLEN, J. B. 1980. Cochlear micromechanics---A physical model of transduction. *Journal of the Acoustical Society of America,* 68**,** 1660-1670.

ALLEN, J. B. & FAHEY, P. F. 1993. A second cochlear-frequency map that correlates distortion product and neural tuning measurements. *The Journal of the Acoustical Society of America,* 94**,** 809-816.

AMMA, L. L., GOODYEAR, R., FARIS, J. S., JONES, I., NG, L., RICHARDSON, G. & FORREST, D. 2003. An emilin family extracellular matrix protein identified in the cochlear basilar membrane. *Molecular and Cellular Neuroscience,* 23**,** 460-472.

ARNOLD, A., KOMPIS, M., CANDREIA, C., PFIFFNER, F., HÄUSLER, R. & STIEGER, C. 2010. The floating mass transducer at the round window: Direct transmission or bone conduction? *Hearing Research,* 263**,** 120-127.

ASHMORE, J. 2008. Cochlear Outer Hair Cell Motility. *Physiological Reviews,* 88**,** 173-210.

ASHMORE, J., AVAN, P., BROWNELL, W. E., DALLOS, P., DIERKES, K., FETTIPLACE, R., GROSH, K., HACKNEY, C. M., HUDSPETH, A. J., JÜLICHER, F., LINDNER, B., MARTIN, P., MEAUD, J., PETIT, C., SANTOS SACCHI, J. R. & CANLON, B. 2010. The remarkable cochlear amplifier. *Hearing Research,* 266**,** 1-17.

ASSAD, J. & COREY, D. 1992. An active motor model for adaptation by vertebrate hair cells. *The Journal of Neuroscience,* 12**,** 3291-3309.

AVAN, P., BONFILS, P., GILAIN, L. & MOM, T. 2003. Physiopathological significance of distortion-product otoacoustic emissions at 2 f1–f2 produced by high-versus low-level stimuli. *The Journal of the Acoustical Society of America,* 113**,** 430-441.

AVAN, P., LOTH, D., MENGUY, C. & TEYSSOU, M. 1990. Evoked otoacoustic emissions in guinea pig: basic characteristics. *Hearing Research,* 44**,** 151-160.

BÉKÉSY, G. V. 1953. Description of Some Mechanical Properties of the Organ of Corti. *The Journal of the Acoustical Society of America,* 25**,** 770-785.

BÉKÉSY, G. V. 1960. *Experiments in hearing*, McGraw-Hill Book Company.

BÉKÉSY, G. V. 1970. Travelling Waves as Frequency Analysers in the Cochlea. *Nature,* 225**,** 1207-1209.

BENSER, M. E., MARQUIS, R. E. & HUDSPETH, A. J. 1996. Rapid, Active Hair Bundle Movements in Hair Cells from the Bullfrog's Sacculus. *The Journal of Neuroscience,* 16**,** 5629-5643.

BEURG, M., NAM, J.-H., CRAWFORD, A. & FETTIPLACE, R. 2008. The Actions of Calcium on Hair Bundle Mechanics in Mammalian Cochlear Hair Cells. *Biophysical Journal,* 94**,** 2639-2653.

BIAN, L. 2004. Cochlear compression: Effects of low-frequency biasing on quadratic distortion product otoacoustic emission. *The Journal of the Acoustical Society of America,* 116**,** 3559-3571.

BIAN, L., CHERTOFF, M. E. & MILLER, E. 2002. Deriving a cochlear transducer function from low-frequency modulation of distortion product otoacoustic emissions. *The Journal of the Acoustical Society of America,* 112**,** 198-210.

BIAN, L., LINHARDT, E. E. & CHERTOFF, M. E. 2004. Cochlear hysteresis: Observation with low-frequency modulated distortion product otoacoustic emissions. *The Journal of the Acoustical Society of America,* 115**,** 2159-2172.

BIAN, L. & SCHERRER, N. M. 2007. Low-frequency modulation of distortion product otoacoustic emissions in humans. *The Journal of the Acoustical Society of America,* 122**,** 1681-1692.

BILGER, R. C., MATTHIES, M. L., HAMMEL, D. R. & DEMOREST, M. E. 1990. Genetic Implications of Gender Differences in the Prevalence of Spontaneous Otoacoustic Emissions. *J Speech Hear Res,* 33**,** 418-432.

BILLONE, M. & RAYNOR, S. 1973. Transmission of radial shear forces to cochlear hair cells. *The Journal of the Acoustical Society of America,* 54**,** 1143-1156.

BOHNKE, F. & ARNOLD, W. 1998. Nonlinear mechanics of the organ of Corti caused by Deiters cells. *Biomedical Engineering, IEEE Transactions on,* 45**,** 1227-1233.

BORRMANN, A. & ARNOLD, W. 2007. Non-syndromal round window atresia: an autosomal dominant genetic disorder with variable penetrance? *European Archives of Oto-Rhino-Laryngology,* 264**,** 1103-1108.

BROWN, A. M., MCDOWELL, B. & FORGE, A. 1989. Acoustic distortion products can be used to monitor the effects of chronic gentamicin treatment. *Hearing research,* 42**,** 143-156.

BROWN, S. D. M., HARDISTY-HUGHES, R. E. & MBURU, P. 2008. Quiet as a mouse: dissecting the molecular and genetic basis of hearing. *Nature Reviews Genetics,* 9**,** 277-290.

BROWNELL, W. E., BADER, C. R., BERTRAND, D. & DE RIBAUPIERRE, Y. 1985. Evoked mechanical responses of isolated cochlear outer hair cells. *Science,* 227**,** 194-196.

CABEZUDO, L. M. 1978. The ultrastructure of the basilar membrane in the cat. *Acta Oto-Laryngologica,* 86**,** 160-175.

CHAN, D. K. & HUDSPETH, A. J. 2005a. Ca2+ current-driven nonlinear amplification by the mammalian cochlea in vitro. *Nature Neuroscience,* 8**,** 149-155.

CHAN, D. K. & HUDSPETH, A. J. 2005b. Mechanical Responses of the Organ of Corti to Acoustic and Electrical Stimulation In Vitro. *Biophysical Journal,* 89**,** 4382-4395.

CHEATHAM, M. A. & DALLOS, P. 1982. Two-tone interactions in the cochlear microphonic. *Hearing Research,* 8**,** 29-48.

CHEATHAM, M. A., ZHENG, J., HUYNH, K. H., DU, G. G., GAO, J., ZUO, J., NAVARRETE, E. & DALLOS, P. 2005. Cochlear function in mice with only one copy of the prestin gene. *The Journal of Physiology,* 569**,** 229-241.

CHEN, Z., HU, G., GLASBERG, B. R. & MOORE, B. C. J. 2011. A new method of calculating auditory excitation patterns and loudness for steady sounds. *Hearing Research,* 282**,** 204-215.

CLACK, J. A. 2002. Patterns and processes in the early evolution of the tetrapod ear. *Journal of neurobiology,* 53**,** 251-264.

CODY, A. R. & JOHNSTONE, B. M. 1980. Single auditory neuron response during acute acoustic trauma. *Hearing Research,* 3**,** 3-16.

CODY, A. R. & RUSSELL, I. J. 1987. The response of hair cells in the basal turn of the guinea-pig cochlea to tones. *The Journal of Physiology,* 383**,** 551-569.

COHEN-SALMON, M., EL-AMRAOUI, A., LEIBOVICI, M. & PETIT, C. 1997. Otogelin: A glycoprotein specific to the acellular membranes of the inner ear. *Proceedings of the National Academy of Sciences,* 94**,** 14450-14455.

COLLETTI, V., SOLI, S. D., CARNER, M. & COLLETTI, L. 2006. Treatment of mixed hearing losses via implantation of a vibratory transducer on the round window. *International journal of audiology,* 45**,** 600-608.

COOPER, N. P. & RHODE, W. S. 1992. Basilar membrane mechanics in the hook region of cat and guinea-pig cochleae: Sharp tuning and nonlinearity in the absence of baseline position shifts. *Hearing Research,* 63**,** 163-190.

COREY, D. P., GARCÍA-AÑOVEROS, J., HOLT, J. R., KWAN, K. Y., LIN, S. Y., VOLLRATH, M. A., AMALFITANO, A., CHEUNG, E. L. M., DERFLER, B. H. & DUGGAN, A. 2004. TRPA1 is a candidate for the mechanosensitive transduction channel of vertebrate hair cells. *Nature,* 432**,** 723-730.

COREY, D. P. & HUDSPETH, A. J. 1983. Kinetics of the receptor current in bullfrog saccular hair cells. *The Journal of Neuroscience,* 3**,** 962-976.

CRAWFORD, A. C., EVANS, M. G. & FETTIPLACE, R. 1989. Activation and adaptation of transducer currents in turtle hair cells. *J Physiol,* 419**,** 405-34.

CRAWFORD, A. C., EVANS, M. G. & FETTIPLACE, R. 1991. The actions of calcium on the mechano-electrical transducer current of turtle hair cells. *The Journal of Physiology,* 434**,** 369-398.

CRAWFORD, A. C. & FETTIPLACE, R. 1981. An electrical tuning mechanism in turtle cochlear hair cells. *The Journal of Physiology,* 312**,** 377-412.

CRAWFORD, A. C. & FETTIPLACE, R. 1985. The mechanical properties of ciliary bundles of turtle cochlear hair cells. *The Journal of Physiology,* 364**,** 359-379.

CULLER, E., FINCH, G. & GIRDEN, E. 1935. Function of the round window in hearing. *American Journal of Physiology--Legacy Content,* 111**,** 416-425.

DALLOS, P. 1970. Low-Frequency Auditory Characteristics: Species Dependence. *The Journal of the Acoustical Society of America,* 48**,** 489.

DALLOS, P. 1986. Neurobiology of cochlear inner and outer hair cells: intracellular recordings. *Hearing Research,* 22**,** 185-198.

DALLOS, P. 1992. The active cochlea. *The Journal of Neuroscience,* 12**,** 4575-4585.

DALLOS, P. 2003. Some pending problems in cochlear mechanics. *Biophysics of the Cochela: From Molecules to Models. A. Gummer, editor. World Scientific, Hackensack, NJ***,** 97-109.

DALLOS, P., BILLONE, N. C., DURRANT, J. D., WANG, C. Y. & RAYNOR, S. 1972. Cochlear Inner and Outer Hair Cells: Functional Differences. *Science,* 177**,** 356-358.

DALLOS, P. & CHEATHAM, M. A. 1976. Compound action potential (AP) tuning curves. *The Journal of the Acoustical Society of America,* 59**,** 591-597.

DALLOS, P. & CHEATHAM, M. A. 1989. Nonlinearities in cochlear receptor potentials and their origins. *The Journal of the Acoustical Society of America,* 86**,** 1790-1796.

DALLOS, P. & EVANS, B. N. 1995. High-frequency motility of outer hair cells and the cochlear amplifier. *Science,* 267**,** 2006-2009.

DALLOS, P. & HARRIS, D. 1978. Properties of auditory nerve responses in absence of outer hair cells. *Journal of Neurophysiology,* 41**,** 365-383.

DALLOS, P., WU, X., CHEATHAM, M. A., GAO, J., ZHENG, J., ANDERSON, C. T., JIA, S., WANG, X., CHENG, W. H. Y., SENGUPTA, S., HE, D. Z. Z. & ZUO, J. 2008. Prestin-Based Outer Hair Cell Motility Is Necessary for Mammalian Cochlear Amplification. *Neuron,* 58**,** 333-339.

DALLOS, P., ZHENG, J. & CHEATHAM, M. A. 2006. Prestin and the cochlear amplifier. *The Journal of Physiology,* 576**,** 37-42.

DAVIS, H. 1958. A mechano-electrical theory of cochlear action. *Trans Am Otol Soc.,* 46**,** 180-96.

DAVIS, H. 1965. A Model for Transducer Action in the Cochlea. *Cold Spring Harbor Symposia on Quantitative Biology,* 30**,** 181-190.

DAVIS, H. 1983. An active process in cochlear mechanics. *Hearing Research,* 9**,** 79-90.

DAVIS, R. L. 2003. Gradients of Neurotrophins, Ion Channels, and Tuning in the Cochlea. *The Neuroscientist,* 9**,** 311-316.

DE ALARCON, A., JAHRSDOERFER, R. A. & KESSER, B. W. 2008. Congenital absence of the oval window: diagnosis, surgery, and audiometric outcomes. *Otology & neurotology,* 29**,** 23.

DEANS, M. R., PETERSON, J. M. & WONG, G. W. 2010. Mammalian Otolin: a multimeric glycoprotein specific to the inner ear that interacts with otoconial matrix protein Otoconin-90 and Cerebellin-1. *PloS one,* 5**,** e12765.

DECRAEMER, W. F., KHANNA, S. M. & FUNNELL, W. R. J. 1989. Interferometric measurement of the amplitude and phase of tympanic membrane vibrations in cat. *Hearing Research,* 38**,** 1-17.

DECRAEMER, W. F., KHANNA, S. M. & FUNNELL, W. R. J. 1991. Malleus vibration mode changes with frequency. *Hearing Research,* 54**,** 305-318.

DENK, W., HOLT, J. R., SHEPHERD, G. M. G. & COREYTT, D. P. 1995. Calcium imaging of single stereocilia in hair cells: Localization of transduction channels at both ends of tip links. *Neuron,* 15**,** 1311-1321.

DONG, W. & OLSON, E. S. 2009. In Vivo Impedance of the Gerbil Cochlear Partition at Auditory Frequencies. *Biophysical Journal,* 97**,** 1233-1243.

DREXL, M., MELLADO LAGARDE, M. M., ZUO, J., LUKASHKIN, A. N. & RUSSELL, I. J. 2008. The Role of Prestin in the Generation of Electrically Evoked Otoacoustic Emissions in Mice. *Journal of Neurophysiology,* 99**,** 1607-1615.

DURRANT, J. D. & DALLOS, P. 1972. The Effects of dc Current Polarization on Cochlear Harmonics. *The Journal of the Acoustical Society of America,* 52**,** 1725-1728.

EATOCK, R. A., COREY, D. P. & HUDSPETH, A. J. 1987. Adaptation of mechanoelectrical transduction in hair cells of the bullfrog's sacculus. *The Journal of Neuroscience,* 7**,** 2821-2836.

ELLIOT, S. J. 24.08.2011 2011. *RE: Personal Communication.*

FETTIPLACE, R. & HACKNEY, C. M. 2006. The sensory and motor roles of auditory hair cells. *Nature Reviews Neuroscience,* 7**,** 19-29.

FLOCK, A. & CHEUNG, H. C. 1977. Actin filaments in sensory hairs of inner ear receptor cells. *The Journal of Cell Biology,* 75**,** 339-343.

FRANK, G., HEMMERT, W. & GUMMER, A. W. 1999. Limiting dynamics of high-frequency electromechanical transduction of outer hair cells. *Proceedings of the National Academy of Sciences,* 96**,** 4420-4425.

FRANK, G. & KOSSL, M. 1996. The acoustic two-tone distortions 2f1-f2 and f2-f1 and their possible relation to changes in the operating point of the cochlear amplifier. *Hear.Res.,* 98/1-2**,** 115.

FRANK, G. & KOSSL, M. 1997. Acoustical and electrical biasing of the cochlea partition. Effects on the acoustic two tone distortions f2-f1 and 2f1-f2. *Hear.Res.,* 113**,** 57-68.

FREEMAN, D. M., ABNET, C. C., HEMMERT, W., TSAI, B. S. & WEISS, T. F. 2003a. Dynamic material properties of the tectorial membrane: a summary. *Hearing Research,* 180**,** 1-10.

FREEMAN, D. M., MASAKI, K., MCALLISTER, A. R., WEI, J. L. & WEISS, T. F. 2003b. Static material properties of the tectorial membrane: a summary. *Hearing Research,* 180**,** 11-27.

FREEMAN, D. M. & WEISS, T. F. 1990. Hydrodynamic forces on hair bundles at high frequencies. *Hearing Research,* 48**,** 31-36.

FRIDBERGER, A., DE MONVEL, J. B., ZHENG, J., HU, N., ZOU, Y., REN, T. & NUTTALL, A. 2004. Organ of Corti Potentials and the Motion of the Basilar Membrane. *The Journal of Neuroscience,* 24**,** 10057-10063.

FRIDBERGER, A., TOMO, I., ULFENDAHL, M. & DE MONVEL, J. B. 2006. Imaging hair cell transduction at the speed of sound: dynamic behavior of mammalian stereocilia. *Proceedings of the National Academy of Sciences of the United States of America,* 103**,** 1918-1923.

FROLENKOV, G. I., BELYANTSEVA, I. A., KURC, M., MASTROIANNI, M. A. & KACHAR, B. 1998. Cochlear outer hair cell electromotility can provide force for both low and high intensity distortion product otoacoustic emissions. *Hearing research,* 126**,** 67-74.

GALE, J. & ASHMORE, J. 1994. Charge displacement induced by rapid stretch in the basolateral membrane of the guinea-pig outer hair cell. *Proceedings of the Royal Society of London. Series B: Biological Sciences,* 255**,** 243-249.

GALE, J. E. & ASHMORE, J. F. 1997. An intrinsic frequency limit to the cochlear amplifier. *Nature,* 389**,** 63-66.

GAO, J., WANG, X., WU, X., AGUINAGA, S., HUYNH, K., JIA, S., MATSUDA, K., PATEL, M., ZHENG, J. & CHEATHAM, M. A. 2007. Prestin-based outer hair cell electromotility in knockin

mice does not appear to adjust the operating point of a cilia-based amplifier. *Proceedings of the National Academy of Sciences,* 104**,** 12542.

GARCÍA-AÑOVEROS, J. & COREY, D. P. 1997. The Molecules Of Mechanosensation. *Annual Review of Neuroscience,* 20**,** 567-594.

GEDLICKA, C., FORMANEK, M. & EHRENBERGER, K. 2009. Analysis of 60 patients after tympanotomy and sealing of the round window membrane after acute unilateral sensorineural hearing loss. *American Journal of Otolaryngology,* 30**,** 157-161.

GEISLER, C. D. 1996. *Physiology of olivocochlea efferents,* New York, Springer.

GEISLER, C. D. 1998. *From Sound to Synapse*, OUP USA.

GEISLER, C. D. & SANG, C. 1995. A cochlear model using feed-forward outer-hair-cell forces. *Hearing Research,* 86**,** 132-146.

GÉLÉOC, G., LENNAN, G., RICHARDSON, G. & KROS, C. 1997. A quantitative comparison of mechanoelectrical transduction in vestibular and auditory hair cells of neonatal mice. *Proceedings of the Royal Society of London. Series B: Biological Sciences,* 264**,** 611-621.

GHAFFARI, R., ARANYOSI, A. J. & FREEMAN, D. M. 2007. Longitudinally propagating traveling waves of the mammalian tectorial membrane. *Proceedings of the National Academy of Sciences,* 104**,** 16510-16515.

GHIZ, A. F., SALT, A. N., DEMOTT, J. E., HENSON, M. M., HENSON JR, O. W. & GEWALT, S. L. 2001. Quantitative anatomy of the round window and cochlear aqueduct in guinea pigs. *Hearing Research,* 162**,** 105-112.

GILLESPIE, P. G. & COREY, D. P. 1997. Myosin and Adaptation by Hair Cells. *Neuron,* 19.

GOLD, T. 1948. Hearing. II. The Physical Basis of the Action of the Cochlea. *Proceedings of the Royal Society of London. Series B, Biological Sciences,* 135**,** 492-498.

GOODHILL, V. 1971. Sudden deafness and round window rupture. *The Laryngoscope,* 81**,** 1462-1474.

GOODYEAR, R. J., MARCOTTI, W., KROS, C. J. & RICHARDSON, G. P. 2005. Development and properties of stereociliary link types in hair cells of the mouse cochlea. *The Journal of Comparative Neurology,* 485**,** 75-85.

GUETA, R., BARLAM, D., SHNECK, R. Z. & ROUSSO, I. 2006. Measurement of the mechanical properties of isolated tectorial membrane using atomic force microscopy. *Proceedings of the National Academy of Sciences,* 103**,** 14790-14795.

GUETA, R., TAL, E., SILBERBERG, Y. & ROUSSO, I. 2007. The 3D structure of the tectorial membrane determined by second-harmonic imaging microscopy. *Journal of Structural Biology,* 159**,** 103-110.

GUINAN, J. J. J. & PEAKE, W. T. 1967. Middle-Ear Characteristics of Anesthetized Cats. *The Journal of the Acoustical Society of America,* 41**,** 1237-1261.

GUINAN JR, J. J. 2012. How are inner hair cells stimulated? Evidence for multiple mechanical drives. *Hearing research,* 292**,** 35-50.

GULLEY, R. L. & REESE, T. S. 1977. Regional specialization of the hair cell plasmalemma in the organ of corti. *The Anatomical Record,* 189**,** 109-123.

GUMMER, A. W., HEMMERT, W. & ZENNER, H. P. 1996. Resonant tectorial membrane motion in the inner ear: its crucial role in frequency tuning. *Proceedings of the National Academy of Sciences,* 93**,** 8727-8732.

HARRISON, R. V. & EVANS, E. F. 1979. Cochlear fibre responses in guinea pigs with well defined cochlea lesions. *Acta Oto-laryngologica* 83-92.

HARRISON, R. V. & PRIJS, V. F. 1984. Single cochlear fibre responses in guinea pigs with long-term endolymphatic hydrops. *Hearing Research,* 14**,** 79-84.

HE, D. Z. Z., JIA, S. & DALLOS, P. 2003. Prestin and the dynamic stiffness of cochlear outer hair cells. *The Journal of neuroscience,* 23**,** 9089-9096.

HE, D. Z. Z., JIA, S. & DALLOS, P. 2004. Mechanoelectrical transduction of adult outer hair cells studied in a gerbil hemicochlea. *Nature,* 429**,** 766-770.

HEFFNER, R. S., KOAY, G. & HEFFNER, H. E. 2001. Audiograms of five species of rodents: implications for the evolution of hearing and the perception of pitch. *Hearing research,* 157**,** 138-152.

HEINRICH, U.-R., MAURER, J. & MANN, W. 1998. Possible Ca²⁺-dependent mechanism of apical outer hair cell modulation within the cochlea of the guinea pig. *Cell and Tissue Research,* 292**,** 57-65.

HELLSTROM, S. O. 1998. Surgical anatomy of the rat middle ear. *Otolaryngology--head and neck surgery : official journal of American Academy of Otolaryngology-Head and Neck Surgery,* 119**,** 556-8.

HEMMERT, W., ZENNER, H.-P. & GUMMER, A. W. 2000. Three-Dimensional Motion of the Organ of Corti. *Biophysical Journal,* 78**,** 2285-2297.

HILDEBRAND, M. S., MORÍN, M., MEYER, N. C., MAYO, F., MODAMIO-HOYBJOR, S., MENCÍA, A., OLAVARRIETA, L., MORALES-ANGULO, C., NISHIMURA, C. J. & WORKMAN, H. 2011. DFNA8/12 caused by TECTA mutations is the most identified subtype of nonsyndromic autosomal dominant hearing loss. *Human mutation*.

HOLLEY, M. C. & ASHMORE, J. F. 1990. Spectrin, actin and the structure of the cortical lattice in mammalian cochlear outer hair cells. *Journal of Cell Science,* 96**,** 283-291.

HOLT, J. R., GILLESPIE, S. K. H., PROVANCE, D. W., SHAH, K., SHOKAT, K. M., COREY, D. P., MERCER, J. A. & GILLESPIE, P. G. 2002. A chemical-genetic strategy implicates myosin-1c in adaptation by hair cells. *Cell,* 108**,** 371-381.

HOWARD, J. & BECHSTEDT, S. 2004. Hypothesis: a helix of ankyrin repeats of the NOMPC-TRP ion channel is the gating spring of mechanoreceptors. *Current biology: CB,* 14**,** R224.

HOWARD, J. & SPUDICH, J. 1996. Is the lever arm of myosin a molecular elastic element? *Proceedings of the National Academy of Sciences of the United States of America,* 93**,** 4462.

HUANG, G. & SANTOS-SACCHI, J. 1994. Motility voltage sensor of the outer hair cell resides within the lateral plasma membrane. *Proceedings of the National Academy of Sciences,* 91**,** 12268-12272.

HUDSPETH, A. J. 2008. Making an Effort to Listen: Mechanical Amplification in the Ear. *Neuron,* 59**,** 530-545.

HUDSPETH, A. J. & COREY, D. P. 1977. Sensitivity, polarity, and conductance change in the response of vertebrate hair cells to controlled mechanical stimuli. *Proceedings of the National Academy of Sciences,* 74**,** 2407-2411.

HUDSPETH, A. J. & JACOBS, R. 1979. Stereocilia mediate transduction in vertebrate hair cells (auditory system/cilium/vestibular system). *Proceedings of the National Academy of Sciences,* 76**,** 1506-1509.

IWASA, K. 1993. Effect of stress on the membrane capacitance of the auditory outer hair cell. *Biophysical journal,* 65**,** 492-498.

JABER, L., HALPERN, G. J. & SHOHAT, T. 2000. Trends in the frequencies of consanguineous marriages in the Israeli Arab community. *Clinical genetics,* 58**,** 106-110.

JENSEN-SMITH, H. & HALLWORTH, R. 2007. Lateral wall protein content mediates alterations in cochlear outer hair cell mechanics before and after hearing onset. *Cell motility and the cytoskeleton,* 64**,** 705-717.

JOHNSON, STUART L., BEURG, M., MARCOTTI, W. & FETTIPLACE, R. 2011. Prestin-Driven Cochlear Amplification Is Not Limited by the Outer Hair Cell Membrane Time Constant. *Neuron,* 70**,** 1143-1154.

JOHNSTONE, J. R. & JOHNSTONE, B. M. 1966. Origin of Summating Potential. *The Journal of the Acoustical Society of America,* 40**,** 1405-1413.

JONES, G. P. 2012. *Acoustic sensitivity of the vestibular system and mechanical analysis of the tectorial membrane in mammals.* Doctoral, University of Sussex.

JONES, G. P., LUKASHKINA, V. A., RUSSELL, I. J., ELLIOTT, S. J. & LUKASHKIN, A. N. 2013. Frequency-Dependent Properties of the Tectorial Membrane Facilitate Energy Transmission and Amplification in the Cochlea. *Biophysical journal,* 104**,** 1357-1366.

KAKEHATA, S. & SANTOS-SACCHI, J. 1995. Membrane tension directly shifts voltage dependence of outer hair cell motility and associated gating charge. *Biophysical journal,* 68**,** 2190-2197.

KANDEL, E. R., SCHWARTZ, J. H. & JESSELL, T. M. 2000. *Principles of Neural Science*, McGraw-Hill Medical.

KATORI, Y., HOZAWA, K., KIKUCHI, T., TONOSAKI, A. & TAKASAKA, T. 1993. Fine structure of the lamina basilaris of guinea pig cochlea. *Acta Oto-Laryngologica,* 113**,** 715-719.

KEMP, D. T. 1978. *Stimulated acoustic emissions from within the human auditory system*, ASA.

KEMP, D. T. 2008. *Otoacoustic Emissions: Concepts and Origins*, Springer.

KEMP, D. T. & BROWN, A. M. 1984. Ear canal acoustic and round window electrical correlates of 2f1- f2 distortion generated in the cochlea. *Hearing Research,* 13**,** 39-46.

KEMP, D. T. & CHUM, R. 1980. Properties of the generator of stimulated acoustic emissions. *Hearing Research,* 2**,** 213-232.

KENNEDY, H. J., CRAWFORD, A. C. & FETTIPLACE, R. 2005. Force generation by mammalian hair bundles supports a role in cochlear amplification. *Nature,* 433**,** 880-883.

KIANG, N. Y. S., SACHS, M. B. & PEAKE, W. T. 1967. Shapes of Tuning Curves for Single Auditory-Nerve Fibers. *The Journal of the Acoustical Society of America,* 42**,** 1341-1342.

KIEFER, J., ARNOLD, W. & STAUDENMAIER, R. 2006. Round window stimulation with an implantable hearing aid (Soundbridge®) combined with autogenous reconstruction of the auricle–a new approach. *ORL,* 68**,** 378-385.

KILLION, M. C. & DALLOS, P. 1979. Impedance matching by the combined effects of the outer and middle ear. *The Journal of the Acoustical Society of America,* 66**,** 599-602.

KIM, D. O. 1986. Active and nonlinear cochlear biomechanics and the role of outer-hair-cell subsystem in the mammalian auditory system. *Hearing Research,* 22**,** 105-114.

KIM, D. O., MOLNAR, C. E. & MATTHEWS, J. W. 1980. Cochlear mechanics: Nonlinear behavior in two-tone responses as reflected in cochlear-nerve-fiber responses and in ear-canal sound pressure. *The Journal of the Acoustical Society of America,* 67**,** 1704-1721.

KIMURA, R. S. 1966. Hairs of the Cochlear Sensory Cells and Their Attachment to the Tectorial Membrane. *Acta Oto-laryngologica,* 61**,** 55-72.

KJAER, B. A. 1976. *Condenser microphones and microphone preamplifiers. Theory and application handbook*.

KJELLEN, L. & LINDAHL, U. 1991. Proteoglycans: Structures and Interactions. *Annual Review of Biochemistry,* 60**,** 443-475.

KOKA, K., HOLLAND, N. J., LUPO, J. E., JENKINS, H. A. & TOLLIN, D. J. 2010. Electrocochleographic and mechanical assessment of round window stimulation with an active middle ear prosthesis. *Hearing Research,* 263**,** 128-137.

KÖSSL, M. & RUSSELL, I. J. 1992. The phase and magnitude of hair cell receptor potentials and frequency tuning in the guinea pig cochlea. *The Journal of Neuroscience,* 12**,** 1575-1586.

KRONESTER-FREI, A. 1978. Ultrastructure of the different zones of the tectorial membrane. *Cell and Tissue Research,* 193**,** 11-23.

KROS, C., MARCOTTI, W., VAN NETTEN, S., SELF, T., LIBBY, R., BROWN, S., RICHARDSON, G. & STEEL, K. 2001. Reduced climbing and increased slipping adaptation in cochlear hair cells of mice with Myo7a mutations. *Nature neuroscience,* 5**,** 41-47.

KROS, C. J., RUSCH, A. & RICHARDSON, G. P. 1992. Mechano-Electrical Transducer Currents in Hair Cells of the Cultured Neonatal Mouse Cochlea. *Proceedings of the Royal Society of London. Series B: Biological Sciences,* 249**,** 185-193.

KUMMER, P., JANSSEN, T. & ARNOLD, W. 1998. The level and growth behavior of the 2 f1− f2 distortion product otoacoustic emission and its relationship to auditory sensitivity in normal hearing and cochlear hearing loss. *The Journal of the Acoustical Society of America,* 103**,** 3431.

LEGAN, P. K., LUKASHKINA, V. A., GOODYEAR, R. J., KÖSSL, M., RUSSELL, I. J. & RICHARDSON, G. P. 2000. A Targeted Deletion in [alpha]-Tectorin Reveals that the Tectorial Membrane Is Required for the Gain and Timing of Cochlear Feedback. *Neuron,* 28**,** 273-285.

LEGAN, P. K., LUKASHKINA, V. A., GOODYEAR, R. J., LUKASHKIN, A. N., VERHOEVEN, K., VAN CAMP, G., RUSSELL, I. J. & RICHARDSON, G. P. 2005. A deafness mutation isolates a second role for the tectorial membrane in hearing. *Nature Neuroscience,* 8**,** 1035-1042.

LEGAN, P. K., RAU, A., KEEN, J. N. & RICHARDSON, G. P. 1997. The Mouse Tectorins. *Journal of Biological Chemistry,* 272**,** 8791-8801.

LIBERMAN, M. C. 1978. Auditory-nerve response from cats raised in a low-noise chamber. *The Journal of the Acoustical Society of America,* 63**,** 442.

LIBERMAN, M. C., GAO, J., HE, D. Z. Z., WU, X., JIA, S. & ZUO, J. 2002. Prestin is required for electromotility of the outer hair cell and for the cochlear amplifier. *Nature,* 419**,** 300-304.

LIM, D. J. 1972. Fine morphology of the tectorial membrane. Its relationship to the organ of Corti. *Arch Otolaryngol,* 96**,** 199-205.

LIM, D. J. 1986. Functional structure of the organ of Corti: a review. *Hearing Research,* 22**,** 117-146.

LINDER, T. E., MA, F. & HUBER, A. 2003. Round window atresia and its effect on sound transmission. *Otology & neurotology,* 24**,** 259.

LIU, Z., LI, G.-H., HUANG, J.-F., MURPHY, R. W. & SHI, P. 2012. Hearing Aid for Vertebrates via Multiple Episodic Adaptive Events on prestin Genes. *Molecular Biology and Evolution*.

LUKASHKIN, A. N., BASHTANOV, M. E. & RUSSELL, I. J. 2005. A self-mixing laser-diode interferometer for measuring basilar membrane vibrations without opening the cochlea. *Journal of Neuroscience Methods,* 148**,** 122-129.

LUKASHKIN, A. N., LUKASHKINA, V. A. & RUSSELL, I. J. 2002. One source for distortion product otoacoustic emissions generated by low- and high-level primaries. *The Journal of the Acoustical Society of America,* 111**,** 2740-2748.

LUKASHKIN, A. N., RICHARDSON, G. P. & RUSSELL, I. J. 2010. Multiple roles for the tectorial membrane in the active cochlea. *Hearing Research,* 266**,** 26-35.

LUKASHKIN, A. N. & RUSSELL, I. J. 1998a. A descriptive model of the receptor potential nonlinearities generated by the hair cell mechanoelectrical transducer. *J.Acoust.Soc.Am.,* 103**,** 973-980.

LUKASHKIN, A. N. & RUSSELL, I. J. 1998b. A descriptive model of the receptor potential nonlinearities generated by the hair cell mechanoelectrical transducer. *The Journal of the Acoustical Society of America,* 103**,** 973-980.

LUKASHKIN, A. N. & RUSSELL, I. J. 1999. Analysis of the f− f and 2 f− f distortion components generated by the hair cell mechanoelectrical transducer: Dependence on the amplitudes of the primaries and feedback gain. *The Journal of the Acoustical Society of America,* 106**,** 2661.

LUKASHKIN, A. N. & RUSSELL, I. J. 2005a. Dependence of the DPOAE amplitude pattern on acoustical biasing of the cochlear partition. *Hear Res,* 203**,** 45-53.

LUKASHKIN, A. N. & RUSSELL, I. J. 2005b. Dependence of the DPOAE amplitude pattern on acoustical biasing of the cochlear partition. *Hearing Research,* 203**,** 45-53.

LUKASHKIN, A. N., SMITH, J. K. & RUSSELL, I. J. 2007a. Properties of distortion product otoacoustic emissions and neural suppression tuning curves attributable to the tectorial membrane resonance. *The Journal of the Acoustical Society of America,* 121**,** 337.

LUKASHKIN, A. N., WALLING, M. N. & RUSSELL, I. J. 2007b. Power Amplification in the Mammalian Cochlea. *Current Biology,* 17**,** 1340-1344.

LUPO, J. E., KOKA, K., HOLLAND, N. J., JENKINS, H. A. & TOLLIN, D. J. 2009. Prospective electrophysiologic findings of round window stimulation in a model of experimentally induced stapes fixation. *Otology & neurotology,* 30**,** 1215.

MAIER, W. 1989. Phylogeny and ontogeny of mammalian middle ear structures. *Netherlands Journal of Zoology, 40,* 1**,** 55-74.

MAMMANO, F. & NOBILI, R. 1993. Biophysics of the cochlea: Linear approximation. *The Journal of the Acoustical Society of America,* 93**,** 3320-3332.

MANLEY, G. A. 2000. Cochlear mechanisms from a phylogenetic viewpoint. *Proceedings of the National Academy of Sciences,* 97**,** 11736-11743.

MANLEY, G. A. 2010. An evolutionary perspective on middle ears. *Hearing research,* 263**,** 3-8.

MARQUARDT, T., HENSEL, J., MROWINSKI, D. & SCHOLZ, G. 2007a. Low-frequency characteristics of human and guinea pig cochleae. *J Acoust Soc Am,* 121**,** 3628-38.

MARQUARDT, T., HENSEL, J., MROWINSKI, D. & SCHOLZ, G. 2007b. Low-frequency characteristics of human and guinea pig cochleae. *The Journal of the Acoustical Society of America,* 121**,** 3628.

MARTIN, C., TRINGALI, S., BERTHOLON, P., POUGET, J. F. & PRADES, J. M. 2002. Isolated congenital round window absence. *The Annals of otology, rhinology, and laryngology,* 111**,** 799.

MARTIN, P., BOZOVIC, D., CHOE, Y. & HUDSPETH, A. J. 2003. Spontaneous Oscillation by Hair Bundles of the Bullfrog's Sacculus. *The Journal of Neuroscience,* 23**,** 4533-4548.

MEAUD, J. & GROSH, K. 2011. Coupling Active Hair Bundle Mechanics, Fast Adaptation, and Somatic Motility in a Cochlear Model. *Biophysical Journal,* 100**,** 2576-2585.

MELLADO LAGARDE, M. M. 2008. *A Role for Prestin in Amplification, Otoacoustic Emissions, and Shaping Mechanical Tuning in the Cochlea.* DPhil, University of Sussex.

MELLADO LAGARDE, M. M. 2011. Personnal Communication.

MELLADO LAGARDE, M. M., DREXL, M., LUKASHKIN, ANDREI N., ZUO, J. & RUSSELL, I. J. 2008. Prestin's Role in Cochlear Frequency Tuning and Transmission of Mechanical Responses to Neural Excitation. *Current Biology,* 18**,** 200-202.

MERTENS, J. 1991. The reaction of the guinea pig cochlea to perforations of the round window membrane with and without perilymph aspiration. *European Archives of Oto-Rhino-Laryngology,* 248**,** 395-399.

MILLS, D. M. 1997. Interpretation of distortion product otoacoustic emission measurements. I. Two stimulus tones. *The Journal of the Acoustical Society of America,* 102**,** 413-429.

MILLS, D. M., NORTON, S. J. & RUBEL, E. W. 1993. Vulnerability and adaptation of distortion product otoacoustic emissions to endocochlear potential variation. *The Journal of the Acoustical Society of America,* 94**,** 2108-2122.

MILLS, D. M. & RUBEL, E. W. 1994. Variation of distortion product otoacoustic emissions with furosemide injection. *Hearing research,* 77**,** 183-199.

MOLLER, A. R. 1970. *The Middle Ear. In Foundations of Modern Auditory Theory,* New York, Academic Press.

MOUNT, D. & ROMERO, M. 2004. The SLC26 gene family of multifunctional anion exchangers. *Pflügers Archiv European Journal of Physiology,* 447**,** 710-721.

MÜLLER, M., HUNERBEIN, K., HOIDIS, S. & SMOLDERS, J. 2005. A physiological place frequency map of the cochlea in the CBA/J mouse. *Hearing Research,* 202**,** 63-73.

MUNYER, P. D. & SCHULTE, B. A. 1991. Immunohistochemical identification of proteoglycans in gelatinous membranes of cat and gerbil inner ear. *Hearing Research,* 52**,** 369-378.

MURUGASU, E. & RUSSELL, I. J. 1995. Salicylate ototoxicity: the effect on the basilar membrane displacement, cochlea microphonics and neural responses in the basal turn of the guinea pig cochlea. *Auditory Neuroscience* 1**,** 139-150.

MUSTAPHA, M., WEIL, D., CHARDENOUX, S., ELIAS, S., EL-ZIR, E., BECKMANN, J. S., LOISELET, J. & PETIT, C. 1999. An α-tectorin gene defect causes a newly identified autosomal recessive form of sensorineural pre-lingual non-syndromic deafness, DFNB21. *Human molecular genetics,* 8**,** 409-412.

NAKAJIMA, H. H., DONG, W., OLSON, E. S., ROSOWSKI, J. J., RAVICZ, M. E. & MERCHANT, S. N. 2010a. Evaluation of round window stimulation using the floating mass transducer by intracochlear sound pressure measurements in human temporal bones. *Otology & neurotology: official publication of the American Otological Society, American Neurotology Society [and] European Academy of Otology and Neurotology,* 31**,** 506.

NAKAJIMA, H. H., MERCHANT, S. N. & ROSOWSKI, J. J. 2010b. Performance considerations of prosthetic actuators for round-window stimulation. *Hearing Research,* 263**,** 114-119.

NEELY, S. T. & KIM, D. O. 1982. *An active model for sharp tuning and high sensitivity in cochlear mechanics*, ASA.

NEELY, S. T. & KIM, D. O. 1983. An active cochlear model showing sharp tuning and high sensitivity. *Hearing Research,* 9**,** 123-130.

NETTEN, S. M. V. & KROS, C. J. 2000. Gating energies and forces of the mammalian hair cell transducer channel and related hair bundle mechanics. *Proceedings of the Royal Society of London. Series B: Biological Sciences,* 267**,** 1915-1923.

NILSEN, K. E. & RUSSELL, I. J. 1999. Timing of cochlear feedback: spatial and temporal representation of a tone across the basilar membrane. *Nature Neuroscience,* 2**,** 642-648.

NOWOTNY, M. & GUMMER, A. W. 2006. Nanomechanics of the subtectorial space caused by electromechanics of cochlear outer hair cells. *Proceedings of the National Academy of Sciences of the United States of America,* 103**,** 2120-2125.

NUTTALL, A. L. & DOLAN, D. F. 1996. Steady-state sinusoidal velocity responses of the basilar membrane in guinea pig. *The Journal of the Acoustical Society of America,* 99**,** 1556-1565.

OLSON, E. S. 1998. *Observing middle and inner ear mechanics with novel intracochlear pressure sensors*, ASA.

OPTICS, S. 1993. *Optical devises and laser diode instrumentation: Product catalogue*.

OSPECK, M., DONG, X. & IWASA, K. H. 2003. Limiting frequency of the cochlear amplifier based on electromotility of outer hair cells. *Biophysical journal,* 84**,** 739-749.

PATUZZI, R. B. & YATES, G. K. 1987. The low-frequency response of inner hair cells in the guinea pig cochlea: implications for fluid coupling and resonance of the stereocilia. *Hearing research,* 30**,** 83-98.

PATUZZI, R. B., YATES, G. K. & JOHNSTONE, B. M. 1989a. Changes in cochlear microphonic and neural sensitivity produced by acoustic trauma. *Hearing Research,* 39**,** 189-202.

PATUZZI, R. B., YATES, G. K. & JOHNSTONE, B. M. 1989b. Outer hair cell receptor current and sensorineural hearing loss. *Hearing Research,* 42**,** 47-72.

PENNER, M. J., GLOTZBACH, L. & HUANG, T. 1993. Spontaneous otoacoustic emissions: Measurement and data. *Hearing Research,* 68**,** 229-237.

PENNER, M. J. & ZHANG, T. 1997. Prevalence of spontaneous otoacoustic emissions in adults revisited. *Hearing Research,* 103**,** 28-34.

PICKLES, J. O. 2008. *An Introduction to the Physiology of Hearing*, Academic Press.

PREYER, S., RENZ, S., HEMMERT, W., ZENNER, H. P. & GUMMER, A. W. 1996. Receptor potential of outer hair cells isolated from base to apex of the adult guinea-pig cochlea: implications for cochlear tuning mechanisms. *Aud Neurosci,* 2**,** 145-157.

PURIA, S. & STEELE, C. 2010. Tympanic-membrane and malleus–incus-complex co-adaptations for high-frequency hearing in mammals. *Hearing Research,* 263**,** 183-190.

RHODE, W. S. 1971. Observations of the Vibration of the Basilar Membrane in Squirrel Monkeys using the M[o-umlaut]ssbauer Technique. *The Journal of the Acoustical Society of America,* 49**,** 1218-1231.

RHODE, W. S. 1978. Some observations on cochlear mechanics. *The Journal of the Acoustical Society of America,* 64**,** 158-176.

RHODE, W. S. 2007. Distortion product otoacoustic emissions and basilar membrane vibration in the 6--9 kHz region of sensitive chinchilla cochleae. *The Journal of the Acoustical Society of America,* 122**,** 2725-2737.

RHODE, W. S. & GEISLER, C. D. 1967. Model of the Displacement between Opposing Points on the Tectorial Membrane and Reticular Lamina. 42**,** 185-190.

RICCI, A. J., CRAWFORD, A. C. & FETTIPLACE, R. 2003. Tonotopic Variation in the Conductance of the Hair Cell Mechanotransducer Channel. *Neuron,* 40**,** 983-990.

RICHARDSON, G. P., DE MONVEL, J. B. & PETIT, C. 2011. How the Genetics of Deafness Illuminates Auditory Physiology. *Annual Review of Physiology,* 73**,** 311-334.

RICHARDSON, G. P., RUSSELL, I. J., DUANCE, V. C. & BAILEY, A. J. 1987. Polypeptide composition of the mammalian tectorial membrane. *Hearing Research,* 25**,** 45-60.

RICHTER, C.-P., EMADI, G., GETNICK, G., QUESNEL, A. & DALLOS, P. 2007. Tectorial Membrane Stiffness Gradients. *Biophysical Journal,* 93**,** 2265-2276.

ROBLES, L. & RUGGERO, M. A. 2001. Mechanics of the Mammalian Cochlea. *Physiological Reviews,* 81**,** 1305-1352.

ROBLES, L., RUGGERO, M. A. & RICH, N. C. 1986. Basilar membrane mechanics at the base of the chinchilla cochlea. I. Input--output functions, tuning curves, and response phases. *The Journal of the Acoustical Society of America,* 80**,** 1364-1374.

ROLAND, P. S. & WRIGHT, C. G. 2006. Surgical aspects of cochlear implantation: mechanisms of insertional trauma.

ROZSASI, A., SIGG, O. & KECK, T. 2003. Persistent inner ear injury after diving. *Otology & neurotology,* 24**,** 195.

RUGGERO, M. A. & RICH, N. C. 1991. Furosemide alters organ of corti mechanics: evidence for feedback of outer hair cells upon the basilar membrane. *The Journal of Neuroscience,* 11**,** 1057-1067.

RUSSELL, I. J., CODY, A. R. & RICHARDSON, G. P. 1986. The responses of inner and outer hair cells in the basal turn of the guinea-pig cochlea and in the mouse cochlea grown in vitro. *Hearing Research,* 22**,** 199-216.

RUSSELL, I. J., KOSSL, M. & RICHARDSON, G. P. 1992. Nonlinear Mechanical Responses of Mouse Cochlear Hair Bundles. *Proceedings of the Royal Society of London. Series B: Biological Sciences,* 250**,** 217-227.

RUSSELL, I. J., LEGAN, P. K., LUKASHKINA, V. A., LUKASHKIN, A. N., GOODYEAR, R. J. & RICHARDSON, G. P. 2007. Sharpened cochlear tuning in a mouse with a genetically modified tectorial membrane. *Nature Neuroscience,* 10**,** 215-223.

RUSSELL, I. J. & NILSEN, K. E. 1997. The location of the cochlear amplifier: Spatial representation of a single tone on the guinea pig basilar membrane. *Proceedings of the National Academy of Sciences,* 94**,** 2660-2664.

RUSSELL, I. J. & SELLICK, P. M. 1978. Intracellular studies of hair cells in the mammalian cochlea. *The Journal of Physiology,* 284**,** 261-290.

RUSSELL, I. J. & SELLICK, P. M. 1983. Low-frequency characteristics of intracellularly recorded receptor potentials in guinea-pig cochlear hair cells. *The Journal of Physiology,* 338**,** 179-206.

RYAN, A. & DALLOS, P. 1975. Effect of absence of cochlear outer hair cells on behavioural auditory threshold. *Nature,* 253**,** 44-46.

RYBALCHENKO, V. & SANTOS-SACCHI, J. 2003. Cl− flux through a non-selective, stretch-sensitive conductance influences the outer hair cell motor of the guinea-pig. *The Journal of physiology,* 547**,** 873-891.

SACHS, M. B. & KIANG, N. Y. S. 1968. Two-Tone Inhibition in Auditory-Nerve Fibers. *The Journal of the Acoustical Society of America,* 43**,** 1120-1128.

SAITO, K. 1983. Fine structure of the sensory epithelium of guinea-pig organ of Corti: Subsurface cisternae and lamellar bodies in the outer hair cells. *Cell and Tissue Research,* 229**,** 467-481.

SANTOS-SACCHI, J. 1993. Harmonics of outer hair cell motility. *Biophysical Journal,* 65**,** 2217-2227.

SANTOS-SACCHI, J. 2008. Cochlear Mechanics: No Shout but a Twist in the Absence of Prestin. *Current biology : CB,* 18**,** R304-R306.

SCHRAVEN, S. P., HIRT, B., GOLL, E., HEYD, A., GUMMER, A. W., ZENNER, H. P. & DALHOFF, E. 2012. Conditions for Highly Efficient and Reproducible Round-Window Stimulation in Humans. *Audiology and Neurotology,* 17**,** 133-138.

SCHRAVEN, S. P., HIRT, B., GUMMER, A. W., ZENNER, H. P. & DALHOFF, E. 2011. Controlled round-window stimulation in human temporal bones yielding reproducible and functionally relevant stapedial responses. *Hearing research*.

SELLICK, P. M., PATUZZI, R. & JOHNSTONE, B. M. 1982. Measurement of basilar membrane motion in the guinea pig using the M[o-umlaut]ssbauer technique. *The Journal of the Acoustical Society of America,* 72**,** 131-141.

SELLICK, P. M. & RUSSELL, I. J. 1980. The responses of inner hair cells to basilar membrane velocity during low frequency auditory stimulation in the guinea pig cochlea. *Hearing Research,* 2**,** 439-445.

SHAH, D. M., FREEMAN, D. M. & WEISS, T. F. 1995. The osmotic response of the isolated, unfixed mouse tectorial membrane to isosmotic solutions: effect of Na+, K+, and Ca2+ concentration. *Hearing Research,* 87**,** 187-207.

SHERA, C. A. 2004. Mechanisms of Mammalian Otoacoustic Emission and their Implications for the Clinical Utility of Otoacoustic Emissions. *Ear and Hearing,* 25**,** 86-97.

SIEGEL, J. H. & HIROHATA, E. T. 1994. Sound calibration and distortion product otoacoustic emissions at high frequencies. *Hear.Res.,* 80**,** 146-152.

SPINDEL, J. H., LAMBERT, P. R. & RUTH, R. A. 1995. The round window electromagnetic implantable hearing aid approach. *Otolaryngologic Clinics of North America,* 28**,** 189.

SPOENDLIN, H. 1969. Innervation Patterns in the Organ of Corti of the Cat. *Acta Oto-laryngologica,* 67**,** 239-254.

STAUFFER, E. A., SCARBOROUGH, J. D., HIRONO, M., MILLER, E. D., SHAH, K., MERCER, J. A., HOLT, J. R. & GILLESPIE, P. G. 2005. Fast adaptation in vestibular hair cells requires myosin-1c activity. *Neuron,* 47**,** 541-553.

STEEL, K. P. 1983. The tectorial membrane of mammals. *Hearing Research,* 9**,** 327-359.

STEELE, C. R. A. P., S 2005. Force on inner hair cell stereocilia. *International Journal of Solids and Structures***,** 5885-5904.

STERKERS, O., FERRARY, E. & AMIEL, C. 1988. Production of inner ear fluids. *Physiological Reviews,* 68**,** 1083-1128.

SWARTZ, D. & SANTI, P. 1999. Immunolocalization of tenascin in the chinchilla inner ear1. *Hearing research,* 130**,** 108-114.

TABERNER, A. M. & LIBERMAN, M. C. 2005. Response Properties of Single Auditory Nerve Fibers in the Mouse. *Journal of Neurophysiology,* 93**,** 557-569.

TANAKA, T. 1981. Gels. *Scientific American,* 244**,** 124-136.

TASAKI, I. & SPYROPOULOS, C. S. 1959. Stria Vascularis as Source of Endocochlear Potential. *Journal of Neurophysiology,* 22**,** 149-155.

TEMCHIN, A. N., RICH, N. C. & RUGGERO, M. A. 2008. Threshold tuning curves of chinchilla auditory-nerve fibers. I. Dependence on characteristic frequency and relation to the magnitudes of cochlear vibrations. *Journal of neurophysiology,* 100**,** 2889-2898.

THALMANN, I. 1993. Collagen of accessory structures of organ of corti. *Connective Tissue Research,* 29**,** 191-201.

THALMANN, I., MACHIKI, K., CALABRO, A., HASCALL, V. C. & THALMANN, R. 1993. Uronic Acid-Containing Glycosaminoglycans and Keratan Sulfate Are Present in the Tectorial Membrane of the Inner Ear: Functional Implications. *Archives of Biochemistry and Biophysics,* 307**,** 391-396.

THALMANN, I., THALLINGER, G., COMEGYS, T. H. & THALMANN, R. 1986. Collagen – The Predominant Protein of the Tectorial Membrane. *ORL,* 48**,** 107-115.

TILNEY, L. G., DEROSIER, D. J. & MULROY, M. J. 1980. The organization of actin filaments in the stereocilia of cochlear hair cells. *The Journal of Cell Biology,* 86**,** 244-259.

TONNDORF, J. & KHANNA, S. M. 1972. Tympanic-Membrane Vibrations in Human Cadaver Ears Studied by Time-Averaged Holography. *The Journal of the Acoustical Society of America,* 52**,** 1221-1233.

TONNDORF, J. & TABOR, J. 1962. Closure of the cochlear windows: its effect upon air-and bone-conduction. *The Annals of otology, rhinology, and laryngology,* 71**,** 5.

TRINGALI, S., KOKA, K., DEVEZE, A., HOLLAND, N. J., JENKINS, H. A. & TOLLIN, D. J. 2010. Round window membrane implantation with an active middle ear implant: a study of the effects on the performance of round window exposure and transducer tip diameter in human cadaveric temporal bones. *Audiology and Neurotology,* 15**,** 291-302.

TSUPRUN, V. & SANTI, P. 2001. Proteoglycan arrays in the cochlear basement membrane. *Hearing research,* 157**,** 65-76.

VAN WANROOIJ, M. M. & VAN OPSTAL, A. J. 2004. Contribution of Head Shadow and Pinna Cues to Chronic Monaural Sound Localization. *The Journal of Neuroscience,* 24**,** 4163-4171.

VATER, M. & KÖSSL, M. 2011. Comparative aspects of cochlear functional organization in mammals. *Hearing Research,* 273**,** 89-99.

VATER, M., MENG, J. & FOX, R. C. 2004. *Hearing organ evolution and specialization: early and later mammals,* New York, Springer.

VERHOEVEN, K., LAER, L. V., KIRSCHHOFER, K., LEGAN, P. K., HUGHES, D. C., SCHATTEMAN, I., VERSTREKEN, M., HAUWE, P. V., COUCKE, P., CHEN, A., SMITH, R. J. H., SOMERS, T., OFFECIERS, F. E., HEYNING, P. V. D., RICHARDSON, G. P., WACHTLER, F., KIMBERLING, W. J., WILLEMS, P. J., GOVAERTS, P. J. & CAMP, G. V. 1998. Mutations in the human [alpha]-tectorin gene cause autosomal dominant non-syndromic hearing impairment. *Nat Genet,* 19**,** 60-62.

VOSS, S. E., ROSOWSKI, J. J. & PEAKE, W. T. 1996a. Is the pressure difference between the oval and round windows the effective acoustic stimulus for the cochlea? *The Journal of the Acoustical Society of America,* 100**,** 1602.

VOSS, S. E., ROSOWSKI, J. J. & PEAKE, W. T. 1996b. *Is the pressure difference between the oval and round windows the effective acoustic stimulus for the cochlea?*, ASA.

WALSH, T., ABU RAYAN, A., ABU SA'ED, J., SHAHIN, H., SHEPSHELOVICH, J., LEE, M., HIRSCHBERG, K., TEKIN, M., SALHAB, W., AVRAHAM, K., KING, M. & KANAAN, M. 2006. Genomic analysis of a heterogeneous Mendelian phenotype: multiple novel alleles for inherited hearing loss in the Palestinian population. *Human Genomics,* 2**,** 201-11.

WEDDELL, T. D., MELLADO LAGARDE, M. M., LUKASHKINA, V. A., LUKASHKIN, A. N., ZUO, J. & RUSSELL, I. J. 2011. Prestin links extrinsic tuning to neural excitation in the mammalian cochlea. *Current Biology,* epub ahead of print.

WEISS, T. F. & FREEMAN, D. M. 1997. Equilibrium behavior of an isotropic polyelectrolyte gel model of the tectorial membrane: effect of pH. *Hearing Research,* 111**,** 55-64.

WEITZEL, E. K., TASKER, R. & BROWNELL, W. E. 2003. Outer hair cell piezoelectricity: frequency response enhancement and resonance behavior. *The Journal of the Acoustical Society of America,* 114**,** 1462.

WEVER, E. G., LAWRENCE, M. & VON BÉKÉSY, G. 1954. A note on recent developments in auditory theory. *Proceedings of the National Academy of Sciences of the United States of America,* 40**,** 508.

WHITEHEAD, M. L. 1998. Species differences of distortion-product otoacoustic emissions: Comment on ``Interpretation of distortion product otoacoustic emission measurements. I. Two stimulus tones'' [J. Acoust. Soc. Am. 102, 413--429 (1997)]. *The Journal of the Acoustical Society of America,* 103**,** 2740-2742.

WHITEHEAD, M. L., LONSBURY-MARTIN, B. L. & MARTIN, G. K. 1992. Evidence for two discrete sources of 2f[sub 1] - f[sub 2] distortion-product otoacoustic emission in rabbit. II: Differential physiological vulnerability. *The Journal of the Acoustical Society of America,* 92**,** 2662-2682.

WIEDERHOLD, M. L. & MAHONEY, J. W. 1985. Acoustic overstimulation reduces 2f[sub 1] - f[sub 2] cochlear emissions at low and high primary levels in the cat. *The Journal of the Acoustical Society of America,* 77**,** S95-S95.

WOLLENBERG, B., BELTRAME, M., SCHÖNWEILER, R., GEHRKING, E., NITSCH, S., STEFFEN, A. & FRENZEL, H. 2007. Integration of the active middle ear implant Vibrant Soundbridge in total auricular reconstruction]. *HNO,* 55**,** 349.

WOOLF, N. K., KOEHRN, F. J. & RYAN, A. F. 1992. Immunohistochemical localization of fibronectin-like protein in the inner ear of the developing gerbil and rat. *Developmental brain research,* 65**,** 21-33.

YATES, G. K. 1990. Basilar membrane nonlinearity and its influence on auditory nerve rate-intensity functions. *Hearing Research,* 50**,** 145-162.

YOST, W. A., SCHLAUCH, A. R. S. & REVIEWER 2001. Fundamentals of Hearing: An Introduction (4th edition). *The Journal of the Acoustical Society of America,* 110**,** 1713-1714.

YU, N. & ZHAO, H.-B. 2009a. Modulation of Outer Hair Cell Electromotility by Cochlear Supporting Cells and Gap Junctions. *PLoS ONE,* 4**,** e7923.

YU, N. & ZHAO, H. B. 2009b. Modulation of outer hair cell electromotility by cochlear supporting cells and gap junctions. *PloS one,* 4**,** e7923.

ZAGAESKI, M., CODY, A. R., RUSSELL, I. J. & MOUNTAIN, D. C. 1994. Transfer characteristic of the inner hair cell synapse: Steady-state analysis. *The Journal of the Acoustical Society of America,* 95**,** 3430-3434.

ZENNARO, O., DUMON, T., ERRE, J., GUILLAUME, A. & ARAN, J. Year. Piezo-electric middle ear implant hearing aid experimental model in guinea-pig. *In*, 1992. IEEE, 1316-1317.

ZHENG, J., DEO, N., ZOU, Y., GROSH, K. & NUTTALL, A. L. 2007. Chlorpromazine alters cochlear mechanics and amplification: In vivo evidence for a role of stiffness modulation in the organ of corti. *Journal of neurophysiology,* 97**,** 994-1004.

ZHENG, J., MILLER, K. K., YANG, T., HILDEBRAND, M. S., SHEARER, A. E., DELUCA, A. P., SCHEETZ, T. E., DRUMMOND, J., SCHERER, S. E., LEGAN, P. K., GOODYEAR, R. J., RICHARDSON, G. P., CHEATHAM, M. A., SMITH, R. J. & DALLOS, P. 2011. Carcinoembryonic antigen-related cell adhesion molecule 16 interacts with α-tectorin and is mutated in autosomal dominant hearing loss (DFNA4). *Proceedings of the National Academy of Sciences,* 108**,** 4218-4223.

ZHENG, J., SHEN, W., HE, D. Z., LONG, K. B., MADISON, L. D. & DALLOS, P. 2000. Prestin is the motor protein of cochlear outer hair cells. *Nature,* 405**,** 149-155.

ZUREK, P. M. 1981. *Spontaneous narrowband acoustic signals emitted by human ears*, ASA.

ZUREK, P. M. & LESHOWITZ, B. H. 1976. Measurement of the combination tones f[sub 2] - f[sub 1] and 2f[sub 1] - f[sub 2]. *The Journal of the Acoustical Society of America,* 60**,** 155-168.

ZWAENEPOEL, I. 2002. Otoancorin, an inner ear protein restricted to the interface between the apical surface of sensory epithelia and their overlying acellular gels, is defective in autosomal recessive deafness DFNB22. *Proceedings of the National Academy of Sciences,* 99**,** 6240-6245.

ZWICKER, E. 1977. Masking-period patterns produced by very-low-frequency maskers and their possible relation to basilar-membrane displacement. *The Journal of the Acoustical Society of America,* 61**,** 1031-1040.

ZWISLOCKI, J. J. 1980. Theory of cochlear mechanics. *Hearing Research,* 2**,** 171-182.

ZWISLOCKI, J. J. 1986. Analysis of cochlear mechanics. *Hearing Research,* 22**,** 155-169.

ZWISLOCKI, J. J. & CEFARATTI, L. K. 1989. Tectorial membrane II: Stiffness measurements in vivo. *Hearing Research,* 42**,** 211-227.

ZWISLOCKI, J. J., CHAMBERLAIN, S. C. & SLEPECKY, N. B. 1988. Tectorial membrane I: Static mechanical properties in vivo. *Hearing Research,* 33**,** 207-222.

ZWISLOCKI, J. J. & KLETSKY, E. J. 1979. Tectorial membrane: a possible effect on frequency analysis in the cochlea. *Science,* 204**,** 639-641.

APPENDIX 1

In pigmented guinea pigs, low-frequency modulated DPOAEs were recorded in 6 healthy individuals. All animals underwent surgery under anaesthetic to allow recordings to be made and the middle ear was opened with a ventrolateral approach to equalise pressure either side of the tympanum. Anaesthetic regime, monitoring and surgical approach were as previously described in Lukashkin and Russell, 2005b see also chapter 2.2.1 . The equipment set-up was as previously described in Lukashkin and Russell, 2005b and chapter. Sound was delivered to the tympanic membrane by two Brüel & Kjær 4134 1/2 in. microphones for high frequency sound and a Beyer Dynamic DT48 dynamic headphone for delivering low frequency, high intensity biasing tones. Sound was recorded at the tympanum by a Brüel & Kjær 4133 1/2 in. microphone. All speakers and microphones were coupled to the ear canal of the animals via a closed sound system manufactured in house (chapter 2.2.3.1). The 30 Hz low frequency-biasing signal was supplied by a Philips PM5193 programmable synthesizer. Tone sequences for sound stimulation were synthesised by a Data Translation 3010 board and all Experimental control, data acquisition and data analysis were performed using a PC with programmes written in Test-Point (CEC, MA, USA). The closed sound system was calibrated in situ using a multi-harmonic signal for frequencies between 1 and 50 kHz. The sound system calibration for the 30 Hz low frequency tone was performed separately for this particular frequency.

Stimuli for DPOAE growth function modulation by a low frequency tone were presented with durations of 102 ms, a rise/fall time of 2 ms and inter burst intervals of 100ms. Primary tones at levels between 30 and 80 dB SPL and at frequencies of 22, 26 and 28kHz were used. Responses to 50 tone bursts were averaged in the time domain. A low-frequency tone (30 Hz) at a level of 120 dB SPL was employed to bias the cochlear partition. Sampling of the responses to every tone burst was triggered at the same phase of the biasing tone. All data were sampled at 250 kHz.

Guinea pig experimental procedure

DPOAE growth functions with different f_1/f_2 ratios and DPOAE-grams were used to establish optimal f_1/f_2 ratios for evoking CDPOAEs and to monitor inner ear integrity respectively (see Lukashkin and Russell, 2005b.

Low-frequency biased DPOAEs growth functions were evoked with f_2 = 1.690 kHz or 2 kHz and a f_2/f_1 ratio dependent on the optimal value obtained during the f_1-run. L_1 was set 10 dB above L_2 for all levels of L_2. Biasing tone frequency and level were 30 Hz and 120 dB SPL respectively in all experiments.

APPENDIX 2

Construction of the Otoa knockout mouse.

BAC 285M3 containing the Otoa gene was identified by screening a mouse 129Sv CITB CJ7 BAC library (Invitrogen) with an otoancorin cDNA probe and used to assemble a targeting construct. The construct is composed of a long arm of 3692 bp ending with the first seven codons of exon 2 from Otoa and fused in frame with EGFP, followed by a bovine growth hormone polyadenylation signal, a neomycin resistance cassette from PGKneopA and a short arm of 1150 bp, beginning 125 bp 5' of exon 3 of Otoa. The vector was constructed with fragments obtained by restriction digestion and by PCR using Pfu polymerase (Stratagene, Belgium) with specific primers (Invitrogen, UK). The finished vector was fully sequenced to confirm correct construction. CCB ES cells were electroporated with the NotI linearised construct and screened by Southern blotting BamHI digested ES cell DNA with 32P-labelled probes A and B13. Probes A and B were PCR amplified from BAC 285M3 using specific primers (MmOtoaKOAF1 ACACACTGTGACACACTGCA with MmOtoaKOAR1 CTCTATAAGAGCACTA GGCA and MmOtoaKOBF1 TTGCCTGTTTCCTGTCAACA with MmOtoaKOBR1 CATCTCTCAGCTCTGCTTCA). Probes A and B lie outside the targeting arms and are therefore selective for the endogenous locus. ES cells from correctly targeted lines were introduced into E3.5 blastocysts by microinjection and re-implanted into pseudopregnant female mice13. Chimeras were test bred to confirm germline transmission and a colony established. Mice were genotyped by multiplex PCR of tail snip DNA28 using primers OtoaGF1: CTG AATGATGGACATGTCTTAGACA, OtoaGR1: TGATAGGCACCTCCATGGCT CAGAA and GFPGR1: TGCAGATGAACTTCAGGGTCAGCTT, giving PCR products of 232 bp from the wild type allele and 330 bp from the mutant allele. Expression of Otoa in +/+, +/- and -/- mice was assayed by RT-PCR using primers spanning exon 2 to the pA signal (OtoaEXPF1 GATGTCTCAGGGACCTAGGA, OtoaEXPR1 CTACTCAGACAATGCGATGCA), and exons 3 to 9 (OtoaEXPF2 TTTACATCCATT GTTGCAGA, OtoaEXPR2 CATAGAGGTCTTTGAACACT).

Morphological analysis.

Methods for the preparation of cochlear tissues for light and electron microscopy were as described previously (Legan et al., 2000, Legan et al., 2005 and Russell et al., 2007). Confocal immunofluorescence microscopy was performed using a rabbit serum directed against two

non-overlapping peptides in the mesothelin-like domain of otoancorin described previously (Zwaenepoel, 2002).

APPENDIX 3

A MOUSE MODEL FOR HUMAN DEAFNESS DFNB22 REVEALS THAT HEARING IMPAIRMENT IS DUE TO A LOSS OF INNER HAIR CELL EXCITATION

Andrei N. Lukashkin[1,6], P. Kevin Legan[1], Thomas D. Weddell[1,6], Victoria A. Lukashkina[1,6], Richard J. Goodyear[1], Lindsey Welstead[1], Christine Petit[2,3,4,5], Ian J. Russell[1,6,7] & Guy P. Richardson[1,7]

[1]University of Sussex, School of Life Sciences, Falmer, Brighton BN1 9QG, UK [2]Institut Pasteur, Unité de Génétique et Physiologie de l'Audition, F75015 Paris; France [3]Inserm UMRS587; [4]Université Pierre & Marie Curie; [5]Collège de France [6]Current address: School of Pharmacy and Biomolecular Sciences, University of Brighton, Brighton BN2 4GJ, UK [7]Corresponding authors

Submitted to Proceedings of the National Academy of Sciences of the United States of America

Mutations at the DFNB22 locus encoding the 120 kDa inner-ear specific protein otoancorin that is expressed on the surface of the spiral limbus in the cochlea cause recessive, non-syndromic hearing impairment in humans. Gene targeting in embryonic stem cells was used to create an EGFP knock in, otoancorin knock out (OtoaEGFP/EGFP) mouse. In the OtoaEGFP/EGFP mouse the tectorial membrane, a ribbon-like strip of extracellular matrix that is normally anchored by one edge to the spiral limbus and lies over the organ of Corti, retains its general form and remains in close proximity to Corti's organ, but is detached from the limbal surface. Measurements of cochlear microphonic potentials, distortion product otoacoustic emissions and basilar membrane motion indicate the tectorial membrane remains functionally attached to the electromotile, sensorimotor outer hair cells of the organ of Corti and that the amplification and frequency tuning of the basilar membrane responses to sounds are almost normal. The compound action potential masker tuning curves, a measure of the tuning of the sensory inner hair cells, are also sharply tuned but the thresholds of the compound action potentials, a measure of inner hair cell sensitivity, are significantly elevated. These results indicate that the hearing loss in DFNB22 patients is due to a defect in inner hair cell stimulation, and reveal the limbal attachment of the tectorial membrane plays a critical role in this process.

cochlea | deafness | hearing | otoancorin | tectorial membrane

INTRODUCTION

The sensory epithelium of the cochlea, the organ of Corti (Fig. 1), contains two types of hair cell, the purely sensory inner hair cells (IHCs) and the electromotile, sensori-motor outer hair cells (OHCs). These cells are critically positioned between two strips of extracellular matrix, the basilar and the tectorial membranes (BM and TM respectively). Signal processing in the cochlea is initiated when sound-induced changes in fluid pressure displace the BM in the transverse direction, causing radial shearing displacements between the surface of the organ of Corti (the reticular lamina) and the overlying TM (1). The radial shear is detected by the hair bundles of both the IHCs and the OHCs (2) with the stereocilia of the OHC hair bundles forming an elastic link between the organ of Corti and the overlying TM (3). Deflection of the stereocilia gates the hair cell's mechanoelectrical transducer (MET) channels, thereby initiating a MET current (4) that promotes active mechanical force production by the OHCs which, in turn, influences mechanical interactions between the TM and the BM (5, 6). This nonlinear frequency-dependent enhancement process, which boosts the sensitivity of cochlear responses to low-level sounds and compresses them at high levels, is known as the cochlear amplifier (7).

Whilst the hair bundles of the OHCs are imbedded into the TM and therefore directly excited by relative displacement of the undersurface of the TM and the reticular lamina, those of the IHCs are not in direct contact with the TM, and the way in which they are driven by motion of the BM remains unclear. Intracellular recordings of the receptor potentials in IHCs indicate the bundles are velocity coupled (to fluid flow) at low frequencies, and displacement coupled at higher frequencies of stimulation (2, 8, 9). Direct measurements of the motion of the reticular lamina and the lower surface of the TM in an *ex vivo* preparation of the guinea-pig cochlea provide evidence that, at frequencies below 3 kHz, counterphase transverse movements of the two surfaces generate pulsatile fluid movements in the subtectorial space that could drive the hair bundles of the IHCs (10). At higher frequencies the two surfaces move in phase and radial shear alone is thought to dominate. Theoretical studies (11) reveal that the boundary layers will be vanishingly thin at high frequencies, that the fluid in the gap between the TM and the reticular lamina will be inviscid, and that the hydrodynamic forces on the hair bundle will be inertial. Whilst an overlying TM that is not directly attached to a hair bundle does not apply torque to the hair bundle (11), the inertial force of the fluid driving the hair bundle depends on its mass and therefore the size of the gap between the reticular lamina and the TM (12) (11).

The TM is composed of radially-arrayed collagen fibrils that are imbedded in a non-collagenous matrix composed of a number of different glycoproteins including Tecta, Tectb, otogelin, otolin and Ceacam 16 (13-16). Mutations in Tecta cause recessive (DFNB21) and dominant (DFNA8/12) forms of human hereditary deafness (17-19), and a dominant missense mutation in Ceacam 16 (DFNA4) has been identified recently as a cause of late onset progressive hearing loss in an American family (15). Mutations in Tecta are one of the most common causes of autosomal dominant, non-syndromic hereditary hearing loss (20), and mouse models for both the recessive (21) and dominant (22) forms of deafness arising from mutations in Tecta have been created. Together with data from a Tectb null mutant mouse (23), these studies have provided evidence that the TM plays multiple roles in hearing (24). Although much is known about the structure of the TM, an extracellular matrix that is unique to the cochlea, relatively little is known about how it attaches to the apical surface of the cochlear epithelium. Otoancorin, a product of the DFNB22 locus, is expressed on the apical surface of the spiral

Reserved for Publication Footnotes

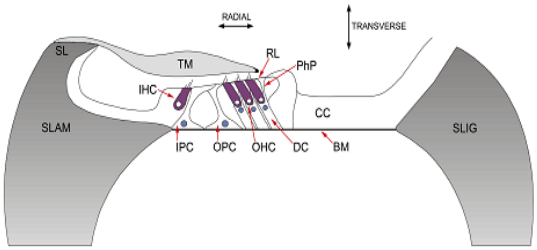

Fig. 1. Schematic cross-section of the wild-type cochlea Spiral lamina (SLAM), spiral ligament (SLIG) inner pillar cells (IPC), outer pillar cells (OPC), Deiters' cells (DC), phalangeal process of DC (PhP) Claudius cells (CC), outer hair cell (OHC), inner hair cell (IHC), reticular laminar [RL] and major non-cellular elements (basilar membrane [BM] and tectorial membrane [TM].

limbus and has been suggested to mediate TM attachment to this region of the cochlear epithelium (25). In this study we use gene targeting to inactivate otoancorin. This provides a mouse model for DFNB22, reveals a loss of IHC sensitivity as the primary cause of deafness, and isolates a specific role for the limbal attachment of the TM in driving the hair bundles of the IHCs.

RESULTS

Gene targeting in embryonic stem (ES) cells was used to replace the first coding exon of the murine *Otoa* gene with a cassette encoding the enhanced green fluorescent protein, EGFP (Fig. 2A). Southern blotting with probes located external to the targeting vector was used to detect and confirm successful targeting (Fig. 2B), and one ES cell line was used to produce a chimeric mouse that transmitted through the germ line. Full length Otoa mRNA cannot be detected in the cochleae of $Otoa^{EGFP/EGFP}$ mice by RT-PCR (Fig. 2C). EGFP is observed in the interdental cells of the spiral limbus in mature mice that are heterozygous ($Otoa^{+/EGFP}$) for the targeted mutation, and otoancorin is detected on the apical surface of the limbus with an antibody (25) raised to two peptides located in the predicted C-terminal region of this protein (Fig. 2D, D'). In homozygous $Otoa^{EGFP/EGFP}$ mice, EGFP expression levels in the interdental cells are higher and otoancorin immunoreactivity cannot be detected on the surface of the spiral limbus (Fig. 2E, E'). Although shorter alternative transcripts are predicted that could be expressed in the $Otoa^{EGFP/EGFP}$ mouse (see Fig. 2A), these should be recognised by the antibody and are therefore unlikely to be expressed. EGFP expression is also observed in the border cells that lie immediately adjacent and just medial to the IHCs, and in the cells of Reissner's membrane between postnatal days 8 and 12 in $Otoa^{EGFP/EGFP}$ mice (Fig. 2 F-I). These results indicate the $Otoa^{EGFP/EGFP}$ mouse is a null mutant at the level of protein expression, and confirm previous immunocytochemical studies (25) showing otoancorin is expressed in the interdental cells of the spiral limbus and, during a brief period of postnatal development, in the border cells that lie next to the IHCs.

The tectorial membrane is detached from the spiral limbus in $Otoa^{EGFP/EGFP}$ mice

In wild-type and $Otoa^{+/EGFP}$ mice the medial edge of the TM is closely apposed and attached to the spiral limbus, and the lateral region lies over the apical surface of the hair cells in the organ of Corti (Fig. 3A). In the $Otoa^{EGFP/EGFP}$ mouse, the TM is detached from the spiral limbus and the lateral-most region is markedly thinner than normal (Fig. 3B). This region is frequently seen to be fenestrated in the homozygous mutants and a typical marginal band, as seen in both wild-type and heterozygous mice, is not present (Fig. 3C, D). Although the TM in the homozygous mutants often appears to be slightly tilted, with the lateral region displaced medially with respect to the organ of Corti,

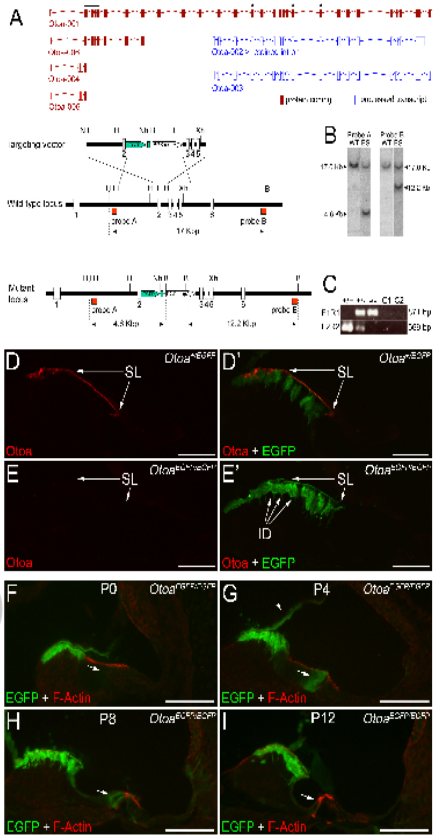

Fig. 2. Targeted insertion of EGFP into exon 2 of *Otoa*(A) The *Otoa* locus in Ensembl, shown above maps of the targeting vector, the 5' region of the *Otoa* gene, and the targeted *Otoa* locus. The full length Otoa transcript and five other putative splice variants predicted from EST clones are shown in the upper part of (A). The horizontal black line indicates exons 2 to 5 of *Otoa*, and the asterisks indicate exons 14, 20 and 21 that encode the peptide sequences used to raise the otoancorin antiserum (25). Splice variants Otoa-001, -004, -005 and -006 would be disrupted by the targeting approach used, and variants Otoa-002 and -003 would contain the peptide epitopes recognised by the otoancorin antiserum if they were independently expressed in the mutant. In the lower part of (A), dark bars represent intronic DNA, open boxes represent exons and red boxes indicate the external probes A and B used to confirm correct targeting. Sizes of the expected restriction fragments are indicated. Dashed lines indicate likely regions of homologous recombination. (B) Southern blots of *BamH1* digested DNA from wild type and targeted ES cell DNA probed with external probes A and B as indicated in panel A. In addition to the wild type band of 17 kb, a band of 4.6 kb is observed with probe A, and a band of 12.2 kb with probe B. (C) RT-PCR using primers spanning exon 2 to the bovine growth hormone pA signal (F1R1), and exons 3 to 9 (F2R2). A PCR product indicating mRNA expression from the targeted locus is observed in $Otoa^{+/EGFP}$ (+/-) and $Otoa^{EGFP/EGFP}$ (-/-) RT-PCR reactions only, whilst the wild type PCR product is observed only in $Otoa^{+/+}$ and $Otoa^{+/EGFP}$ RT-PCR reactions. C1 = no RT control, C2 = no DNA control. (D-E) Confocal images of cryosections from the cochleae of $Otoa^{+/EGFP}$ (D, D') and $Otoa^{EGFP/EGFP}$ (E, E') mice double immunolabelled with antibodies to otoancorin (red channel; D, D', E, E') and GFP (green channel; D', E'). SL = spiral limbus, ID = interdental cells. (F-I) Confocal images of cryosections from the cochleae of $Otoa^{EGFP/EGFP}$ mice at P0 (F), P4 (G), P8 (H) and P12 (I) double labelled with Texas Red phalloidin to reveal F-actin (red channel) and GFP (green channel). Arrows indicate border cell region, arrowhead in panel G indicates Reissner's membrane. Bars = 50 µm (D-E'), 100 µm (F-I).

hair bundle imprints, the sites at which the hair bundles of the OHCs attach to the lower surface of the TM, are observed by both transmission and scanning electron microscopy (Fig. 3E, F). Despite these changes in the structure and attachment of the TM

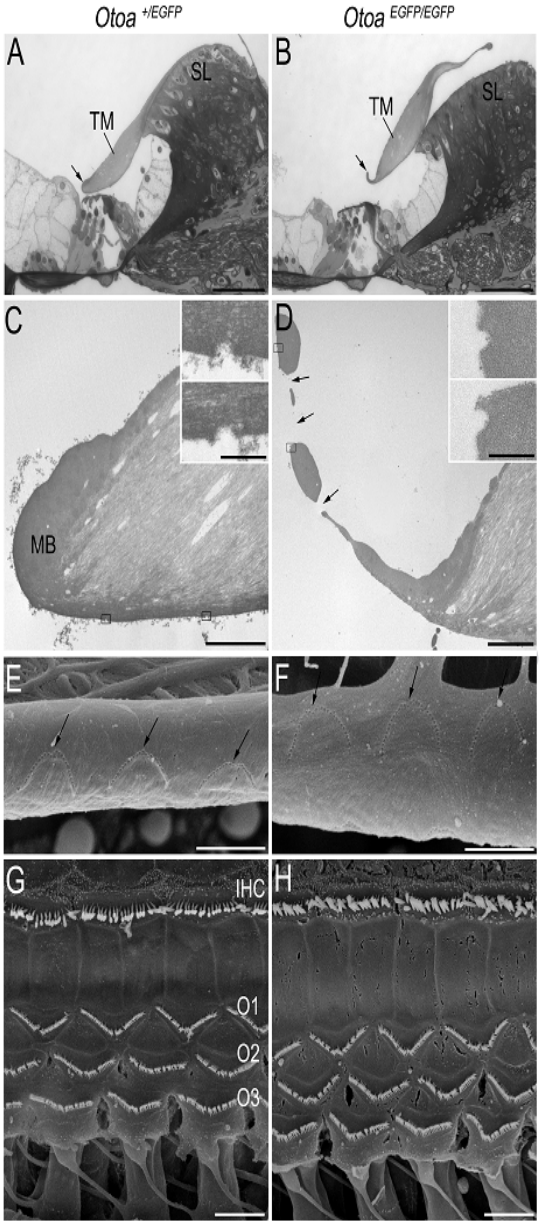

Fig. 3. Characterisation of the mutant phenotype Structure of organ of Corti and tectorial membrane in mature *Otoa*$^{+/EGFP}$ (A, C, E andG) and *Otoa*$^{EGFP/EGFP}$ (B, D, F and H) mice. (A, B) Toluidin blue stained, one micron thick plastic sections. The tectorial membrane (TM) is detached from the spiral limbus (SL) in the *Otoa*$^{EGFP/EGFP}$ mouse. Arrows indicate the marginal band (A) and equivalent region in the mutant (B). (C, D) Transmission electron micrographs showing ultrastructural details of the lateral margin of the TM. A prominent marginal band (MB) is visible in the *Otoa*$^{+/EGFP}$mouse (C). This region is thinned and fenestrated (arrows) in the *Otoa*$^{EGFP/EGFP}$ mouse (D). Details of the boxed areas are shown at higher magnification in insets revealing the imprints of the tallest stereocilia of the OHCs. (E, F) Scanning electron micrographs of the lower surface of the TM revealing the W-shaped imprints (arrows) of the OHC hair bundles. These are observed around the fenestrae in the *Otoa*$^{EGFP/EGFP}$ mouse. (G, H) Scanning electron micrographs revealing the hair bundles of the inner (IHC) and 3 rows of outer (O1, O2 and O3) hair cells in the organ of Corti. The structure and arrangement of these hair bundles is similar in mice of both genotype. Bars = 50 µm (A, B), 5 µm (C-H), 500 nm (insets in C, D).

in the *Otoa*$^{EGFP/EGFP}$ mouse, scanning electron microscopy reveals that the orientation and organisation of the hair bundles of the IHCs and OHCs in the organ of Corti are normal, and similar

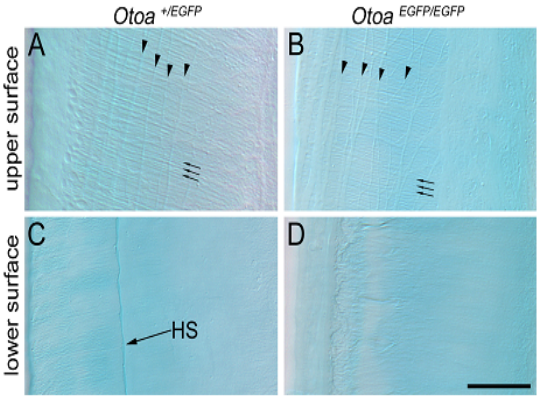

Fig. 4. Differential interference contrast microscopy of tectorial membranes Images of the upper (A, B) and lower (C, D) surfaces of unfixed, Alcian blue stained TMs from the basal end of the cochlea of *Otoa*$^{+/EGFP}$ (A, C) and *Otoa*$^{EGFP/EGFP}$ (B, D) mice at 7 weeks of age. Covernet fibrils (arrowheads) and radial collagen fibril (arrows) are visible in mice of both genotype. Hensen's stripe (HS) is not visible in the *Otoa*$^{EGFP/EGFP}$ mice. Bar = 20 µm.

to that observed in both wild-type (not shown) and heterozygous mice (Fig. 3G, H). Differential interference contrast microscopy indicates the collagen fibril bundles of the TM are, as in heterozygotes and wild-types, distributed radially within the core of the matrix in the homozygous mutants (Fig. 4A, B). The covernet, a network formed by fibrils that are aligned mainly along the length of the upper surface of the TM, is also of normal appearance (Fig. 4A, B). Hensen's stripe, a ridge that runs longitudinally along the lower surface of the TM and is thought to engage the hair bundle of the IHCs is, however, not visible in the homozygous mutants (Fig. 4C, D).These observations show that otoancorin is required for adhesion of the TM to the spiral limbus and that the TM, despite the structural abnormalities described above, retains its gross overall form, remaining in close proximity with the organ of Corti.

Cochlear microphonic potentials are symmetrical in Otoa$^{EGFP/EGFP}$ *mice*

Cochlear microphonic (CM) potentials are extracellular potentials derived from the transducer currents of the OHCs (1, 26-28) and their symmetrical nature is known to be due to the presence of the TM biasing the operating point of the hair bundle (21, 29). Although the TM is detached from the spiral limbus in the *Otoa*$^{EGFP/EGFP}$ mice, the CM potentials recorded from the round window of *Otoa*$^{EGFP/EGFP}$ mice are similar to those recorded from wild type mice (Fig. 5A) being symmetric at low to moderate sound levels, becoming negatively and then positively asymmetrical with increasing sound levels above 80 dB SPL (Russell et al., 1986). The DC component of the CM potentials, a measure of their symmetry, only differs significantly ($p \leq 0.001$) at 85 dB SPL, the inflection point in wild type *Otoa* mice, an indication that attachment of the TM to the limbus may be important for controlling this point of apparent mechanical instability. These data provide functional evidence that the hair bundles of OHCs are, as suggested by the presence of hair-bundle imprints, attached to the TM in the homozygous mutants.

Cochlear amplification is not significantly affected in Otoa$^{EGFP/EGFP}$ *mice*

Distortion product otoacoustic emissions (DPOAEs) are a non-linear acoustical response produced by the cochlea in response to simultaneous stimulation with two pure tones. A 10-35 dB elevation in threshold is observed for DPOAEs in the 8-65 kHz, low-threshold region of the cochlea (30) in *Otoa*$^{EGFP/EGFP}$ mice (Fig. 5B), with the difference being restricted to ≤20 dB in the basal region where we are able to measure basilar membrane responses.. If one assumes that these changes in DPOAE thresh-

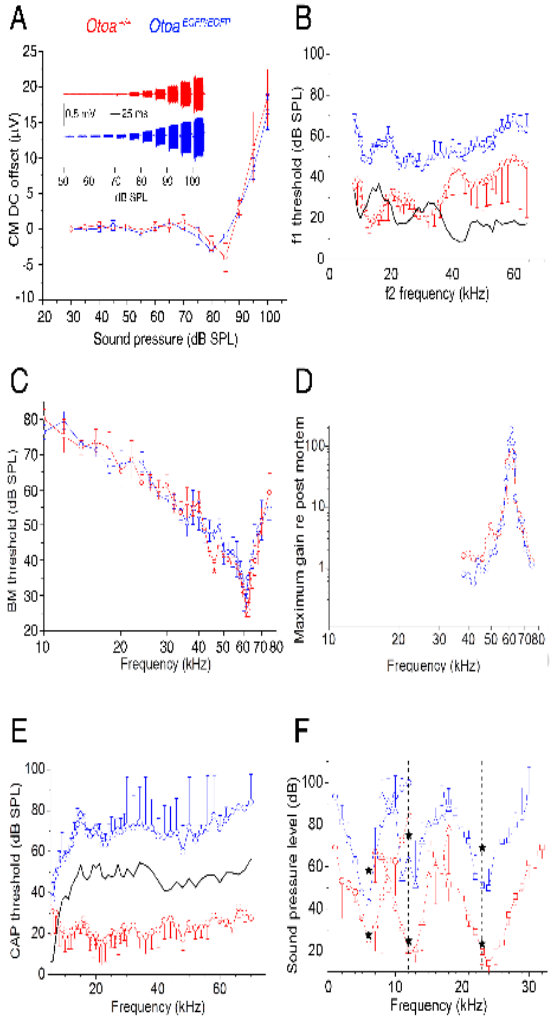

Fig. 5. Physiological responses of the cochlea of wild-type (red) and *Otoa*$^{EGFP/EGFP}$ (blue) mice (A) Inset: Cochlear microphonic potentials recorded from round window in response to 10 kHz tones of increasing levels (low-pass filtered at 12 kHz). DC component of the CM (mean +/- standard deviation, n = 10 preparations each for wild type and *Otoa*$^{EGFP/EGFP}$ mice). (B) Distortion product otoacoustic emission (2f1 – f2, 0 dB SPL, criterion mean +/- standard deviation) as a function of the f2 frequency (f2/f1 ratio = 1.23). Black line: mean difference between measurements from n = 4 wild-type and n = 4 *Otoa*$^{EGFP/EGFP}$. (C) Isoresponse basilar membrane frequency tuning curves (0.2 nm criterion) (mean +/- standard deviation, n = 4 wild-type and n = 4 *Otoa*$^{EGFP/EGFP}$ mice with CFs between 59 kHz – 61 kHz). Red asterisk indicates a second peak of sensitivity on the low frequency shoulder of the wild type tuning curve where the values for frequencies of 44, 46 and 48 kHz are significantly different (p≤0.001) from those in the mutant tuning curve. (D)difference in maximum gain measured alive in a single preparation with respect to (re) post mortem. (E) Auditory nerve, compound action-potential threshold-curves as a function of stimulus tone frequency (mean +/- standard deviation). Black line: mean difference between n = 5 wild-type and n = 4 *Otoa*$^{EGFP/EGFP}$ mice. (F) Masking tuning curves (mean +/- standard deviation, n = 10 preparations) for auditory nerve compound action potential (probe tone frequencies indicated by vertical dashed lines; levels are indicated by black stars; lower stars: probe level for the wild-type mice; upper stars:level for *Otoa*$^{EGFP/EGFP}$. Q_{10dB} (bandwidth measured 10dB above tip / probe tone frequency) at the probe tone frequencies of 6, 12 and 23 kHz are 2.3±0.4, 4.6±0.5 and 7.2±0.7 for wild-type; and 3.2±0.2, 7.5±0.5 and 12.1±3.8 for *Otoa*$^{EGFP/EGFP}$ mice respectively. All mice < 3 months old littermates.

old reflect changes in the gain of the cochlear amplifier, and that the amplifier provides a gain of 60 dB in the low-threshold region of the mammalian cochlea, then the feedback efficiency from the OHCs in the 8-65 kHz region of the cochlea in *Otoa*$^{EGFP/EGFP}$ mice is only decreased by about 3%. Measurements of the BM responses from the 55-65 kHz, high-frequency end of the cochlea in *Otoa*$^{EGFP/EGFP}$ mice provide direct confirmation that cochlear amplification remains close to normal when the TM is detached from the spiral limbus (Fig. 5C, D). The sensitivity and sharpness of tuning given by the $Q_{10\,dB}$ (ratio of the CF to the bandwidth measured 10 dB from the tip) in the *Otoa*$^{EGFP/EGFP}$ and the wild-type mice do not differ significantly (P = 0.15, Table 1). The low-frequency shoulder of the BM tuning curves is, however, modified and at frequencies between 44 and 48 kHz sensitivities are significantly different (p≤0.001) and the threshold minimum observed in the tuning curve of the wild type mice (red asterisk in Fig. 5C) is absent from that of the *Otoa*$^{EGFP/EGFP}$ mice..

Compound Action Potential thresholds are significantly elevated in the Otoa$^{EGFP/EGFP}$ *mouse*

The compound action potential (CAP) is the synchronized activity of the auditory nerve fibres that is measured at the beginning of pure-tone stimulation. The thresholds for these potentials are elevated by 35-55 dB in the 8-70 kHz range in the *Otoa*$^{EGFP/EGFP}$ mice (Fig. 5E). Derived simultaneous masking neural tuning curves closely resemble the tuning of single auditory nerve fibres (31) and are known to become less sharp when cochlear amplification is compromised (32). Although the CAP thresholds of *Otoa*$^{EGFP/EGFP}$ mice are elevated, the CAP masking tuning curves derived from simultaneous tone-on-tone masking (31) are sharp, as would be expected if mechanical amplification were preserved (Fig. 5F). Two characteristics of the CAP masker tuning curves recorded from *Otoa*$^{EGFP/EGFP}$ mice further indicate cochlear amplification is not compromised and that non-linear suppression (the basis for the tuning curves) is already manifested in the mechanical responses of the cochlear partition before the latter elicit neural excitation. First, the masker levels used are about 20 dB below the relatively high probe tone levels (upper black stars in Fig. 5F) necessary to elicit a measurable neural response for frequencies around the probe frequency. Second, the tuning curves are significantly sharper than those of wild-type mice (Fig. 5F), as has been observed previously for probe tone levels well above the mechanical threshold in sensitive, wild-type cochleae (22). These observations provide further evidence that the threshold of the mechanical responses is not significantly changed in the *Otoa*$^{EGFP/EGFP}$ mice, but that it is the transmission of these responses to the IHCs that is attenuated.

DISCUSSION

The EGFP knock-in, Otoa knock-out mouse created in this study provides direct evidence that otoancorin is, as predicted (25), necessary for attachment of the TM to the spiral limbus. Whilst the TM is detached from the spiral limbus in the *Otoa*$^{EGFP/EGFP}$ mouse, it remains in close proximity to the sensory epithelium, possibly via its attachment to the hair bundles of the OHCs. This is in contrast to the situation in the *Tecta*$^{\Delta ENT/\Delta ENT}$ mouse, in which a residual TM is completely divorced from the organ of Corti and ectopically associated with Reissner's membrane (20). Otoancorin is not expressed in OHCs and another protein must therefore mediate adhesion of the OHC stereocilia to the TM. Although otoancorin and stereocilin share some long range homology (33), and despite the absence of hair-bundle imprints in the TMs of stereocilin null mice (25), functional interactions between the TM and the OHCs do not require stereocilin (34). Distinct molecular mechanisms may therefore mediate interactions between the TM and the OHCs on the one hand, and the TM and the spiral limbus on the other.

The TM proteins with which otoancorin interacts are not yet known. Collagens are still present in the detached TMs of the *Tecta*$^{\Delta ENT/\Delta ENT}$ mouse (20) so limbal attachment is un-

Table 1. Parameters of the basilar membrane tuning curves for wild-type and *Otoa*$^{EGFP/EGFP}$ mice.

Genotype	CF (kHz)	Q10dB	Threshold (dB SPL)	Gain re post mortem (dB)	Number of animals
Wild-type *Otoa*$^{+/+}$	55-68	9.3±1.50	27 ± 7	33±7	5
Otoa$^{EGFP/EGFP}$	55-65	8.2±1.0	29 ± 4	30±6	8

likely to be mediated by this class of protein. Whilst all the major non-collagenous proteins of the TM (Tecta, Tectb and Ceacam16) are absent from the residual, detached TMs of the *Tecta*$^{\Delta ENT/\Delta ENT}$ mouse (20), and the TM remains limbally attached in the *Tectb*$^{-/-}$ mouse, the *Otog*$^{-/-}$ mouse and the *Ceacam16*$^{-/-}$ mouse (13, 22, 32). One can therefore deduce that Tecta is a likely interaction partner of otoancorin, although the more recently identified TM protein otolin (15) may also mediate adherence of the TM to the limbus via otoancorin.

Although the limbally detached TMs of *Otoa*$^{EGFP/EGFP}$ mice are grossly normal, Hensen's stripe is absent and the lateral region is thinned and fenestrated, lacking a distinct marginal band. Hensen's stripe forms during the later stages of postnatal development from a region on the lower surface of the TM known as the homogeneous stripe, a region that remains in contact with the surface of the cochlear epithelium medial to the IHCs whilst the spiral sulcus is forming. Contact with the epithelium, mediated by otoancorin, may therefore be required for the development of Hensen's stripe. It is unclear why the lateral region of the TM fails to develop correctly in the *Otoa*$^{EGFP/EGFP}$ mice, as *Otoa* is not expressed by the supporting cells of the organ of Corti; the pillar cells, Dieters' cell or Hensen's cells.

The loss of limbal attachment and the abnormalities in TM structure described above have very little effect on the sensitivity and tuning of the BM response, cause a mild (~20 dB) reduction in the threshold of the DPOAEs, and result in a substantial (50 dB) increase in the threshold of the neural tuning curves, although the neural responses remain sharply tuned. The limbal attachment of the TM is not therefore necessary for cochlear amplification and tuning, but is critically required to ensure that the response of the BM and the reticular lamina are transmitted to the hair bundles of the IHCs without any loss of sensitivity. Whilst it may seem surprising that the loss of TM attachment to the spiral limbus has little effect on BM sensitivity and tuning, this finding is indeed predicted by a lever and springs model of the cochlea (35). The radial motion of the reticular lamina is largely controlled by the displacement of its attachment point at the pillar head, its rotation being of secondary importance. Consequently, a change in the angular rotation of the reticular laminar is predicted to have little effect on radial shear of the OHC hair bundles and increases amplification of BM motion by a factor of 1.5 at most, i.e., 3 dB or less, an outcome supported by our findings.

The symmetry of the CM observed in *Otoa*$^{EGFP/EGFP}$ mice implies that the OHCs are working, as in wild type mice, around the most sensitive point on their input-output function and therefore able to provide BM amplification with optimal gain (21). Furthermore, the symmetry of the CM implies that the OHCs are not acting, as previously suggested, against the radial stiffness of the TM provided by the limbal attachment to set their operating point (21, 29, 36), unless the TM is attached to some other structure lateral to the OHCs in an otoancorin-independent manner. Whilst there have been indications that the TM may be attached to the surface of Hensen's cells (37), morphological evidence for such an attachment is lacking (see Fig 3A). The operating point is therefore more likely to be set by the resting open probability of the MET channels, which is close to 50% in artificial endolymph containing low (0.02 mM) calcium, (38). This raises the interesting possibility that the TM may passively regulate the local calcium ionic environment in the vicinity of the MET channels (39)and may also explain why the CM recorded from the organ of Corti of *Tecta*$^{\Delta ENT/\Delta ENT}$ (21) and *Tecta*$^{C1509G/C1509G}$ (40) mice, where the TM is completely detached from the organ of Corti, is typically asymmetrical in form.

The timing of the forces that are fed back to the cochlear partition by the OHCs is crucial for cochlear amplification to be effective (20, 33-35) and depends on whether the OHC hair bundles are driven by the elastic or inertial forces delivered by the TM (33). For frequencies well below the characteristic frequency (CF, the frequency that produces the most sensitive response), the TM imposes an elastic load on the OHC bundles and they are displaced maximally in the excitatory direction (i.e., towards the tallest row of stereocilia) during maximum displacement of the cochlear partition towards the scala vestibuli (1) (36-38) (37-40). For frequencies at and around the CF, however, it has been suggested that the OHCs are excited by the inertial force imposed by the TM (23). This excitation lags cochlear partition displacement by 0.5 cycles, so that the OHC stereocilia are displaced maximally when the partition is displaced maximally towards the scala tympani (23). As a consequence of this, and as a result of the additional 0.25 cycle delay imposed by the membrane time constant, which appears to track the CF of the IHCs up tp 8 kHz (38), the receptor potentials and the forces produced by somatic electromotility are in phase with the velocity of the cochlear partition. The sensitivity and sharpness of BM tuning found in the *Otoa*$^{EGFP/EGFP}$ mouse indicate that the elasticity of the TM attachment to the spiral limbus is not a crucial factor for exciting the OHCs near their characteristic frequency, and that the OHCs must react against, and therefore be excited by, the inertial load provided by the TM at CF to effectively boost the mechanical responses of the cochlea (22).

A second resonance has been observed approximately one half an octave below the tip of the BM tuning curve in measurements obtained from the basal, high-frequency end of the murine cochlea (20, 21). This feature of BM tuning curves has been previously attributed to the TM resonance (20, 23) and is thought to result from a reduction in the load imposed by the TM at its resonance frequency. Whilst the TM's role as both an inertial mass and a source of the second resonance had been deduced from previous studies of the *Tecta*$^{\Delta ENT/\Delta ENT}$ mouse, it was not possible to isolate a specific role for the elasticity of the limbal attachment region as the residual TM is completely detached from both the spiral limbus and the surface of the organ of Corti in the *Tecta*$^{\Delta ENT/\Delta ENT}$ mouse. The absence of a second resonance in the BM tuning curves of *Otoa*$^{EGFP/EGFP}$ mouse in which the TM is detached from the spiral limbus now provides evidence that this resonance derives specifically from the elasticity of the TM's attachment to the spiral limbus, combined with its effective mass.

Whilst the sensitivities of the BM responses recorded from wild type and *Otoa*$^{EGFP/EGFP}$ mice are similar, DPOAEs recorded at similar frequencies differ by about 20 dB. Slight changes in

the motion of the reticular lamina due to changes in loading of the cochlear partition by the modified TM of the *Otoa*$^{EGFP/EGFP}$ mouse might cause this increase in DPOAE thresholds. The reticular lamina is, however, coupled compliantly to the BM via the OHC-Deiter's cell complex (41-44), so any change in the load on the cochlear partition would be expected to affect amplification of BM motion and be reflected in the vibrations of the BM. It is therefore more likely that this mild loss in the sensitivity of the DPOAEs in *Otoa*$^{EGFP/EGFP}$ mice is due to the detachment of the TM from the spiral limbus altering the transmission pathway between the source of the DPOAEs and the point of measurement at the eardrum.

The loss of limbal attachment in the *Otoa*$^{EGFP/EGFP}$ mouse causes a substantial increase in the CAP threshold, but does not affect the sharpness of neural tuning. Increased neural thresholds with preserved BM sensitivity have been described previously for the *Tecta*$^{Y1870C/+}$ mouse in which the TM remains attached to the spiral limbus but the subtectorial space in the vicinity of the IHCs is much increased, but are accompanied by a broadening of the neural tuning curves despite the BM remaining sharply tuned. Due to likely changes in the relative position of the TM and the hair cells caused by fixation and dehydration in the absence of firm attachment to the spiral limbus, it is not possible to determine whether or not the dimensions of the subtectorial space are altered in the *Otoa*$^{EGFP/EGFP}$ mouse. Nonetheless, modelling studies (12) indicate only a small change (2 fold, from 5-10 microns) in the dimensions of this space would severely reduce hydrodynamic input to the IHC bundle. Loss of limbal attachment may be sufficient to cause such a change, or reduce the pressure difference between the inner sulcus and the hair bundles of the OHCs (45) caused by organ of Corti motion, and therefore reduce the sensitivity of the IHCs without affecting neural tuning. Abrogation of pulsatile fluid motion caused by a rocking reticular lamina (10) seems an unlikely possibility, at least at CF, as the mouse cochlea operates at frequencies in excess of 3 kHz. Likewise it seems unlikely that the absence of Hensen's stripe leads to a loss in neural sensitivity, as it is only a prominent feature in the basal, high-frequency half of the murine cochlea and cannot be responsible for sensitivity in the low-frequency region of the CAP audiogram in the mouse.

The results also inform as to the cause of deafness in DFNB22 families. Three different recessive mutations in *OTOA*, a splice site mutation, a missense mutation and a large genomic deletion, have been identified in Palestinian families as the cause of prelingual, sensorineural deafness (26, 47). The degree of deafness of the affected individuals in two of these three families has been reported and has been described as being moderate-to-severe, i.e., similar or slightly more severe than the 35-55 dB hearing loss found in the *Otoa*$^{EGFP/EGFP}$ mouse over the 8-55 kHz range. Whilst the exact consequences of the splice site and missense mutation are unknown, both are recessive and therefore likely to cause loss of function, as is also expected for the deletion which encompasses the first 19 of the 28 coding exons. The *Otoa*$^{EGFP/EGFP}$ mouse lacks expression of otoancorin and should be a faithful

model for the recessive human mutations that have been identified thus far. The hearing loss in patients with recessive loss-of-function mutations in *OTOA* is therefore predicted to be due to a failure in the excitation of the IHCs, and not due to a loss of cochlear amplification.

ACKNOWLEDGEMENTS.

The work was supported by the Wellcome Trust (Programme Grant 087737), the MRC (Programme Grant G0801693/2), ANR-11 BSV5 01102 EARMEC and ERC-2011-AdG 294570 "Auditory Hair Bundle". The authors thank James Hartley for technical support.

1. Davis H (1965) A model for transducer action in the cochlea. *Cold Spring Harb Symp Quant Biol* 30:181-190.
2. Sellick PM & Russell IJ (1980) The responses of inner hair cells to basilar membrane velocity during low frequency auditory stimulation in the guinea pig cochlea. *Hear Res* 2(3-4):439-445.
3. Kimura RS (1966) Hairs of the cochlear sensory cells and their attachment to the tectorial membrane. *Acta Otolaryngol* 61(1):55-72.
4. Hudspeth AJ & Corey DP (1977) Sensitivity, polarity, and conductance change in the response of vertebrate hair cells to controlled mechanical stimuli. *Proc Natl Acad Sci U S A* 74(6):2407-2411.
5. Allen JB (1980) Cochlear micromechanics--a physical model of transduction. *J Acoust Soc Am* 68(6):1660-1670.
6. Zwislocki JJ (1980) Theory of cochlear mechanics. *Hear Res* 2(3-4):171-182.
7. Davis H (1983) An active process in cochlear mechanics. *Hear Res* 9(1):79-90.
8. Dallos P, Billone MC, Durrant JD, Wang C, & Raynor S (1972) Cochlear inner and outer hair cells: functional differences. *Science* 177(4046):356-358.
9. Patuzzi RB & Yates GK (1987) The low-frequency response of inner hair cells in the guinea pig cochlea: implications for fluid coupling and resonance of the stereocilia. *Hear Res* 30(1):83-98.
10. Nowotny M & Gummer AW (2006) Nanomechanics of the subtectorial space caused by electromechanics of cochlear outer hair cells. *Proc Natl Acad Sci U S A* 103(7):2120-2125.
11. Freeman DM & Weiss TF (1990) Hydrodynamic forces on hair bundles at high frequencies. *Hear Res* 48(1-2):31-36.
12. Smith ST & Chadwick RS (2011) Simulation of the response of the inner hair cell stereocilia bundle to an acoustical stimulus. *PLoS One* 6(3):e18161.
13. Legan PK, Rau A, Keen JN, & Richardson GP (1997) The mouse tectorins. Modular matrix proteins of the inner ear homologous to components of the sperm-egg adhesion system. *J Biol Chem* 272(13):8791-8801.
14. Cohen-Salmon M, El-Amraoui A, Leibovici M, & Petit C (1997) Otogelin: a glycoprotein specific to the acellular membranes of the inner ear. *Proc Natl Acad Sci U S A* 94(26):14450-14455.
15. Zheng J, *et al.* (2011) Carcinoembryonic antigen-related cell adhesion molecule 16 interacts with alpha-tectorin and is mutated in autosomal dominant hearing loss (DFNA4). *Proc Natl Acad Sci U S A* 108(10):4218-4223.
16. Deans MR, Peterson JM, & Wong GW (2010) Mammalian Otolin: a multimeric glycoprotein specific to the inner ear that interacts with otoconial matrix protein Otoconin-90 and Cerebellin-1. *PLoS One* 5(9):e12765.
17. Verhoeven K, *et al.* (1998) Mutations in the human alpha-tectorin gene cause autosomal dominant non-syndromic hearing impairment. *Nat Genet* 19(1):60-62.
18. Mustapha M, *et al.* (1999) An alpha-tectorin gene defect causes a newly identified autosomal recessive form of sensorineural pre-lingual non-syndromic deafness, DFNB21. *Hum Mol Genet* 8(3):409-412.
19. Alasti F, *et al.* (2008) A novel TECTA mutation confirms the recognizable phenotype among autosomal recessive hearing impairment families. *Int J Pediatr Otorhinolaryngol* 72(2):249-255.
20. Hildebrand MS, *et al.* (2011) DFNA8/12 caused by TECTA mutations is the most identified subtype of nonsyndromic autosomal dominant hearing loss. *Hum Mutat* 32(7):825-834.
21. Legan PK, *et al.* (2000) A targeted deletion in alpha-tectorin reveals that the tectorial membrane is required for the gain and timing of cochlear feedback. *Neuron* 28(1):273-285.
22. Legan PK, *et al.* (2005) A deafness mutation isolates a second role for the tectorial membrane in hearing. *Nat Neurosci* 8(8):1035-1042.
23. Russell IJ, *et al.* (2007) Sharpened cochlear tuning in a mouse with a genetically modified tectorial membrane. *Nat Neurosci* 10(2):215-223.
24. Lukashkin AN, Richardson GP, & Russell IJ (2009) Multiple roles for the tectorial membrane in the active cochlea. *Hear Res*.
25. Zwaenepoel I, *et al.* (2002) Otoancorin, an inner ear protein restricted to the interface between the apical surface of sensory epithelia and their overlying acellular gels, is defective in autosomal recessive deafness DFNB22. *Proc Natl Acad Sci U S A* 99(9):6240-6245.
26. Brownell WE, Manis PB, Zidanic M, & Spirou GA (1983) Acoustically evoked radial current densities in scala tympani. *J Acoust Soc Am* 74(3):792-800.
27. Zidanic M & Brownell WE (1990) Fine structure of the intracochlear potential field. I. The silent current. *Biophys J* 57(6):1253-1268.
28. Zidanic M & Brownell WE (1992) Fine structure of the intracochlear potential field. II. Tone-evoked waveforms and cochlear microphonics. *J Neurophysiol* 67(1):108-124.
29. Russell IJ, Cody AR, & Richardson GP (1986) The responses of inner and outer hair cells in the basal turn of the guinea-pig cochlea and in the mouse cochlea grown in vitro. *Hear Res* 22:199-216.
30. Muller M, von Hunerbein K, Hoidis S, & Smolders JW (2005) A physiological place-frequency map of the cochlea in the CBA/J mouse. *Hear Res* 202(1-2):63-73.
31. Dallos P & Cheatham MA (1976) Compound action potential (AP) tuning curves. *J Acoust Soc Am* 59(3):591-597.
32. Harrison RV & Prijs VF (1984) Single cochlear fibre responses in guinea pigs with long-term endolymphatic hydrops. *Hear Res* 14(1):79-84.
33. Sathyanarayana BK, Hahn Y, Patankar MS, Pastan I, & Lee B (2009) Mesothelin, Stereocilin, and Otoancorin are predicted to have superhelical structures with ARM-type repeats. *BMC Struct Biol* 9:1.
34. Verpy E, *et al.* (2008) Stereocilin-deficient mice reveal the origin of cochlear waveform distortions. *Nature* 456(7219):255-258.
35. Dallos P (2002) Some pending problems in cochlear mechanics.
36. Geisler CD & Sang C (1995) A cochlear model using feed-forward outer-hair-cell forces. *Hear Res* 86(1-2):132-146.
37. Kronester-Frei A (1979) Localization of the marginal zone of the tectorial membrane in situ, unfixed, and with in vivo-like ionic milieu. *Arch Otorhinolaryngol* 224(1-2):3-9.

38. Johnson SL, Beurg M, Marcotti W, & Fettiplace R (2011) Prestin-driven cochlear amplification is not limited by the outer hair cell membrane time constant. *Neuron* 70(6):1143-1154.
39. Shah DM, Freeman DM, & Weiss TF (1995) The osmotic response of the isolated, unfixed mouse tectorial membrane to isosmotic solutions: effect of Na+, K+, and Ca2+ concentration. *Hear Res* 87(1-2):187-207.
40. Xia A, *et al.* (2010) Deficient forward transduction and enhanced reverse transduction in the alpha tectorin C1509G human hearing loss mutation. *Dis Model Mech* 3(3-4):209-223.
41. Mammano F & Ashmore JF (1995) A laser interferometer for sub-nanometre measurements in the cochlea. *J Neurosci Methods* 60(1-2):89-94.
42. Russell IJ & Nilsen KE (1997) The location of the cochlear amplifier: spatial representation of a single tone on the guinea pig basilar membrane. *Proc Natl Acad Sci U S A* 94(6):2660-2664.
43. Chen F, *et al.* (2011) A differentially amplified motion in the ear for near-threshold sound detection. *Nat Neurosci* 14(6):770-774.
44. Yu N & Zhao HB (2009) Modulation of outer hair cell electromotility by cochlear supporting cells and gap junctions. *PLoS One* 4(11):e7923.
45. Steele CR, Puria S (2005) Force on inner hair cell stereocilia. *Int J Solid and Structures* 42:5885-5904.